NASA Contractor Report 3706

Low-Temperature Forming of Beta Titanium Alloys

R. S. Kaneko and C. A. Woods
Lockheed-California Company
Burbank, California

Prepared for
Langley Research Center
under Contract NAS1-15568

National Aeronautics
and Space Administration

Scientific and Technical
Information Branch

1983

FOREWORD

This final report summarizes a study performed for the NASA Langley Research Center under Contract NAS1-15568, Investigation of Low Temperature Forming of Beta Titanium Alloys for Supersonic Cruise Research (SCR) Applications, for the period December 1978 to December 1982. Mr. D. M. Royster was the technical monitor for NASA. Results from concurrent Lockheed internal research studies on beta titanium alloys are also reported.

The program was conducted by the Lockheed-California Company, Burbank, with Mr. R.S. Kaneko of the Materials and Processes Department the Project Leader. Lockheed personnel who made key contributions to the program were:

Materials and Producibility	C.M. Garcia, R.J. Reiseck
Structures	C.A. Woods, G.W. Davis, J.C. Ekvall, M.D. McMaster, L. Young, P. Schell
Manufacturing Research	J.K. Lawson, F.H. Ruge, T.F. Imholz, L. Moses
Structures and Materials Laboratory	R.L. Lowe, J.M. Cox, T. Gillette, F. Pickel, W. Renslen, T.K. Mukherji
Quality Assurance	W.W. Leuders, J.F. Crocker, M.J. Berg

Creep and elevated temperature compression coupon tests were conducted at the Battelle Columbus Laboratories under the direction of J. Van Echo.

TABLE OF CONTENTS

TABLE OF CONTENTS (Continued)

LIST OF FIGURES

LIST OF FIGURES (Continued)

LIST OF FIGURES (Continued)

LIST OF FIGURES (Continued)

LIST OF TABLES

LIST OF TABLES (Continued)

LIST OF TABLES (Continued)

LOW-TEMPERATURE FORMING OF BETA TITANIUM ALLOYS

Russell S. Kaneko and Carolyn A. Woods

Lockheed-California Company

SUMMARY

Low-cost methods for titanium structural fabrication using advanced cold-formable beta alloys were investigated for application in a Mach 2.7 supersonic cruise vehicle. This work focuses on improving processing and structural efficiencies as compared with standard hot-formed and riveted construction of all Ti-6Al-4V sheet structure. The principal alloy investigated was Ti-15V-3Cr-3Sn-3Al (Ti-15-3), and a more limited evaluation of the Ti-3Al-8V-6Cr-4Mo-4Zr (Beta-C) alloy was made.

The beta alloys were readily cold-formable, brazable, and weldable in the solution-treated condition, and the aged mechanical properties appear suitable for postulated service at -65°F to 600°F. Skin/stringer panels were made by a new approach whereby cold-formed beta Ti stringers and Ti-6Al-4V face sheets were joined using a unique out-of-furnace isothermal brazing process, followed by low-temperature aging to achieve optimum properties. Structural verification included room and elevated temperature crippling tests of small skin/stringer assemblies, and column buckling, fatigue and damage-tolerance testing of large-scale representative wing surface panels of a supersonic cruise vehicle. This new methodology can reduce production costs by at least 25 percent and weight by 16 percent compared with the conventional Ti-6Al-4V hot-formed and riveted assembly.

Increasing the structural capability of beta titanium components by local reinforcement with continuous fiber SiC/Ti-6Al-4V metal matrix composite (MMC) was shown feasible using the isothermal brazing process. Conversely spot-weldability of the MMC was poor and requires further development to eliminate local composite weakening. Present costs of the MMC selective reinforcement concepts studied are very high.

INTRODUCTION

For several years NASA has been conducting a supersonic cruise research (SCR) program to develop a strong technology base for providing rational decisions concerning the development of future supersonic aircraft. Titanium alloys are of interest to the SCR program because of their structural efficiency at elevated temperature. Conventional titanium sheet structure, however, has a history of being difficult and expensive to fabricate because of the extensive hot forming, machining, drilling and fastening involved. Alpha-beta alloys possess very limited formability. For example, the minimum bend radius of Ti-6Al-4V (Ti-6-4) sheet at room temperature is about five times the thickness. Therefore, it is usually hot formed at 1300 to 1500°F to obtain the required dimensions with minimal springback.

Metastable beta titanium alloys possess a body centered cubic crystal lattice having a relatively large number of active slip systems that result in increased ductility and the ability to be formed at, or near, room temperature. This considerably reduces fabrication costs. Being strip rollable they are also more economical than alpha-beta alloys such as Ti-6Al-4V produced on a hand mill.

With simple aging treatments, the beta alloys can attain a higher specific strength than conventional alpha-beta alloys. Further weight savings are possible by exploiting selective cold-roll taper forming and the close tolerances and long lengths achieved by continuous strip processing.

Based on the potential structural efficiency and formability virtues of the beta titanium alloys, this study was initiated to verify their advantages over conventional titanium alloys for SCR applications. The general approach taken to accomplish this objective was (1) developing the manufacturing parameters and mechanical property data for efficiently cold forming, brazing, welding, and heat treating advanced beta titanium alloys, and (2) demonstrating cost and structural payoffs through design, fabrication, and evaluation of large structural panels.

The program consisted of eight major tasks, briefly described below:

- Task 1 - Material Identification and Screening. - Identify and screen three candidate beta titanium alloys for mechanical properties and relative applicability to low temperature forming.

- Task 2 - Room Temperature Formability Study. - Investigate the room temperature forming capability of the two most promising alloys.

- Task 3 - Process Optimization. - Develop forming parameters and optimum heat treatment for the two beta alloys.

- Task 4 - Material Characterization. - Develop and conduct a test program to determine effects of forming, joining, and SCR environment on the basic material properties of the two beta alloys.

- Task 5 - Joining Studies. - Develop low-cost, efficient joining methods for the two beta alloys.

- Task 6 - Panel Specimen Fabrication. - Design, fabricate, and test hat-stiffened crippling specimens from the two beta alloys.

- Task 7 - Wing Panel Fabrication. - Design and fabricate representative hat-stiffened SCR upper wing surface panels from a selected beta alloy and joining method. Perform static compression and variable amplitude flight-by-flight fatigue loading spectrum tests. Assess the relative merits of low-temperature forming of beta titanium alloys for fabricating SCR structural wing panels compared to state-of-the-art fabrication methods for Ti-6Al-4V alloy.

- Task 8 - Metal Matrix Composite (MMC) Selective Reinforcement Concepts. - Design, analyze, fabricate and test selectively reinforced beta titanium skin-stringer compression elements, and assess the data for scaling up the concepts to fabricate a full-size wing panel.

Preliminary results of Tasks 1 through 7 were presented in Reference 1. Final results of Tasks 1 through 8 are reported herein.

Use of trade names or names of manufacturers in this report does not constitute an official endorsement of such products or manufacturers, either expressed or implied, by the National Aeronautics and Space Administration or the Lockheed-California Company.

SYMBOLS AND ABBREVIATIONS

a	Crack length, inch
Δa	Effective crack extension, inch
A	Aged, (thermal treatments are noted in text)
CT	Compact tension
CW	Cold work (refers primarily to tension strain; a minus sign denotes compression strain)
da/dN	Fatigue crack growth rate, in/cycle
e	Elongation in 4w (w=specimen width), percent
E	Elastic modulus (tensile or compressive), Msi
EDAX	Energy dispersive analysis of X-rays
f_{1gRef}	Mean stress during climb

fcg	Fatigue crack growth
F_{cy}	Compressive yield strength at 0.2 percent offset, ksi
F_{tu}	Ultimate tensile strength, ksi
F_{ty}	Tensile yield strength at 0.2 percent offset, ksi
FLD	Forming limit diagram
h	Hour
K	Stress intensity factor, ksi-$in^{1/2}$
ΔK	Stress intensity factor range, ksi-$in^{1/2}$
L	Longitudinal
K_c	Plane stress fracture toughness (The value of K_R at the instability condition), ksi-$in^{1/2}$
K_R	Crack growth resistance, ksi-$in^{1/2}$
K_t	Geometric stress concentration factor
MMC	Metal matrix composite
n	Strain hardening coefficient
r	Radius, inch
R	Stress ratio, min stress/max stress
R_c	Stress ratio below which compression loading is ineffective
$\bar{R}$	Planar average plastic strain ratio, $e_{width}/e_{thickness}$
ρ	Density, lb/in^3
SCR	Supersonic cruise research
SCV	Supersonic cruise vehicle
SEM	Scanning electron microscopy
ST	Solution treated
STA	Solution treated and aged
t	Thickness, inch
T	Transverse
TIG	Tungsten inert gas (welding;

TASK 1 - MATERIAL IDENTIFICATION AND SCREENING

Literature Survey

A cursory review was made initially of references covering beta alloys which had been produced experimentally or commercially as flat-rolled products. Further review was then limited to alloys which were commercially available and which lend themselves to low-temperature forming with the potential of being age-hardened to strength levels of high structural efficiency.

A comparison of published properties and formability of the principal beta alloy candidates is summarized in tables 1 and 2. Formability data are given for the solution-treated (ST) condition. Other values reported in these tables were selected to correspond with a common strength level near 170 ksi to facilitate property comparisons in the solution treated and aged (STA) condition.

Thermal stability characteristics of the six candidate alloys are presented in table 2. Creep data were not available for all the alloys, but the limited data obtained from this literature search shows that the creep resistance of the beta alloys compares favorably with Ti-6Al-4V. Exposure to 600°F for various times up to 1500 hours had little effect on the tensile properties of these alloys. However, a direct comparison of thermal or creep stability cannot be made because of the differences in the exposure times and stress conditions.

Assessment of the data led to selecting Ti-15V-3Cr-3Al-3Sn(Ti-15-3), Ti-3Al-8V-6Cr-4Mo-4Zr(Beta-C), and Ti-13V-11Cr-3Al(B-120) for screening tests in task 1. Ti-15-3 is recognized as a superior Ti sheet alloy based on a series of previous Air Force programs having the goal of developing a strip-producible, formable, economical, and "forgivable" Ti sheet alloy (references 2 through 5). B-120 was the first beta alloy of commercial importance, and was chosen to serve only as a baseline for the screening tests in task 1. Beta-C has exhibited a good combination of cold formability and aged mechanical properties including creep stability, and was the most readily available alloy for this program of the remaining candidates.

Test Materials

Beta alloys Ti-15-3, Beta-C, and B-120 were selected from the literature survey for screening in task 1, with Ti-15-3 and Beta-C for the ensuing tasks. Properties of the as-received sheet materials and their program usage are listed in table 3.

RMI Company experienced difficulties producing the hot-roll Beta-C sheets for the program. It was not available for task 1 screening and the thinner of the two ordered gages (0.040 and 0.080 inch) was cancelled. Nominal gage of the Beta-C received was 0.065 inch. Ductility was rather low as evidenced by the tensile elongation and minimum bend radii reported in the mill certification (table 3).

On receipt of the Beta-C material, the tensile properties and microstructure were checked. The tensile properties shown below agreed with the supplier data and were acceptable although elongation was marginal.

As-Solution Treated 1600°F, 30 Min., Air Cool:

Dir	F_{tu}, ksi	F_{ty}, ksi	e,%
L	130.0	129.6	13.0
T	133.4	132.8	8.0

Metallographic examination of the Beta-C revealed a mixed beta grain size consisting of fine and very large grains (> ASTM No. 1). Also the surface appeared heavily etched resulting in an uneven and rough texture. Microstucture is shown in figure 1. The grain size inhomogeneity is greater than normal and can be attributed to the cumulative effects of reprocessing applied to this lot of material. To correct earlier deficiencies including high hydrogen, low ductility, and high directionality, the material was subjected to an additional vacuum anneal cycle and a 1600°F resolution treatment.

Based on this preliminary assessment, the Beta-C was considered to be below its normal quality. Consequently the Beta-C evaluation was reduced in scope to selectively perform sufficient heat treat, mechanical property, forming, and joining characterization to accomplish the task 6 panel evaluation; and the characterization of the Ti-15-3 alloy was increased.

Screening Tests

Three heat-treat conditions were selectively evaluated; the solution treated condition for formability, and two aging treatments for mechanical properties, representing near-peak and an intermediate strength level as follows:

Alloy	Peak Strength	Intermediate Strength
B-120	900°F - 36h*	900°F - 12h
Ti-15-3	850°F - 16h	900°F - 12h

*Although strength increases slowly with longer aging time, 36 hours was chosen as a practical cutoff point.

A matrix of the screening tests is shown in table 4.

Formability Indices. - Applicability to room temperature forming was initially assessed on the basis of tension and compression tests of annealed material in three grain directions (L,T,45°). Table 5 summarizes the results obtained for Ti-15-3 and B-120 alloys. Ti-15-3 shows better overall formability characteristics than B-120, and little directionality as well.

The lower yield strength (hence, flow stress) and modulus of Ti-15-3 in both tension and compression are favorable from a forming standpoint. Both alloys exhibit high ductility, while strain hardening coefficients were suitably low. Above about 10 percent elongation, the B-120 appears to have a significantly higher strain hardening rate than Ti-15-3. Planar average plastic strain ratios ($\bar{R}$) greater than unity were obtained for both Ti-15-3 and B-120. This characterizes the materials as being resistant to thinning and, therefore, suitable for such forming operations as drawing, stretch forming, and hydroforming (reference 17 through 20). Note, however, that while directional plastic strain ratios (R_i) were nearly isotropic for Ti-15-3, the B-120 had an R-value less than unity in the longitudinal and transverse grain directions.

Aged Mechanical Properties. - All Ti-15-3 and B-120 test coupon blanks were aged in an argon atmosphere and then pickled in nitric-hydroflouric acid to remove the surface film.

- Tension and Residual Strength. - Room temperature tensile properties were determined for Ti-15-3 and B-120 aged to peak and intermediate strength levels. The residual strength of material stretch-strained to a nominal 8 percent permanent set prior to aging to simulate forming strains was included. The reduced section was premachined oversize and the individual coupons were stretched in a tensile test machine.

  A test summary is presented in table 6. Ti-15-3 had less directionality and slightly better ductility than B-120, while B-120 had greater stiffness. Uniaxial prestrain tended to reduce the directionality in both alloys. With prestrain, overaging appears to have set in with the peak strength age in B-120 and with both aged conditions in Ti-15-3, indicating that the alloys were fully aged by these treatments. Prestrain accelerated aging to increase strength only for the intermediate strength age in B-120.

- Notched Fatigue. - Constant amplitude axial testing at R = 0.1 was carried out on hole-notched coupons with K_t = 2.6. The S-N fatigue plots for Ti-15-3 and B-120 in two aged conditions are presented in figure 2. Ti-15-3 alloy showed generally improved fatigue behavior compared to B-120. The two aging treatments for B-120 and the peak strength age for Ti-15-3 produced similar fatigue results, while a 15-percent higher endurance strength is indicated for the lower strength Ti-15-3. This apparent fatigue improvement for the lower-strength aging treatment warranted further study and verification in task 4.

- Fracture Toughness. - R-curve determination for Ti-15-3 and B-120 in two aged conditions was conducted based on the guidelines of proposed ASTM Standard E561-76T, using compact specimens. The resulting R-curves are shown in figures 3 and 4 in terms of effective crack extension. The adjustment of the plastic zone size was based on a comparison of the physical crack length at the end of fatigue pre-cracking to the calculated crack length at the start of R-curve testing. The R-curves indicate that for a given alloy, the higher strength heat treat had a discernible effect resulting in a lower fracture resistance. On the other hand, for a similar strength level, the two alloys have comparable R-curve characteristics.

- Creep. - The test temperature was 600°F, the time period 1000 hours, and the stress 100 ksi. There were four test groups representing two alloys (Ti-15-3, B-120) and two aging treatments. One of the three specimens in each group was stretched prior to aging in the manner described earlier for residual-strength specimens to represent the effect of forming strains. The specimens were tension tested after the creep exposure to compare exposed and unexposed properties.

  The results are shown in table 7. B-120 had better creep resistance than Ti-15-3 under these test conditions, displaying lower creep strains and creep rates for both aging treatments. The effect of aging treatment was insignificant with Ti-15-3, but with B-120 the more fully aged condition, 900°F/36 hours, had the best creep resistance. Cold-work before aging (simulating forming prestrain) tended to lower the creep resistance very slightly in both allys. Note that the creep stress of 100 ksi is much higher than the anticipated sustained design loads for an SCR structure. In view of this, a lower stress was evaluated in the creep tests of task 4 (Materials Characterization). Examination of the room-temperature tensile properties indicates generally good creep stability in these alloys. Some strengthening was found in all specimens after creep exposure, however, with little or no loss in ductility.

TABLE 1. - SELECTED ROOM TEMPERATURE PROPERTIES OF CANDIDATE BETA ALLOYS (TASK 1 LITERATURE SURVEY)

Alloy	Density, ρ (lb/in^3)	Heat Treat Condition[1]		Tensile Properties F_{tu} (ksi)	F_{ty} (ksi)	Elong. (%)	Fracture Toughness in STA Cond., K_c ($ksi\sqrt{in.}$)	Tension Modulus in STA Cond., E_t (10^3 ksi)	Et/ρ For STA Cond., (10^6 in.)	Ftu/ρ For STA Cond., (10^3 in.)	Formability in ST Cond. MBR[2]	Formability in ST Cond. Olsen Cup Depth (in.)	Remarks	References
Ti-2Al-11V-2Sn-11Zr (Transage 129)	0.174	ST	1400F, 2h, Fan Air Cool	110	105	20	–	–	–	–	2t	0.28	Not available within program time frame. Laboratory status	6, *
		STA	ST + 900F, 1 h	180	165	6	–	14.6	83.9	1034	–	–		
Ti-3Al-8V-6Cr-4Mo-4Zr (Beta-C)	0.174	ST	1550F, 15 Min, Air Cool	130	125	14	–	–	–	–	2t	0.28	Currently available as hot rolled sheet	3, 7, 8, *
		STA	ST + 1050F, 6h	178	165	8	–	15.4	88.5	1023	–	–		
Ti-8Mo-8V-2Fe-3Al (Ti-8-8-2-3)	0.175	ST	1450F, 10 Min, Air Cool	135	120	17	–	–	–	–	2t	–	Not offered as sheet product, only bar and wire. Laboratory status.	7, 9
		STA	ST + 900F, 8h	200	190	4	54	15.5	88.6	1143	–	–		
Ti-11.5Mo-6Zr-4.5 Sn (Beta III)	0.183	ST	1350F, 3 Min, Air Cool	135	130	10	–	–	–	–	3t	0.25	Produced as sheet or strip. Not available for this program.	7, 10, 11, 12, *
		STA	ST + 1000F, 8h	175	160	6	–	15.0	82.0	956	–	–		
Ti-13V-11Cr-3Al (8-120)	0.175	ST	1450F, 15 Min, Air Cool	125	120	10	–	–	–	–	3t	0.26	First all beta alloy. Some limited use as sheet or strip.	7, 13, 14
		STA	ST + 900F, 24h	180	165	5	48	15.5	88.6	1028	–	–		
Ti-15V-3Cr-3Al-3Sn (Ti-15-3)	0.172	ST	1450F, 20 Min, Air Cool	110	105	18	–	–	–	–	2t	0.34	Available as simulated strip. Will be scaled up to continuous strip process in current air force program.	5, 15
		STA	ST + 925F, 16h	180	165	12	~90 (K_Q)	15.0	87.2	1047	–	–		

[1] Solution treated and aged properties selected commensurate with a minimum baseline of: Ftu = 170 ksi and Fty = 160 ksi.

[2] MBR = minimum bend radius, where t = sheet thickness

*K. A. Wilhelm, "Forming of Transage 129, Beta III and Beta-C Titanium Alloys", CMRI-1821, Lockheed-Calif. Co., Aug. 1974.

TABLE 2. - CREEP RESISTANCE AND THERMAL STABILITY OF CANDIDATE BETA ALLOYS (TASK 1 LITERATURE SURVEY)

Alloy	Aged Condition	Creep Resistance				Tensile Properties						Ref.
		Exposure			Percent Deformation	Before Exposure			After Exposure			
		Temperature	Time (h)	Stress (Ksi)		F_{tu} (ksi)	F_{ty} (ksi)	Elong. (%)	F_{tu} (ksi)	F_{ty} (ksi)	Elong. (%)	
Ti-2Al-11V-2Sn-11Zr	900F, 1 h	600F	100	97	0.10	180	–	–	–	–	–	6
Ti-3Al-8V-6Cr-4Mo-4Zr	1050F, 6 h	600F	800	80	0.10	174	160	13	174	162	14	8
Ti-8Mo-8V-2Fe-3Al	1000F, 6 h	600F	500	0	–	177	158	13	174	156	13	7
Ti-11.5Mo-6Zr-4.5Sn	1000F, 8 h	600F	100	70	0.12	–	160	–	–	–	–	7
Ti-13V-11Cr-3Al	900F, 100 h	600F	1502	95	0.11	199	180	9	200	184	2	16
Ti-15V-3Cr-3Al-3Sn	950F, 8 h	600F	500	0	–	183	170	10	187	173	10	4
	950F, 16 h	600F	500	0	–	184	173	9	185	170	10	4

TABLE 3. - AS-RECEIVED TITANIUM SHEET PROPERTIES AND USAGE

Alloy & Gage		Ti-15-3 (0.063 in.)	B120 (0.063 in.)	Ti-15-3 (0.080 in.)	Ti-15-3 (0.040 in.)	Beta C (0.065 in.)	Ti-6Al-4V (0.040 in.)	Ti-6Al-4V (0.070 in.)
Mill, Heat No.		Timet, Heat P-2360	Timet, Heat D-5955	Timet, Heat P-3357	Timet, Heat P-3357	RMI Heat 801008	Timet, Heat P-2093	RMI, Heat 803093
Program Usage		Task 1, 5, 8	Task 1	Task 2 - 7	Task 2 - 7	Task 2 - 6	Task 5, 8	Task 4 - 7
Remarks		• Sheet Simulated Strip, Mill Annealed 20 Min at 1450F	• Hot Rolled, Mill Annealed, Mil-T-9046	• Sheet Simulated Strip, Mill Annealed 15 Min at 1450F	• Sheet Simulated Strip, Mill Annealed 20 Min at 1450F	• Hot Rolled, Mill Annealed 30 Min at 1600F	• Hot Rolled, Mill Annealed, Mil-T-9046	• Hot Rolled, Mill Annealed, Mil-T-9046
CERTIFIED TEST RESULTS								
Chemical Composition, Wt percent	C	0.015	0.032	0.018	0.018	0.02	0.02[1]	0.02
	N	0.014	0.027	0.017	0.017	0.012	0.014	0.010
	Fe	0.16	0.16	0.14	0.14	0.06	0.10	0.13
	Al	3.2	2.9	3.1	3.1	3.4	6.2	6.0
	V	15.0	13.6	15.2	15.2	8.2	4.2	3.8
	Cr	3.2	11.2	2.7	2.7	6.2	–	–
	Sn	3.1	–	2.9	2.9	–	–	–
	Zr	–	–	0.001	0.001	4.0	–	–
	Mo	–	–	0.001	0.001	4.0	–	–
	Cu	–	–	0.001	0.001	–	–	–
	H	0.018 - 0.022	0.006 - 0.008	0.014 - 0.018	0.027	0.0155	0.015	0.0084
	O	0.13	0.14	0.11	0.11	0.083	0.13	0.13
	Ti	Balance	Balance	Balance	Balance	Balance	Balance	Balance
F_{tu}, ksi	L	107-114	135.6 - 146.5	106-110	115-116	125.0-133.7	144-145	144.2-147.8
	T	108-114		109-112	117-119	129.5-129.9	146	146.6-148.6
F_{ty}, ksi	L	104-108	131.3 - 139.6	105-107	107-110	121.0-125.1	130	132.8-137.0
	T	105-110		105-110	110-112	124.2-125.4	137-138	139.6-141.6
e, percent	L	16 - 20	13.0 - 21.0	11 - 22	11 - 15	9.5	10	10 - 11
	T	15 - 16		13 - 19	10 - 14	8.0 - 9.0	10 - 11	10 - 11
Bend Test	r/t	2.0	2.5 - 3.0	2.0	2.0	3.5/4.0 (T-axis) 5.2/6.0 (L-axis)	4.0	5.9

TABLE 4. MATRIX OF TASK 1 SCREENING TESTS

Type of Test	Specimen Configuration	Test Requirements (Room Temp. Except as Noted)	Alloy & Gage	Grain Dir	Condition[1]
Tension, Forming Data	Figure A1	F_{ty}, uniform e, E_t, plastic strain ratio ($\bar{R}$), strain hardening coeff. (n)	0.063 in. Ti-15-3 0.063 in. B-120	L, T, 45° L, T, 45°	ST ST
Compression, Forming Data	Figure A2	F_{cy}, E_c.	0.063 in. Ti-15-3 0.063 in. B-120	L, T, 45° L, T, 45°	ST ST
Tension	Figure A1	F_{tu}, F_{ty}, e, E_t.	0.063 in. Ti-15-3 0.063 in. B-120	L, T L, T	P, I P, I
Residual Strength	Figure A1	F_{tu}, F_{ty}, e, E_t; all specimens prestrained before aging	0.063 in. Ti-15-3 0.063 in. B-120	L, T L, T	P, I P, I
Creep, 1000 h at 600F, one stress level	Figure A1	ASTM E139; tension test at room temp. after exposure; nonstrained and prestrained before aging	0.063 in. Ti-15-3 0.063 in. B-120	L L	P, I P, I
Fatigue R = 0.1, K_t = 2.6	Figure A5	S-N curve	0.063 in. Ti-15-3 0.063 in. B-120	L L	P, I P, I
Fracture Toughness	Figure A7	ASTM E561-76T, R-Curve	0.063-in. Ti-15-3 0.063 in. B-120	T–L T–L	P, I P, I

[1] ST = Solution Treated, P = Peak Strength Age, I = Intermediate Strength Age

TABLE 5. MATERIAL PROPERTIES OF ANNEALED 0.063 IN. GAGE Ti-15V-3Cr-3Al-3Sn and Ti-13V-11Cr-3Al (TASK 1)

Properties (1)			Ti-13V-11Cr-3Al			Ti-15V-3Cr-3Al-3Sn		
			L	45°	T	L	45°	T
Tension	Yield Strength (F_{ty}), ksi		129	134	137	118	113	108
	Apparent Modulus (E_t), 10^3 ksi		15.4	13.8	16.2	11.2	12.8	11.6
	(2)Elong. (e), %		24	25	15	19	18	15
	(3)Strain Hardening Coefficient (n), $S = Ce^n$	e<10%	0.062	0.036	0.044	0.038	0.028	0.044
		e>10%	0.15	0.14	–	0.083	0.072	–
	Plastic Strain Ratio, $R_i = \frac{e_{width}}{e_{thickness}}$ and $\bar{R} = \frac{R_1 + 2R_2 + R_3}{4}$		$R_1 = 0.81$	$R_2 = 1.48$	$R_3 = 0.90$	$R_1 = 1.35$	$R_2 = 1.14$	$R_3 = 1.38$
			$\bar{R} = 1.17$			$\bar{R} = 1.25$		
Compression	Yield Strength (F_{cy}), ksi		131	134	139	114	116	117
	Apparent Modulus (E_c), 10^3 ksi		14.9	14.3	15.7	12.7	13.3	12.9

(1)Average of duplicate specimens

(2)0.005 min^{-1} to yield, 0.05 min^{-1} thereafter to visible necking

(3)Derived from logarithmic true stress-strain curve by regression analysis.

TABLE 6. EFFECTS OF STRAINING FOLLOWED BY AGING ON TENSILE PROPERTIES OF TWO BETA TITANIUM ALLOYS (TASK 1)

Beta Alloy	Aging Treatment	Grain Direction	Condition	F_{tu} (ksi)	F_{ty} (ksi)	e (%)	Apparent Elastic Modulus (10^3 ksi)
Ti-13V-11Cr-3Al 0.063 in sheet	900°F -36h Peak Strength	L	STA	211	193	5.3	16.8
			STCWA	215	190	5.7	16.6
		T	STA	219	204	4.3	16.7
			STCWA	218	197	4.0	17.0
	900°F -12h Intermediate Strength	L	STA	190	172	8.3	16.4
			STCWA	203	179	6.0	16.3
		T	STA	196	183	6.0	16.6
			STCWA	208	186	6.0	16.7
Ti-15V-3Cr-3Al-3Sn 0.063 in sheet	850°F -16h Peak Strength	L	STA	203	189	6.0	15.4
			STCWA	204	186	5.8	15.3
		T	STA	208	196	6.3	15.6
			STCWA	206	190	5.2	15.6
	900°F -12h Intermediate Strength	L	STA	196	182	7.3	15.5
			STCWA	198	180	6.7	15.3
		T	STA	200	189	5.5	15.6
			STCWA	199	182	6.8	15.5

STA = Solution treated and aged. (Average of two specimens).

STCWA = Solution treated, cold worked and aged. Represents "residual strength" of material stretched nominally 8% to simulate cold forming prior to aging. (Average of three specimens).

TABLE 7. CREEP RESULTS FOR TWO BETA TITANIUM ALLOYS TESTED AT 600°F AND 100 KSI FOR 1000 HOURS (TASK 1)

Alloy	Aging Treatment	Prestrain,[1] %	Creep Strain, %	Min Creep Rate, %/h	Room-Temperature Tensile Properties					
					After Exposure			No Exposure[2]		
					F_{tu} (ksi)	F_{ty} (ksi)	e (%)	F_{tu} (ksi)	F_{ty} (ksi)	e (%)
Ti-15V-3Cr-3Al-3Sn 0.063 in. Sheet, Longitudinal	850°F/16h	0	0.324	0.00016	209	197	5	203	189	6.8
	850°F/16h	0	0.293	0.00015	211	199	5	203	189	6.8
	850°F/16h	8	0.384	0.00018	214	202	3	204	186	5.8
	900°F/12h	0	0.293	0.00017	203	190	5	196	182	7.3
	900°F/12h	0	0.[illegible]	0.00020	204	193	7	196	182	7.3
	900°F/12h	8	0.377	0.00020	219	198	5	198	188	6.7
Ti-13V-11Cr-3Al 0.063 in. Sheet, Longitudinal	900°F/36h	0	0.079	0.000018	216	198	6	211	193	5.3
	900°F/36h	8	0.084	0.000020	214	199	5	211	193	5.3
	900°F/36h	8	0.097	0.000025	–	–	–	215	198	5.7
	900°F/12h	0	0.114	0.000057	202	185	7	198	172	8.3
	900°F/12h	0	0.109	0.000054	198	186	7	198	172	8.3
	900°F/12h	8	0.127	0.000055	211	186	5	203	179	5.8

[1] Nominal amount of stretch prior to aging to simulate forming strains

[2] Average properties, from table 6

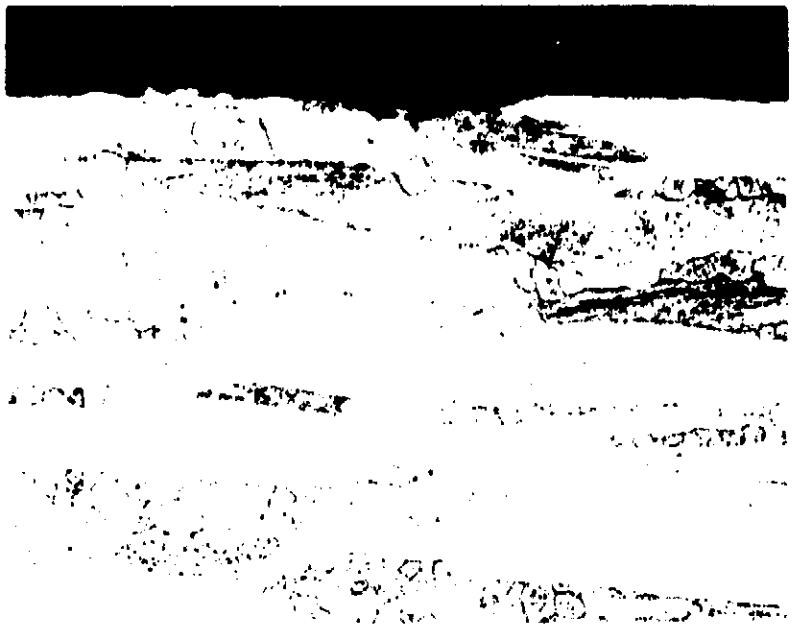

Longitudinal

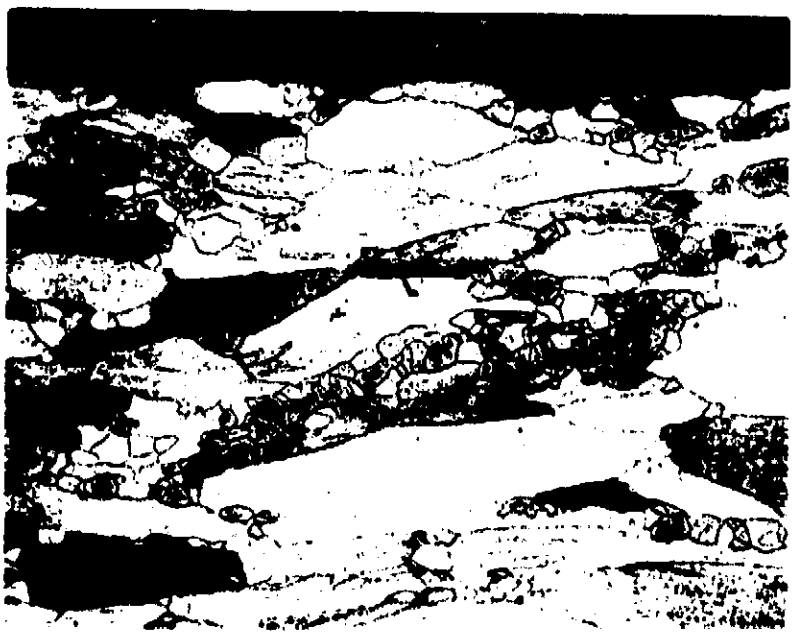

Transverse

Figure 1. - Microstructure of 0.065 in. Beta-C sheet solutioned 1600°F for 30 minutes and air cooled. Longitudinal (upper) and transverse (lower) cross-sections. Note rough surface. Mag 100X.

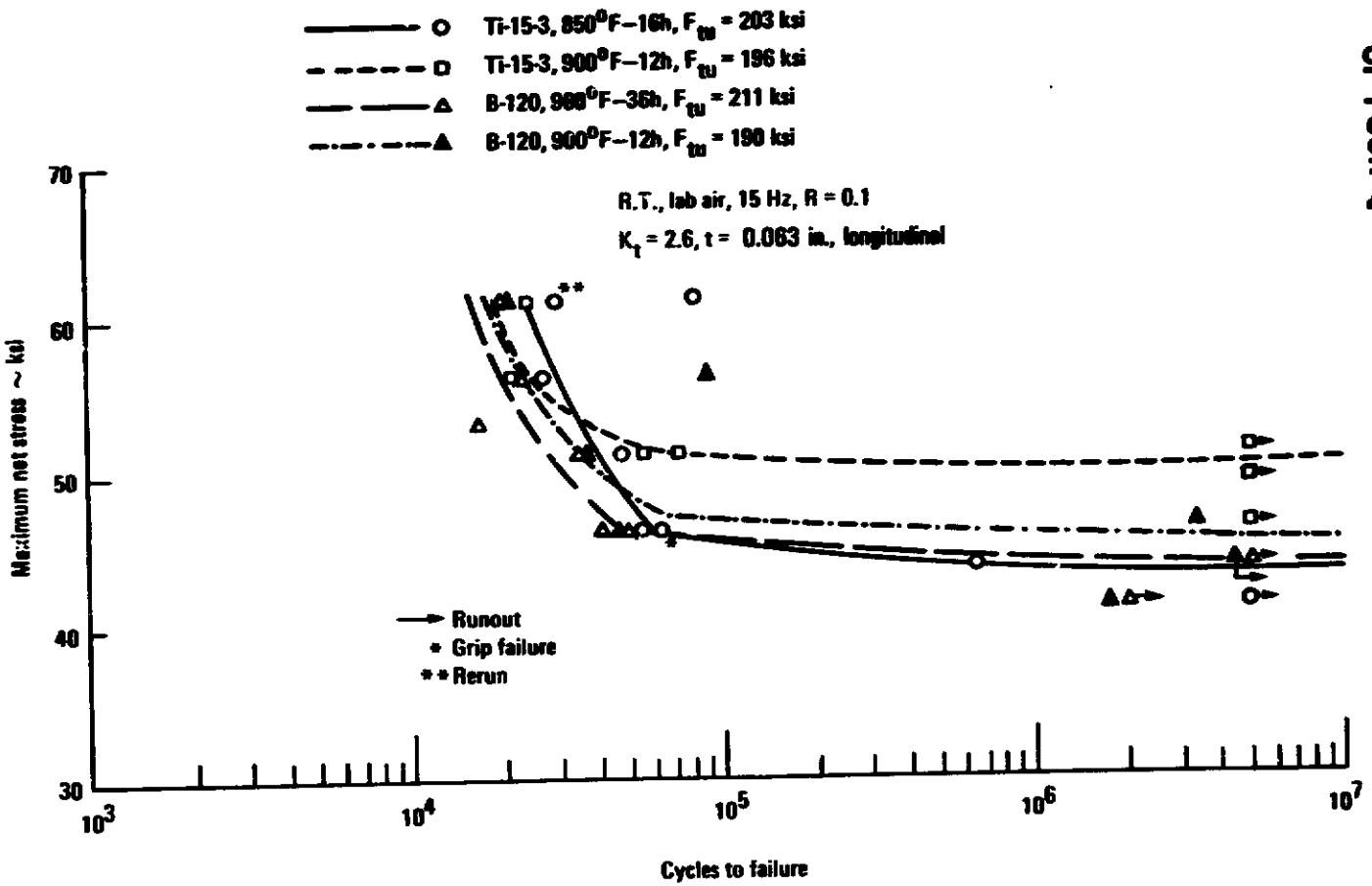

ORIGINAL PAGE IS
OF POOR QUALITY

Figure 2. Constant amplitude fatigue test results for two beta titanium alloys - task 1

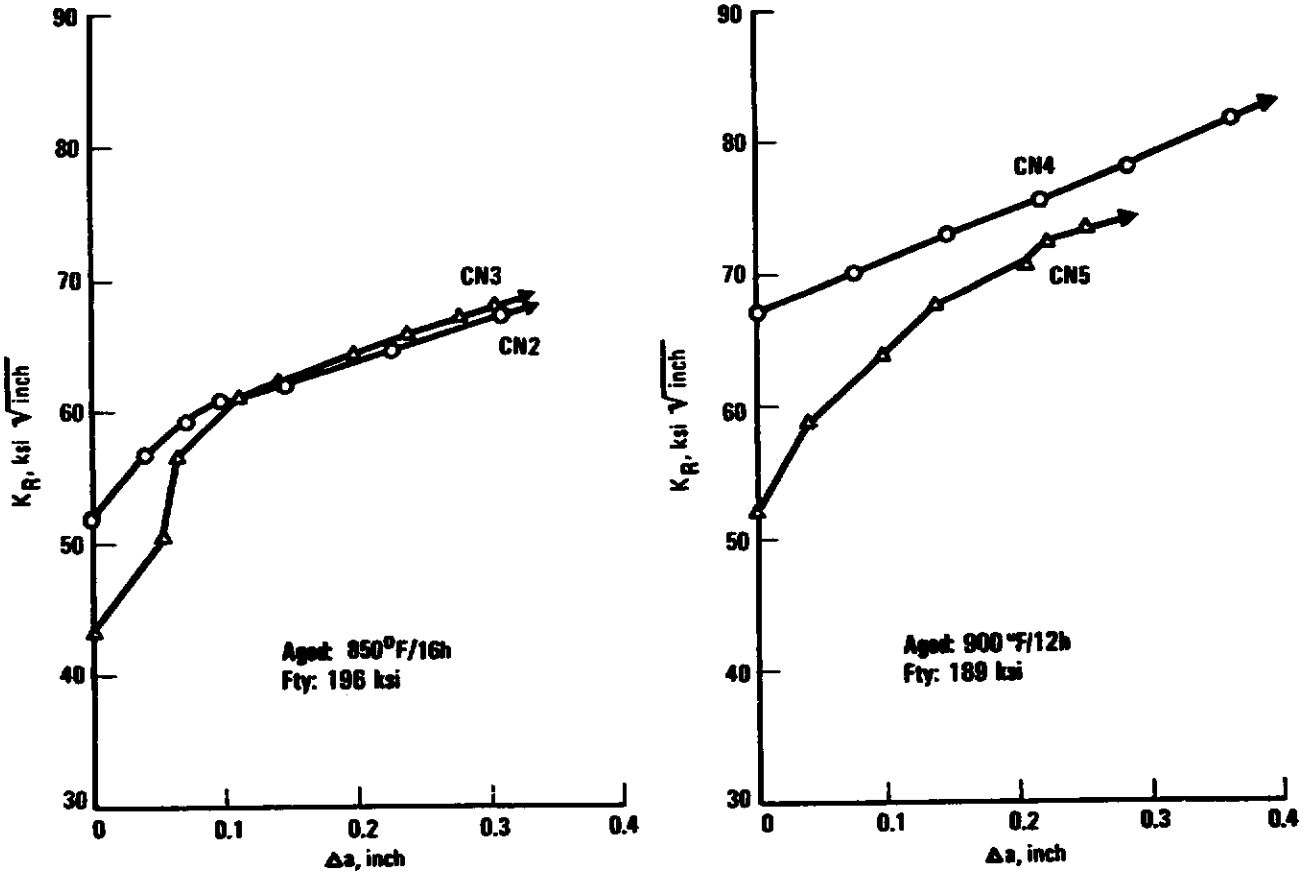

Figure 3. - K_R versus effective crack extension, Ti-15V-3Cr-3Al-3Sn 0.063 inch sheet, T-L orientation - task 1.

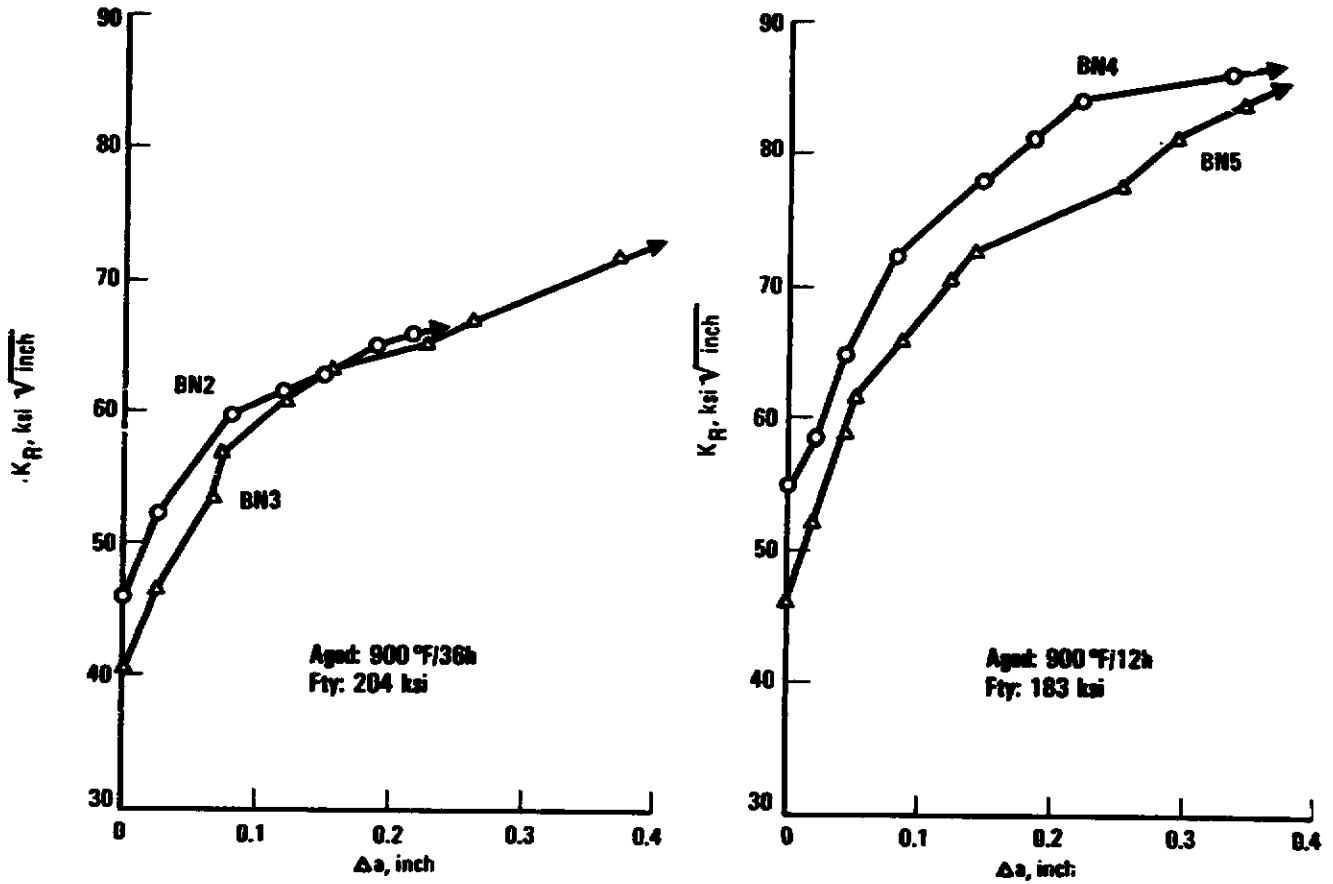

Figure 4. - K_R versus effective crack extension, Ti-13V-11Cr-3Al 0.063 inch sheet, T-L orientation - task 1.

TASK 2 - ROOM TEMPERATURE FORMABILITY STUDY

Forming trials for Ti-15-3 alloy were conducted for press brake bending, stretch press, and hydropress operations. These three processes account for the majority of formed sheet-metal parts on current airplanes. The forming evaluation for the Beta-C was limited to developing optimum bending parameters for brake forming the hat-stringers for the task 6 panels.

Press Brake Bending

Minimum bend radius, springback, and bending strains were determined for the Ti-15-3 material. Tests were conducted on two thickness of material, 0.040 inch and 0.080 inch, with the bend axis both parallel to the rolling direction (L) and across the rolling direction (T). Bending was done in a Chicago Hydraulic press, Model 150-HF-8, using forming dies of the general configuration shown in figure 5.

Generally, the minimum bend radius of a sheet metal is determined by making bends of successively smaller radii until rupture occurs, and then reporting the next larger bend radius. But the beta alloys, unlike most alpha or alpha-beta alloys, exhibit a severe orange peel effect before rupture which makes it difficult to establish bend ratings. For perspective, 0.063 inch Ti-13V-11Cr-3Al beta alloy specimens with the 3.0t minimum bend radius specified in Mil-T-9046 were used as a visual guide for acceptable orange peel appearance. After preliminary tests with standard 1-inch wide specimens, 6-inch wide specimens having a bend span-to-thickness ratio of 75 for 0.80-inch gage and 150 for the 0.040-inch gage were used to ensure a more representative evaluation of bending behavior. The specimens were bent through various angles from 25 to 135 deg. with the following results:

Grain Direction	Gage (in.)	Ti-15-3 Orange Peel Appearance for Given R/t Ratio				Min Bend Radius (r/t)
		0.4 to 1.2	1.6	2.0 to 2.4	2.7	
L&T	0.040	Heavy	Heavy	Light to moderate	Light	2.0
L&T	0.080	–	Heavy	Light to moderate	Light	2.0
Note: No rupture occurred.						

The minimum bend radius in terms of acceptable orange peel appears conservatively to be about 2.4t for both gages of Ti-15-3, and bending behavior was uniform with respect to grain direction.

Springback information taken from 1-inch wide specimens is shown in figure 6. The springback increases with bend angle and radius, and is greater in the thinner gage. Again, results were uniform relative to grain direction.

Circumferential strain after springback, as a function of bend angle and radius, was measured on the OD of 6-inch wide bends using an etched grid of 0.25-inch diameter circles. Figure 7 shows that the peak strain becomes nearly constant at bend angles over 90 degrees and the tighter radii had higher strains. The similarity of the curves for 2.0t and 2.4t is compatible with the similar orange peel appearance results noted earlier.

Brake-formed Ti-15-3 Z and L sections in a free state were aged at 940°F for 12 hours (optimum age determined in task 3) to measure aging effect on dimensional stability of the bends. This information is useful in predicting the need for forming compensations or heat-treat fixturing. As shown in table 8, angular movement was only 2 degrees or less, and in most cases the bend angle decreased.

Room-temperature and warm-bending studies were conducted on the 0.065-inch gage Beta-C. Room temperature tests were conducted to determine minimum bend radius and springback for (L) and (T) bends. Results of 45-, 90-, and 135-degree bends using 6-inch wide specimens are summarized in table 9. Visual examination at 20X was very difficult due to the rough surface texture, therefore, bend quality was further evaluated by penetrant inspection and metallographic examination.

Selected cross-sections in the bend area are shown in figures 8 and 9. These photomicrographs illustrate the difficulty in judging bend quality due to the poor as-received surface condition. Minimum bend radius appears to be 4t for (T) bends and 6t for (L) bends. These results generally confirm those reported by RMI (table 3). They are considered further evidence of the marginal ductility of this lot of Beta-C sheet, especially in the transverse grain direction (L bends). Springback increased with bend angle and radius as expected.

Warm bending was done at 350°F and 420°F using heated dies to examine the effect on bend radius and springback. Results of (L) and (T) 90-degree bends using 6-inch wide specimens are give in table 10. Cross-sections of warm bends to verify bend quality are also shown in figures 8 and 9. Acceptable bend radius was effectively decreased from 4t to 2t for (T) bends, and from 6t to 4t for (L) bends.

Stretch Forming

For the stretch-forming experiment, 36-inch long, 0.080-inch gage Ti-15-3 brake formed right angle sections were formed into heel-out angles as depicted in figure 10, on a 60-ton Hufford press fitted with numerical control. Section

height (H) was varied to approach splitting and buckling limits. Only the three runs presented in table 11 were considered satisfactory due to equipment problems. The 28 percent maximum stretch is considered excellent.

Hydroforming

Hydroforming of 0.040-and 0.080-inch gage Ti-15-3 was evaluated by forming stretch and shrink flanges on each test blank to the test configuration of figure 11, and adjusting the flange height to vary the severity of forming strains. Form tooling is shown in figure 12.

The primary hydroforming experiments were conducted in a production Verson Wheelan press, using a maximum bladder pressure of 6000 psi which is the limit normally permitted on this production equipment. The rubber blanket had a Type-D Shore hardness of 45. Effect of a higher forming pressure was assessed in a 1000-ton HPM Hydraulic Press (Guerin trapped-rubber process), using a pressure of 7800 psi and a rubber with Type-A Shore hardness of 80.

Test results are presented in table 12, and examples of acceptable and unacceptable hydroformed test parts are shown in figure 13. The 0.080-inch gage was more formable than the 0.040-inch gage achieving a maximum net stretch of 20 percent compared with 12 percent for the 0.040-inch sheet. The prescribed shrink was not obtained because of a tooling error. Slightly better forming quality was obtained using the Guerin process, indicating that higher forming pressures are beneficial. Although forming limits were not determined, these limited tests have demonstrated the adequate stretch flange formability of Ti-15-3 sheet.

Comparison With Other Alloys

Table 13 gives a summary of the brake bend, stretchform, and hydroform characteristics observed for Ti-15-3 sheet. In each case, they compare favorably with the design limits of A40 grade commercially pure titanium and Ti-6Al-4V.

TABLE 8. - EFFECT OF AGING ON BEND ANGLE OF 0.080 IN.
T1-15-3 BRAKE FORMED PARTS

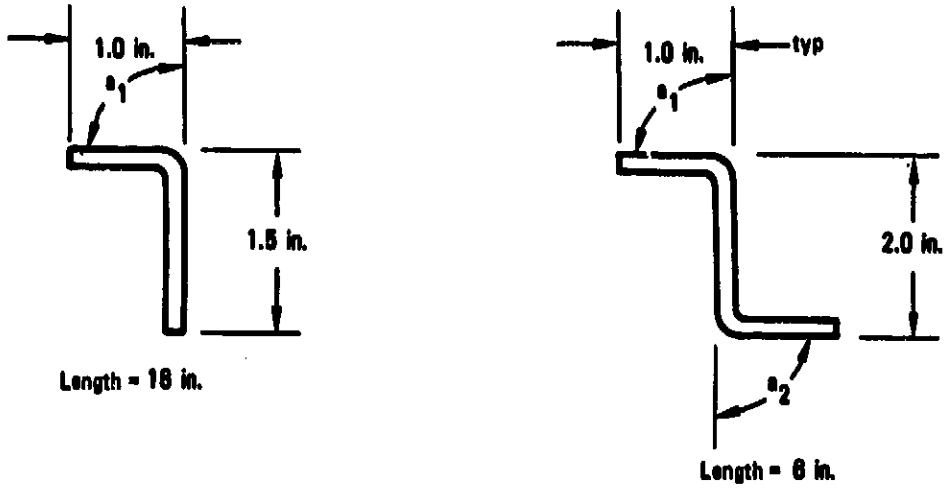

Bend Angle "a" (Deg.)	Punch Radius	Specimen Config.	Bend Axis	Angle Change After Aging (Deg.)**			
				End 1*		End 2*	
				θ_1	θ_2	θ_1	θ_2
45	2t	Z	L	+0.8	+1.2	+1.2	+1.2
90	2t	Z	L	-0.8	-1.3	-0.9	-1.2
90	2t	Z	T	-1.4	+1.1	-0.8	0
90	2.3t	Z	L	-1.2	-1.4	-1.2	-2.1
90	2.3t	L	L	+0.1	-	-0.2	-
90	2.7t	Z	L	+0.7	-1.2	+1.7	-0.5
135	2t	Z	L	+2.0	+0.5	-0.4	-0.9

* Angle measured 1 in. from each end.
** Aging Treatment: 940 °F for 12 hours.

TABLE 9. - ROOM TEMPERATURE BRAKE BENDING OF 0.065 IN. BETA-C SHEET

Bend Axis Dir	Bend Radius	Avg. Free Bend Angle (Deg.)	Avg. Spring-Back (Deg.)	Visual Examination at 20X	Flourescent Penetrant Inspection	Metallographic Examination
L	6.0 t	40	17	Acceptable	No Indications	–
		87	30	Acceptable	No Indications	Acceptable (Figure 9b)
		121	28	Acceptable	No Indications	–
	5.0 t	39	7	Apparent Metal Separation(2)	No Indications	–
		45	11	Apparent Metal Separation(2)	No Indications	–
		94	23	Apparent Metal Separation(2)	No Indications	Minor Separations (Figure 9c)
		132	24	Apparent Metal Separation(2)	No Indications	–
	4.0 t	90	15	Apparent Metal Separation(2)	Two indications on one of the bends.	–
	3.5 t	(1)	–	–	–	–
T	4.0 t	43	13	Acceptable	No Indications	–
		90	16	Acceptable	No Indications	Acceptable (Figure 9b)
		120	33	Acceptable	No Indications	–
	3.5 t	90	–	Apparent Metal Separation(2)	No Indications	Acceptable (Figure 9c)

NOTES:

(1) Specimen fractured at bend before reaching 90 degrees.

(2) In most cases what appeared visually as metal separation did not retain penetrant.

TABLE 10. - WARM BRAKE BENDING OF 0.065 IN. BETA-C SHEET

Bend Axis Dir	Bend Radius	Forming Temperature (°F)	Average Free Bend Angle (Degrees)	Average Spring-Back (Degrees)	Visual Examination at 15X	Metallographic Examination
L	5.0t	350	90	15	Acceptable	Acceptable (Figure 9d)
	4.0t	350	92	14	Apparent Separations	Acceptable (Figure 9e)
	3.0t	350	88	12	Apparent Crack	Unacceptable Separation (Figure 9f)
	2.0t	350	90	6	Cracked	Cracked (Figure 9g)
	2.0t	420	90	7	Cracked	Cracked (Figure 9h)
T	3.0t	350	89	11	Acceptable	Acceptable (Figure 8d)
	2.0t	350	87	8	Acceptable	–
	2.0t	420	90	8	Acceptable	Acceptable (Figure 8e)

TABLE 11. - EVALUATION OF STRETCH FORMED SPECIMENS

Specimen No.	Section Height (in.)	Stretch Direction	Percentage Stretch	Strain Rate, Min^{-1}	Remarks
CL Z5	1.5	Longitudinal	8	0.013	Good part*
CT Z1	2.0	Transverse	14	0.023	Good part*
CL Z1	3.5	Longitudinal	28	0.046	Good part except that horizontal flange had slight wave and vertical flange drew into die block due to die block separation.*

*Slight local distortion of vertical flange attributed to inadequate die pressure.

TABLE 12. - Ti-15-3 HYDROFORMING RESULTS

Thickness, in.	Flange Design (1) Stretch Flange Height (in.)	Flange Design (1) Shrink Flange Height (in.)	Hydro-Forming Process (2)	Specimen No.	Grain Direction	Flange Height (in.) (3) Stretch Center (B1)	Flange Height (in.) (3) Stretch Ends ((A1+C1)/2)	Flange Height (in.) (3) Shrink Center (B2)	Flange Height (in.) (3) Shrink Ends ((A2+C2)/2)	Bend Angle (Deg.) (3) Stretch Center (b1)	Bend Angle (Deg.) (3) Stretch Ends ((a1+c1)/2)	Bend Angle (Deg.) (3) Shrink Center (b2)	Bend Angle (Deg.) (3) Shrink Ends ((a2+c2)/2)	Strain on Stretch Flange After Forming, Percent (4) ϵ_C	Strain on Stretch Flange After Forming, Percent (4) ϵ_N	Remarks
0.080	2.0	2.0	V(6)	CHL2	L	1.9	2.2	1.9	1.9	90	92	78	79	+16 (+28)	-6	Acceptable quality with minor irregularities in stretch flange.
				CHT2	T	2.1	2.2	1.9	1.9	88	92	79	80	+18 (+28)	-8	Same as CHL2.
			G(7.8)	CHT6	T	2.0	2.2	1.9	1.9	90	97	77	79	+28 (+28)	-8	Acceptable Quality.
	1.5	1.5	V(6)	CHL6	L	1.7	1.9	1.8	1.5	88	94	78	79	+16 (+28)	-6	Same as CHL2.
				CHT3	T	1.7	1.9	1.8	1.5	88	94	78	79	+12 (+28)	-6	Same as ChL2.
			G(7.8)	CHT4	T	1.7	1.9	1.8	1.8	90	97	77	78	+16 (+28)	-8	Acceptable Quality.
0.040	2.0	2.0	V(5)	CHL2	T	1.8	2.3	1.9	1.9	98	94	80	73	8 (+28)	0	Rejectable quality due to severe humps along bend radius of stretch flange.
			G(7.8)	CHT6	T	2.0	2.2	1.9	1.9	105	94	82	73	+16 (+28)	-4	Rejectable quality due to severe buckling of stretch flange resulting in contour reversal.
	1.75	1.5	V(5)	CHT1	L	1.7	1.9	1.6	1.5	93	70	75	72	+18 (+24)	-4	Rejectable quality due to severe cunning in web between views B-B and C-C and cramming at view B-B. Also contour reversal of stretch flange and excessive distortion of stretch flange.
				CHT5	T	1.8	1.9	1.6	1.5	96	80	77	73	+18 (+24)	-4	Rejectable quality due to buckling in web and stretch flange originating in bend radius.
				CHT3	T	1.7	1.7	1.5	1.5	111	76	71	72	+20 (+24)	-6	Salvageable quality with moderate hand work to remove small web and stretch flange distortions.
			G(7.8)	CHT2	T	1.7	1.9	1.5	1.5	102	79	78	71	+20 (+24)	-8	Same as CHT3.
	1.5	1.0	V(5)	CHT4	T	1.5	1.7	1.1	1.1	90	77	76	73	+12 (+28)	-6	Same as CHT3, except less severe distortions.
	1.25	0.75	V(5)	CHL5	L	1.3	1.4	0.7	0.7	96	77	74	72	+12 (+16)	-5	Acceptable quality with minor work and flange distortion.

NOTES:

(1) Flanges formed to 90 deg, without springback compensation to the bend and contour radii shown in figure 11.

(2) V = Varson-Wheelon Pressure Bladder; G = Guerin Trapped Rubber; ( ) = Forming Pressure in ksi.

(3) Measured at views A-A, B-B and C-C as shown in figure 11.

(4) Measured at detail "Y" of stretch flange as shown in sketch herein. Strains at detail "X" and "Z" locations of stretch flange and at the root locations of shrink flange were "zero" in all cases. Positive (+) and negative (-) values represent tension and compression strains, respectively. Value in parentheses are calculated strains.

(5) See figure 11.

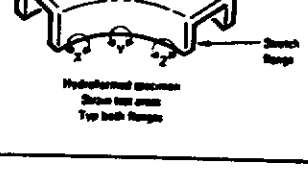

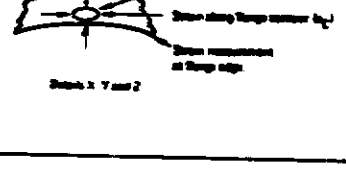

TABLE 13. - ROOM TEMPERATURE FORMABILITY OF TITANIUM ALLOYS

Alloy	Yield Strength (ksi)	Gage (in.)	Min Bend Radius	Stretch Form Limit (%)	Hydroform Limit (%)	
					Stretch	Shrink
Ti-15-3, ANN	110	0.040 0.080	2.4t 2.4t	– 28	12 20	– –
C.P., ANN	40	0.040 0.080	3.0t 3.0t	20 20	12 12	1.0 1.5
Ti-6Al-4V, ANN	120	0.040 0.080	4.7t 5.5t	7 7	8 8	1.0 –

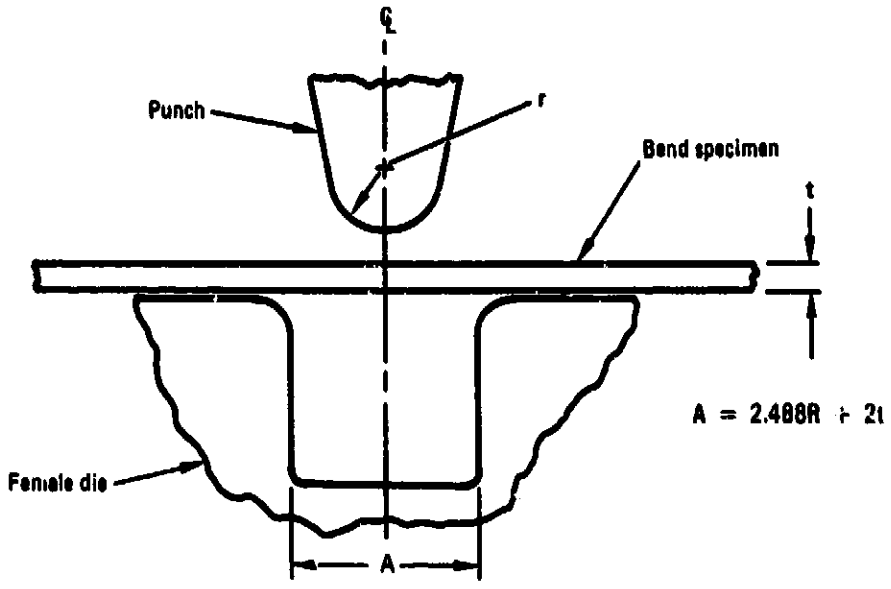

Figure 5. - Brake bending die configuration.

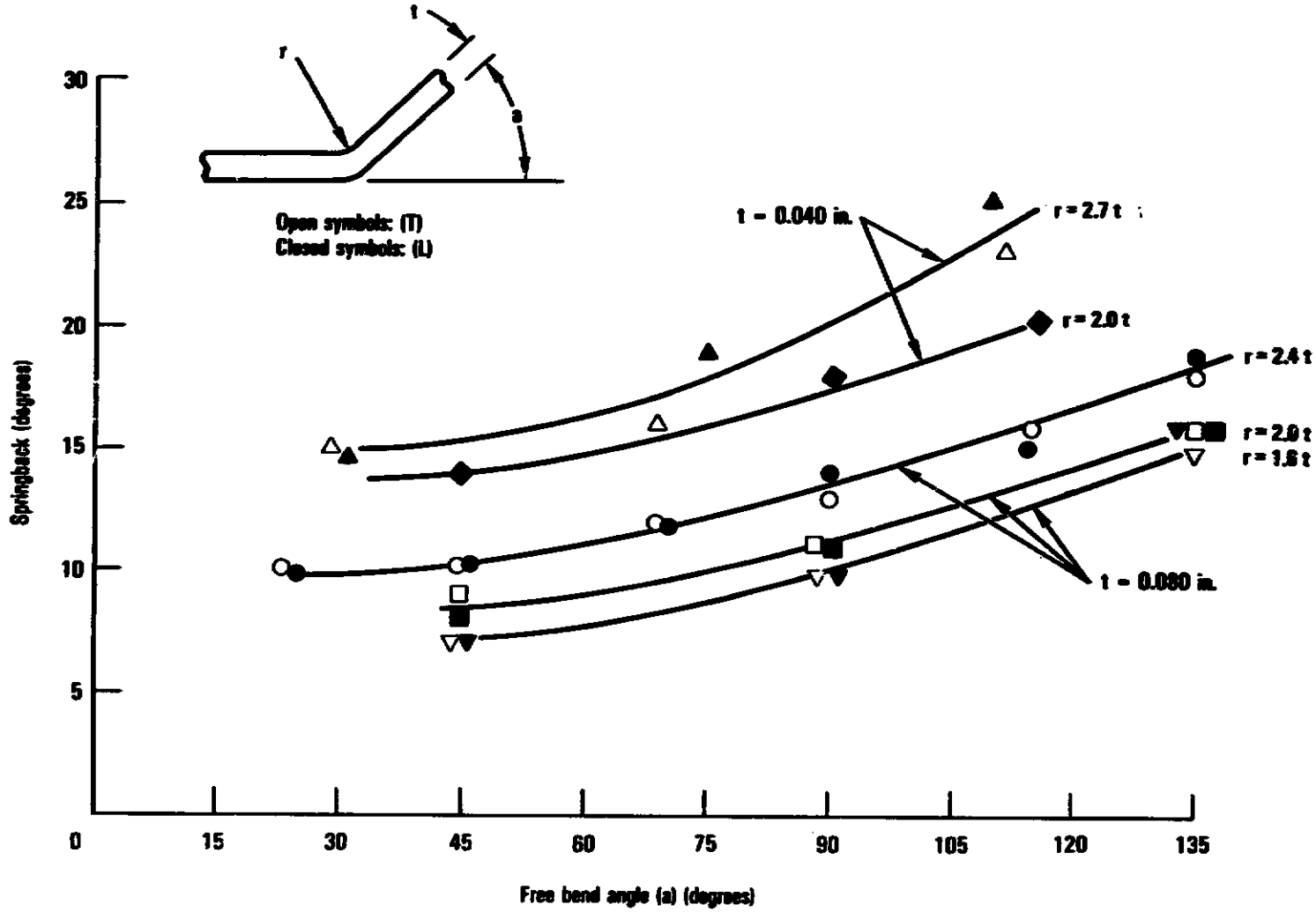

Figure 6. - Room temperature springback of annealed Ti-15-3.

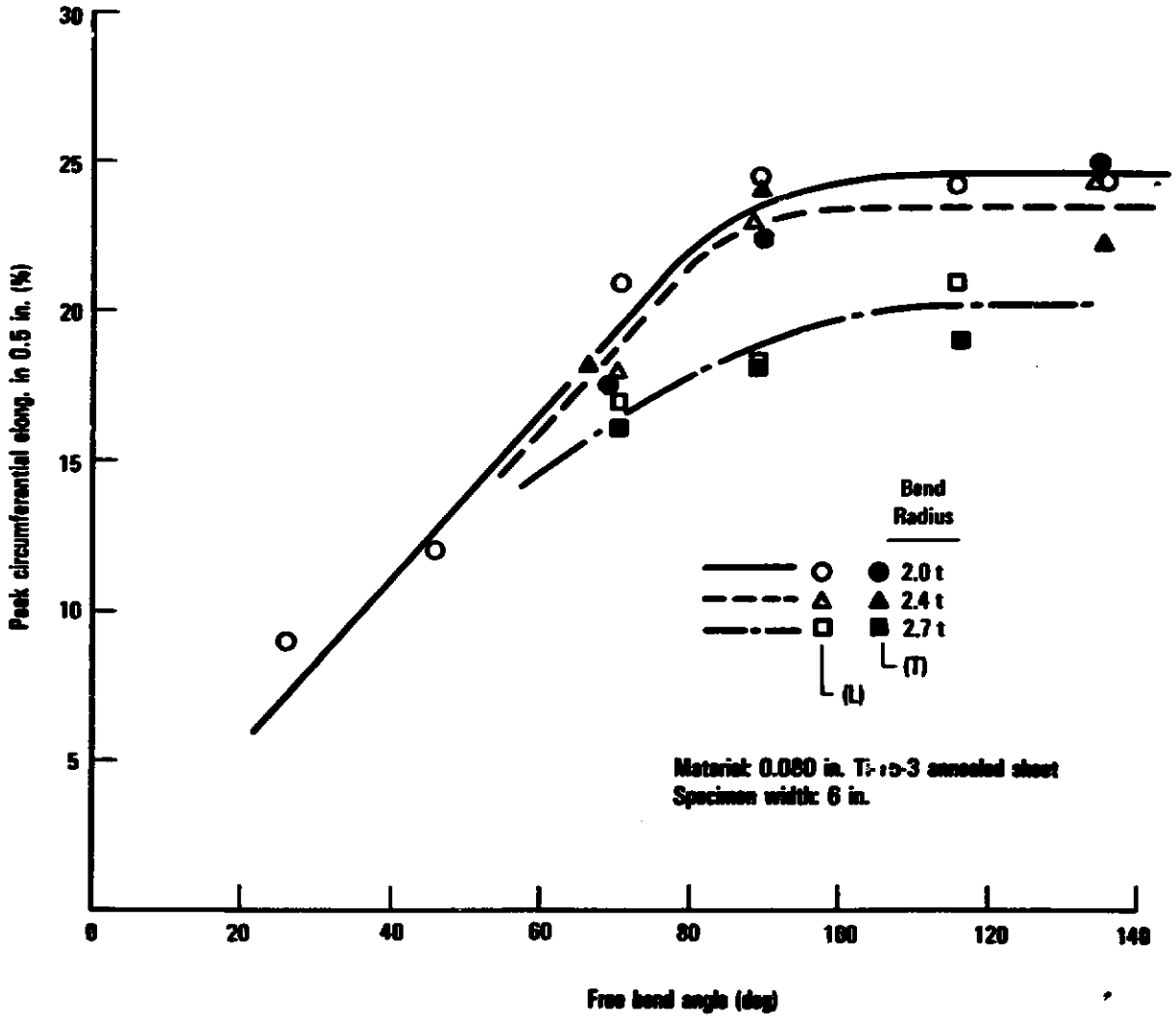

Figure 7. - Influence of bend angle and radius on circumferential strain.

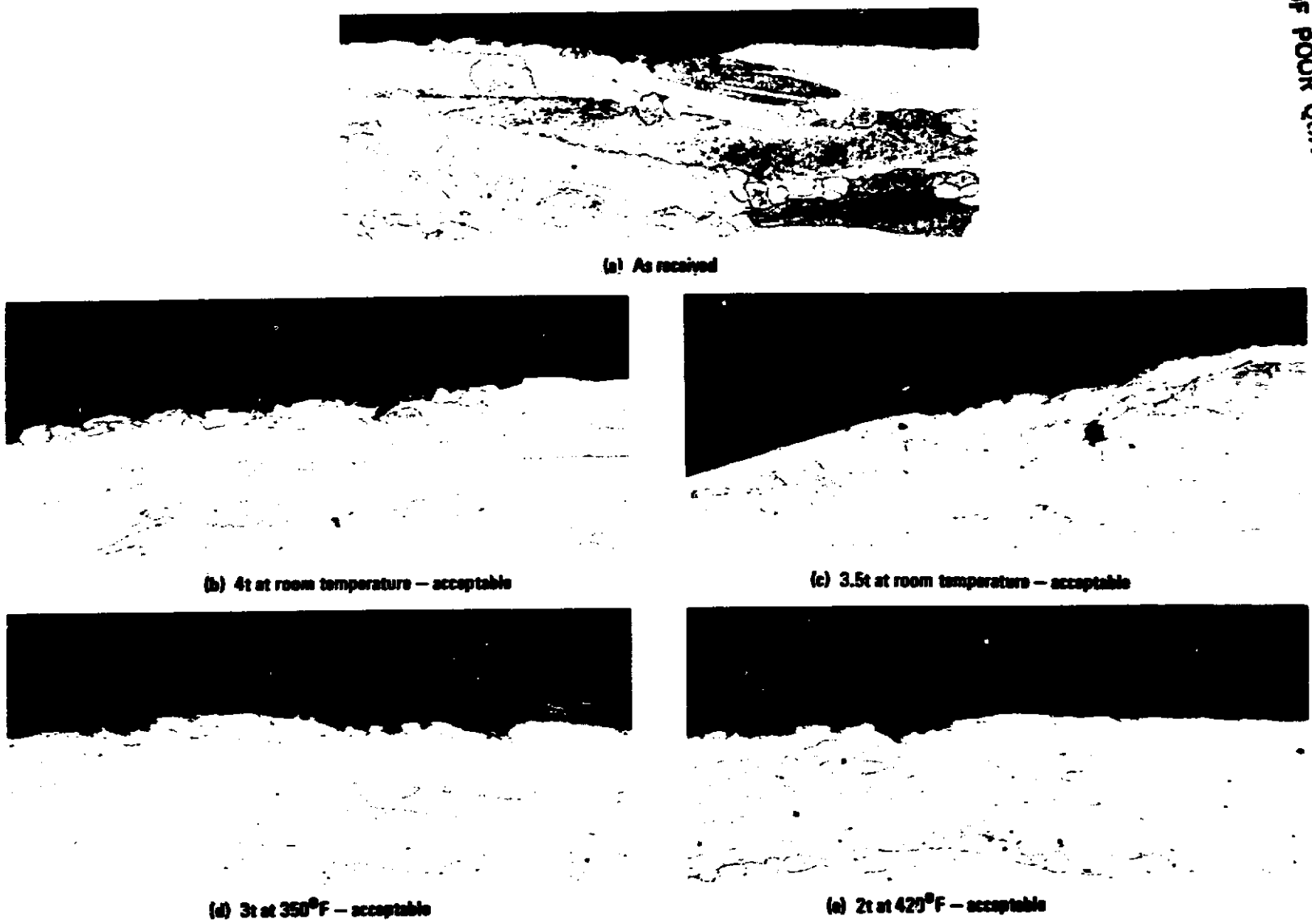

Figure 8. - Cross sections of (T) bends in 0.065 in. Beta-C. Mag. 100X

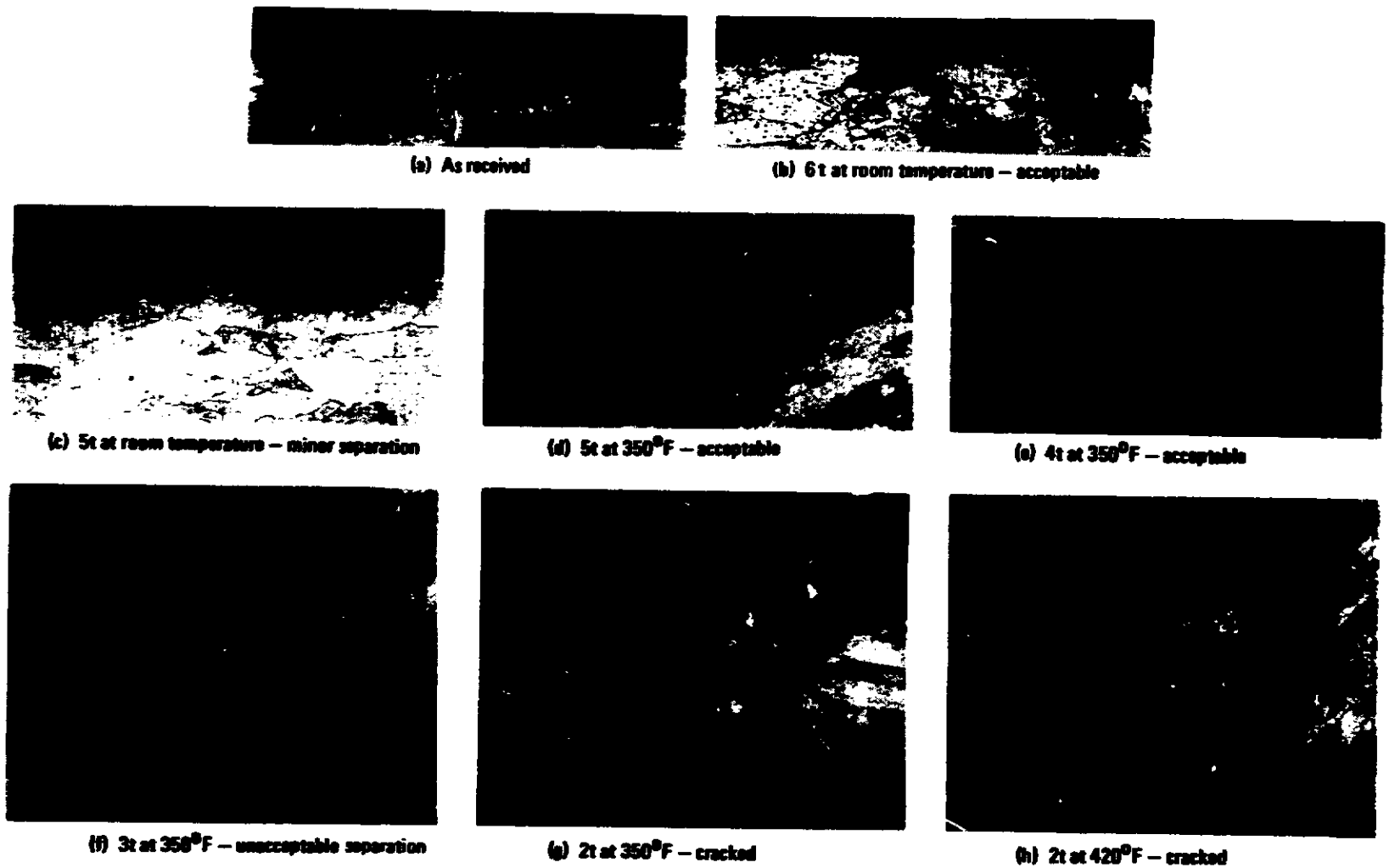

Figure 9. - Cross sections of (L) bends in 0.065 in Beta-C.
Mag. 100X (Reduced 63%)

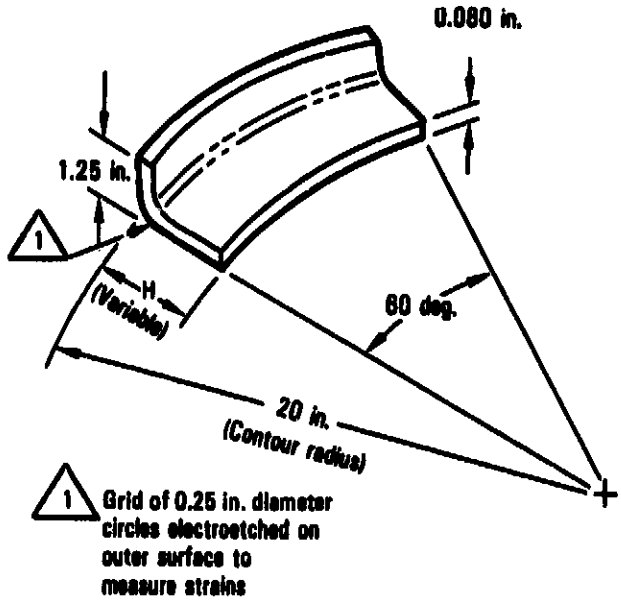

Figure 10. - Stretch formed specimen configuration (heel-out angle).

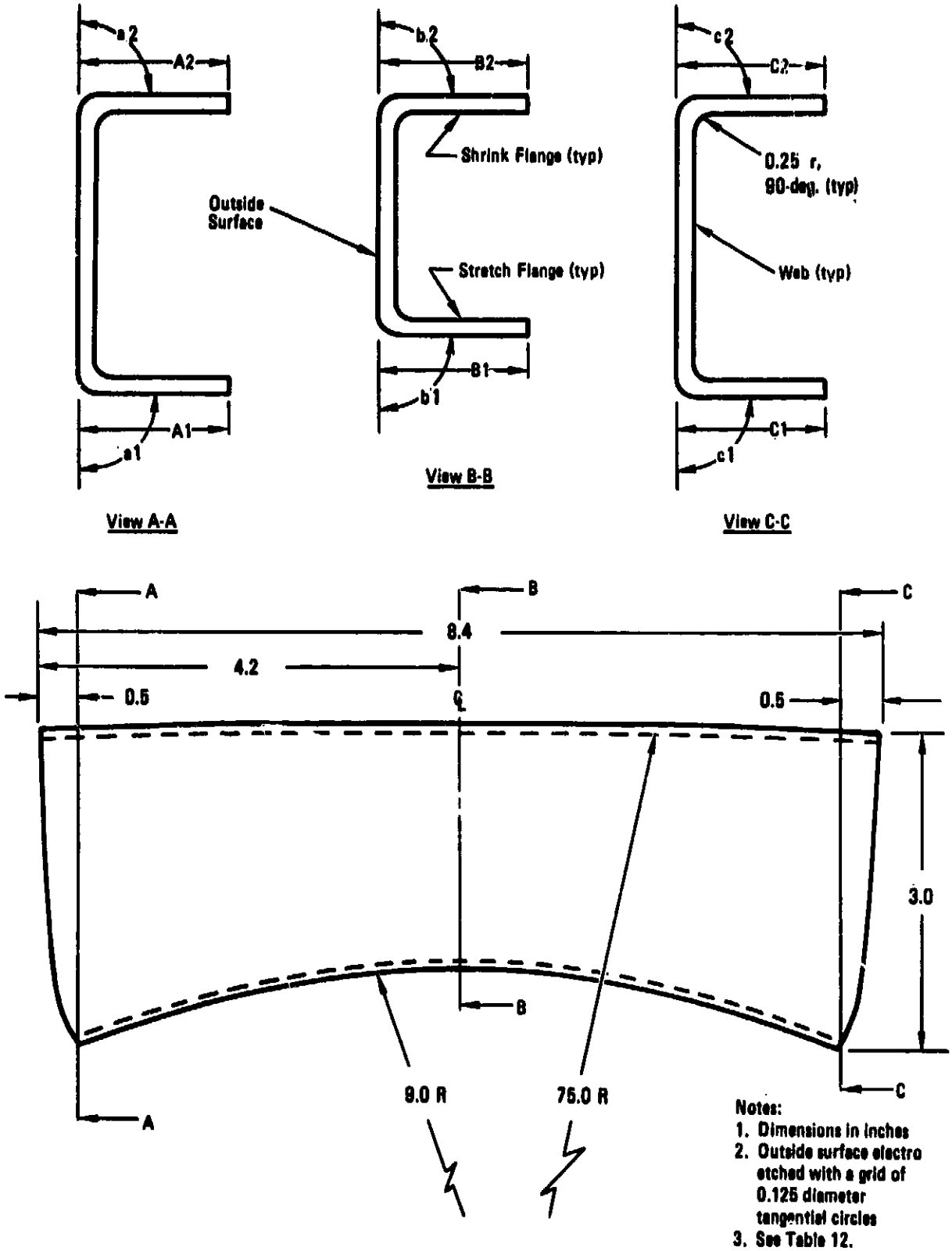

Figure 11. - Hydroforming test configuration illustrating selected locations for formability evaluation.

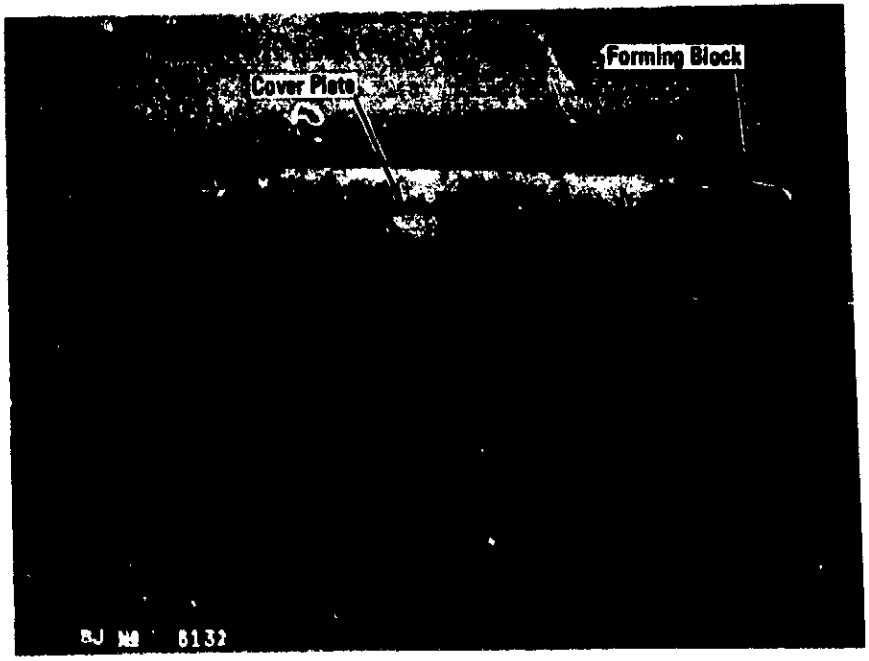

Figure 12. - Hydroform tooling.

(a) 0.080 in. gage, 20 percent stretch – ACCEPTABLE

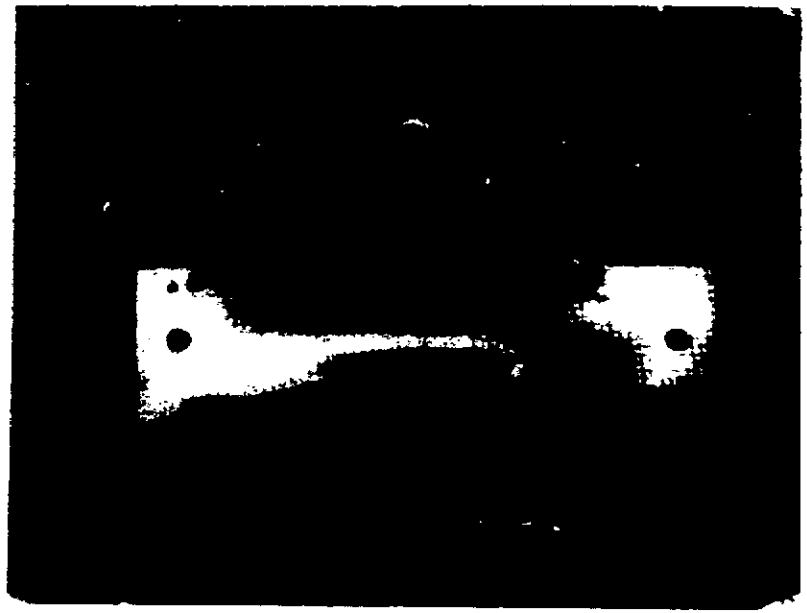

(c) 0.040 in. gage, – UNACCEPTABLE

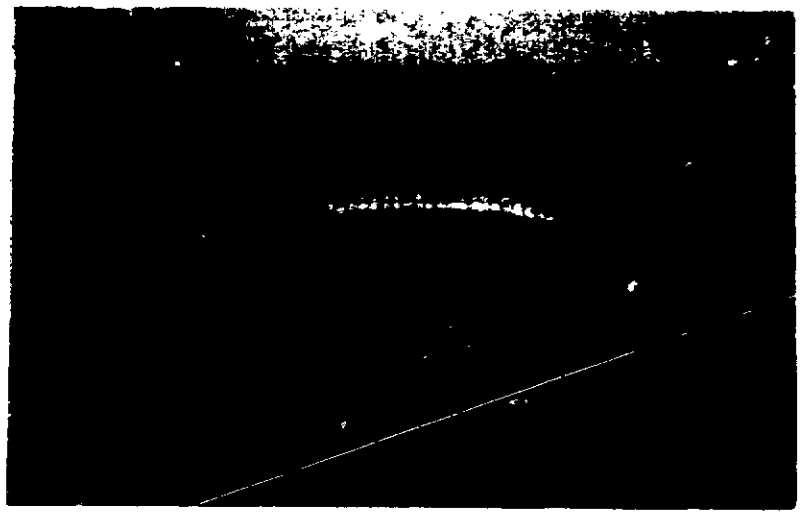

(b) 0.040 in. gage, 12 percent stretch – ACCEPTABLE

Figure 13. - Examples of acceptable and unacceptable hydroformed Ti-15-3 specimens.

TASK 3 - PROCESS OPTIMIZATION

Aging Studies

Ti-15-3 and Beta-C are air-hardening metastable beta compositions that are very formable in the solution-treated (annealed) condition. Precipitation hardening occurs on direct aging from the annealed condition by decomposition of beta to alpha. The heat treatment objective was, therefore, to obtain a combination of cold formability in the annealed condition with subsequent aged properties suitable for the intended Mach 2.7 service. With the program directed toward wing upper surface panels, the mechanical property goals favor high compressive strength and modulus. Heat treat variables were the aging temperature and time.

Ti-15-3. - Task 1 screening tests at tensile strength levels of the order of 200 ksi indicated possibly marginal ductility and toughness with some degradation of notched fatigue strength. Therefore, a lower-strength aging treatment seemed appropriate. Using the task 1 results along with aging data from references 4 and 16 as a guide, the aging cycle selections were 925°F for 8 and 12 hours and 950°F for 12 hours. To represent forming effects, prestrains of nominally 10 percent stretch and 2.5 percent shrink (compression) were included. Prestraining was accomplished on individual specimens in static test machines, then the test coupons were finish machined from the strained section. Evaluations consisted of tension and compression testing at room temperature and 600°F, plus metallurgical examination.

Tensile property data are listed in tables 14 and 15, and plotted in figure 14. Compressive properties are listed in table 16 and plotted in figure 15. All three aging cycles gave suitable property sets at room and 600°F test temperatures. The ultimate tensile strength retained at 600°F was particularly high. Aging 950°F for 12 hours shows slightly more tensile ductility with a corresponding lower strength than the 925°F, 8- and 12-hour treatments. Also the 950°F, 12-hour age shows less difference in strength between nonstrained and prestrained conditions, probably reflecting a fuller degree of aging than the two 925°F aging cycles. Modulus was essentially the same for the three aging cycles, both in tension and in compression.

Examination of the microstructures revealed the desired fine, homogeneous precipitate distribution for each of the aging cycles. Figure 16 shows typical structures for the 925°F, 12-hour age. The prestrained material revealed a worked structure indicative of slip deformation, and the 600°F tensile specimens showed no evident microstructural changes.

From the above evaluation, a 940°F, 12-hour aging cycle was selected for the Ti-15-3 alloy. Test data show that satisfactory mechanical properties can be expected given a normal aging temperature variation of ±10°F.

Beta-C. - Table 17 gives some preliminary 8-hour aging data at 950-1050°F in 25°F increments developed by RMI Company for this lot of material. Inferior transverse ductility found in the solution-treated condition is evident again in the solution-treated and aged condition. From these data, aging temperatures of 1000°F and 1025°F were selected for further evaluation. Five percent minimum elongation in the transverse direction was selected as a target. Room temperature and 600°F tensile properties, r. temperature compressive properties, and microstructures were evaluated.

Tensile property data are listed in tables 18 and 19, and plotted in figure 17. Compression data are given in table 20 and figure 18. Tensile ductility, tensile modulus, and compressive modulus were relatively consistent among the four aging cycles, i.e., 1000°F and 1025°F for 6 and 10 hours. The higher-strength 1000°F age appears more attractive in view of the superior strength retention at the 600°F test temperature.

Microstructures were similar for the four aging treatments. Figure 19 shows a typical well-dispersed precipitate distribution, in this case for the 1000°F, 6-hour aged Beta-C. With reference to the duplex beta grain size (refer also to as-solutioned structure in figure 1), the large elongated grains evidently promoted denser nucleation, indicating a higher residual work content in these large grains. Partial recrystallization could account for the smaller, more equiaxed grains.

Based on the foregoing aging temperature/time evaluations, 1000°F for 8 hours was selected as the aging cycle for the Beta-C. Test results for 6 and 10 hours indicate that 8 hours will produce acceptable strength-ductility levels coupled with heat treat economics of lower temperatures and shorter aging periods.

Forming Limit Diagram (FLD)

This punch-stretch technique for laboratory formability evaluation was developed by Hecker (references 21 and 22), and it has been used by other investigators for evaluating the formability of steel, brass, aluminum, and titanium alloys (references 23 and 24). The FLD may be used to characterize limiting strains under the influence of uniaxial or biaxial straining. In the diagram, major strain is defined as the largest increment of deformation in the formed area and minor strain as the corresponding increment of deformation normal to the major strain.

An FLD was developed for the 0.080-inch Ti-15-3. Steel tooling conforming to the dimensions in figure 20 was used, and the punch loads were applied in a hydraulic tensile test machine. The forming limit curve was generated by using square specimens and increasing lubrication on the positive minor strain side, and by decreasing specimen width using dogbone specimens for the negative minor strain side. Strain measurements were taken from an etched grid pattern of 0.125-inch diameter circles on the test blanks. Figure 21 shows typical Ti-15-3 tested specimens.

The FLD is plotted in figure 22. Little difference was seen between the two punch speeds that were used, and a limit tension strain of about 28 percent is indicated near the uniaxial strain condition ($e_2 = 0$). In figure 23 the FLD boundary zone is compared with some actual forming strains from task 2, and with forming limit curves recently developed by Battelle for various alloys. Reasonable correlation is seen between FLD limit strains and the forming strains for 2t bends and the stretch-formed flange with 3.5 inch flange height. Hydroforming results fell considerably below the FLD limit, and it is conceivable that higher forming pressures would improve the hydroformability of Ti-15-3. Good agreement with Battelle's Ti-15-3 curve is seen, and the formability of Ti-15-3 appears to be comparable to 2024-0 aluminum and much better than annealed Ti-6Al-4V.

TABLE 14. - ROOM TEMPERATURE TENSION TEST RESULTS OF 0.080 IN. Ti-15-3 SHEET, LONGITUDINAL GRAIN

Aged Condition	Specimen No.(2)	(1)Prestrain, Percent (+) Tension (-) Compression	F_{tu} (ksi)	F_{ty} (ksi)	e (%)	E (Msi)
925°F -8h	T3	No Prestrain	180	164	9.5	16.2
925°F -8h	T4	No Prestrain	181	165	10.0	14.1
925°F -12h	T1	No Prestrain	18[illegible]	172	7.5	15.2
925°F -12h	T2	No Prestrain	186	171	9.0	14.6
950°F -12h	T5	No Prestrain	176	161	11.0	14.1
950°F -12h	T6	No Prestrain	175	164	10.0	14.6
925°F -8h	TT3	+9.5	194	179	8.0	15.0
925°F -8h	TT4	+10.0	197	181	8.0	15.4
925°F -12h	TT2	+9.5	196	182	8.0	15.4
950°F -12h	TT5	+10.0	180	170	11.0	14.6
950°F -12h	TT6	+10.0	186	172	10.0	14.6
925°F -8h	TC5	-2.0	176	166	11.0	15.0
925°F -8h	TC6	-2.5	175	165	8.0	15.0
925°F -12h	TC3	-3.0	179	167	12.0	15.4
925°F -12h	TC4	-2.5	179	168	12.0	15.0
950°F -12h	TC7	-2.0	171	161	10.0	15.0
950°F -12h	TC8	-2.0	175	160	13.0	15.0

(1)Strained prior to aging. Nonstrained specimens had 0.500 in. wide gage section; others were 0.250 in.

(2)Specimen Configuration: Figure A1

TABLE 15. - SHORT TIME TENSION TEST RESULTS OF 0.080 IN. Ti-15-3 SHEET AT 600°F, LONGITUDINAL GRAIN

Aged Condition	Specimen No.(2)	(1)Prestrain in Tension, Percent	F_{tu} (ksi)	F_{ty} (ksi)	e (%)	E (Msi)
925°F -8h	T9	No Prestrain	160	138	7.5	12.8
925°F -8h	T10	No Prestrain	159	136	7.0	12.3
925°F -12h	T7	No Prestrain	162	140	7.0	13.2
925°F -12h	T8	No Prestrain	162	142	7.0	12.8
950°F -12h	T11	No Prestrain	163	133	8.0	12.3
950°F -12h	T12	No Prestrain	154	132	8.5	13.1
925°F -8h	TT9	10.5	178	149	10.0	13.4
925°F -8h	TT10	10.0	179	152	8.0	14.4
925°F -12h	TT7	10.0	177	151	9.0	13.1
925°F -12h	TT8	9.5	177	154	9.0	13.6
950°F -12h	TT11	10.0	166	143	10.0	13.3
950°F -12h	TT12	10.0	167	140	9.0	13.8

(1)Strained prior to aging. Nonstrained specimens had 0.500 in. wide gage section; others were 0.250 in.

(2)Specimen Configuration: Figure A1

TABLE 16. - COMPRESSION TEST RESULTS OF 0.080 IN. T1-15-3 SHEET AT ROOM TEMPERATURE AND 600°F, LONGITUDINAL GRAIN

Aged Condition	Specimen No.(3)	Test Temperature	(1)Prestrain in Tension, Percent	F_{cy} (ksi)	E (Msi)
925°F -8h	C1	Room	No Prestrain	174	15.2
925°F -8h	C2	Room	No Prestrain	177	15.2
925°F -12h	C3	Room	No Prestrain	179	15.2
925°F -12h	C4	Room	No Prestrain	178	15.6
950°F -12h	C5	Room	No Prestrain	170	15.2
950°F -12h	C6	Room	No Prestrain	171	15.4
925°F -8h	CT1	Room	10.5	Buckled	15.0
925°F -8h	CT2	Room	10.0	Buckled	15.0
925°F -12h	CT3	Room	10.0	192	15.6
925°F -12h	CT4	Room	10.5	193	15.1
950°F -12h	CT5	Room	11.0	184	15.0
950°F -12h	CT6	Room	11.0	185	15.2
925°F -8h	C7-C8(2)	600°F	No Prestrain	145	15.0
925°F -12h	C9-C10(2)	600°F	No Prestrain	150	15.1
950°F -12h	C11-C12(2)	600°F	No Prestrain	143	15.0
925°F -8h	CT7-CT8(2)	600°F	10.5	162	14.4
925°F -12h	CT9-CT10(2)	600°F	10.0 - 10.5	161	14.8
950°F -12h	CT11-CT12(2)	600°F	10.5	152	14.7

(1)Strained prior to aging.

(2)Paired specimens butted side-to-side in compression fixture. Specimens had to be remachined and tested in this manner since the originally intended fixture was not available.

(3)Specimen Configuration: Figure A2

TABLE 17. - PRELIMINARY AGING RESPONSE OF 0.065 IN. BETA-C SHEET, HEAT NO. 801008 (SOURCE: RMI)

Aging Treatment	Dir	F_{tu} (ksi)	F_{ty} (ksi)	e (%)
950°F–8h – A.C.	L	195.5	171.9	5.5
	L	195.4	178.7	5.0
	T	198.7	178.5	3.5
	T	195.5	177.5	3.5
975°F–8h – A.C.	L	190.8	173.0	6.0
	L	187.8	167.7	6.0
	T	192.0	173.0	3.5
	T	191.1	173.5	4.5
1000°F–8h – A.C.	L	184.3	159.5	7.75
	L	178.7	159.8	7.75
	T	184.9	166.6	4.5
	T	183.4	166.5	4.75
1025°F–8h – A.C.	L	175.0	155.5	8
	L	174.7	155.5	8
	T	173.5	158.5	6
	T	174.2	158.5	6.5
1050°F–8h – A.C.	L	167.7	148.2	8
	L	164.3	144.6	8
	T	167.2	147.9	6.5
	T	167.6	149.5	6.5

TABLE 18. - ROOM TEMPERATURE TENSION TEST RESULTS OF 0.065 IN. BETA-C SHEET

Aged Condition	(1) Dir	F_{tu} (ksi)	F_{ty} (ksi)	e (%)	E_{app} (Msi)
1000°F -6h	L	176	161	8.5	15.3
	L	177	161	8.5	15.4
	avg.	176.5	161	8.5	15.3
	T	173	160	5.0	15.6
	T	174	161	5.5	15.4
	T	175	161	6.0	15.4
	avg.	174	161	5.5	15.5
1000°F -10h	L	181	166	8.0	15.9
	L	183	167	7.5	16.1
	avg.	182	166.5	7.7	16.0
	T	181	168	4.0	16.0
	T	184	170	6.0	15.6
	T	183	171	5.0	15.8
	avg.	183	170	5.0	15.8
1025°F -6h	L	173	158	8.0	15.7
	L	169	154	9.0	15.4
	avg.	171	156	8.5	15.5
	T	167	155	5.5	15.5
	T	173	160	6.0	16.0
	avg.	170	157	5.7	15.7
1025°F -10h	L	172	158	8.5	15.5
	L	172	159	7.5	15.7
	avg.	172	158.5	8.0	15.6
	T	174	161	6.0	15.9
	T	172	160	6.5	15.7
	avg.	173	160.5	6.2	15.8

(1)Specimen Configuration: Figure A1

TABLE 19. - SHORT TIME TENSION TEST RESULTS OF 0.065 IN. BETA-C SHEET AT 600°F

Aged Condition	(1) Dir	F_{tu} (ksi)	F_{ty} (ksi)	e (%)	E_{app} (Msi)
1000°F -8h	L	164	136	7.5	13.7
	L	168	139	9.0	13.5
	avg.	166	137	8.2	13.6
1000°F -10h	L	166	139	6.0	13.6
	L	169	141	7.0	14.5
	avg.	167	140	6.5	14.0
1025°F -8h	L	154	126	9.5	13.5
	L	153	125	9.0	14.0
	avg.	153.5	125.5	9.2	13.7
1025°F -10h	L	157	129	9.0	14.0
	L	158	130	9.5	13.9
	avg.	157.5	129.5	9.2	13.9

(1) Specimen Configuration: Figure A1

TABLE 20. - ROOM TEMPERATURE COMPRESSION TEST RESULTS OF 0.065 IN. BETA-C SHEET

Aged Condition	(1) Dir	F_{cy} (ksi)	E_{app} (Msi)
1000°F -8h	L	164	13.8
	L	161	13.9
	avg.	163	13.8
	T	168	14.5
	T	174	14.4
	avg.	171	14.4
1000°F -10h	L	170	14.0
	L	170	14.2
	avg.	170	14.1
	T	176	14.8
	T	173	14.0
	avg.	174	14.4
1025°F -8h	L	158	14.0
	L	162	14.2
	avg.	160	14.1
	T	169	14.2
	T	167	15.0
	avg.	168	14.6
1025°F -10h	L	161	14.7
	L	159	13.5
	avg.	160	14.1
	T	175	14.7
	T	174	14.7
	avg.	174.5	14.7

(1) Specimen Configuration: Figure A2

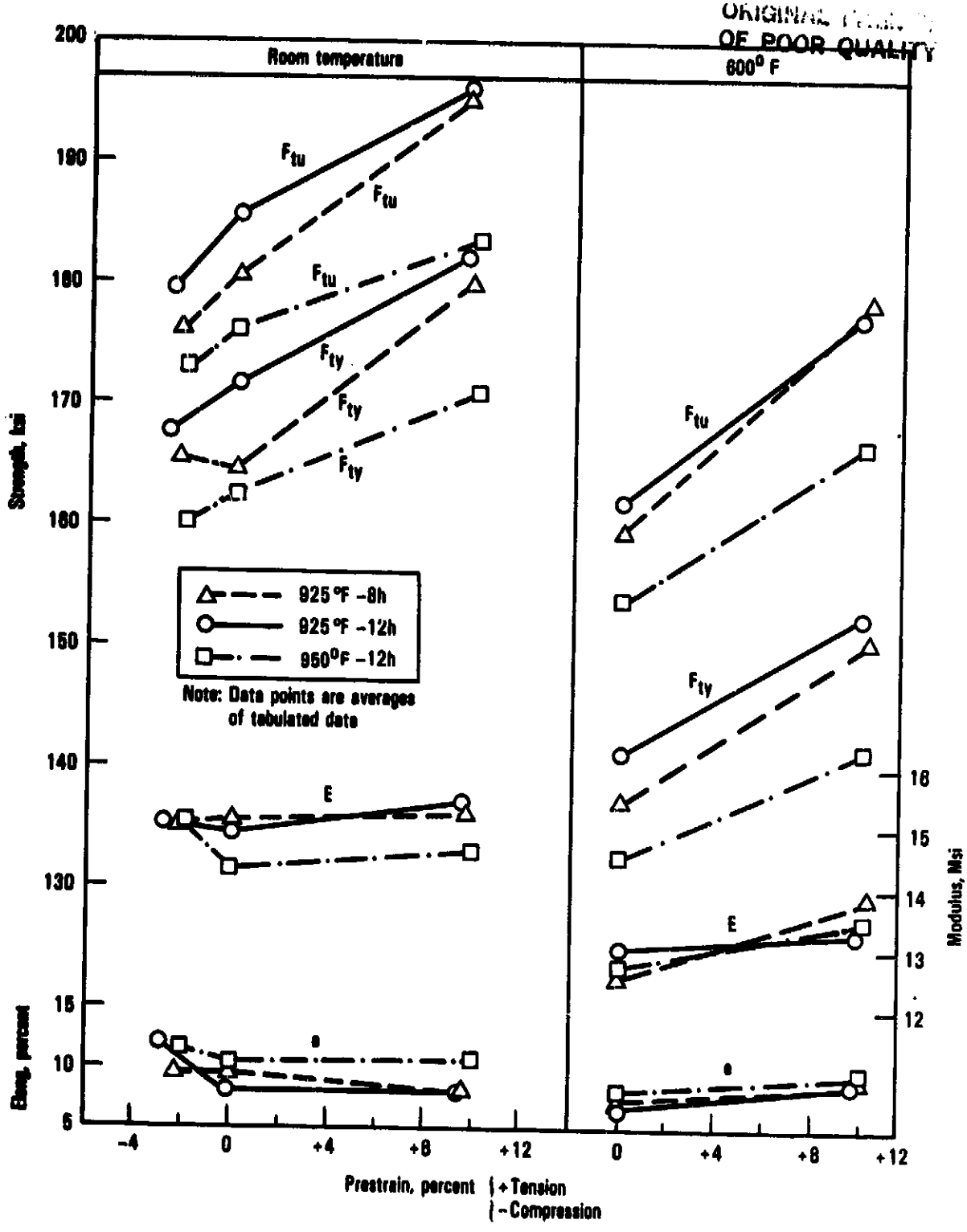

Figure 14. - Longitudinal tensile properties of 0.080 in. Ti-15-3 sheet at room temperature and 600°F for various aging cycles.

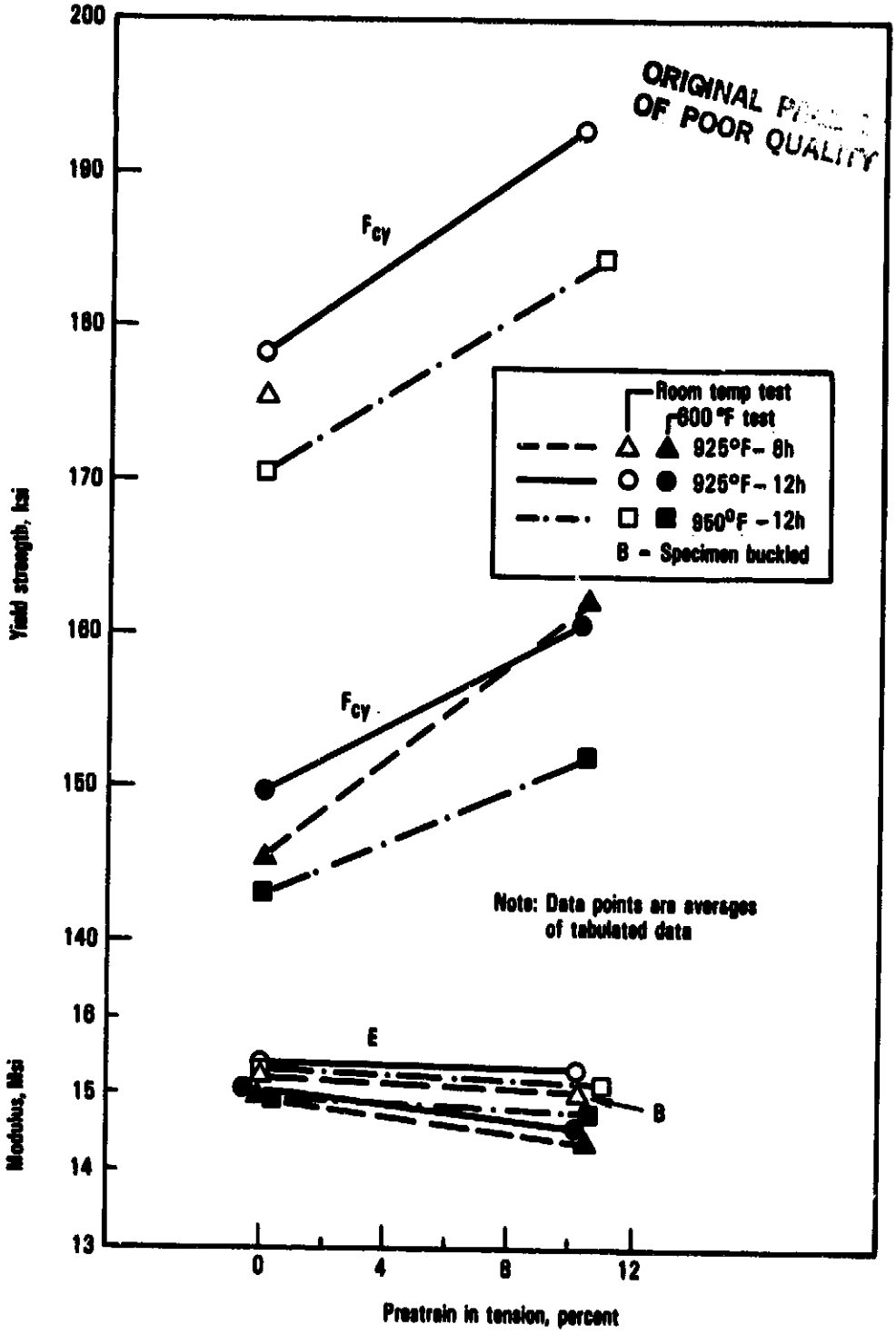

Figure 15. Longitudinal compressive properties of 0.080 in. Ti-15-3 sheet at room temperature and 600°F for various aging cycles.

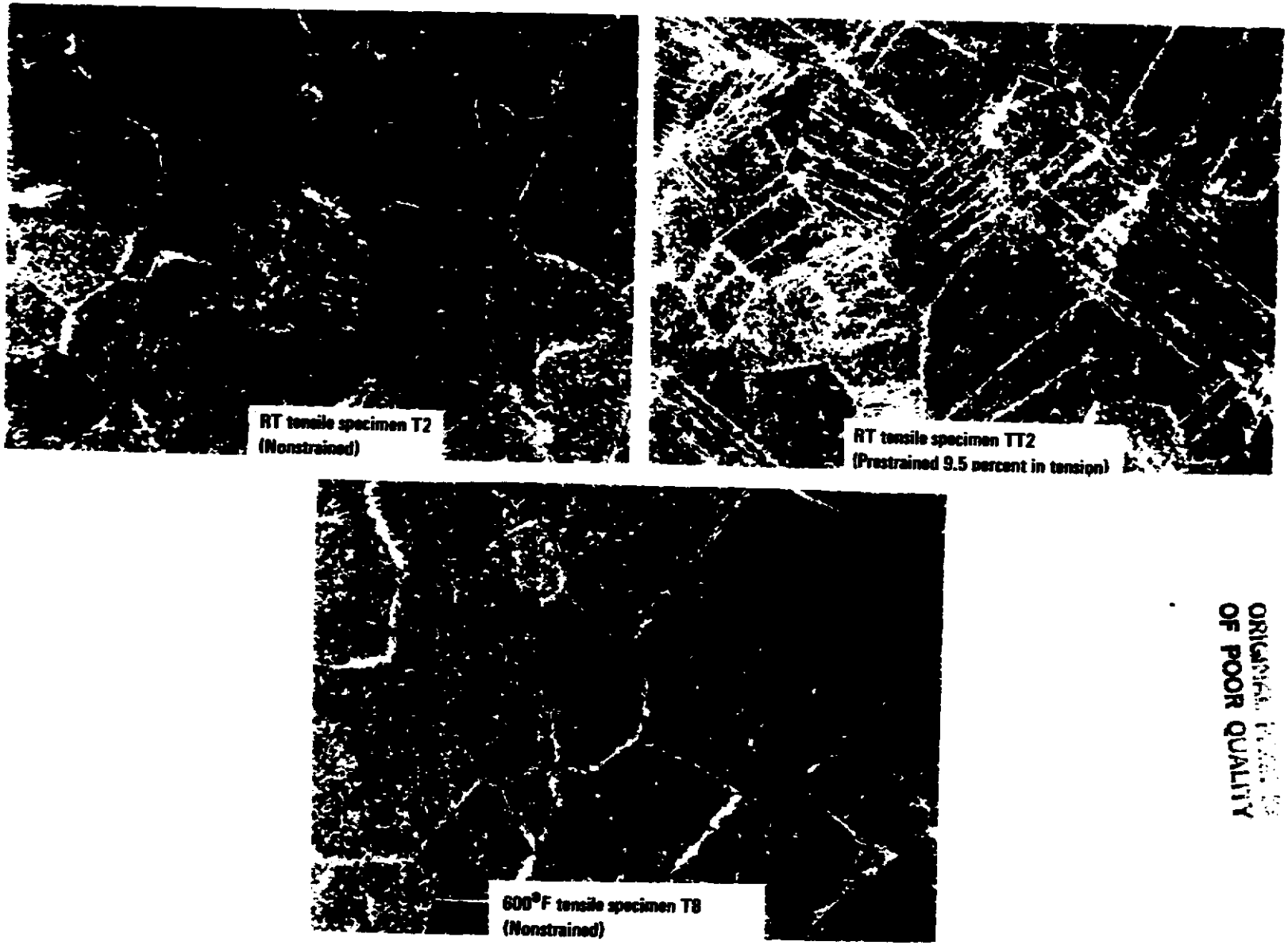

Figure 16. - Microstructure of Ti-15-3 tensile specimens (grip area) aged 925°F - 12 hours. Mag 400X.

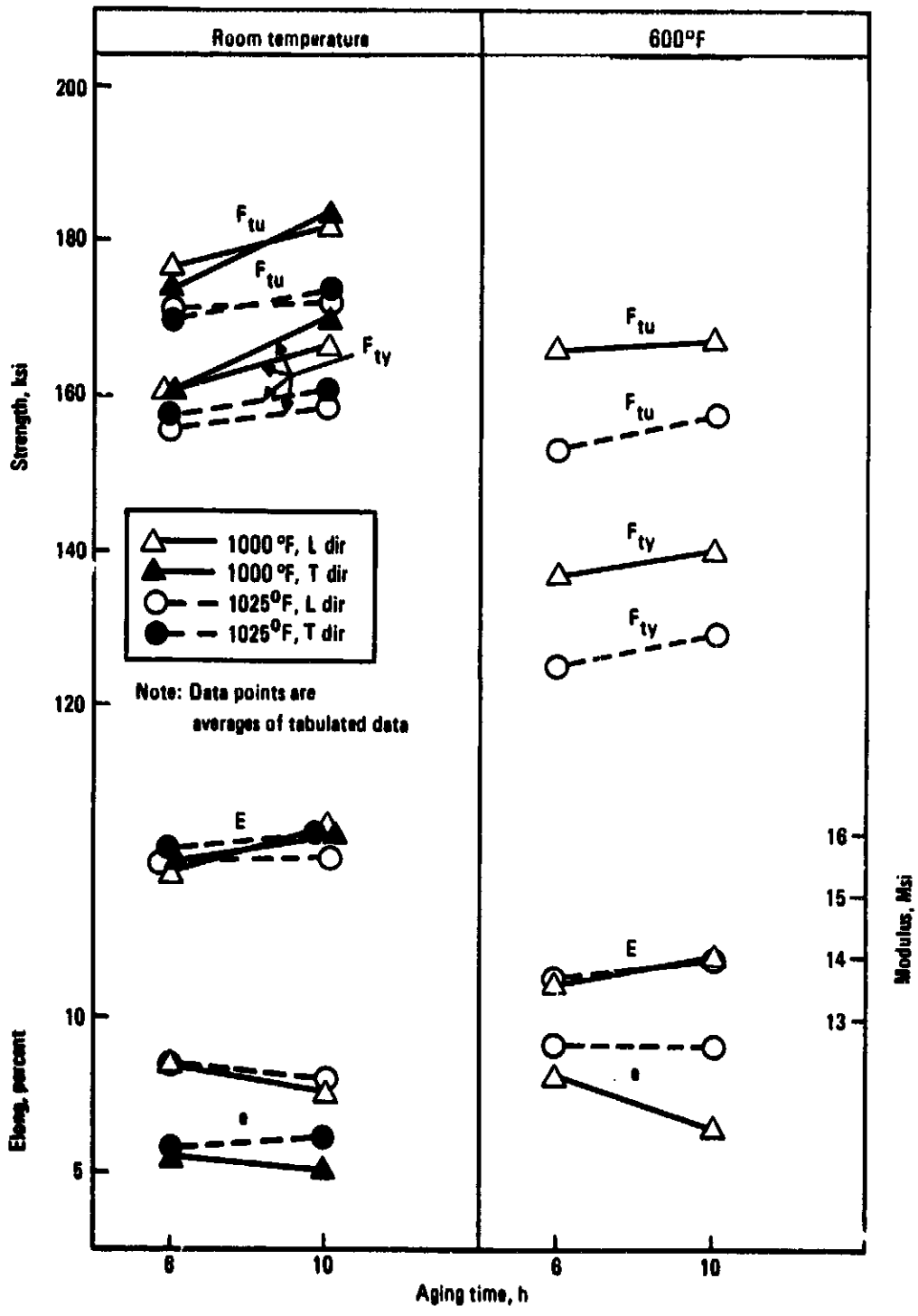

Figure 17. - Tensile properties of 0.065 in. Beta-C sheet at room temperature and 600°F for various aging cycles.

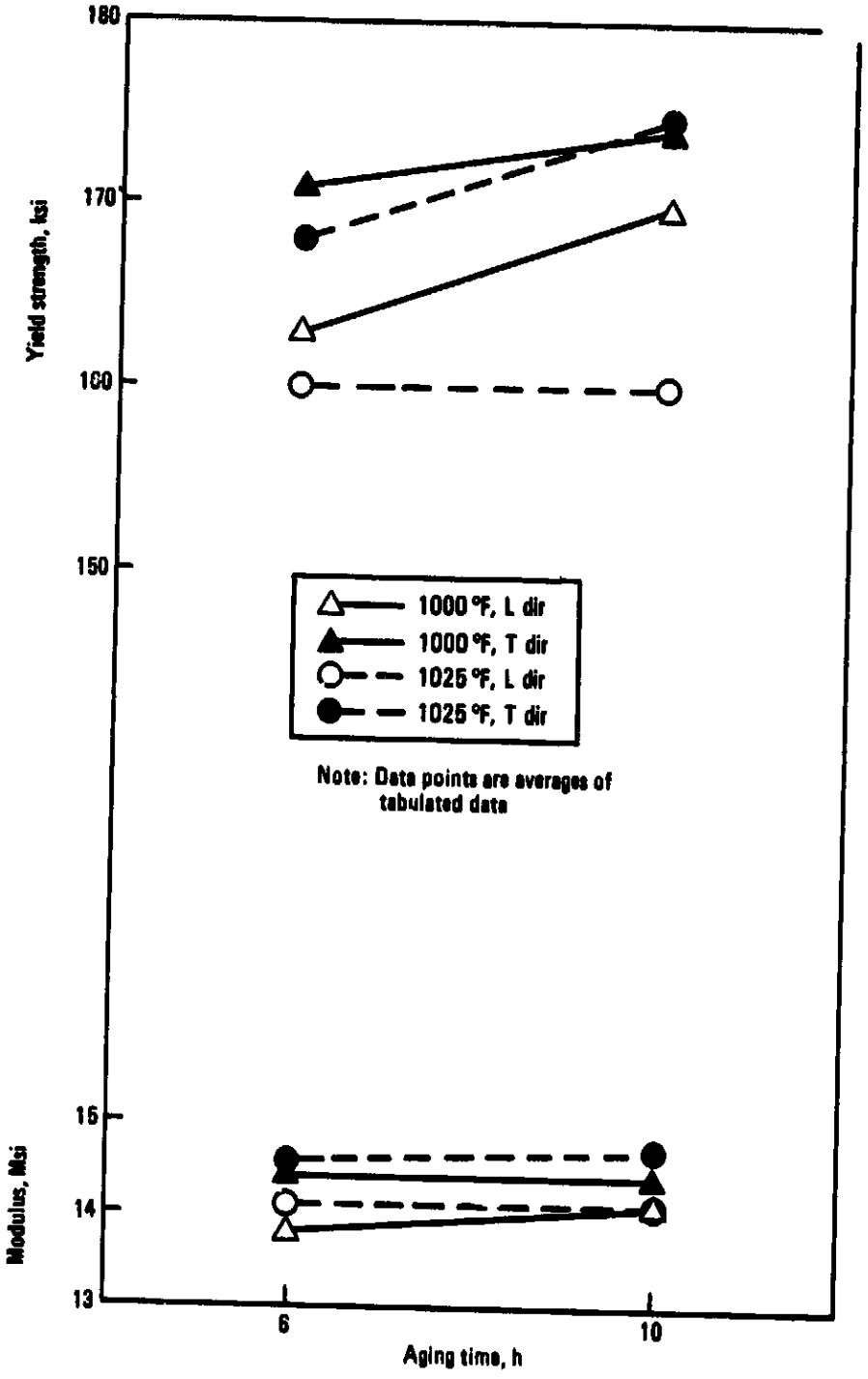

Figure 18. - Room temperature compressive properties of 0.065 in. Beta-C sheet for various aging cycles.

Mag.100X

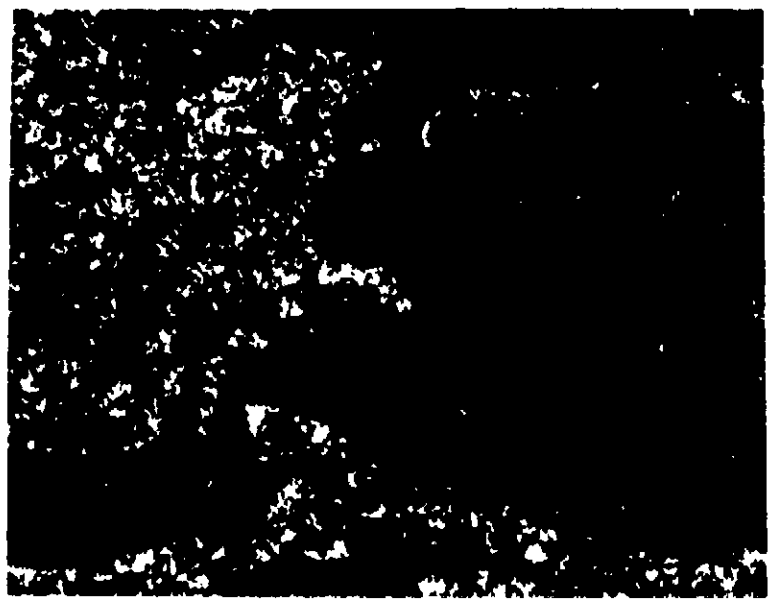

Mag.304X

Figure 19. - Microstructure of 0.065 in. Beta-C aged 1000°F - 6 hours. Longitudinal direction.

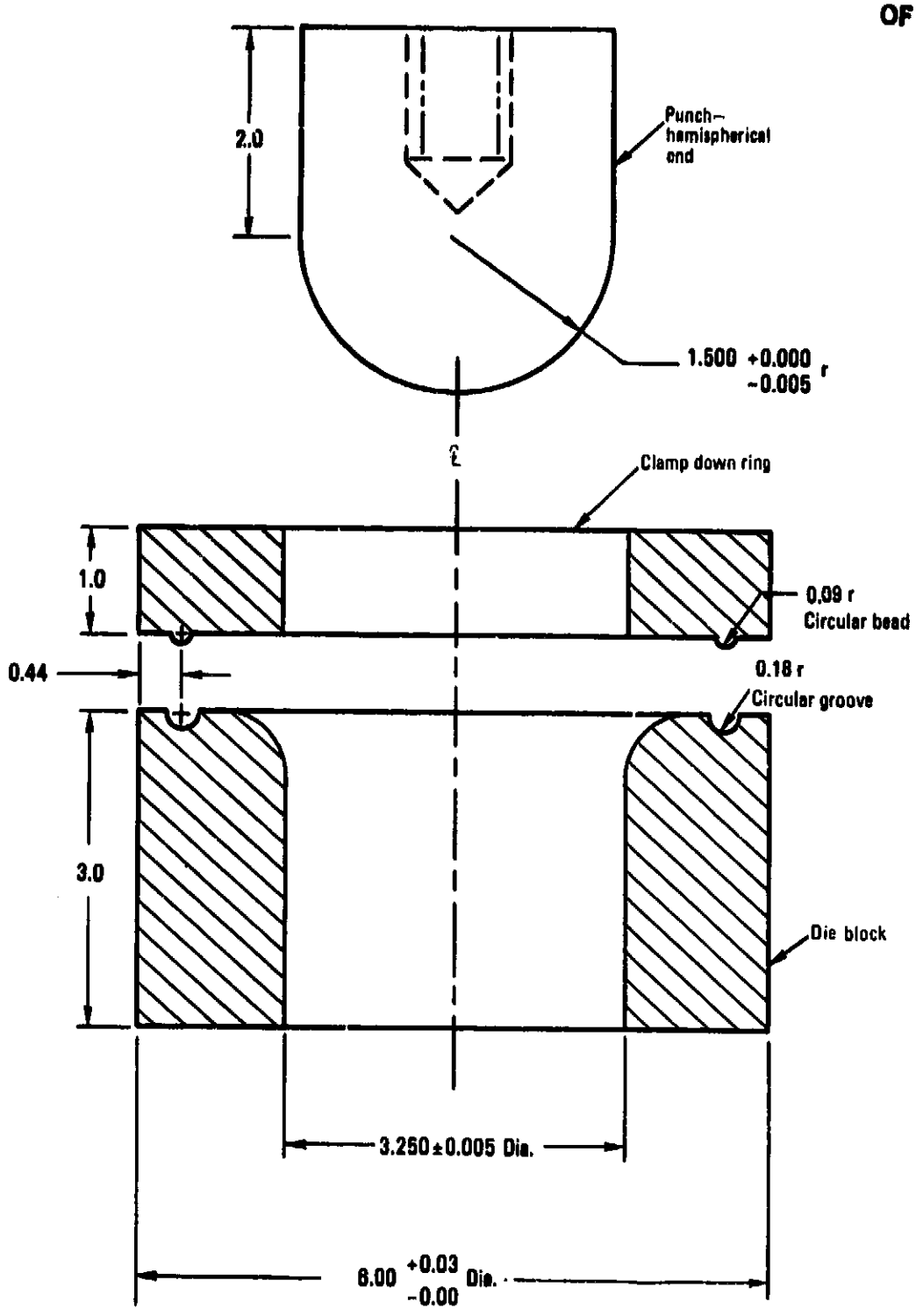

Note: dimensions in inches

Figure 20. - Punch and die set for FLD test.

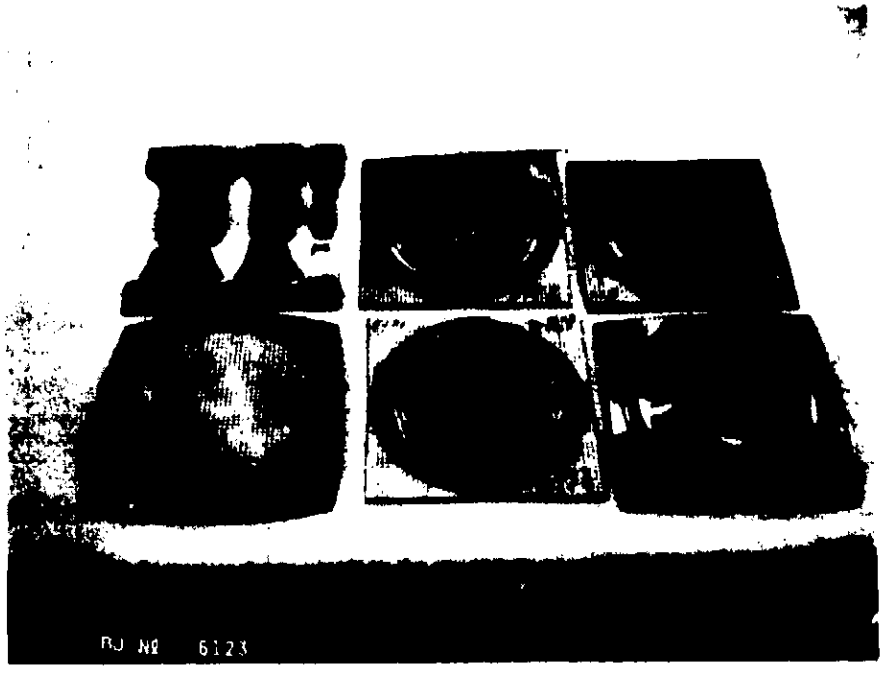

Figure 21. - Ti-15-3 FLD test specimens, 0.080 in. sheet.

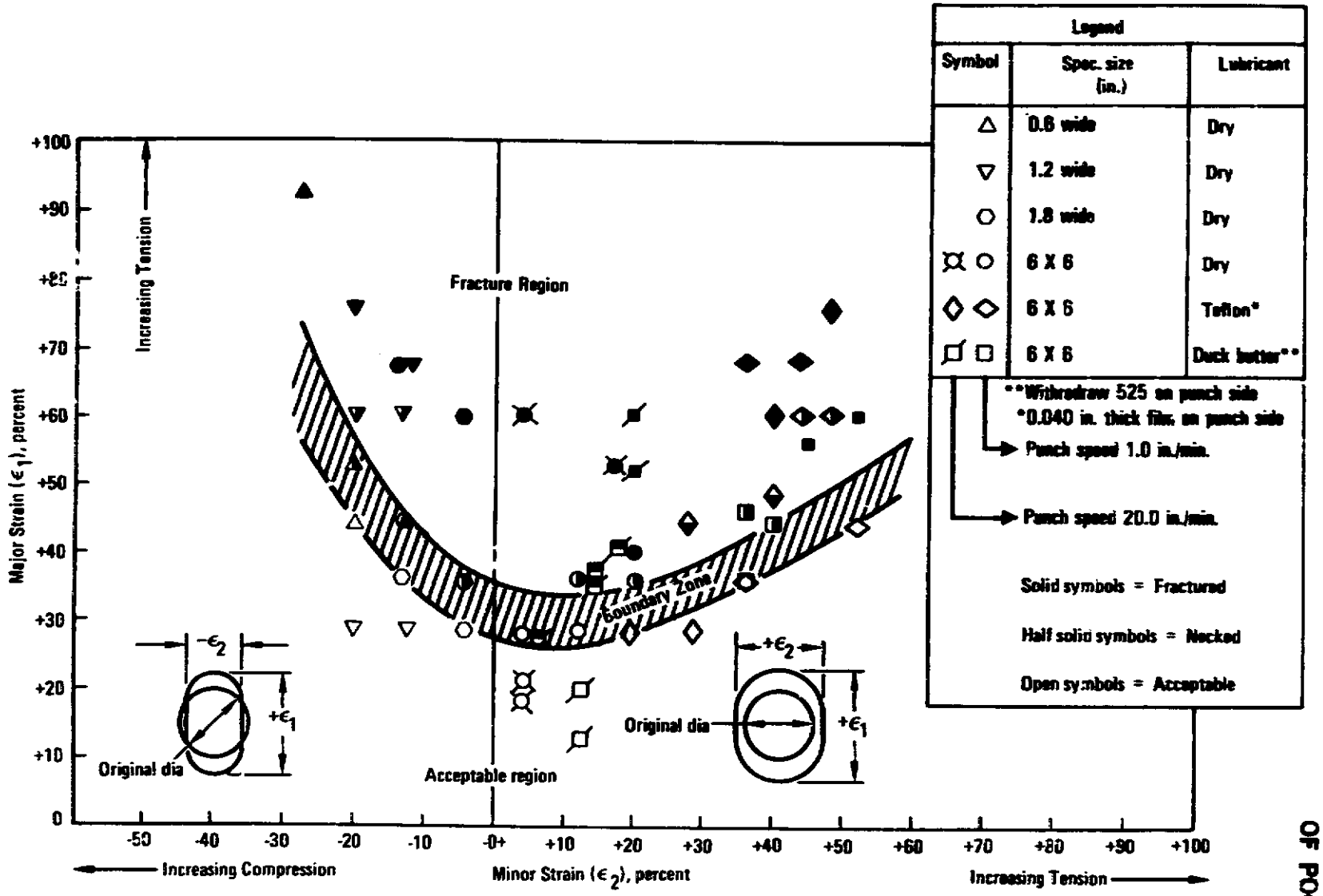

Figure 22. - Forming limit diagram for 0.080 in. Ti-15-3 sheet.

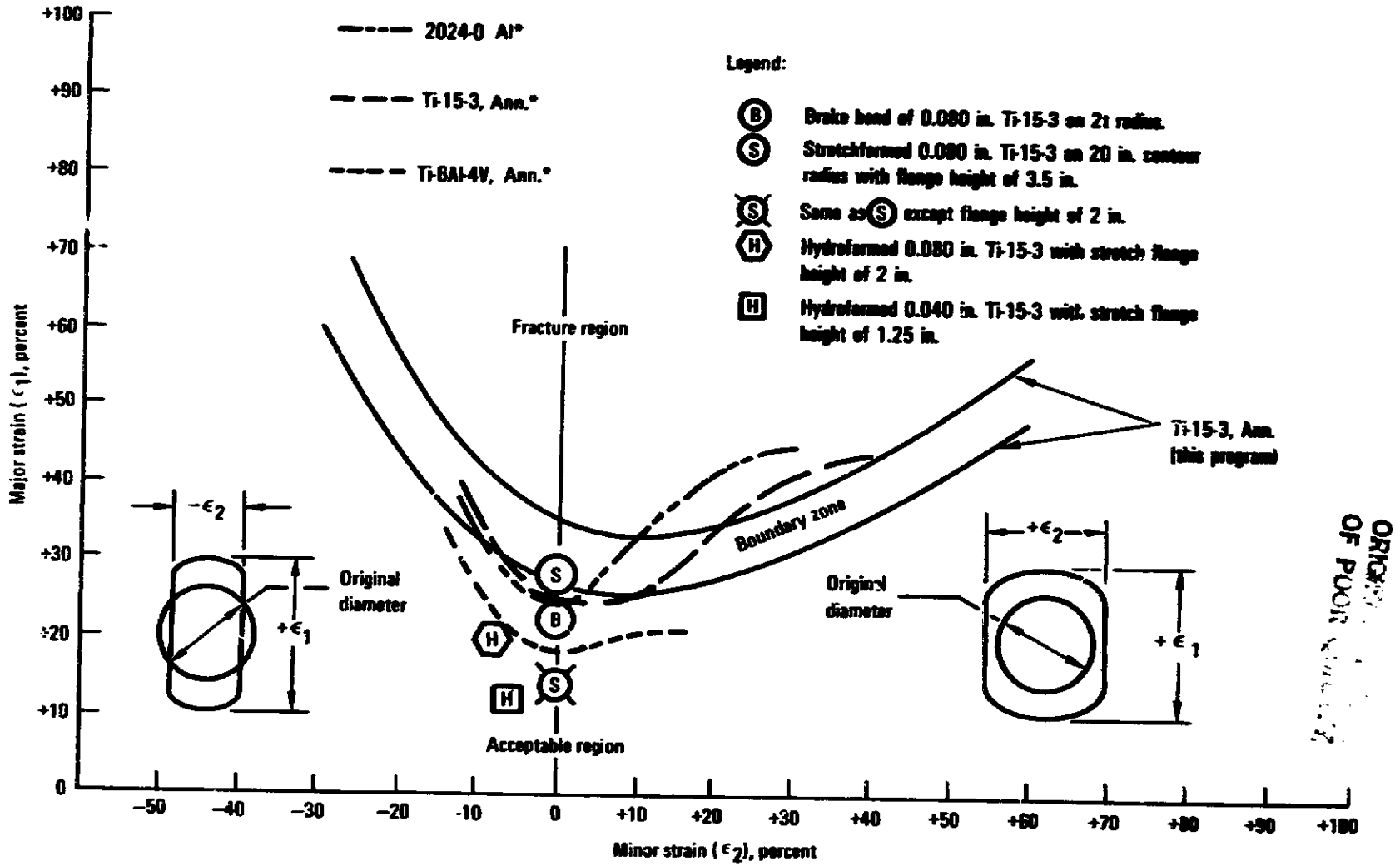

*V. Nagpal and W. W. Sutherland, "Formability Limits for Some Aerospace Sheet Materials," Battelle Columbus Lab., Feb. 1980

Figure 23. - Comparison of FLD strains for 0.080 in. Ti-15-3 with actual forming strains and other alloys.

TASK 4 - MATERIAL CHARACTERIZATION

The effects of forming, joining, and supersonic cruise environment on structural performance of the Ti-15-3 and Beta-C sheet have been studied. To simulate cold forming strains, sheet stock in the form of large dogbone panels having a 1-inch square grid scribed over the reduced area to measure elongation, were stretched in a Universal test machine. Plastic strain levels in the test coupons machined from the test section of the panels ranged from 4 to 9.5 percent in the Ti-15-3 sheet and 3 to 5.5 percent in the Beta-C, over a 4-inch gage length. A typical Ti-15-3 stretched panel may be viewed in figure 24.

Parent, isothermal brazed, simulated braze cycle, and TIG welded specimens from both nonstrained and strained sheet were tested in the aged condition, using the optimum aging cycles developed in task 3, i.e., 940°F-12h for Ti-15-3 and 1000°F-8h for Beta-C. All test specimens were aged in either argon or vacuum atmospheres. Brazing employed 3003Al braze alloy and a peak temperature of 1275°F. The test program included smooth and notched tension, compression, creep, smooth and notched fatigue, brazed lap shear fatigue, fracture toughness (R-curve), and fatigue crack growth (fcg). Test temperatures were -65°F, RT, and 600°F, as stipulated for a Mach 2.7 supersonic cruise vehicle (SCV).

Tension and Compression

Tests were conducted according to standard ASTM procedures. Conventional radiant heating was used for the 600°F specimens as provided by a resistance-wound furnace. The -65°F specimens were cooled within a chamber by vaporizing liquid nitrogen. Strain rate for tensile tests was 0.005 min^{-1} to yield, then about 1 minute to failure. A strain rate of 0.005 min^{-1} was used for -65°F and RT compression tests, and 0.002 min^{-1} for the 600°F tests.

The test results are listed in the following tables, and the average properties are compared graphically in the figures:

RT tension, Ti-15-3	- table 21, figure 25
-65°F tension, Ti-15-3	- table 22, figure 26
600°F tension, Ti-15-3	- table 23, figure 27
RT tension, Beta-C	- table 24, figure 28
-65°F tension, Beta-C	- table 25, figure 29
600°F tension, Beta-C	- table 26, figure 30

RT	compression, Ti-15-3	- table 27, figure 31
-65°F	compression, Ti-15-3	- table 28, figure 32
600°F	compression, Ti-15-3	- table 29, figure 33
RT	compression, Beta-C	- table 30, figure 34
-65°F	compression, Beta-C	- table 31, figure 35
600°F	compression, Beta-C	- table 32, figure 36

Consistent trends may be noted from these static test data:

- Tensile prestrain (cold work) enhances aged strength of Ti-15-3 and Beta-C with little loss of ductility (tensile). The strength increases were greater in the direction normal to the prestrain direction. No Bauschinger effect (loss of compressive yield strength) was noted in either alloy when aged after the tension strain.

- The simulated brazing cycle prior to aging resulted in a small strength loss presumed due to overaging. Tensile prestrain prior to the brazing cycle further reduced strength in the direction of prestrain on subsequent aging. Compression tests of the Beta-C alloy show, however, that strength increases can occur in the direction normal to the prestrain. The kinetics of these combined prestrain/brazing effects need to be metallurgically investigated.

- Actual brazed (composite) specimens of either Ti-15-3 or Beta-C to Ti-6-4 displayed properties intermediate to those of the two alloys joined, as expected.

- Welded and aged Ti-15-3 sheet exhibited full joint efficiencies. Cold work after welding reduced subsequent aged tensile strength but appeared to have little effect on compressive yield strength.

- Tensile and compressive moduli for a given alloy remained fairly consistent for the various processing conditions tested.

Notch Tension

Sharp notch tensile strengths for Ti-15-3 and Beta-C are compared at three test temperatures, in table 33. Tests were conducted according to ASTM E338. Notch radius varied rather widely from the specified radius of 0.0007 inch maximum, so the actual radius and calculated K_t factor are given for each coupon. Despite the variation in K_t, certain trends are seen. Ti-15-3 showed higher notch strength and notch strength/yield strength ratios (NTS/YS) than the Beta-C at all three test temperatures. For a given alloy, the

notch strengths were reasonably similar at -65°F and room temperature, and highest at 600°F, while NTS/YS ratio increases with test temperature. Notch strengths were also fairly uniform with respect to grain direction. Prestrain generally lowered the notch strength of both alloys.

Creep

Table 34 summarizes results of creep tests of 500 hours duration at 600°F and applied stress levels of 50 and 75 ksi. Test procedures of ASTM E139-79 recommended practice were followed. The Beta-C alloy showed lower minimum creep rates and produced less creep at both stress levels than the Ti-15-3 alloy for comparable material conditions. However, the composite specimens of either Beta-C or Ti-15-3 when brazed to Ti-6Al-4V displayed equivalent creep strength. The creep properties of the brazed (composite) specimens appeared to be strongly influenced by the Ti-6Al-4V portion of the composite.

Examining effects of processing variants upon the creep behavior of Ti-15-3, the creep strengths show an almost inverse relation to degree of overaging (or strength level), for the various processing conditions. That is, the highest strength cold worked plus aged material had the lowest creep strength, while the braze cycle or cold work plus braze cycle before aging lowered aged tensile strength (overaging effect) but were beneficial to creep strength. Minimum creep rates for the Beta-C were identical with or without the braze cycle prior to aging.

All creep specimens were tensile tested at room temperature after creep exposure. Table 35 compares tensile properties of exposed and unexposed specimens in comparable material conditions. Good creep stability is indicated for both alloys after 500 hours at 600°F and the two applied stress levels. Only slight strengthening was found after creep exposure with essentially no loss of ductility.

Fatigue

Room temperature constant amplitude fatigue data for unnotched (K_t=1.0), hole notched (K_t=2.6), and brazed lap shear tests of the Ti-15-3 and Beta-C alloys are detailed in table 36. The tests were run at an R-ratio of 0.1, and a frequency of 10 Hz for the lap shears and 15 Hz for the others.

The parent metal S-N curves are plotted in figures 37 (K_t=1.0) and 38 (K_t=2.6). Ti-15-3 was superior to the Beta-C for both smooth and notched conditions. However, the abnormally rough surface texture and nonuniform grain size of this lot of Beta-C are conditions which could have negatively influenced the fatigue behavior. Also tension and bend tests of the Beta-C have shown inferior ductility in the transverse grain direction. Note that somewhat inferior fatigue performance for transverse K_t=1.0 Beta-C specimens is seen

as well. In figure 38 a previous curve from task 1 (Screening) of 0.063 inch Ti-15-3 with K_t=2.6, is included. Results for the 0.080-inch Ti-15-3 are comparable, which tends to confirm a particularly high endurance limit at K_t=2.6 for Ti-15-3 sheet product.

S-N fatigue curves showing the effects of processing variants on notched fatigue characteristics of Ti-15-3 are presented in figure 39. Low-cycle notched fatigue behavior of Ti-15-3 in various conditions was consistent with Lockheed reference curves for Ti-6-4. The parent Ti-15-3 STA material displays superior high-cycle fatigue strength, while brazing and cold work processes lowered the fatigue endurance strength.

Unnotched fatigue curves showing effects of processing are plotted in figure 40. Here, brazing and welding lowered fatigue strength of Ti-15-3, but cold work appears to enhance fatigue endurance strength considerably. Cold work after welding, however, had a minor adverse effect.

Constant amplitude fatigue test results of single overlap isothermal brazed joints are plotted in figure 41. The S-N curves for either Ti-15-3/Ti-6-4 joints or Beta-C/Ti-6-4 joints are in good agreement with reference curves shown for weld-brazed joints taken from NASA-Langley and Northrop Aircraft programs.

Failure at high cycles of the braze lap-joint specimens typically propagated through the beta alloy sheet at the edge of the overlap (exception specimen No. 11-3). Two of the Ti-15-3 and two of the Beta-C failures, figure 42, were examined. Significant observations made on these samples are summarized below.

Optical metallography and SEM fractography revealed multiple crack origins along the braze interface in all specimens. Some of the origins were located around voids in the braze, and some cracks originated within the braze or at the braze fillet. The Ti-Al intermetallic layer formed at the braze interface was found to be around 0.0001-0.0002 inch thick. Although some small grain boundary (secondary) cracking was present in the Ti-Al layer, no obvious crack origins were found there. Previous work at Northrop on weld-brazed Ti-6Al-4V joints (Ref. 25) revealed fatigue cracks originating from the brittle Ti-Al layer which was about 0.0005 inch thick. Furnace brazing with 4043A1 braze alloy was used in that program. The thinner Ti-Al intermetallic layer formed in the isothermal brazed joints appears to at least minimize fatigue crack initiation in this layer.

Fatigue crack propagation in the Ti-15-3 or Beta-C sheet was for the most part transgranular; however, in places, the crack followed the grain boundary alpha precipitates. This can be seen in figure 43 for the Ti-15-3 and figure 44 for the Beta-C. The heating and cooling cycles that the beta alloy undergoes during brazing and subsequent aging appeared to cause precipitation of a semicontinuous alpha film along a grain boundary denuded zone presumed to be beta. It was reported above that the brazing process reduced fatigue

strength of unnotched (K_t=1.0) and notched (K_t=2.6) Ti-15-3 specimens compared with the parent material. Metallurgical evidence now suggests that the brazing cycle increased growth of the grain boundary alpha film, resulting in integranular crack propagation which could be a factor in reducing fatigue strength. It is believed that shortening the time at temperatures above the aging temperature during the brazing cycle would produce more desirable aging response.

Fatigue Crack Growth

Fatigue crack growth tests of Ti-15-3 were carried out in ambient air and a continuously flowing 3.5% NaCl solution, using compact tension (CT) specimens per ASTM E561-78T (figure A7, appendix). All tests were conducted according to ASTM E647 in a closed-loop electrohydraulic MTS fatigue machine at a frequency of 6 Hz and R=0.1.

Figure 45 compares fcg rates (da/dN) of Ti-15-3 in air and saltwater, figure 46 compares nonstrained material in two directions, and figure 47 compares prestrained material in two directions. The fcg rates of Ti-15-3 were insensitive to the saltwater environment and showed no discernible effect of directionality. Both of these findings corroborate earlier Timet results (ref. 4). Also, very similar crack growth behavior between nonstrained and prestrained material is seen in both L-T (figure 48), and T-L (figure 49) orientations.

Fracture Toughness (R-Curve)

Tests were conducted according to ASTM E561-78T recommended practice using compact specimens (figure A7, appendix). The specimens were tested in a closed-loop electrohydraulic MTS fatigue machine, using antibuckling guides, at a head defection rate of 0.025 inch per minute. (One specimen, K-7, was inadvertently tested at 0.05 inch per minute).

R-curves for nonstrained and prestrained (cold worked) Ti-15-3 are compared in figure 50. Crack growth resistance parameter, K_R, is plotted against crack extension as the precrack is driven stably under increasing crack extension forces. Pronounced differences in K_R behavior of the nonstrained and prestrained material are seen. The lower fracture resistance is believed related to both the higher strength level and reduced plasticity as a result of cold working. The differences in K_R appear much greater than differences indicated earlier in notch tensile behavior. This suggests the need for K_R as well as notch tensile or K_{Ic} data in assessing residual strength of damaged structure in thin gages that are typical of real aircraft structure.

TABLE 21. - ROOM TEMPERATURE TENSILE PROPERTIES OF Ti-15-3 WITH VARIOUS PROCESSING CYCLES

Spec. No. (4)	Condition	Test Dir	Prestrain Dir	F_{tu} (ksi)	F_{ty} (ksi)	e (%)	Eapp (Msi)
7-4	STA	L	–	176	161	12	15.0
7-5	STA	L	–	175	159	12	15.1
7-6	STA	L	–	176	161	11	15.2
avg.		L	–	176	160	12	15.1
7A-2	ST + CW + A	L	L	180	–	8	14.2
7A-5	ST + CW + A	L	L	189	173	7	14.5
avg.		L	L	185	173	8	14.4
8A-1	ST + CW + A	L	T	193	181	7	14.6
8A-2	ST + CW + A	L	T	194	181	7	14.7
8A-3	ST + CW + A	L	T	196	184	6	14.7
avg.		L	T	194	182	7	14.7
7-16	ST + Braze (Ti-15-3/Ti-6-4) + A	L	–	155	141	13	15.2
7-17	ST + Braze (Ti-15-3/Ti-6-4) + A	L	–	154	140	12	15.1
7-36	ST + Braze (Ti-15-3/Ti-6-4) + A	L	–	150	136	14	15.0
avg.		L	–	153	138	13	15.1
7-25	ST + Braze Cycle + A	L	–	165	151	10	14.4
7-26	ST + Braze Cycle + A	L	–	164	149	10	14.7
7-27	ST + Braze Cycle + A	L	–	165	150	10	14.1
avg.		L	–	165	150	10	14.4
7A-3	ST + CW + Braze Cycle + A	L	L	151	137	14	14.7
7D-5	ST + CW + Braze Cycle + A	L	L	148	134	15	14.9
avg.		L	L	150	136	15	14.8
8-1	STA	T	–	181	168	10	15.7
8-3	STA	T	–	181	168	10	15.8
8-4	STA	T	–	177	164	7	14.8
avg.		T	–	180	167	9	15.4
8B-8	ST + CW + A	T	T	186	169	7	14.6
8B-10	ST + CW + A	T	T	183	167	7	14.3
avg.		T	T	185	168	7	14.4
7E-1	ST + CW + A	T	L	195	–	7	14.5
7E-2	ST + CW + A	T	L	197	187	6	14.2
7E-3	ST + CW + A	T	L	200	188	6	15.0
avg.		T	L	197	188	6	14.6
W-1	ST + Weld + A	T	–	181 (1)	169	7	15.5
W-2	ST + Weld + A	T	–	183 (1)	171	7	15.1
W-3	ST + Weld + A	T	–	183 (1)	170	8	15.4
avg.		T	–	182	170	7	15.3
2-1	ST + Weld + CW + A	T	T	164 (2)	150	8	14.4
2-2	ST + Weld + CW + A	T	T	164 (1)	149	7	14.0
2-3	ST + Weld + CW + A	T	T	164 (3)	152	5	14.4
avg.		T	T	164	150	6	14.3

(1) Failed in parent metal
(2) Failed in weld
(3) Failed edge of weld
(4) Specimen Configuration: Figure A1

TABLE 22. - -65°F TENSILE PROPERTIES OF T1-15-3 WITH VARIOUS PROCESSING CYCLES

Spec. No. (1)	Condition	Test Dir	Prestrain Dir	F_{tu} (ksi)	F_{ty} (ksi)	e (%)	Eapp (Msi)
7-1	STA	L	–	194	183	8	15.2
7-2	STA	L	–	196	185	10	15.2
7-3	STA	L	–	197	186	9	15.2
avg.		L	–	196	185	9	15.2
7A7	ST + CW + A	L	L	207	194	7	15.8
7A10	ST + CW + A	L	L	194	177	7	16.8
avg.		L	L	200	185	7	16.3
7-13	ST + Braze (Ti-15-3/Ti-6-4) + A	L	–	174	164	10	16.7
7-14	ST + Braze (Ti-15-3/Ti-6-4) + A	L	–	174	165	10	16.2
7-15	ST + Braze (Ti-15-3/Ti-6-4) + A	L	–	172	162	10	16.1
avg.		L	–	173	164	10	16.3
7-22	ST + Braze Cycle + A	L	–	185	173	8	15.9
7-23	ST + Braze Cycle + A	L	–	186	176	7	16.1
7-24	ST + Braze Cycle + A	L	–	185	176	8	15.6
avg.		L	–	185	175	8	15.9
7D1	ST + CW + Braze Cycle + A	L	L	172	163	11	15.8
7D3	ST + CW + Braze Cycle + A	L	L	169	159	8	16.1
avg.		L	L	170	161	9	15.9

(1) Specimen Configuration: Figure A1

TABLE 23. - 600°F TENSILE PROPERTIES OF Ti-15-3 WITH VARIOUS PROCESSING CYCLES

Spec. No. (2)	Condition	Test Dir	Prestrain Dir	F_{tu} (ksi)	F_{ty} (ksi)	e (%)	Eapp (Msi)
7-7	STA	L	–	150.9	129.9	8.0	(1)
7-8	STA	L	–	150.8	131.8	7.0	(1)
7-9	STA	L	–	150.7	130.7	7.5	(1)
avg.		L	–	150.8	130.8	7.5	(1)
7A-1	ST + CW + A	L	L	152.4	129.9	11.0	13.4
7A-4	ST + CW + A	L	L	166.7	143.1	8.0	13.5
avg.		L	L	159.6	136.5	9.5	13.4
7-18	ST + Braze (Ti-15-3/Ti-6-4) + A	L	–	124.3	103.6	10.0	13.5
7-19	ST + Braze (Ti-15-3/Ti-6-4) + A	L	–	116.4	97.8	11.0	12.0
7-20	ST + Braze (Ti-15-3/Ti-6-4) + A	L	–	123.3	102.6	11.0	13.2
avg.		L	–	121.3	101.3	10.7	12.9
7-28	ST + Braze Cycle + A	L	–	142.0	121.0	9.0	13.1
7-29	ST + Braze Cycle + A	L	–	141.9	120.2	10.0	13.1
7-30	ST + Braze Cycle + A	L	–	139.2	120.3	9.0	13.1
avg.		L	–	141.0	120.5	9.3	13.1
7D-4	ST + CW + Braze Cycle + A	L	L	127.5	109.2	11.0	13.9
7D-6	ST + CW + Braze Cycle + A	L	L	125.5	106.6	13.0	13.2
avg.		L	L	126.5	107.9	12.0	13.5
8-5	STA	T	–	156.3	137.8	7.0	(1)
8-6	STA	T	–	155.9	137.4	7.0	(1)
avg.		T	–	156.1	137.6	7.0	(1)
8B-9	ST + CW + A	T	T	164.5	141.3	8.0	13.7
8B-11	ST + CW + A	T	T	159.8	135.8	8.0	13.6
avg.		T	T	162.2	138.6	8.0	13.6

(1) Not obtained
(2) Specimen Configuration: Figure A1

TABLE 24. - ROOM TEMPERATURE TENSILE PROPERTIES OF BETA-C WITH VARIOUS PROCESSING CYCLES

Spec. No. (1)	Condition	Test Dir	Prestrain Dir	F_{tu} (ksi)	F_{ty} (ksi)	e (%)	Eapp (Msi)
1-4	STA	L	–	193	177	7	15.5
1-5	STA	L	–	190	175	9	15.2
1-6	STA	L	–	191	176	7.5	15.7
avg.		L	–	191	176	8	15.5
1C1	ST + CW + A	L	L	194	178	6	16.0
1C3	ST + CW + A	L	L	195	177	6	15.5
1C5	ST + CW + A	L	L	198	180	6	16.1
avg.		L	L	196	178	6	15.9
1-34	ST + Braze (Beta-C/Ti-6-4) + A	L	–	158	145	10	14.9
1-38	ST + Braze (Beta-C/Ti-6-4) + A	L	–	161	152	12	15.0
3-27	ST + Braze (Beta-C/Ti-6-4) + A	L	–	159	149	11	15.3
avg.		L	–	159	149	11	15.1
1-44	ST + Braze Cycle + A	L	–	174	162	9	15.0
1-45	ST + Braze Cycle + A	L	–	178	164	9	15.2
avg.		L	–	176	163	9	15.1
1C6	ST + CW + Braze Cycle + A	L	L	174	160	8	15.2
1C8	ST + CW + Braze Cycle + A	L	L	165	152	11	15.2
1C10	ST + CW + Braze Cycle + A	L	L	164	152	8	14.6
avg.		L	L	168	155	9	15.0
1-63	STA	T	–	188	177	4	16.0
1-64	STA	T	–	190	179	5	16.0
1-65	STA	T	–	190	179	4.5	15.9
avg.		T	–	189	178	4.5	16.0
1B1	ST + CW + A	T	L	198	189	7	15.6
1B2	ST + CW + A	T	L	198	189	3	15.6
1B3	ST + CW + A	T	L	200	189	2	15.6
avg.		T	L	199	189	4	15.6

(1) Specimen Configuration: Figure A1

TABLE 25. - -65°F TENSILE PROPERTIES OF BETA-C WITH VARIOUS PROCESSING CYCLES

Spec. No. (1)	Condition	Test Dir	Prestrain Dir	F_{tu} (ksi)	F_{ty} (ksi)	e (%)	Eapp (Msi)
1-1	STA	L	–	214	205	3	15.5
1-2	STA	L	–	217	206	5	15.5
1-3	STA	L	–	217	210	3	15.6
avg.		L	–	216	207	3.7	15.5
1A1	ST + CW + A	L	L	214	–	4	16.6
1A3	ST + CW + A	L	L	212	201	4	16.6
1A4	ST + CW + A	L	L	217	207	3	14.9
avg.		L	L	214	204	4	16.0
1-33	ST + Braze (Beta-C/Ti-6-4) + A	L	–	178	169	8	16.4
1-48	ST + Braze (Beta-C/Ti-6-4) + A	L	–	172	165	9	16.7
3-26	ST + Braze (Beta-C/Ti-6-4) + A	L	–	179	173	7	16.3
avg.		L	–	176	169	8	16.5
1-42	ST + Braze Cycle + A	L	–	198	193	5	15.0
1-43	ST + Braze Cycle + A	L	–	201	195	5	15.9
avg.		L	–	199	194	5	15.4
1A6	ST + CW + Braze (Beta-C/Ti-6-4) + A	L	L	174	165	9	15.7
1A8	ST + CW + Braze (Beta-C/Ti-6-4) + A	L	L	175	166	9	16.6
avg.		L	L	174	165	9	16.1

(1) Specimen Configuration: Figure A1

TABLE 26. - 600°F TENSILE PROPERTIES OF BETA-C WITH VARIOUS PROCESSING CYCLES

Spec. No. (2)	Condition	Test Dir	Prestrain Dir	F_{tu} (ksi)	F_{ty} (ksi)	e (%)	Eapp (Msi)
1-7	STA	L	–	172.9	137.1	5.5	(1)
1-8	STA	L	–	174.4	139.9	5.0	(1)
1-9	STA	L	–	173.8	142.0	5.5	(1)
avg.		L	–	173.6	139.6	5.3	(1)
1C-2	ST + CW + A	L	L	174.6	141.4	7.5	13.7
1C-4	ST + CW + A	L	L	176.4	145.0	7.5	13.8
1A-2	ST + CW + A	L	L	172.8	142.2	8.5	13.5
avg.		L	L	174.6	142.9	7.8	13.7
1-39	ST + Braze (Beta-C/Ti-6-4) + A	L	–	131.2	107.3	11.0	13.3
1-40	ST + Braze (Beta-C/Ti-6-4) + A	L	–	130.0	104.5	11.0	13.4
1-41	ST + Braze (Beta-C/Ti-6-4) + A	L	–	133.9	107.9	12.0	13.4
avg.		L	–	131.7	106.6	11.3	13.4
1-46	ST + Braze Cycle + A	L	–	162.0	132.5	8.0	14.0
1-47	ST + Braze Cycle + A	L	–	158.4	129.5	8.0	13.9
avg.		L	–	160.2	131.0	8.0	14.0
1C-7	ST + CW + Braze Cycle + A	L	L	144.7	120.1	9.0	13.7
1C-9	ST + CW + Braze Cycle + A	L	L	147.8	119.4	12.0	13.7
avg.		L	L	146.3	120.0	10.5	13.7
1-66	STA	T	–	171.1	142.2	4.0	(1)
1-67	STA	T	–	175.3	143.1	5.0	(1)
1-68	STA	T	–	170.8	141.3	5.0	(1)
avg.		T	–	172.4	142.2	4.7	(1)
1B-5	ST + CW + A	T	L	182.1	154.7	5.0	14.0
1B-6	ST + CW + A	T	L	176.2	158.1	2.5	14.1
1B-7	ST + CW + A	T	L	182.7	153.5	9.0	14.2
avg.		T	L	180.3	155.4	5.5	14.1

(1) Not obtained
(2) Specimen Configuration: Figure A1

TABLE 27. - ROOM TEMPERATURE COMPRESSIVE PROPERTIES OF Ti-15-3 WITH VARIOUS PROCESSING CYCLES

Spec. No. (1)	Condition	Test Dir	Prestrain Dir	F_{cy} (ksi)	Eapp (Msi)
4-3	STA	L	–	169	14.4
4-4	STA	L	–	167	14.9
avg.		L	–	168	14.7
4C-6	ST + CW + A	L	L	185	15.0
4C-11	ST + CW + A	L	L	182	14.7
avg.		L	L	183	14.9
8A-4	ST + CW + A	L	T	195	15.6
8A-5	ST + CW + A	L	T	200	14.5
avg.		L	T	197	15.1
4-29	ST + Braze (Ti-15-3/Ti-6-4) + A	L	–	146	14.6
4-47	ST + Braze (Ti-15-3/Ti-6-4) + A	L	–	147	15.6
avg.		L	–	147	15.1
4-41	ST + Braze Cycle + A	L	–	164	15.2
4-42	ST + Braze Cycle + A	L	–	165	16.0
avg.		L	–	164	15.6
4C-8	ST + CW + Braze Cycle + A	L	L	145	14.9
4C-10	ST + CW + Braze Cycle + A	L	L	140	17.9
avg.		L	L	142	16.4
7-70	STA	T	–	180	16.0
7-70X	STA	T	–	178	15.2
avg.		T	–	179	15.6
8A-8	ST + CW + A	T	T	183	14.8
8A-9	ST + CW + A	T	T	182	14.2
avg.		T	T	182	14.5
I-2	ST + Weld + A	T	–	177	15.3
I-3	ST + Weld + A	T	–	178	16.6
avg.		T	–	178	16.0
2-4	ST + Weld + CW + A	T	T	175	16.3
2-5	ST + Weld + CW + A	T	T	178	12.5
avg.		T	T	177	14.4

(1) Specimen Configuration: Figure A2

TABLE 28. - -65°F COMPRESSIVE PROPERTIES OF Ti-15-3 WITH VARIOUS PROCESSING CYCLES

Spec. No. (1)	Condition	Test Dir	Prestrain Dir	F_{cy} (ksi)	Eapp (Msi)
4-5	STA	L	–	173	15.4
4-8	STA	L	–	180	15.6
avg.		L	–	177	15.4
4C-7	ST + CW + A	L	L	188	14.6
4C-12	ST + CW + A	L	L	188	17.0
avg.		L	L	188	15.8
4-26	ST + Braze (Ti-15-3/Ti-6-4) + A	L	–	155	14.7
4-27	ST + Braze (Ti-15-3/Ti-6-4) + A	L	–	160	13.7
avg.		L	–	158	14.2
4C-14	ST + CW + Braze (Ti-15-3/Ti-6-4) + A	L	L	149	14.8
4-32	ST + Braze Cycle + A	L	–	175	15.4
4-33	ST + Braze Cycle + A	L	–	173	15.0
avg.		L	–	174	15.2
4C-9	ST + CW + Braze Cycle + A	L	L	156	14.7

(1) Specimen Configuration: Figure A2

TABLE 29. - 600°F COMPRESSIVE PROPERTIES OF Ti-15-3 WITH VARIOUS PROCESSING CYCLES

Spec. No. (2)	Condition	Test Dir	Prestrain Dir	F_{cy} (ksi)	Eapp (Msi)
4-43	STA	L	–	139	15.1
4-44	STA	L	–	139	15.1
avg.		L	–	139	15.1
4C3	ST + CW + A	L	L	158	14.6
4C5	ST + CW + A	L	L	160	14.6
avg.		L	L	159	14.6
4-30	ST + Braze (Ti-15-3/Ti-6-4) + A	L	–	110 (1)	14.6
4-31	ST + Braze (Ti-15-3/Ti-6-4) + A	L	–	109 (1)	14.5
avg.		L	–	109	14.5
4-45	ST + Braze Cycle + A	L	–	132	14.7
4-46	ST + Braze Cycle + A	L	–	133	14.9
avg.		L	–	132	14.8
4C2	ST + CW + Braze Cycle + A	L	L	112	14.7
4C4	ST + CW + Braze Cycle + A	L	L	114	15.1
avg.		L	L	113	14.9

(1) Permanent Bending Noted.
(2) Specimen Configuration: Figure A2

TABLE 30. - ROOM TEMPERATURE COMPRESSIVE PROPERTIES OF BETA-C WITH VARIOUS PROCESSING CYCLES

Spec. No. (1)	Condition	Test Dir	Prestrain Dir	F_{cy} (ksi)	Eapp (Msi)
1-10	STA	L	–	179	15.5
1-11	STA	L	–	180	14.7
avg.		L	–	179	15.1
3A5	ST + CW + A	L	L	180	14.9
3A6	ST + CW + A	L	L	182	15.0
avg.		L	L	181	14.9
3-3	STA	T	–	189	15.5
3-4	STA	T	–	183	16.2
avg.		T	–	186	15.8
3A9	ST + CW + A	T	L	192	14.6
3A14	ST + CW + A	T	L	195	15.5
avg.		T	L	193	15.0
10-1	ST + Weld + A	T	–	Specimen Bent	–
10-2	ST + Weld + A	T	–	Specimen Bent	–
10-3	ST + Weld + A	T	–	181	16.5
12-4	ST + Weld + A	T	–	179	17.0
12-5	ST + Weld + A	T	–	178	16.7
avg.		T	–	179	16.7
3-42	ST + Braze (Beta-C/Ti-6-4) + A	T	–	153	14.6
3-43	ST + Braze (Beta-C/Ti-6-4) + A	T	–	154	15.2
avg.		T	–	154	14.9
3-44	ST + Braze Cycle + A	T	–	177	15.6
3-59	ST + Braze Cycle + A	T	–	179	15.5
avg.		T	–	178	15.5
3A10	ST + CW + Braze Cycle + A	T	L	191	15.3
3A17	ST + CW + Braze Cycle + A	T	L	183	15.6
avg.		T	L	187	15.4

(1) Specimen Configuration: Figure A2

TABLE 31. - -65°F COMPRESSIVE PROPERTIES OF BETA-C WITH VARIOUS PROCESSING CYCLES

Spec. No. (1)	Condition	Test Dir	Prestrain Dir	F_{cy} (ksi)	Eapp (Msi)
3-5	STA	T	–	202	15.6
3-6	STA	T	–	198	15.7
avg.		T	–	200	15.6
3A8	ST + CW + A	T	L	Specimen Bent	–
3A15	ST + CW + A	T	L	Specimen Bent	–
3-38	ST + Braze (Beta-C/Ti-6-4) + A	T	–	Specimen Bent	–
3-39	ST + Braze (Beta-C/Ti-6-4) + A	T	–	153	14.9
3-53	ST + Braze (Beta-C/Ti-6-4) + A	T	–	167	15.4
avg.		T	–	160	15.1
3-40	ST + Braze Cycle + A	T	–	187	15.1
3-41	ST + Braze Cycle + A	T	–	181	17.3
avg.		T	–	184	16.2
3A11	ST + CW + Braze Cycle + A	T	L	192	16.5
JA16	ST + CW + Braze Cycle + A	T	L	189	16.4
avg.		T	L	190	16.4

(1) Specimen Configuration: Figure A2

TABLE 32. - 600°F COMPRESSIVE PROPERTIES OF BETA-C WITH VARIOUS PROCESSING CYCLES

Spec. No. (2)	Condition	Test Dir	Prestrain Dir	F_{cy} (ksi)	Eapp (Msi)
3-46	STA	T	–	160	15.6
3-47	STA	T	–	163	15.5
avg.		T	–	161	15.5
385	ST + CW + A	T	L	172	16.1
386	ST + CW + A	T	L	174	16.3
avg.		T	L	173	16.2
3-48	ST + Braze (Beta-C/Ti-6-4) + A	T	–	115 (1)	14.9
3-49	ST + Braze (Beta-C/Ti-6-4) + A	T	–	113 (1)	14.9
avg.		T	–	114	14.9
3-50	ST + Braze Cycle + A	T	–	147	15.8
3-51	ST + Braze Cycle + A	T	–	144	15.7
avg.		T	–	145	15.7
387	ST + CW + Braze Cycle + A	T	L	148	16.0
388	ST + CW + Braze Cycle + A	T	L	144	15.8
avg.		T	L	146	15.9

(1) Permanent Bending Noted.
(2) Specimen Configuration: Figure A2

TABLE 33. SHARP NOTCH TENSILE STRENGTH (NTS) OF TWO BETA TITANIUM ALLOYS

Test Temp	Alloy	Condition	Prestrain Dir	Test Dir	Notch Radius (in.) (1)	K_t	NTS (ksi)	$\overline{YS}$(3)	NTS / YS
Room	Ti-15-3	STA	–	L	0.004	9.3	108	160	0.68
		STA	–	L	0.004	9.3	112		0.70
		ST + CW + A	L	L	0.003	10.6	92	173	0.53
		ST + CW + A	L	L	0.0025	11.5	104		0.60
		STA	–	T	0.003	10.6	127	167	0.76
		STA	–	T	0.004	9.3	124		0.74
		ST + CW + A	T	T	0.0025	11.6	90	168	0.53
		ST + CW + A	T	T	0.003	10.6	95		0.57
	Beta-C	STA	–	L	0.005	8.4	94	176	0.53
		STA	–	L	0.003	10.6	90		0.51
		ST + CW + A	L	L	0.0025	11.6	88	178	0.49
		ST + CW + A	L	L	0.0025	11.6	86		0.48
		STA	–	T	0.003	10.6	91	178	0.51
		STA	–	T	0.003	10.6	84		0.47
-65°F	Ti-15-3	STA	–	L	0.0025	11.5	110	185	0.59
		STA	–	L	0.0025	11.6	99		0.54
		ST + CW + A	L	L	0.005	8.3	83	185	0.45
		ST + CW + A	L	L	0.005	8.4	91		0.49
	Beta-C	STA	–	L	0.0012	16	93	207	0.45
		ST + CW + A	L	L	0.0025	11.5	77	204	0.38
		ST + CW + A	L	L	0.005	8.4	83		0.40
600°F	Ti-15-3	STA	–	L	0.0012	16	138	131	1.05
		STA	–	L	0.0025	11.5	>137(2)		>1.05
		STA	–	T	0.0012	16	149	138	1.08
	Beta-C	STA	–	L	0.0012	16	127	140	0.91
		STA	–	L	0.0012	16	122		0.87
		ST + CW + A	L	L	0.005	8.3	111	143	0.78
		ST + CW + A	L	L	0.006	7.7	111		0.78
		STA	–	T	0.0012	16	115	142	0.81
		STA	–	T	0.0012	16	107		0.75

(1) Specified radius (r) was 0.0007 in., (Spec. Configuration: Figure A3)

(2) Failed through loading pin hole

(3) Average yield strength (ref. Tables 21-28)

TABLE 34. 500 HOUR CREEP TEST RESULTS AT 600°F FOR TWO BETA TITANIUM ALLOYS

Spec. No. (3)	Alloy	Material Conditions(1)	Strain, percent			Minimum Creep Rate, percent/hour(2)
			Initial	Final	Creep	
75,000 psi						
7-11	Ti-15-3	STA	0.475	0.610	0.135	0.00010
7A6	Ti-15-3	ST + CW + A	0.650	0.842	0.192	0.00019
7-33	Ti-15-3	ST + Braze Cycle + A	0.516	0.640	0.124	0.00012
7A8	Ti-15-3	ST + CW + Braze Cycle + A	0.614	0.730	0.116	0.00010
7-31	Ti-15-3/Ti-6-4	ST + Braze + A	0.588	0.696	0.108	0.00009
1-12	Beta C	STA	0.550	0.608	0.058	0.00003
3-30	Beta C	ST + Braze Cycle + A	0.521	0.590	0.069	0.00003
3-28	Beta C/Ti-6-4	ST + Braze + A	0.516	0.626	0.110	0.00008
50,000 psi						
7-12	Ti-15-3	STA	0.267	0.344	0.077	0.00007
7A9	Ti-15-3	ST + CW + A	0.446	0.556	0.110	0.00010
7-34	Ti-15-3	ST + Braze Cycle + A	0.474	0.538	0.064	0.00006
7D2	Ti-15-3	ST + CW + Braze Cycle + A	0.358	0.430	0.044	0.00005
7-32	Ti-15-3/Ti-6-4	ST + Braze + A	0.400	0.456	0.056	0.00006
1-13	Beta C	STA	0.408	0.460	0.052	0.00002
3-31	Beta C	ST + Braze Cycle + A	0.438	0.484	0.046	0.00002
3-29	Beta C/Ti-6-4	ST + Braze + A	0.322	0.378	0.056	0.00005

(1) Tests and cold work (tensile prestrain) are in the longitudial grain direction

(2) Creep rates may still be decreasing

(3) Specimen configuration: Figure A1

TABLE 35. SUMMARY OF CREEP STABILITY FOR Ti-15-3 AND BETA-C SHEET

Specimen[1]	Alloy	Creep Results[2]		RT Tensile Properties			
		Stress (ksi)	Creep Def. (%)	F_{tu} (ksi)	F_{ty} (ksi)	e (%)	E (Msi)
Solution Treat + Age							
(4)	Ti-15-3	Unexposed	–	176	160	12	15.1
7-11	Ti-15-3	75	0.135	176	163	3	14.8
7-12	Ti-15-3	50	0.077	179	162	10	14.8
(4)	Beta-C	Unexposed	–	191	176	8	15.5
1-12	Beta-C	75	0.058	190	176	8	15.2
1-13	Beta-C	50	0.052	191	178	9	15.4
Solution Treat + Cold Work[3] + Age							
(4)	Ti-15-3	Unexposed	–	184	173	7	14.4
7A6	Ti-15-3	75	0.192	195	178	7	14.9
7A9	Ti-15-3	50	0.110	185	168	7	14.7
Solution Treat + Braze Cycle + Age							
(4)	Ti-15-3	Unexposed	–	164	150	10	14.4
7-33	Ti-15-3	75	0.124	169	155	10	14.9
7-34	Ti-15-3	50	0.064	169	154	10	14.8
(4)	Beta-C	Unexposed	–	176	163	9	15.1
3-30	Beta-C	75	0.069	178	164	9	15.7
3-31	Beta-C	50	0.046	176	163	10	15.2
Solution Treat + Cold Work[3] + Braze Cycle + Age							
(4)	Ti-15-3	Unexposed	–	160	136	14	14.8
7A8	Ti-15-3	75	0.116	153	139	13	14.4
7D2	Ti-15-3	50	0.044	153	137	11	15.0
Solution Treat + Braze + Age							
(4)	Ti-15-3/Ti-6-4	Unexposed	–	153	139	13	15.1
7-31	Ti-15-3/Ti-6-4	75	0.108	159	145	12	15.2
7-32	Ti-15-3/Ti-6-4	50	0.056	154	134	11	15.2
(4)	Beta-C/Ti-6-4	Unexposed	–	159	149	11	15.1
3-28	Beta-C/Ti-6-4	75	0.110	163	148	10	15.3
3-29	Beta-C/Ti 6-4	50	0.056	162	150	11	15.4

(1) Longitudinal

(2) Exposure conditions: 600°F, 500 hours (Reference Table 34)

(3) Tensile strain in L direction

(4) Baseline properties (Reference Tables 21, 24)

TABLE 36. SUMMARY OF FATIGUE DATA FOR TWO BETA TITANIUM ALLOYS (RT, LAB AIR, R = 0.1, 15 Hz) (SHEET 1 OF 3)

Configuration	Coupon No.	Maximum Net Stress, ksi	Cycles to Failure, N
0.080 in. Ti-15-3: STA. Grain = Transverse, K_t = 1.0 (Figure A4)	7-77	100	41,770
	7-75	90	58,294
	7-72	80	81,085 (1)
	7-73	70	159,645 (1)
	7-79	70	2,000,000 NF
	7-78	65	125,796 (1)
	7-76	65	2,008,110 NF
	7-74	60	2,590,820 NF
0.065 in. Beta-C: STA, Grain = Transverse, K_t = 1.0 (Figure A4)	1-80	80	14,796
	1-75	60	41,259
	1-81	55	38,084
	1-76	50	– (2)
	1-77	50	91,090
	1-82	48	78,766
	1-79	44	107,812
	1-78	40	2,004,889 NF
0.065 in. Beta-C: STA, Grain = Longitudinal, K_t = 1.0 (Figure A4)	1-21	90	16,790
	1-15	80	27,459
	1-16	70	37,500
	1-17	60	70,587
	1-18	50	270,400
	1-20	45	218,455
	1-19	40	2,069,318 NF
0.080 in. Ti-15-3: ST + CW + A Grain = Transverse, CW = Transverse, K_t = 1.0 (Figure A4)	8B-4	100	44,857
	8B-6	95	35,064
	8B-2	90	81,047
	8B-5	87.5	44,824
	8B-7	87.5	67,900
	8B-3	85	2,000,000 NF
	8B-1	80	2,000,000 NF
0.080 in. Ti-15-3/0.070 in. Ti-6-4: ST + Braze + A, Grain = Transverse, K_t = 1.0 (Figure A4)	7-85	80	39,418
	7-86	70	47,248
	8-7	60	530,916
	7-91	55	423,531
	7-92	52.5	958,897
	7-90	50	349,050 (3)
	8-8	50	1,471,264
	7-93	45	2,000,000 NF
0.080 in. Ti-15-3: ST + Weld + A Grain = Transverse K_t = 1.0 (Figure A4)	W-8	90	33,377 W
	W-7	80	30,050 PM
	W-10	70	55,100 W
	W-9	65	35,147 EOW
	W-13	65	732,338 W
	W-14	60	54,810 W
	W-11	60	2,000,000 NF

TABLE 36. CONTINUED (SHEET 2 OF 3)

Configuration	Coupon No.	Maximum Net Stress, ksi	Cycles to Failure, N
0.080 in. Ti-15-3: ST + Weld + CW + A, Grain = Transverse, CW = Transverse, K_t = 1.0 (Figure A4)	1-6	80	63,253
	1-1	70	81,920
	1-4	60	164,796
	1-2	50	172,066
	1-5	45	2,000,000 NF
	1-3	40	2,000,000 NF
0.080 in. Ti-15-3: STA, Grain = Longitudinal K_t = 2.6 (Figure A5)	7-47	80	9,260
	7-46	70	12,560
	7-52	60	30,840
	7-50	55	39,020
	7-48	55	2,319,100 NF
	7-51	50	679,060
	7-49	50	2,000,000 NF
0.065 in. Beta-C: STA, Grain = Longitudinal, K_t = 2.6 (Figure A5)	1-24	89.5	4,080
	1-25	67	8,380
	1-30	60	14,810
	1-26	40	53,530
	1-27	35	114,270
	1-28	32.5	230,090
	1-29	30	2,000,000 NF
0.080 in. Ti-15-3: ST + CW + A, Grain = Longitudinal, CW = Longitudinal, K_t = 2.6 (Figure A5)	7C-1	60	22,686
	7C-2	50	123,785
	7C-4	45	56,650
	7C-3	40	85,136
	7C-7	37.5	179,097
	7C-6	35	2,000,000 NF
	7C-5	30	2,000,000 NF
0.080 in. Ti-15-3: ST + Braze cycle + A, Grain = Longitudinal, K_t = 2.6 (Figure A5)	4-58	60	25,664
	4-59	50	40,148
	4-60	40	88,181
	4-64	37.5	236,243
	4-61	35	216,588
	4-63	32.5	2,000,000 NF
	4-62	30	2,000,000 NF
0.080 in. Ti-15-3/0.070 in. Ti-6-4: ST + Braze + A Grain = Longitudinal, K_t = 2.6 (Figure A6)	7-53	60	24,841
	7-67	50	45,707
	7-54	40	64,900
	7-56	35	104,510
	7-68	32.5	168,180
	7-55	30	1,405,644 (3)
	7-69	27.5	2,000,000 NF

TABLE 36. CONCLUDED (SHEET 3 OF 3)

Configuration	Coupon No.	Maximum Net Stress, ksi	Cycles to Failure, N
0.080 in. Ti-15-3/0.070 in. Ti-6-4: ST + Braze + A, Grain = Longitudinal, Lap shear (Figure A6)	4-9	60	1,351 (4)
	4-11	40	1,293 (4)
	4-12	30	32,334 (4)
	4-20	25	28,879 (4)
	4-22	20	168,060 PM (Ti-15-3)
	4-21	17.5	180,513 PM (Ti-15-3)
	4-17	15	833,938 PM (Ti-15-3)
	4-19	12.5	2,000,000 NF
	4-18	10	2,000,000 NF
0.065 in. Beta-C/0.070 in. Ti-6-4: ST + Braze + A, Grain = Longitudinal, Lap shear (Figure A6)	11-1	30	36,000 - 72,000 (4) (5)
	11-7	30	45,000 PM (Beta-C)
	11-6	25	56,412 PM (Beta-C)
	11-9	25	60, 262 PM (Beta-C)
	11-2	20	127,879 PM (Beta-C)
	11-3	15	295,838 (4) & PM (Beta-C)
	11-8	12.5	196,290 PM (Beta-C)
	11-4	10	570,261 PM (Beta-C)
	11-5	7.5	2,000,000 NF

(1) Failed away from center
(2) Machine malfunction, test invalid
(3) Failed at grips
(4) Joint shear failure
(5) Counter did not stop
NF = no failure, W = weld failure, PM = parent metal failure, EOW = edge of weld failure

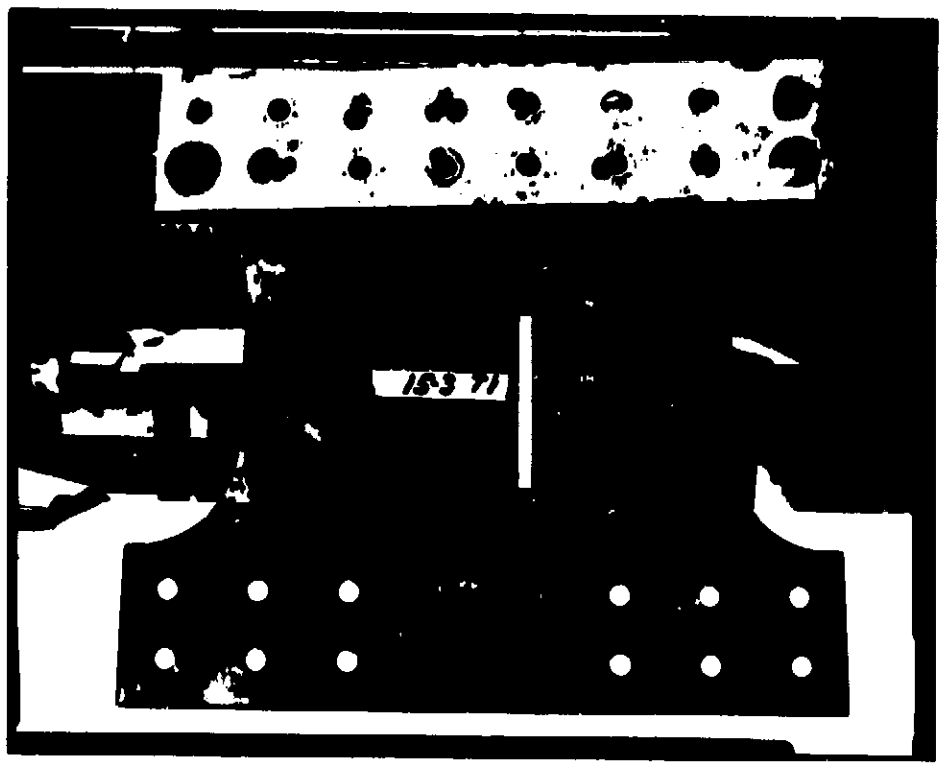

Figure 24. - Typical Ti-15-3 panel after stretching.

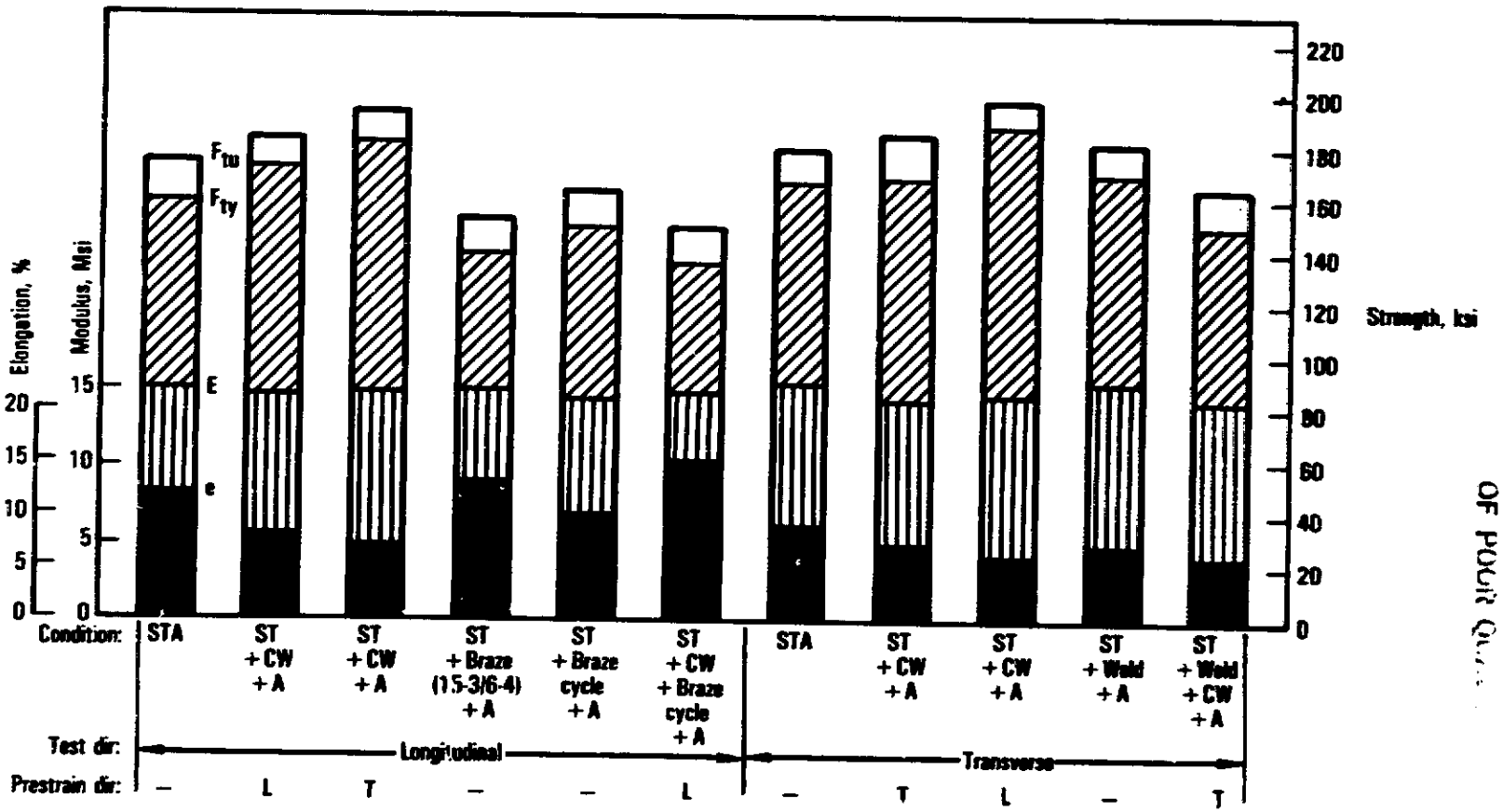

Figure 25. - Processing effects on room temperature tensile properties of Ti-15-3 (average data).

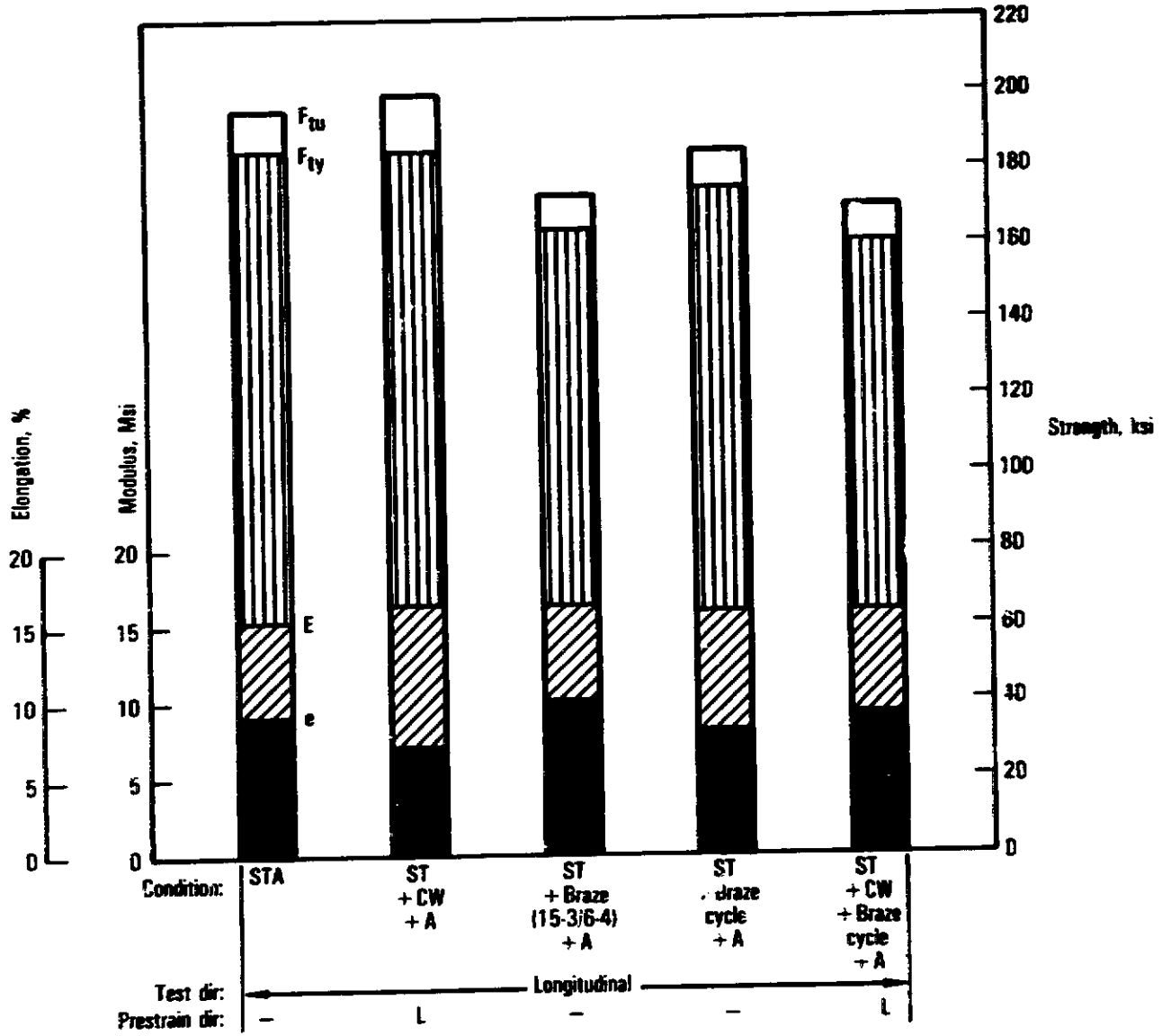

Figure 26. - Processing effects on -65°F tensile properties of Ti-15-3 (average data).

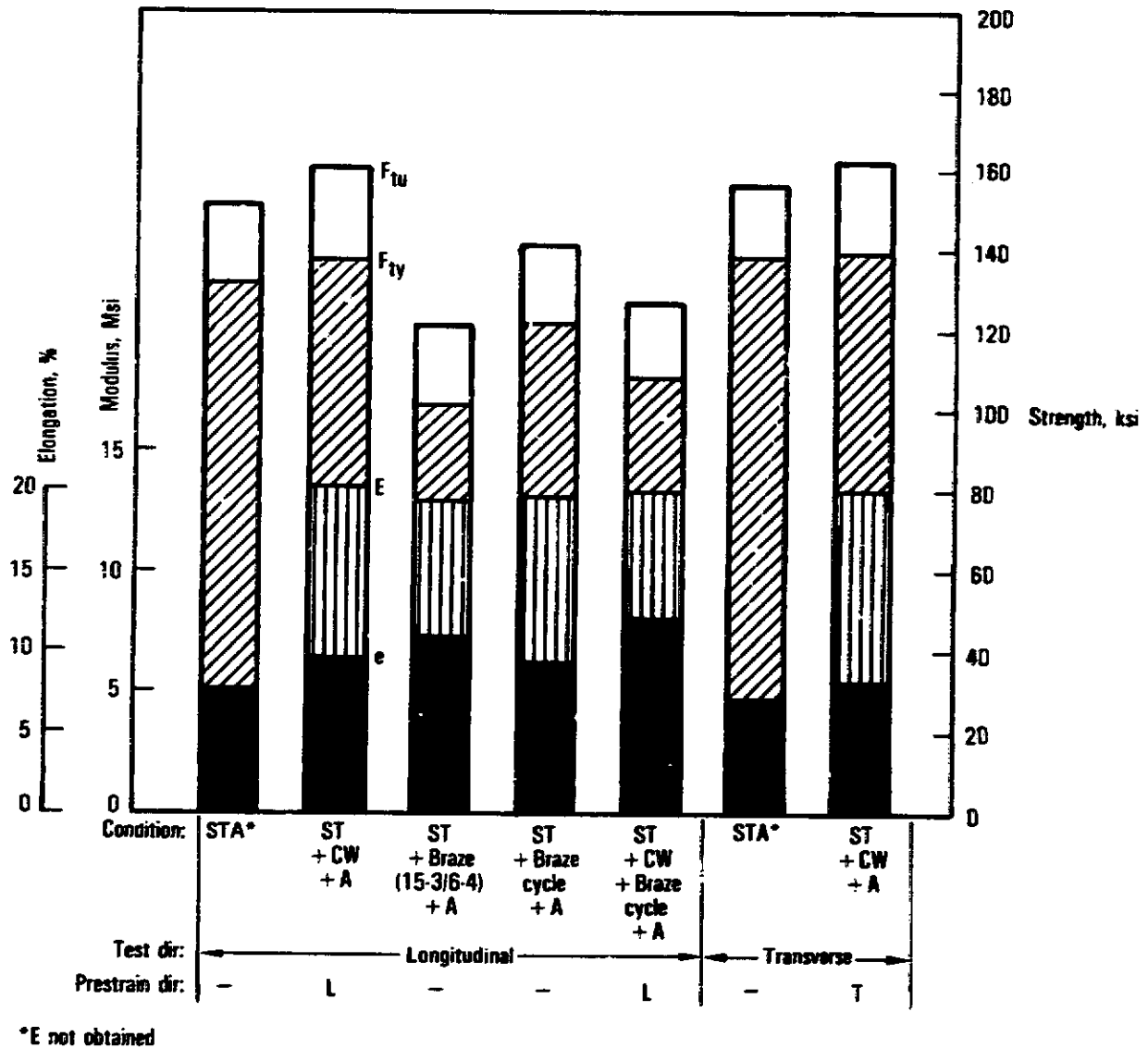

Figure 27. - Processing effects on 600°F tensile properties of Ti-15-3 (average data).

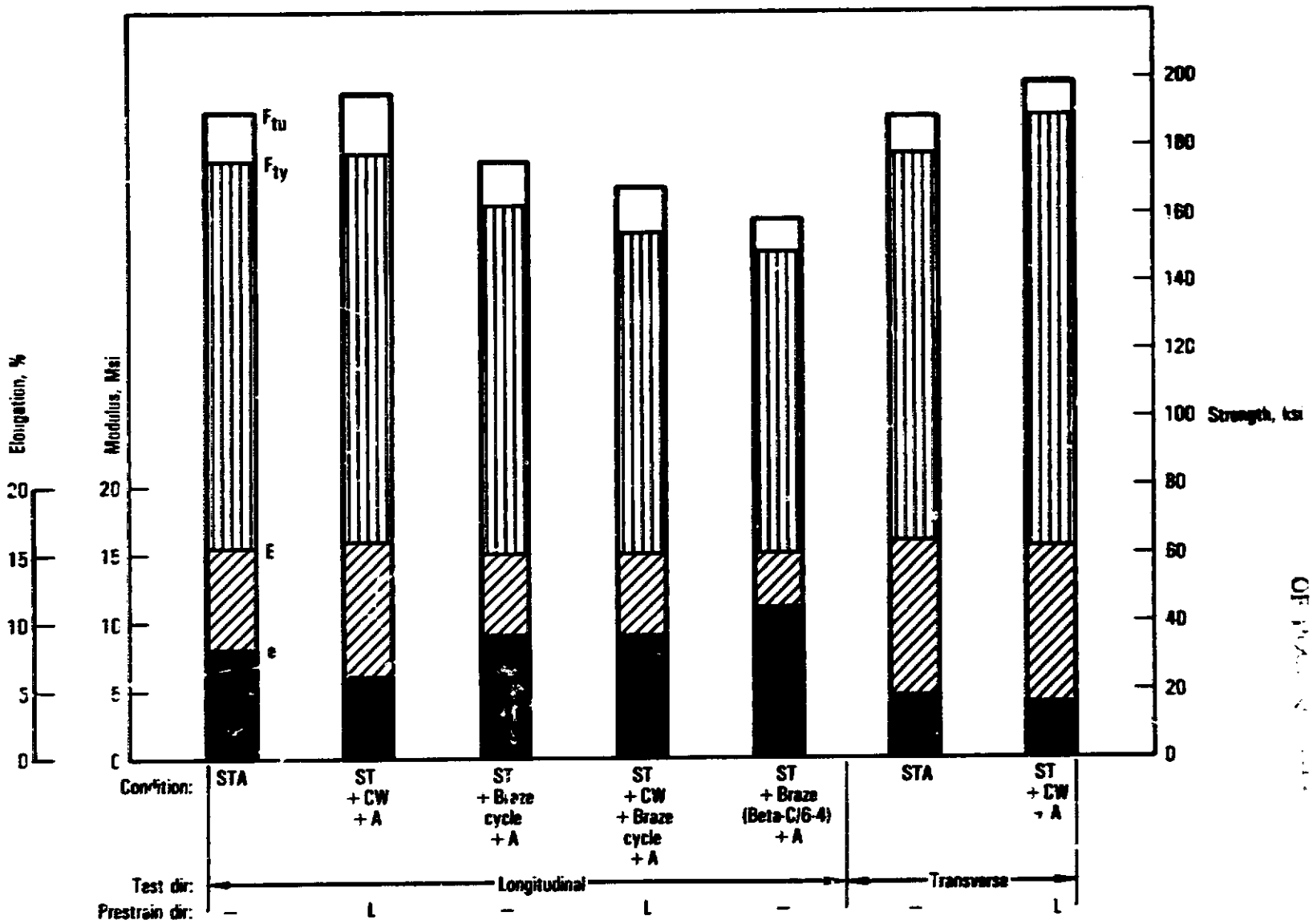

Figure 28. - Processing effects on room temperature tensile properties of Beta-C (average data).

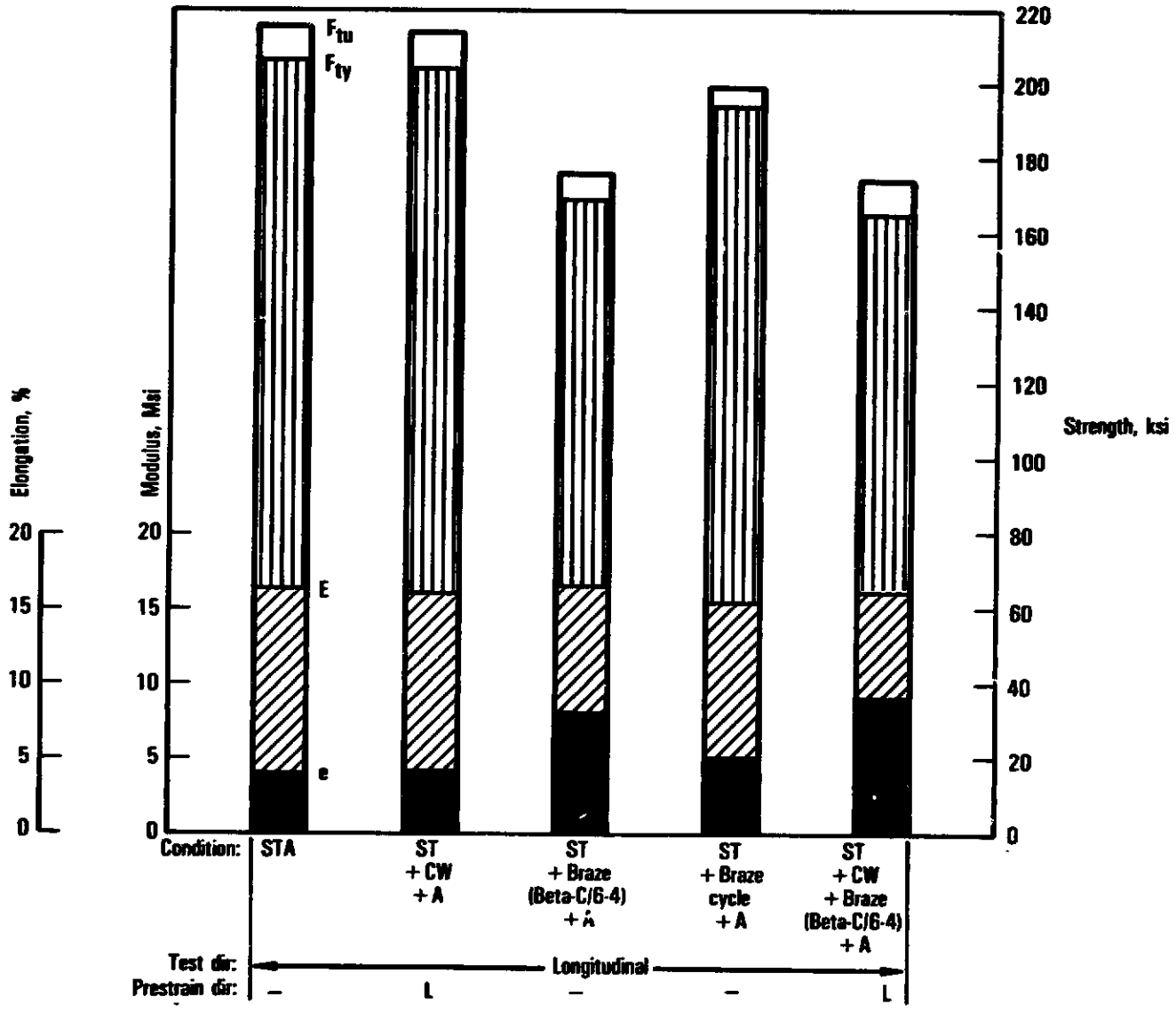

Figure 29. - Processing effects on -65°F tensile properties of Beta-C (average data).

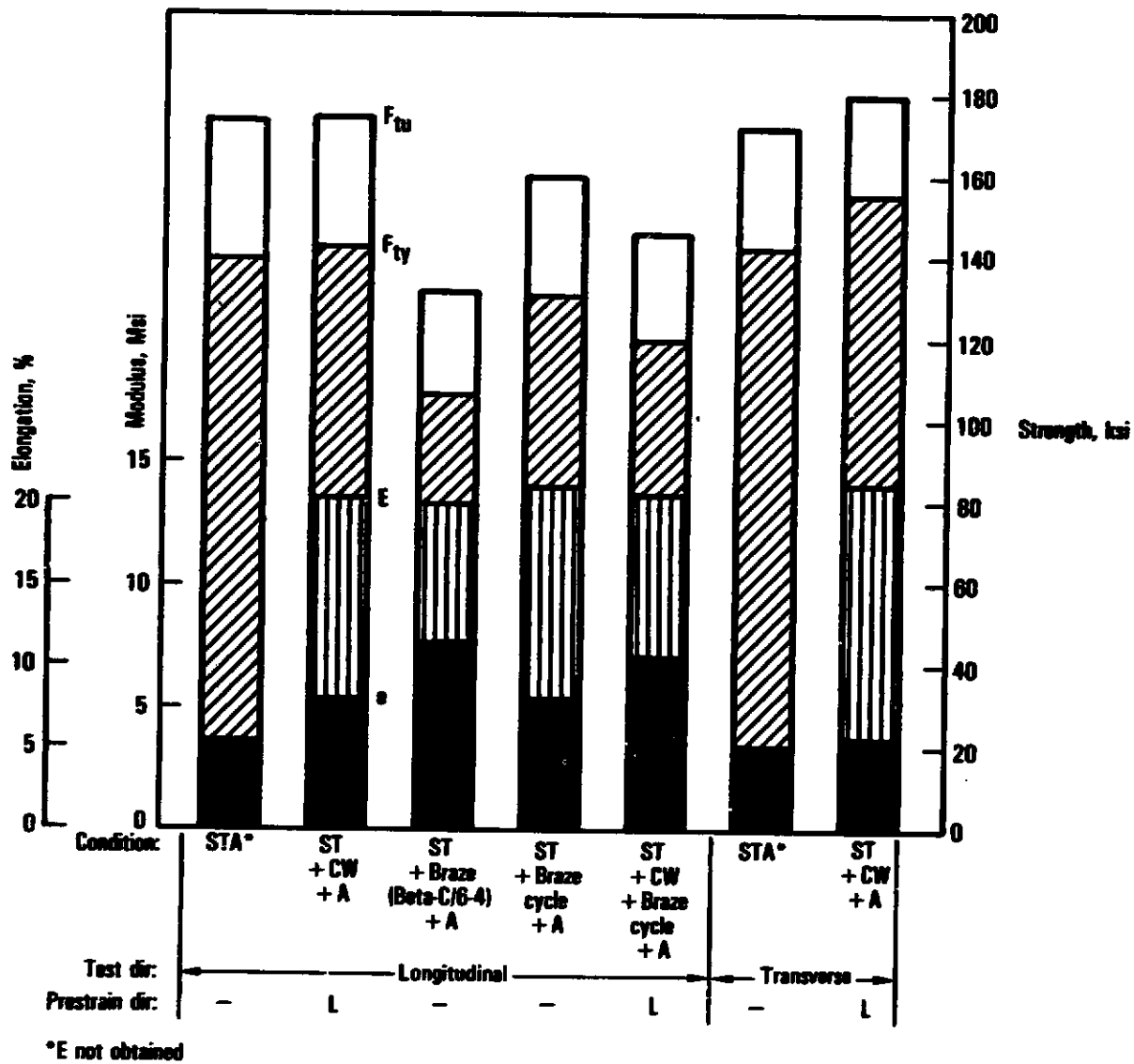

Figure 30. - Processing effects on 600°F tensile properties of Beta-C (average data).

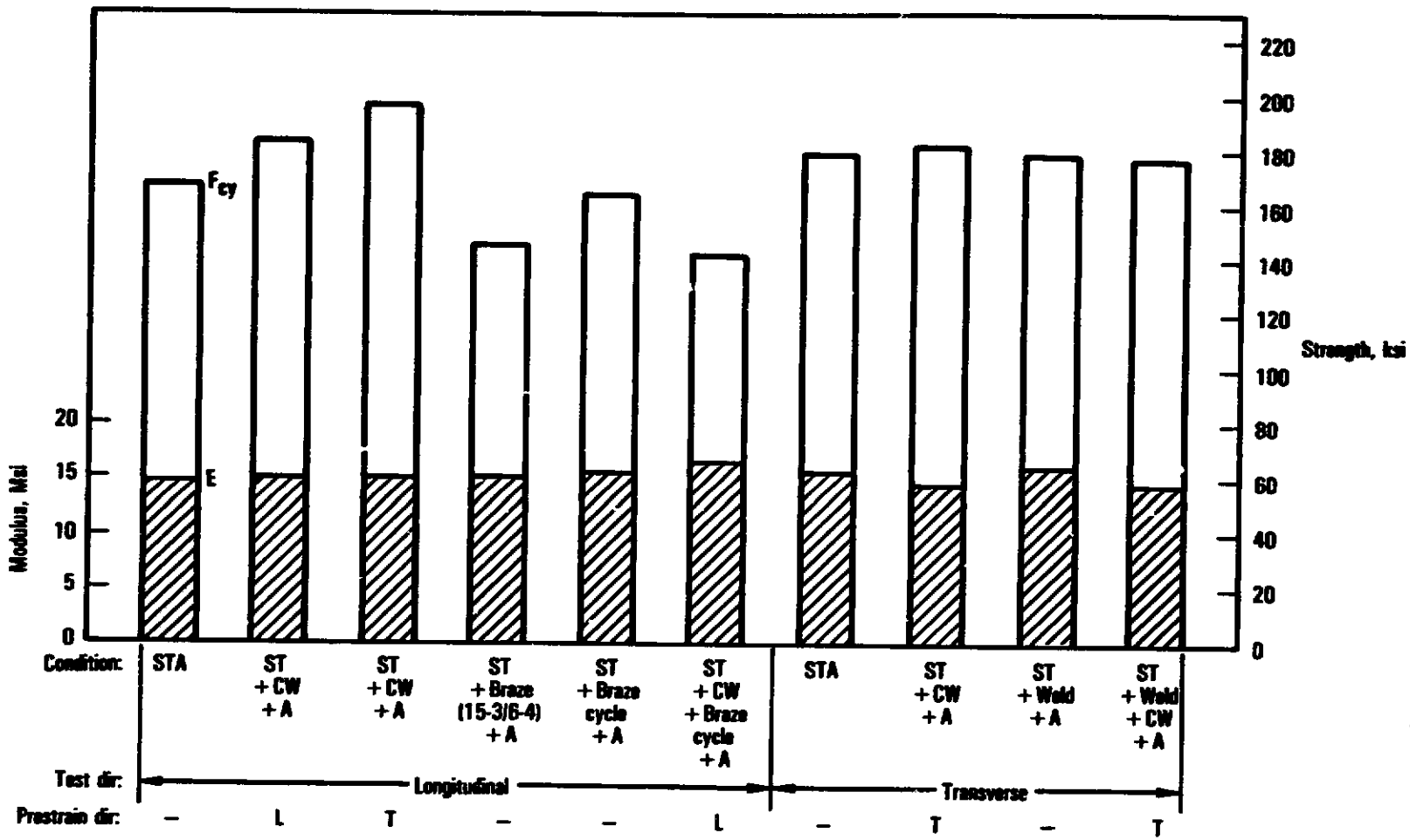

Figure 31. - Processing effects on room temperature compressive properties of Ti-15-3 (average data).

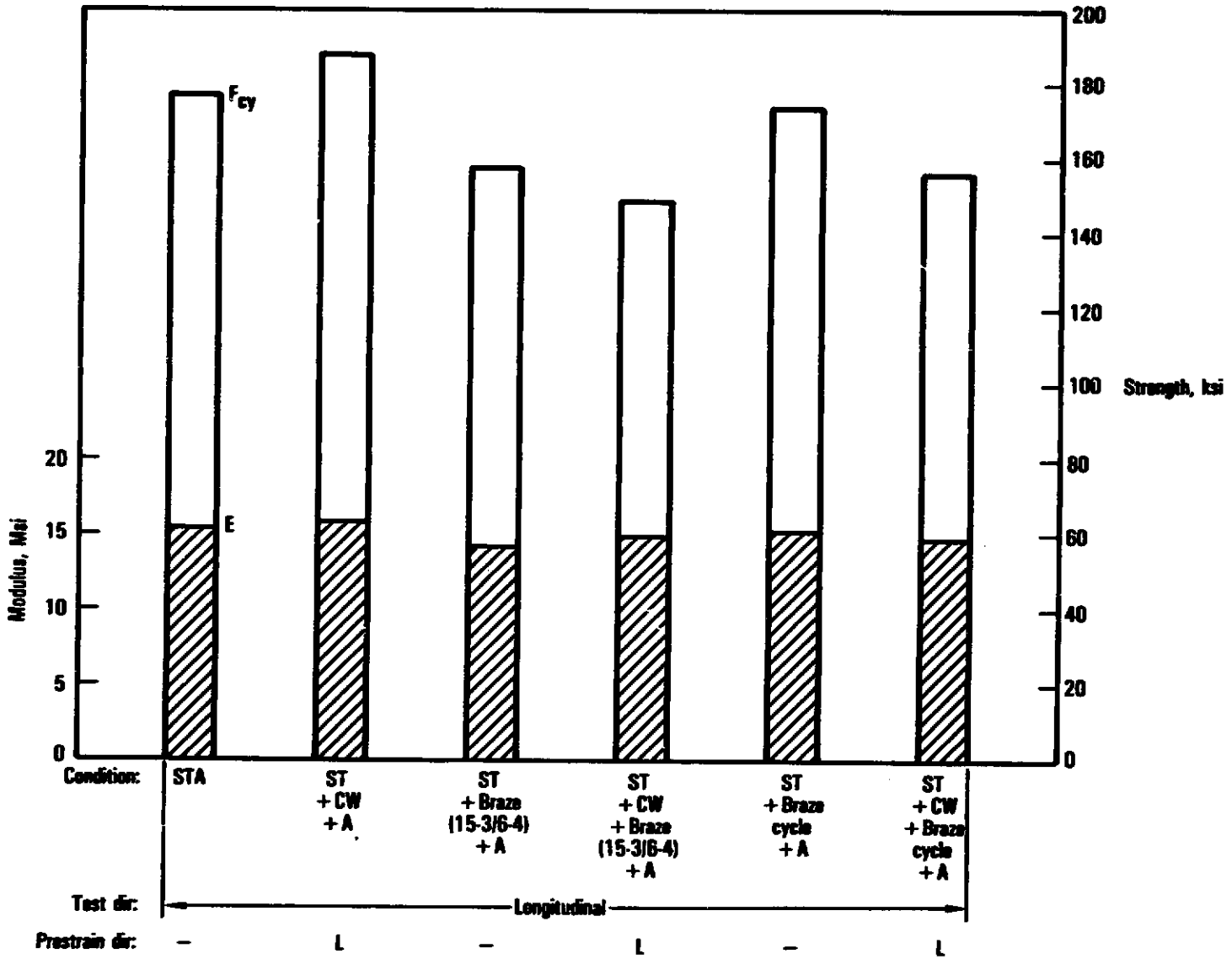

Figure 32. - Processing effects on -65°F compressive properties of Ti-15-3 (average data).

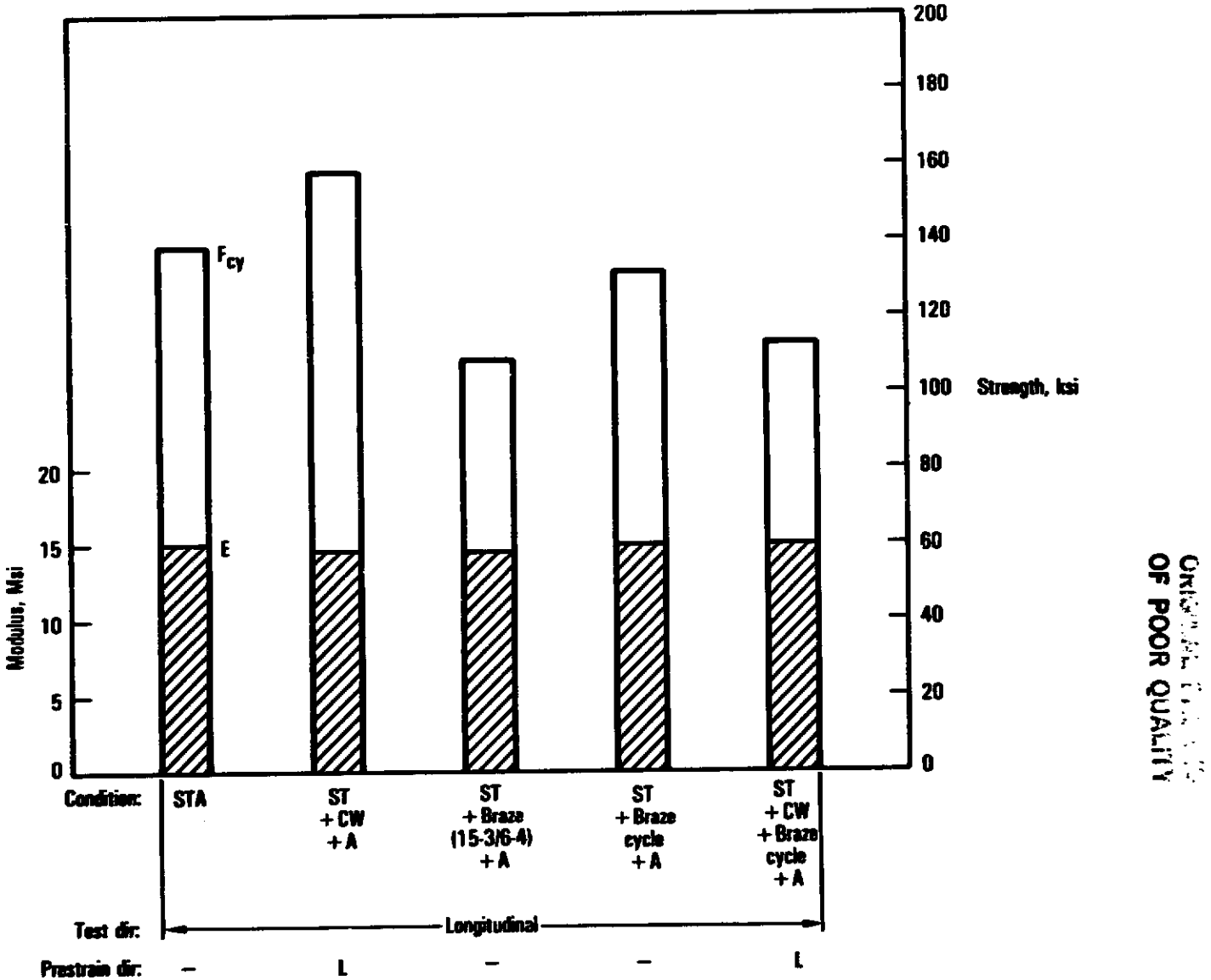

Figure 33. - Processing effects on 600°F compressive properties of Ti-15-3 (average data).

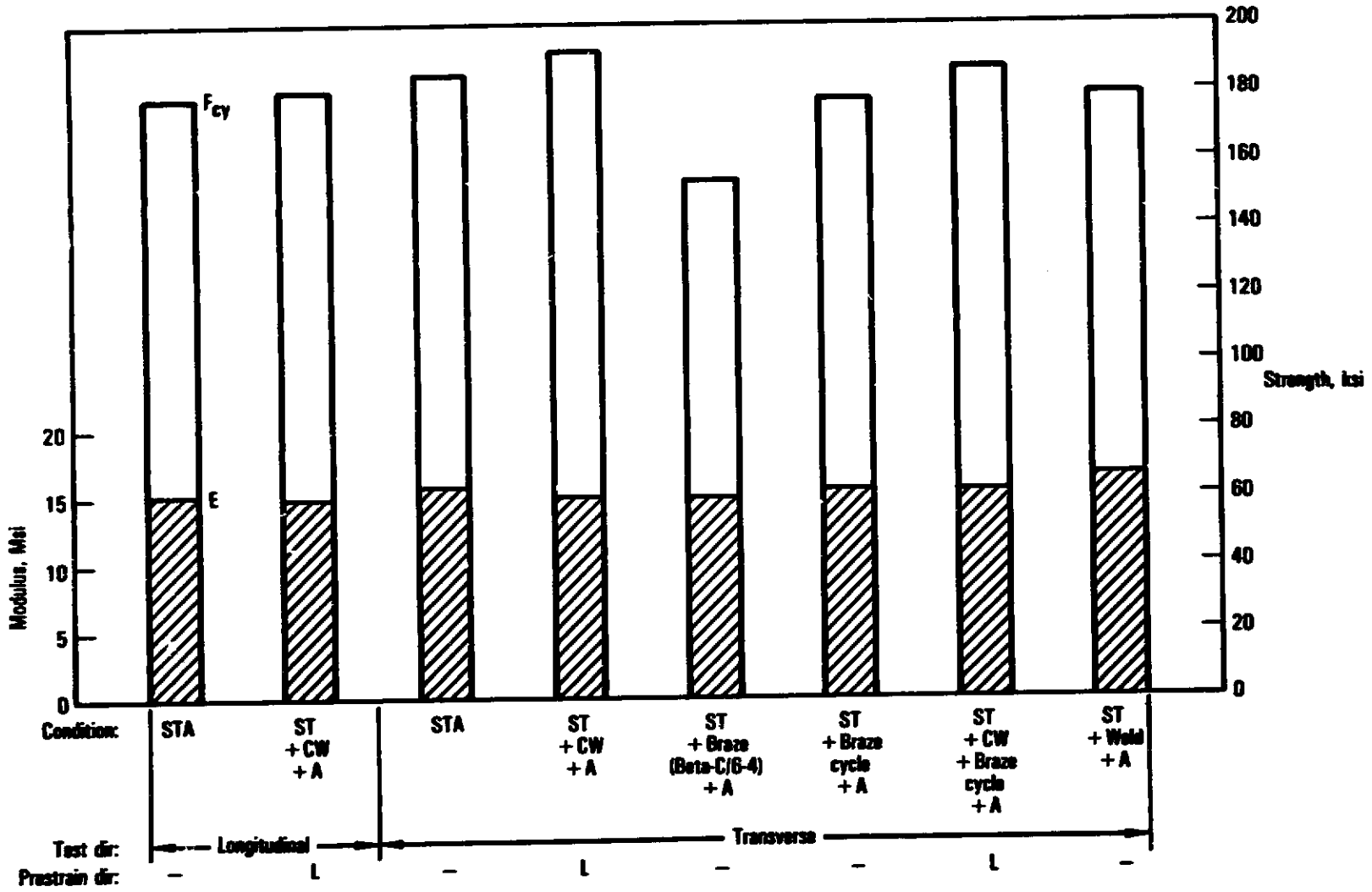

Figure 34. Processing effects on room temperature compressive properties of Beta-C (average data).

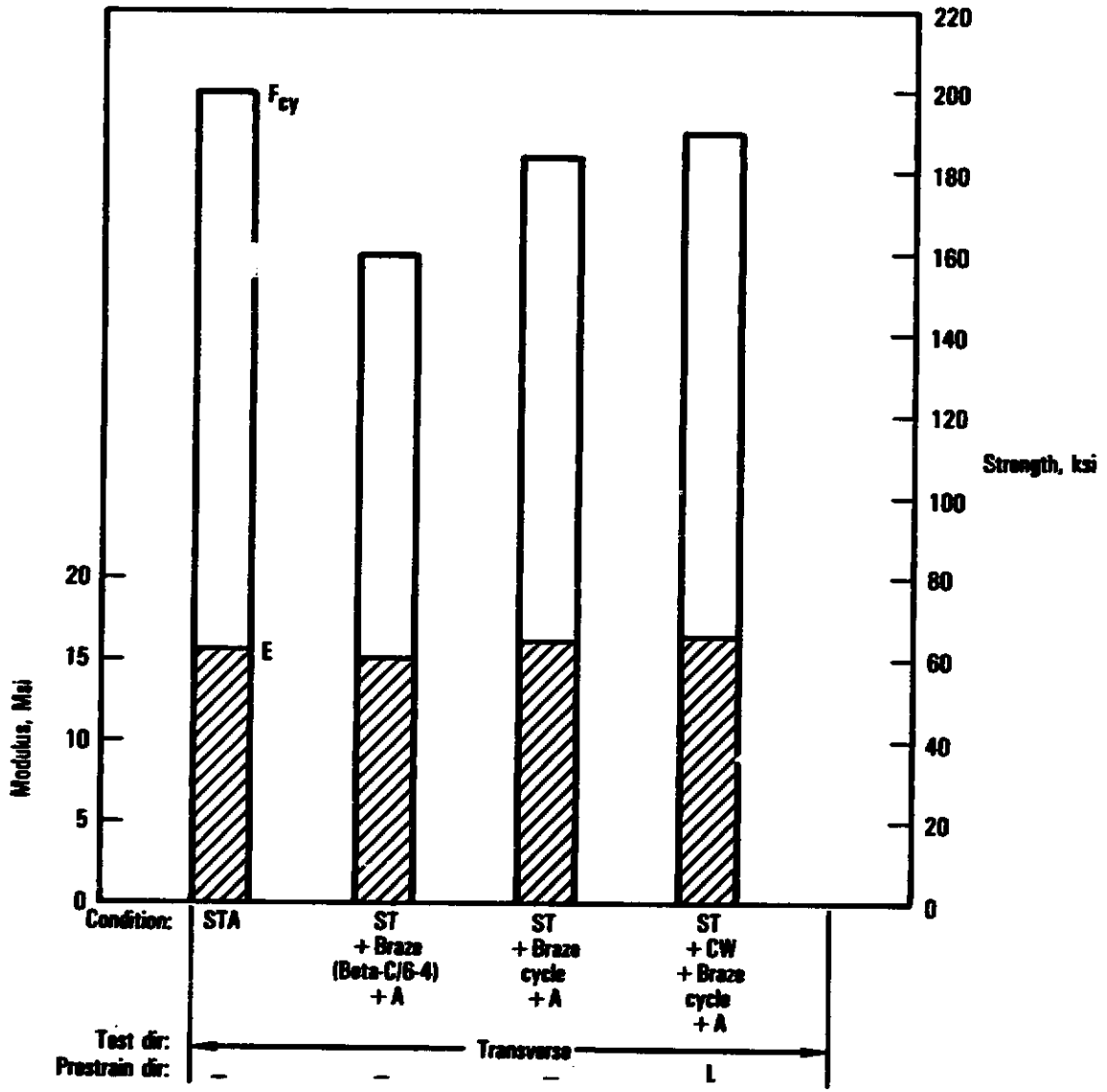

Figure 35. - Processing effects on -65°F compressive properties of Beta-C (average data).

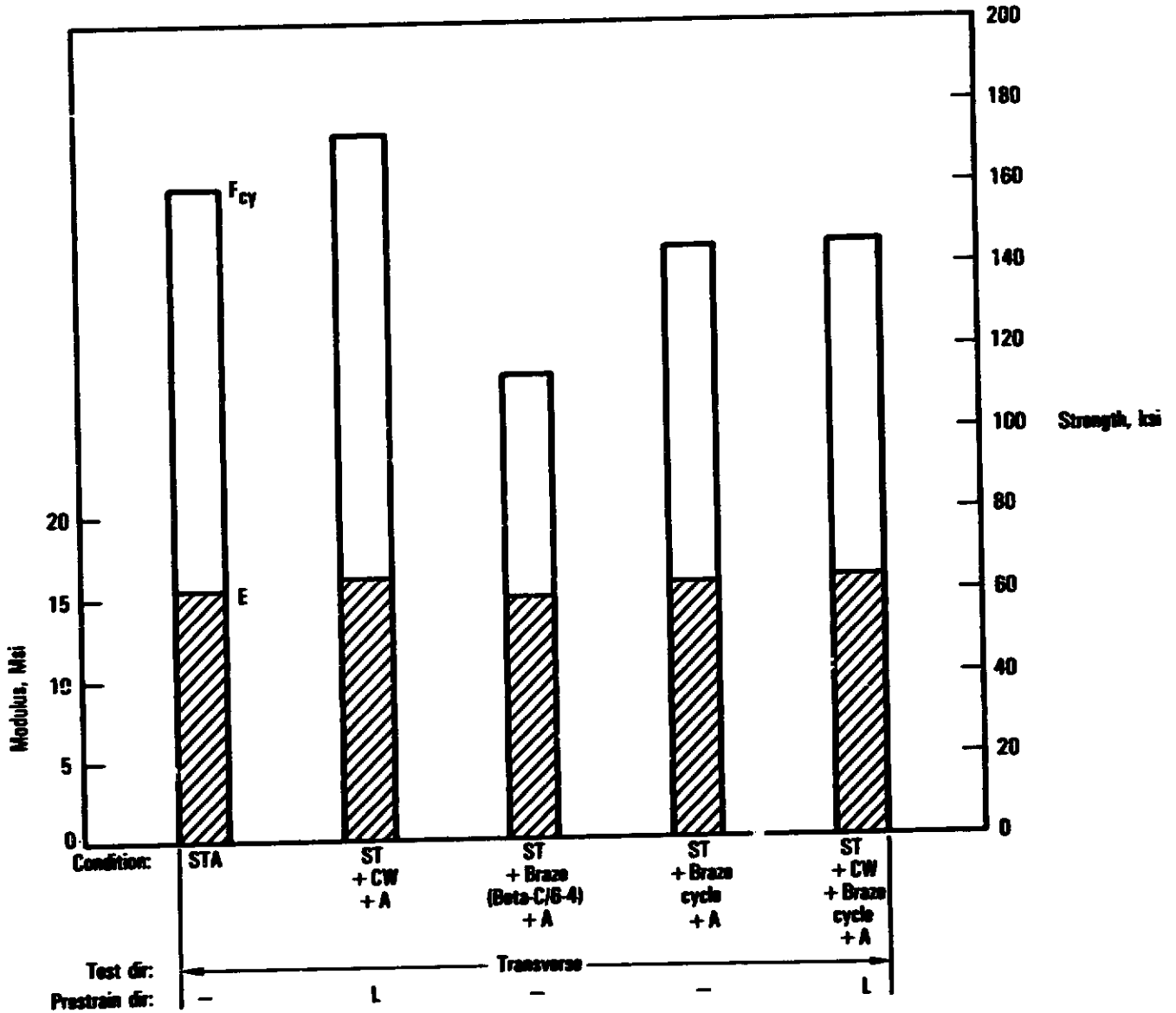

Figure 36. - Processing effects on 600°F compressive properties of Beta-C (average data).

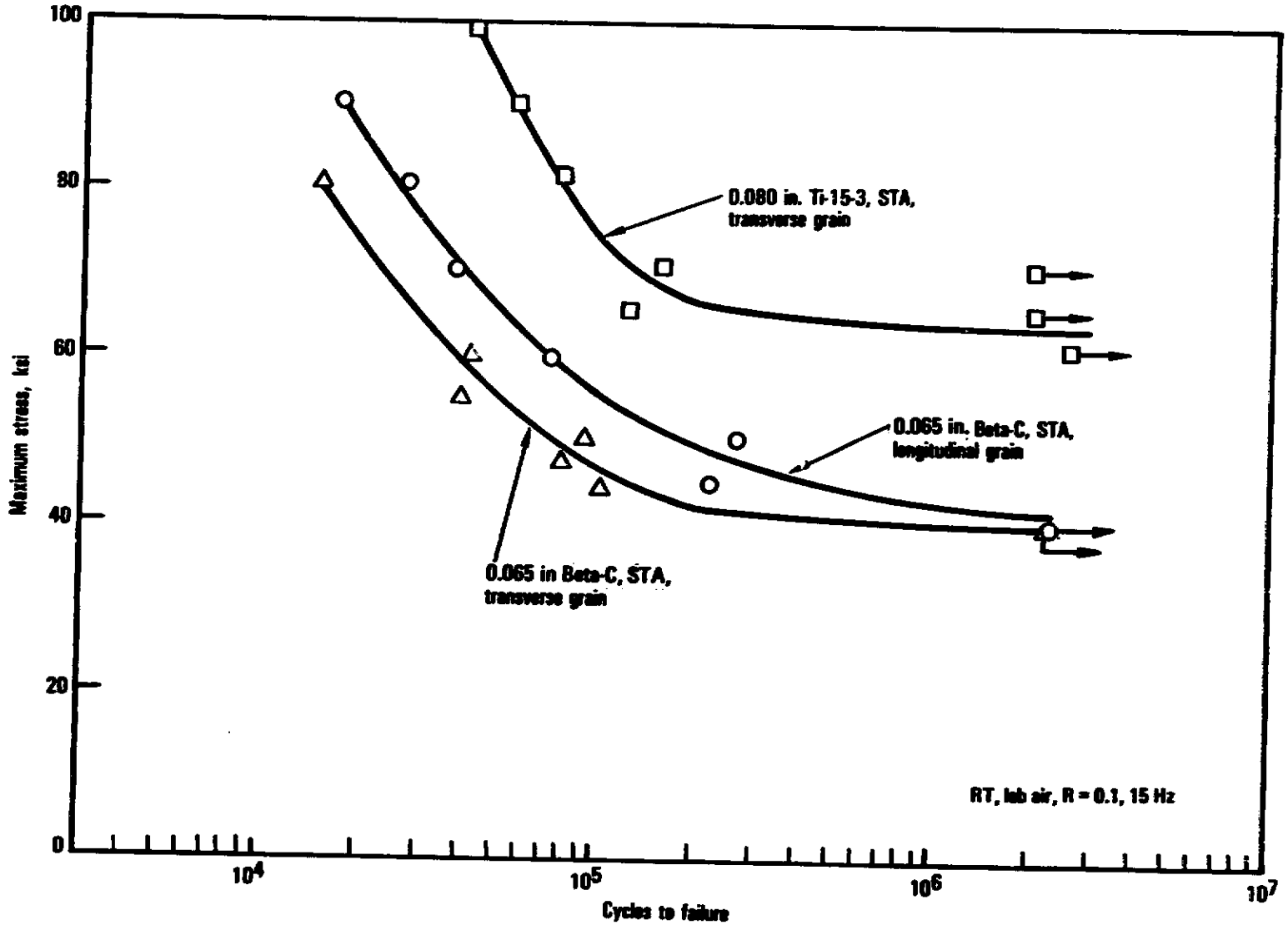

Figure 37. Parent unnotched (K_t = 1.0) fatigue test results for two beta titanium alloys

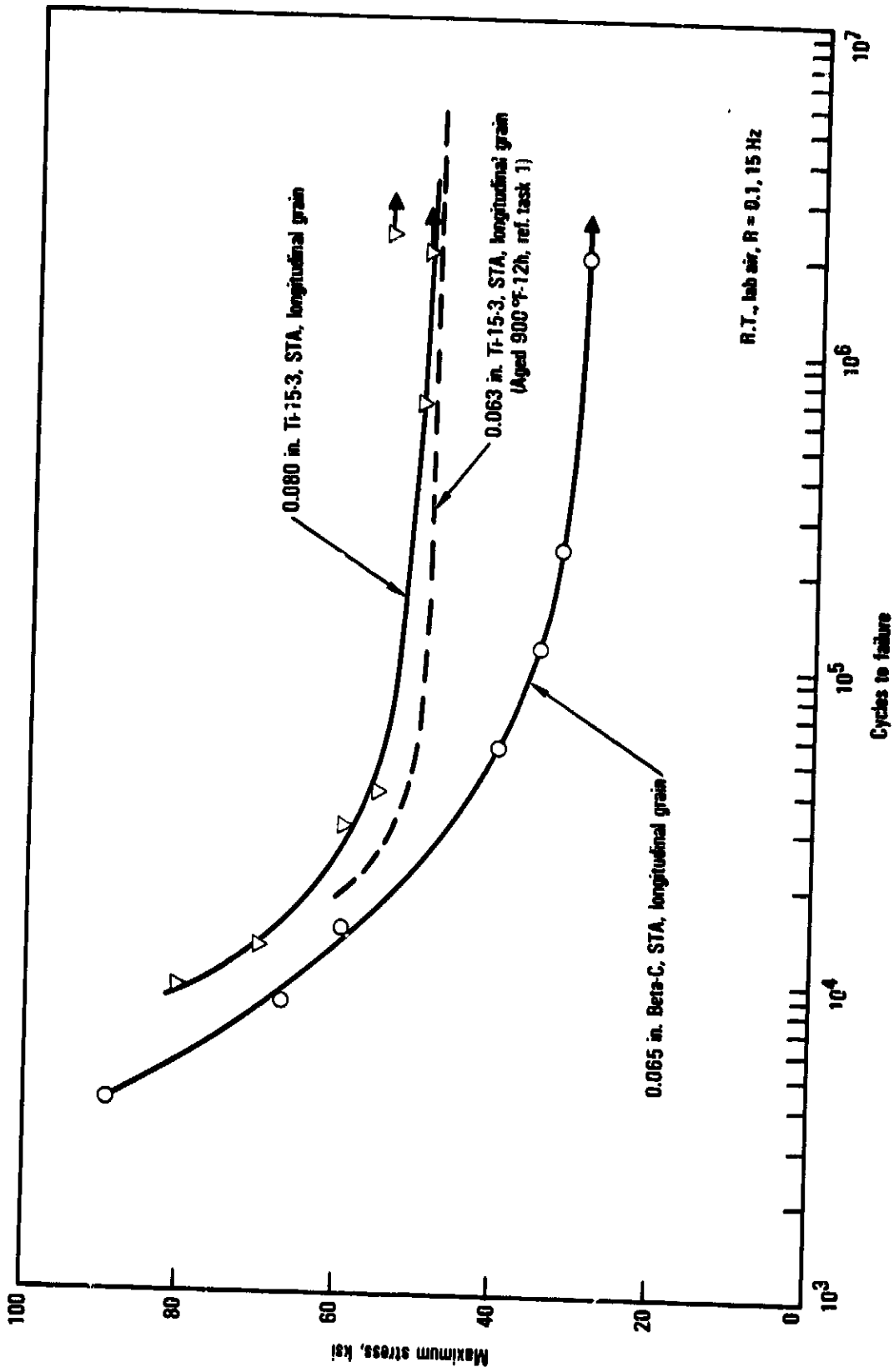

Figure 38. Parent notched (K_t = 2.6) fatigue test results for two beta titanium alloys

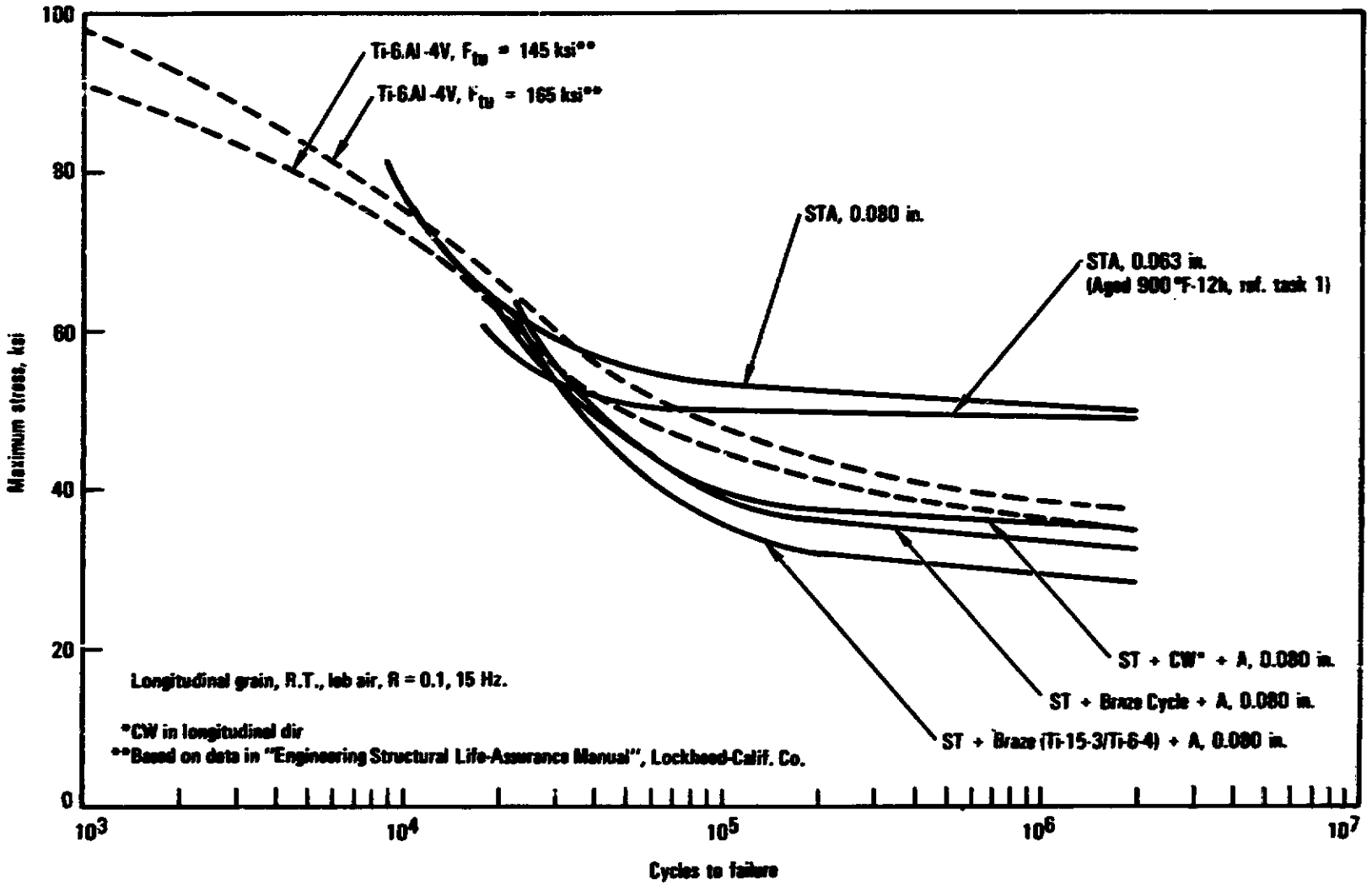

Figure 39. - Constant amplitude notched (K_t = 2.6) fatigue test results for 0.080 in. and 0.063 in. Ti-15-3 in various conditions

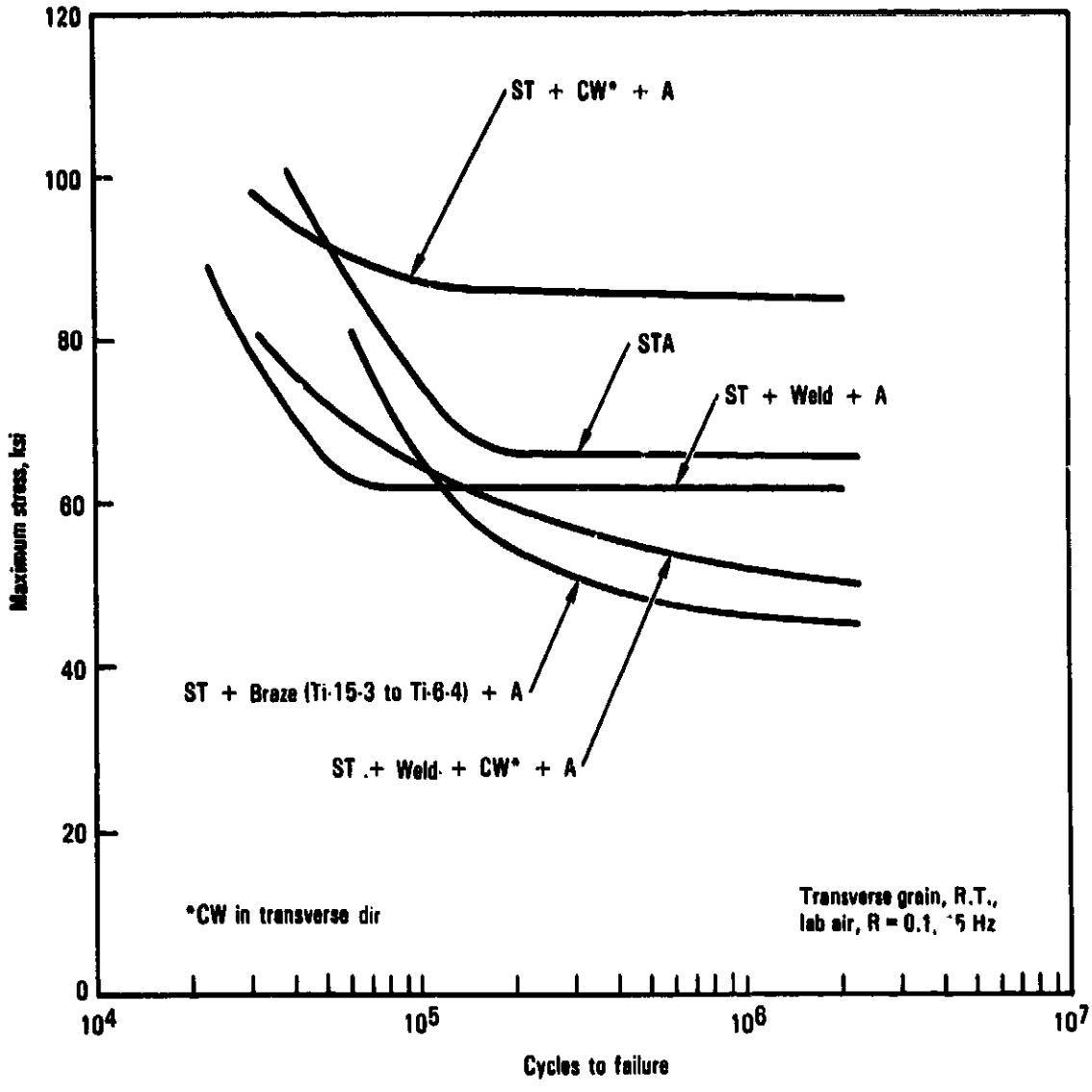

Figure 40. - Constant amplitude unnotched (K_t = 1.0) fatigue test results for 0.080 in. Ti-15-3 in various conditions

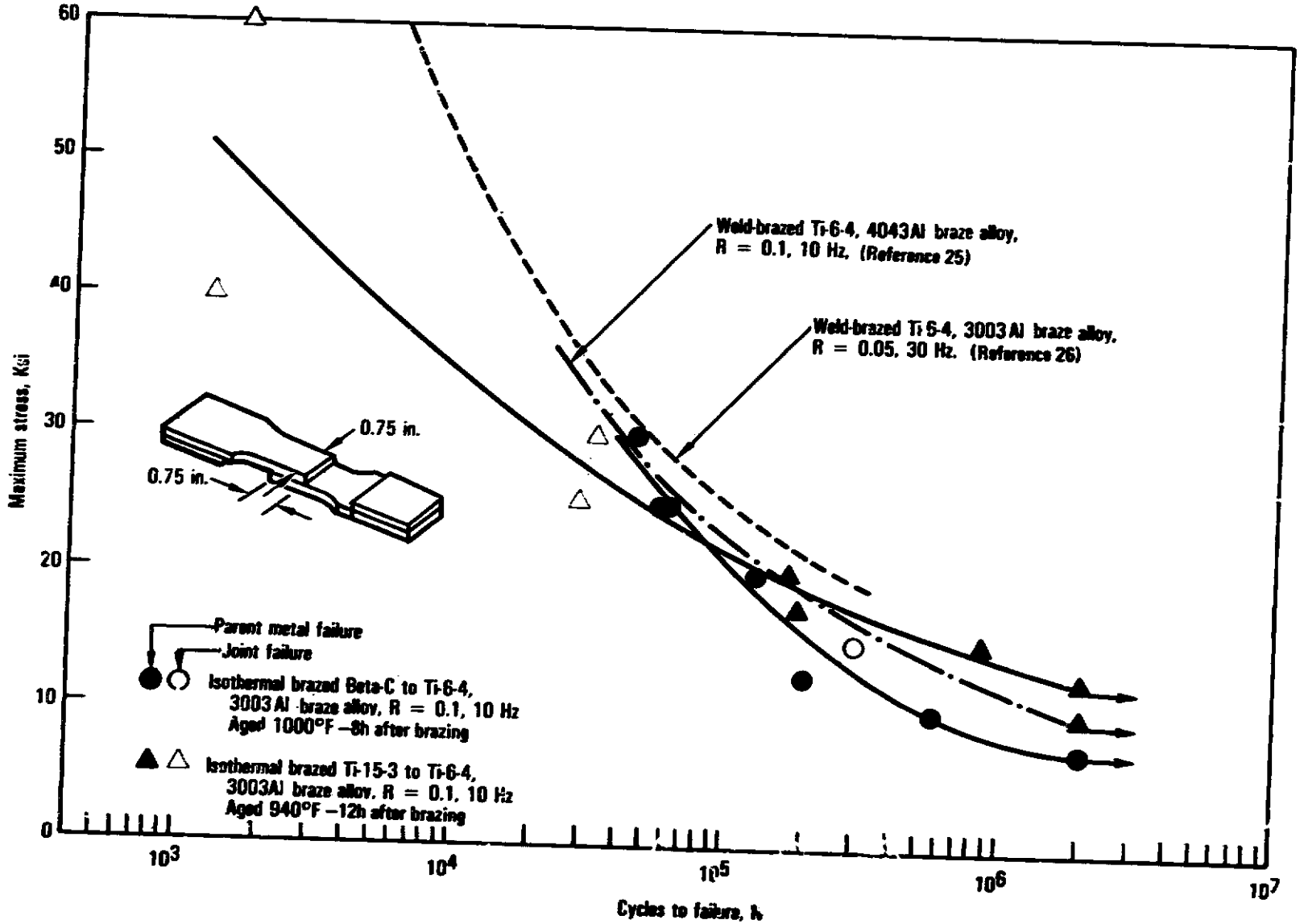

Figure 41. Room temperature fatigue test of single overlap brazed titanium joints.

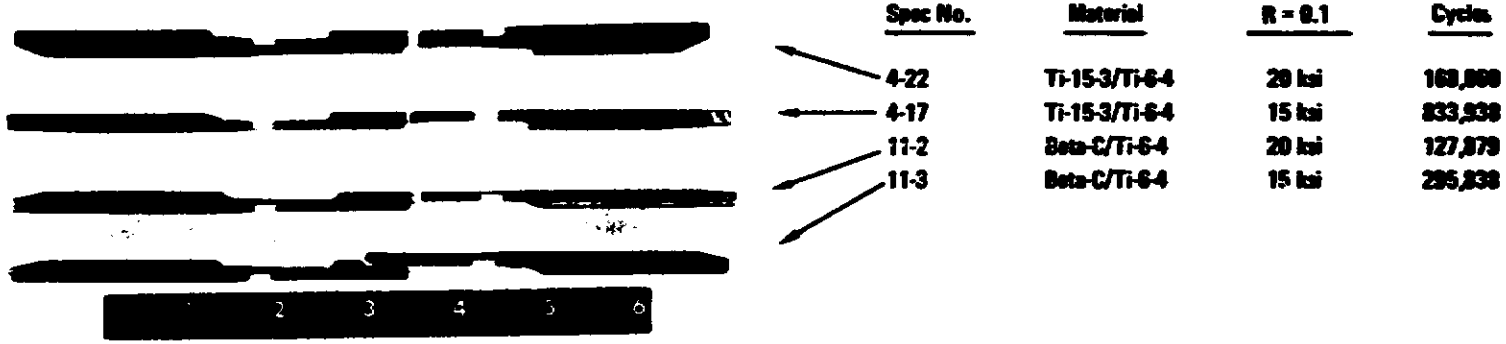

Spec No.	Material	Max. stress R = 0.1	Cycles
4-22	Ti-15-3/Ti-6-4	20 ksi	169,800
4-17	Ti-15-3/Ti-6-4	15 ksi	833,938
11-2	Beta-C/Ti-6-4	20 ksi	127,879
11-3	Beta-C/Ti-6-4	15 ksi	295,838

Figure 42. - Brazed lap shear fatigue samples selected for fractography.

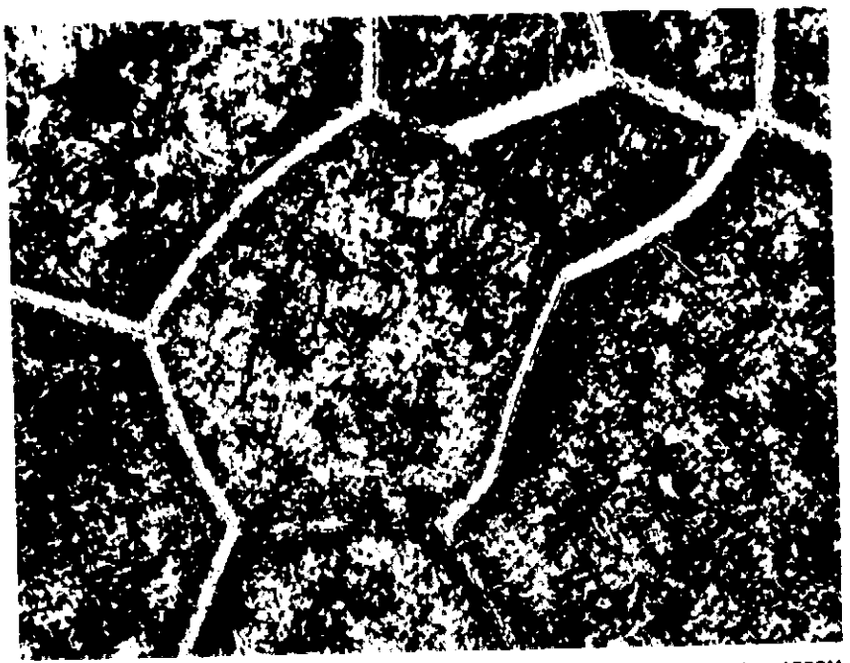

Mag. 1500X

Mag. 2000X

Figure 43. - Microstructure and fatigue crack path of brazed and aged lap shear specimen no. 4-17. Arrows denote grain boundary alpha-phase precipitate in the Ti-15-3.

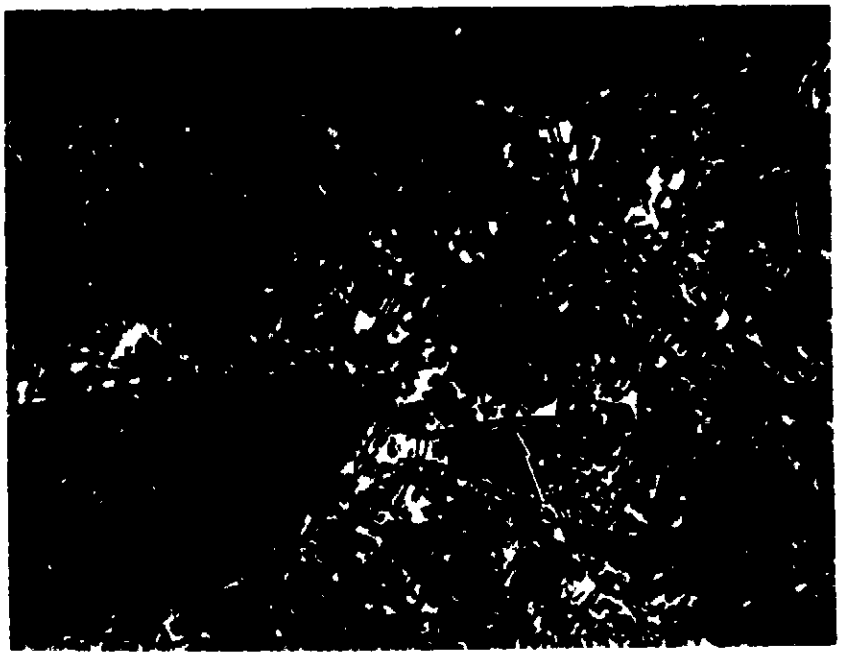

Mag. 1500X

Mag. 2000X

Figure 44. - Microstructure and fatigue crack path of brazed and aged lap shear specimen no. 11-2. Arrows denote grain boundary alpha-phase precipitate in the Beta-C.

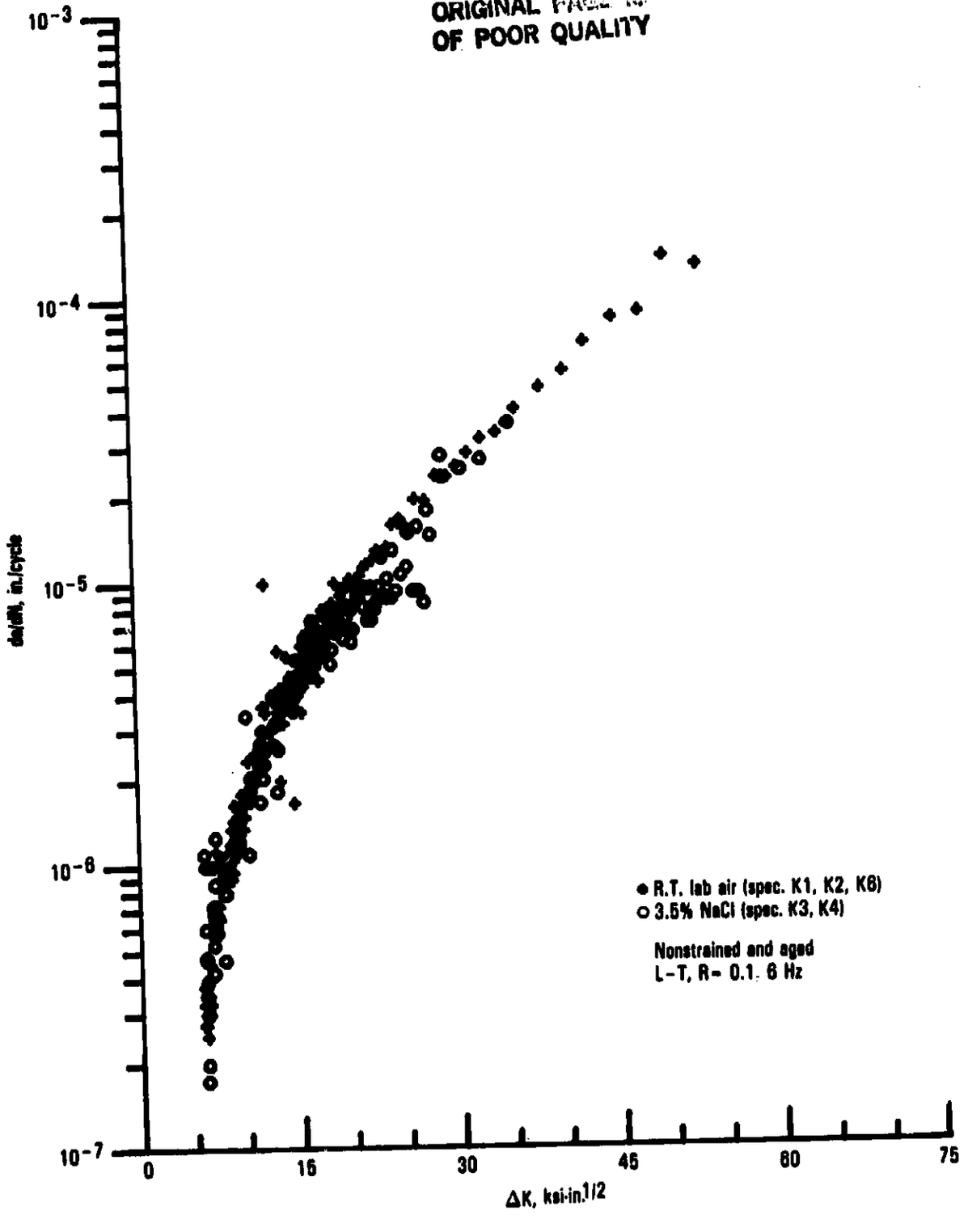

Figure 45. - Fatigue crack growth rates of 0.080 in. Ti-15-3 in air and saltwater.

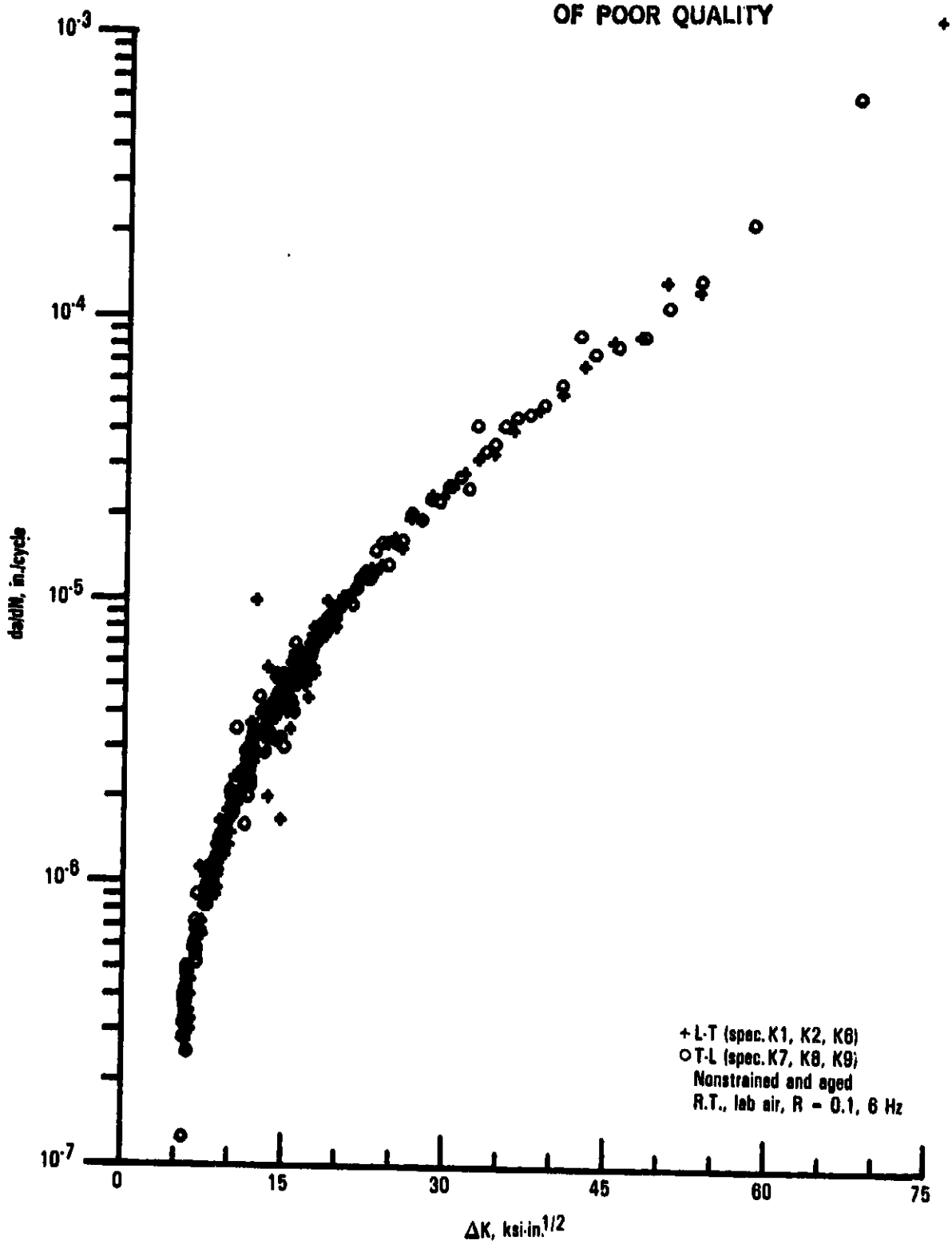

Figure 46. - Fatigue crack growth rates of nonstrained 0.080 in. Ti-15-3 in two directions.

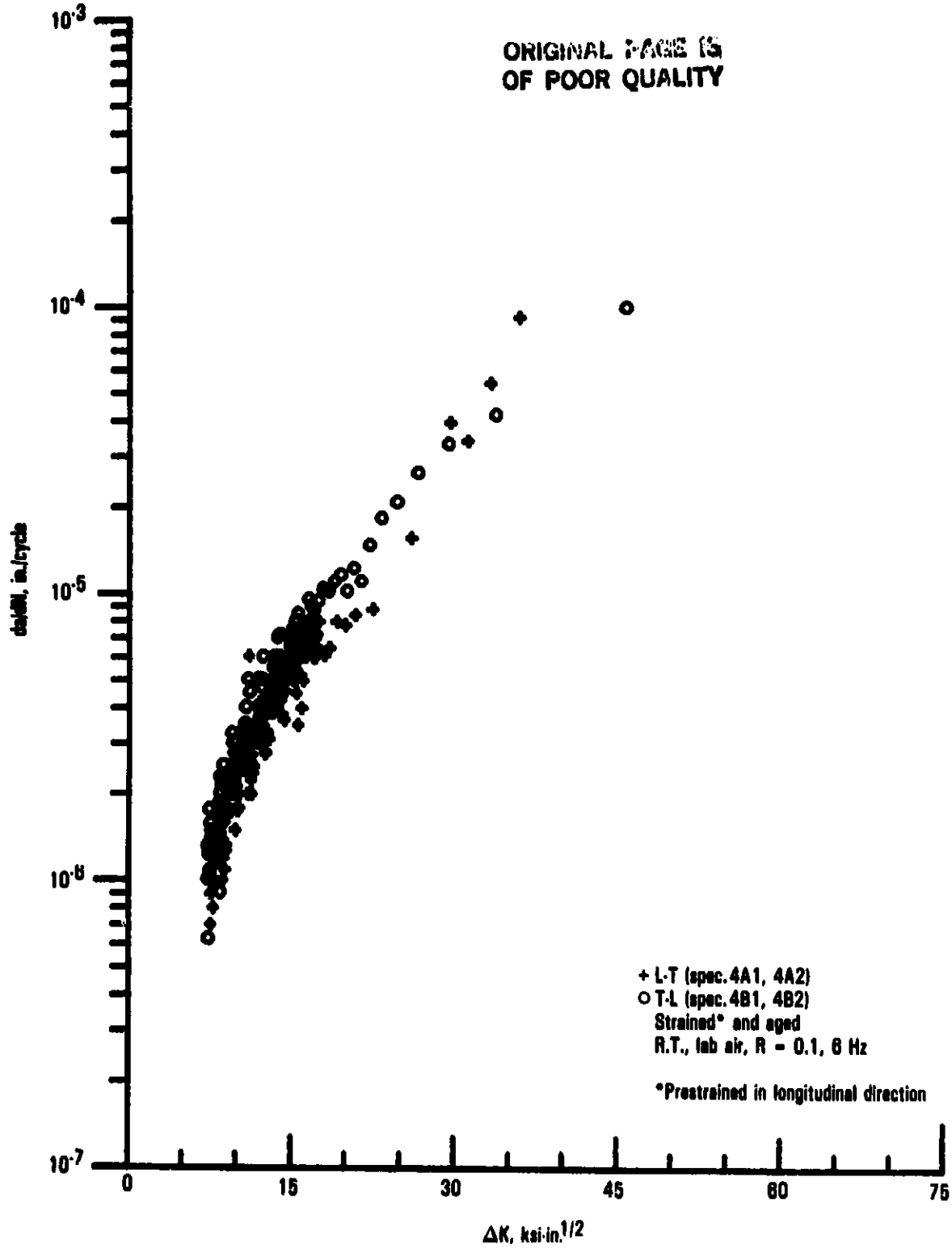

Figure 47. - Fatigue crack growth rates of prestrained 0.080 in. Ti-15-3 in two directions.

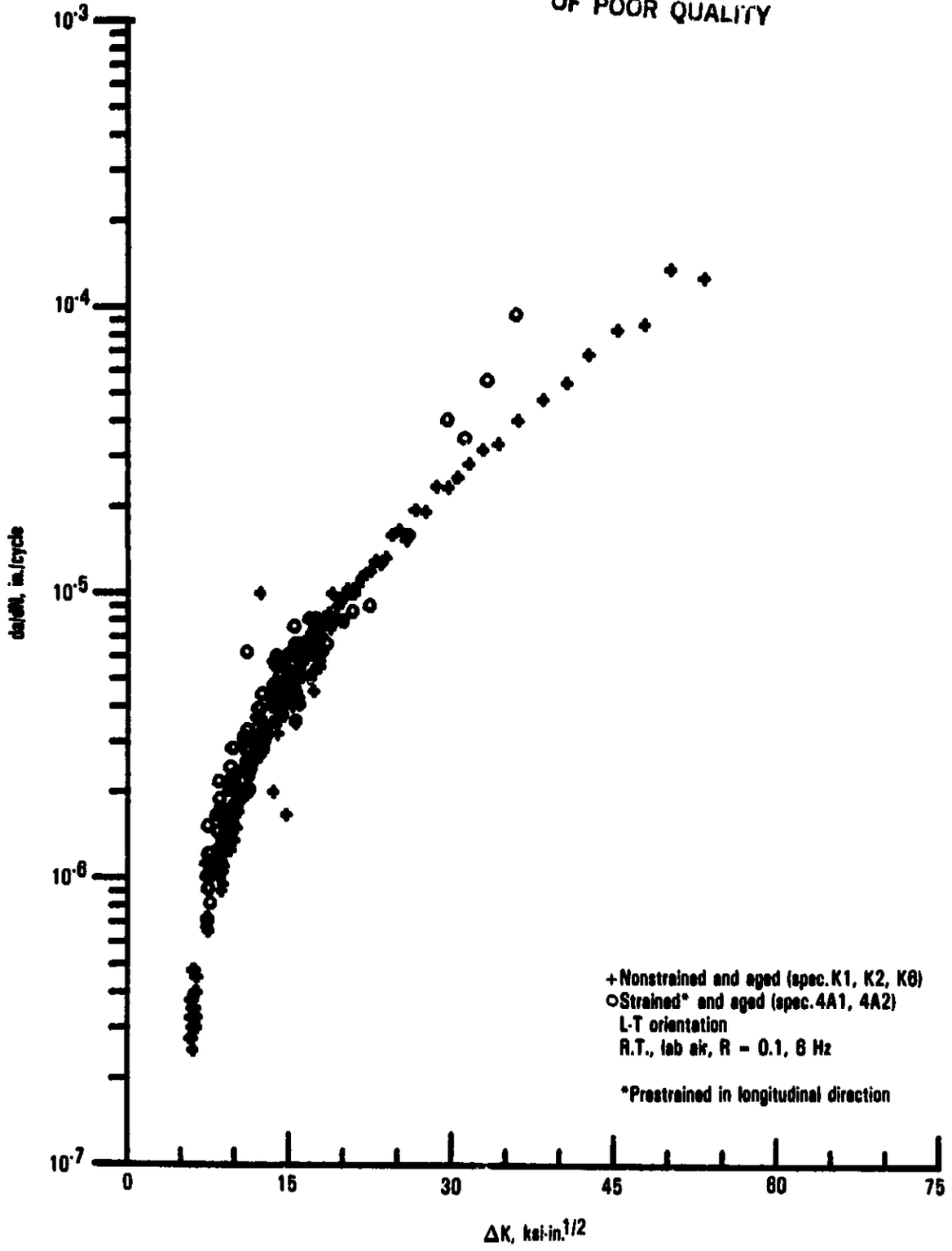

Figure 48. - Fatigue crack growth rates of nonstrained and prestrained 0.080 in. Ti-15-3 in L-T direction.

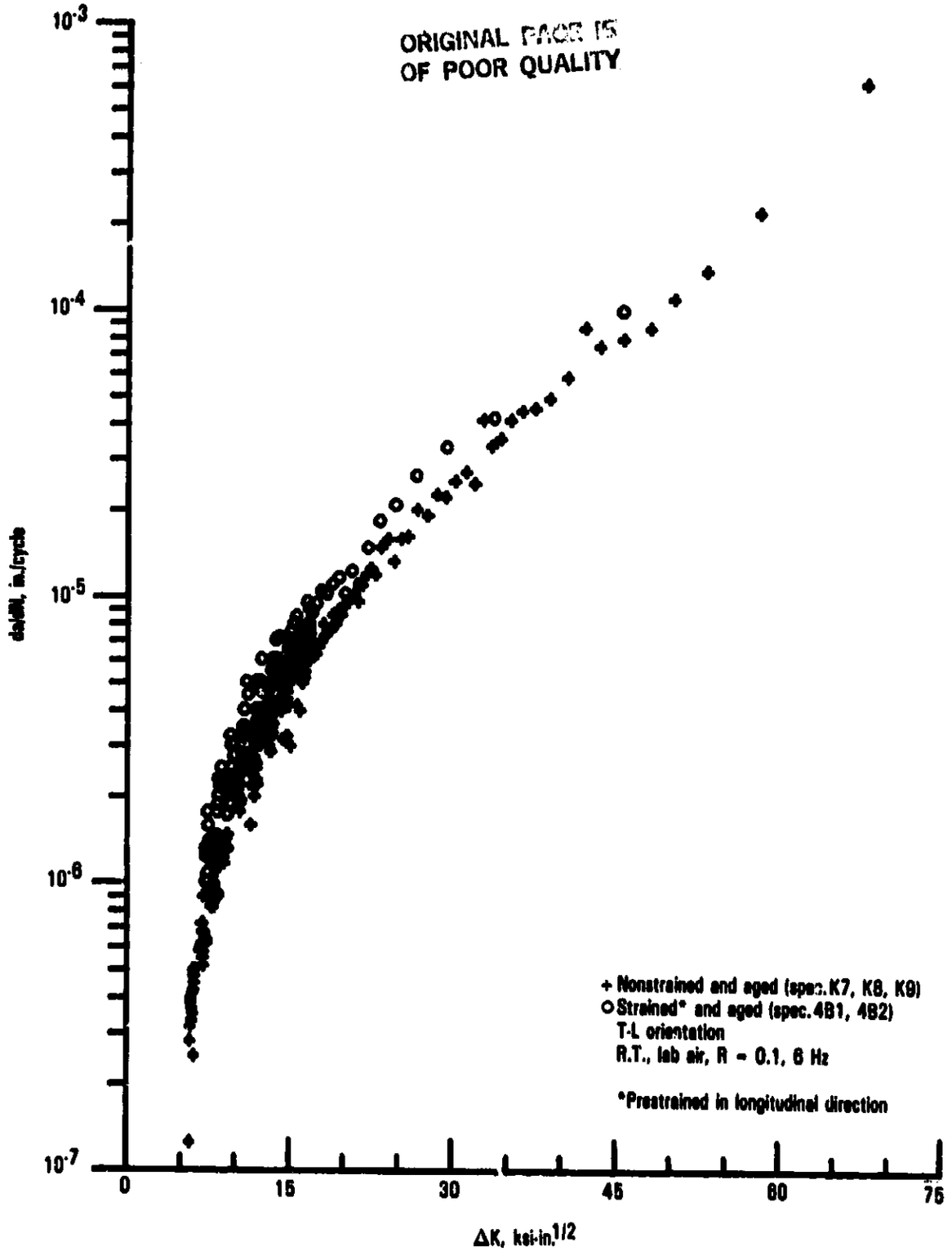

Figure 49. - Fatigue crack growth rates of nonstrained and prestrained 0.080 in. Ti-15-3 in T-L direction.

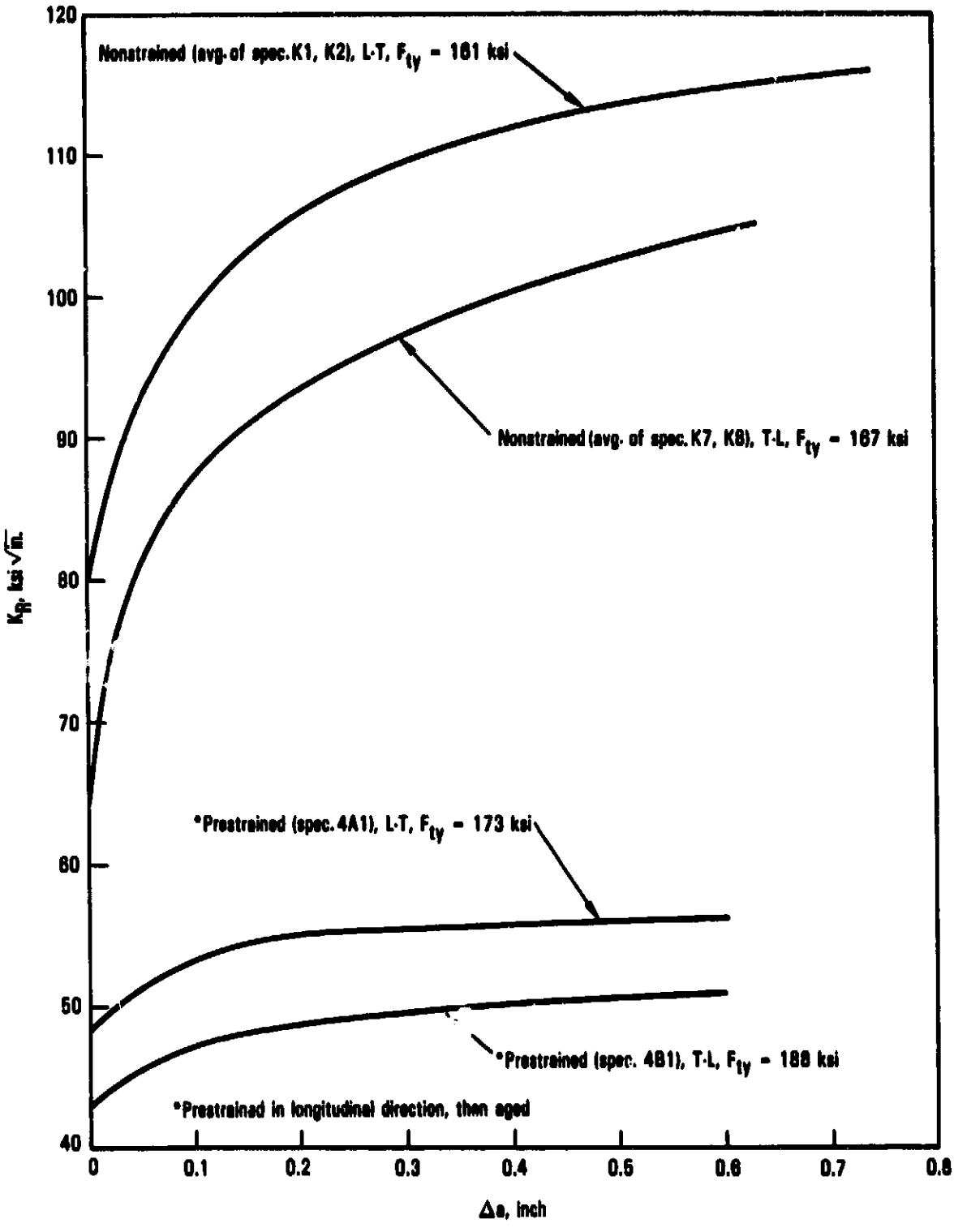

Figure 50. - K_R vs effective crack extension of aged 0.080 in. Ti-15-3.

TASK 5 - JOINING STUDIES

Low-cost brazing and welding methods were investigated as a means of more efficiently joining the beta alloys compared with conventional mechanical joints.

Brazing Development

An isothermal (hot die) brazing system was developed for joining beta alloy structural members, such as stringers, to beta alloy or Ti-6-4 skins. The brazing concept, illustrated in figure 51, employs aluminum-base brazing alloys and heated dies in a high purity argon atmosphere to achieve rapid out-of-furnace heating.

Initial efforts were directed at brazing the beta alloys in the STA condition. Tensile tests to explore the brazing cycle/aging compatibility, figure 52, indicated that a brazing temperature below about 1150°F was needed to minimize the strength loss due to overaging. Room temperature lap shear strengths of some candidate aluminum brazing alloys covering a range of brazing temperatures are shown in figure 53. Unfortunately, candidate brazing alloys with flow points below 1150°F, such as 718 (Al, 12 percent Si), Andry 389 (Al,Si, Mg, Sn, rare earths), and 391 (Al, Si, Mg, Cu, rare earths) were eliminated because of inferior shear strength and wettability.

In terms of shear strength and wetting, the two best aluminum braze alloys tested were 3003 (Al, 1.2 percent Mn), and 1100 (99 percent min. Al). But their liquidus temperature is about 1215°F, which dictated age-hardening after the brazing operation. Braze alloy 3003 was favored over 1100 because of its higher shear strength in all conditions tested (room temperature, 600°F, as-brazed, aged) for both Ti-15-3 and Beta-C brazements, as shown in figures 54 and 55, and its slightly better flow characteristics. Braze alloy 1100, however, showed an advantage in forming the thinnest titanium-aluminide intermetallic layer (0.00005 inch) of the materials studied.

A nominal joint gap of 0.003 inch was controlled using small dimples suitably spaced on one of the joint members. Thicker gaps provided no advantages while adding weight, and gaps of 0.001 inch or less were virtually uninspectable by conventional X-ray technique mainly because of the large difference in densities between the titanium members and the thin aluminum braze layer.

Ultrasonic C-scan and high sensitivity X-ray techniques verified good braze coverage with scattered voids. Representative ultrasonic standards having 1/16, 1/8, and 1/4 inch flat-bottom holes at the faying surface were used. Post shear and peel test examinations revealed good correlation between the non-destructive inspection (NDI) results and the void areas in the braze zone. Total aggregate area of voids not exceeding 15 percent of the joint faying surface was established as an acceptance level guide. Braze test joints and panels of tasks 4 thru 8 were X-ray and ultrasonic inspected, and for the most part met this braze quality level.

Photomicrographs of typical isothermal brazed joints of the beta alloys to Ti-6-4 using 3003 are shown in figure 56. Typical aging response (precipitate distribution) of the beta alloys as well as formation of a titanium-aluminide layer nominally 0.0002 inch thick may be seen.

Crippling tests. - Four small skin/stringer elements, each composed of a single beta alloy zee stiffener brazed to a skin segment of Ti-6Al-4V, were subjected to short column (crippling) tests at room temperature. This testing was performed to provide substantiating data on the integrity of the isothermal brazed section under compression loading and some preliminary design data for the task 6 panel crippling tests. Two specimens had Ti-15-3 stringers and two had Beta-C stringers. The basic specimen configuration and nominal dimensions are shown in figure 57.

The Ti-15-3 stringers were made from 0.063 inch thick annealed sheet, room temperature brake formed on a 2t radius in the longitudinal direction to the zee shape. The stringers were brazed to the annealed 0.040-inch thick Ti-6-4 skin segment, one specimen using 3003 aluminum brazing alloy and the other using 1100 aluminum brazing alloy. After brazing, the specimens were aged in air at 940°F for 12 hours.

The Beta-C stringers were 0.069 inch thick annealed sheet, room temperature brake formed in the transverse direction on a 4t radius. Again, one specimen was brazed with 3003 braze alloy and the other with 1100. After brazing, the specimens were aged in air at 1000°F for 8 hours.

The ends of the specimens were potted and machined flat, square, and parallel. The resulting test length was approximately 4 inches. Two uniaxial strain gages were installed back to back on each specimen, on the skin and attached stringer flange at the midspan of the test length (figure 57).

To ensure uniformity of loading, a 2 inch diameter steel bearing was located between the upper (fixed) test head and the steel compression block that rested directly on the machined surface of the upper potting box. The lower potting box remained in direct contact with the lower (movable) head of the test machine. An LVDT-type deflection transducer was installed parallel to the specimen to measure machine head travel. Testing was performed at ambient conditions in a Universal static test machine. A typical test installation is shown in figure 58.

The initial buckling for these specimens was the local buckling of the widest portion of the Ti-6-4 face sheet, which was the distance from the braze fillet to the free edge of the skin. The initial buckling stresses were calculated using Lockheed Stress Memo No. 80c, considering the widest portion of the face sheet as a flat plate with one edge free.

The calculation of the final failure stresses for these specimens was based on the crippling strength of the combined skin/stringer cross-section, and was made using the procedure outlined in Lockheed Stress Memo No. 126a. The skin/stringer configuration is divided into its component flat and curved elements and a local crippling stress is obtained for each element. This stress and the elemental area are then used to calculate the loading capability of each element. The average crippling stress of the specimen is determined by dividing the sum of these elemental loads by the total area of the cross section. The final failure stress was calculated using the average specimen dimensions for each design.

The analysis indicated that the failure stresses in the Ti-15-3 and the Beta-C were in the elastic regions of their respective stress-strain curves. Although the predicted stress in the skin at failure for the Beta-C specimens did enter the inelastic region of the Ti-6-4 stress-strain curve, the effect of plasticity was so small that it was ignored.

The material property data used for Ti-6-4 in the analyses were taken from reference 13. The properties for Ti-15-3 and Beta-C were based on the data obtained in tasks 3 and 4 of this contract. A summary of the correlation between the analysis and test results is presented in table 37 and discussed below:

- The two Ti-15-3 specimens had equivalent crippling strength regardless of the type of braze alloy used. Less than 1 percent variation was recorded between the failure stresses, and the predicted failure stress was conservative by about 17 percent. The failed specimens are shown in figure 59.

- A much wider variation in actual failure stresses was noted for the two Beta-C specimens. Specimen B had a significantly lower crippling strength than specimen A probably due to the realignment of the head during the testing of this specimen. The crippling strength of specimen A was 10 percent above its calculated failure stress and only 3 percent below that of the two Ti-15-3 specimens. The failed specimens are displayed in figure 60. Typical load/strain and load/deflection curves are presented in figure 61.

- For the Ti-15-3 specimens, the initial compression buckling stresses, as indicated by the divergence in the strain gage recordings, correlated well with the calculated buckling strength of the widest unsupported element on the Ti-6-4 skin segment. Initial buckling stresses of the Beta-C specimens were about 22 percent below the analytical prediction of the buckling strength of the widest unsupported skin element.

- It appears from these tests that the full crippling strength of the cross section can be attained using either 3003 or 1100 braze alloy.

Welding Development

Mechanized TIG arc welding was selected to demonstrate butt joining of beta alloy sheet or strip. Single-pass square butt welds without filler metal addition were made in 0.080 inch Ti-15-3 and 0.065 inch Beta-C sheet. The basic TIG welding machine setup was as follows:

Power Supply - Dimetrics 600 amp DC at 16 kHz, DCSP

Programmer - Dimetrics Gold Track II

Carriage - Dimetrics with AVC head

Torch Gas - Helium

Trailing shield and underside gas - Argon, with Lockheed-designed purge control box to maintain preset flow and pressure to underbead.

Electrode - 2 percent thoriated tungsten, 3/32 inch diameter machined to 25-degree included angle with 0.020 inch diameter point.

Cup - No. 12

Sheet preparation - Milled edge, alkaline clean, Nitric-HF acid pickle, draw file and acetone wipe just prior to welding.

The weld beads were within 0.006 inch of flush and not dressed. Welds met dimensional, X-ray, penetrant, and metallographic inspection criteria for critical structural aircraft welds, with only some minor scattered porosity evident.

Weldments were evaluated as-welded and after aging. Tension and bend test results are given in table 38 for Ti-15-3 and table 39 for Beta-C. Full joint efficiencies with good ductility were attained in both as-welded and weld plus aged conditions. The Ti-15-3 TIG welds withstood a 4t bend radius and the Beta-C welds made 3t, confirming good as-welded ductility.

Microhardness surveys of the Ti-15-3 and Beta-C weldments were made on as-welded and weld plus aged joint cross-sections. The hardness traverses are shown in figures 62 (Ti-15-3) and 63 (Beta-C) along with the cross-sectional photomacrographs. For either alloy the hardness values were substantially uniform across the base metal, heat-affected zone (HAZ) and weld, in both weld conditions, without notable hard or soft zones. The as-welded Ti-15-3 does appear to display a minor aging reaction in the vicinity of the HAZ, which was compatible with the tensile failures occurring in the softer weld zone.

TABLE 37. - ANALYSIS AND TEST RESULTS OF ROOM TEMPERATURE SHORT-COLUMN CRIPPLING TESTS OF ZEE-STIFFENED ELEMENTS

Specimen ID	Description	Initial Buckling, psi		Failure, psi		Comments
		Prediction	Test	Prediction	Test	
2	Ti-15-3 stringer/ Ti-6-4 skin (3003 aluminum braze)	65,900	66,600	94,700	113,400	Showed some evidence of separation at the braze interface between the stringer and skin
4	Ti-15-3 stringer/ Ti-6-4 skin (1100 aluminum braze)	64,500	62,300	94,700	114,300	Showed no visible evidence of separation at the braze interface
A	Beta-C stringer/ Ti-6-4 skin (3003 aluminum braze)	69,500	57,400	99,300	110,300	Stringer contained twist prior to potting Stringer popped loose from the skin segment at maximum load
B	Beta-C stringer/ Ti-6-4 skin (1100 aluminum braze)	66,900	54,100	99,300	89,000	Head realignment noted following initial buckling Load dropped well below maximum value before separation was observed at braze interface

Note: All stresses are averaged

TABLE 38. - MECHANICAL PROPERTIES OF TIG WELDS IN 0.080-INCH T1-15-3

Condition	Weld Dir	Test Dir (1)	Tension Tests (4)				Min Bend Radius (2)
			F_{tu}, ksi	F_{ty}, ksi	e, %	Where Failed	
ST	–	T	110	109	18	–	2t
ST + Weld	L	T	110	107	9	Weld	–
ST + Weld	L	T	111	109	10	Weld	–
ST + Weld	L	T	113	111	8.5	Weld	–
ST + Weld	L	T	–	–	–	–	4t
ST + Weld + Age (3)	L	T	186	176	6.5	Base Metal	–
ST + Weld + Age (3)	L	T	185	175	6.5	Base Metal	–
ST + Weld + Age (3)	L	T	186	174	6	Base Metal	–

(1) Bend axis or loading direction as applicable.
(2) Bent thru 105°, and acceptable with both weld face and root on OD of bend.
(3) 925°F for 12 hours
(4) Specimen Configuration: Figure A1

TABLE 39. - MECHANICAL PROPERTIES OF TIG WELDS IN 0.065-INCH BETA-C

Condition	Weld Dir	Test Dir (1)	Tension Tests (5)				Min Bend Radius (2)
			F_{tu}, ksi	F_{ty}, ksi	e, %	Where Failed	
ST	–	T	133	132	8.0	–	4t
ST + Weld	L	T	129	123	7.5	Weld	–
ST + Weld	L	T	131	125	7.5	Weld	–
ST + Weld	L	T	132	126	7.0	Weld	–
STA (3)	–	T	–	–	–	–	3t
ST + Weld + Age (4)	L	T	179	166	5.2	–	–
ST + Weld + Age (4)	L	T	179	171	3.0	Weld	–
ST + Weld † Age (4)	L	T	178	168	3.0	Weld	–
			182	170	3.0	Weld	–

(1) Bend axis or loading direction as applicable.
(2) Bent thru 105°, and acceptable with both weld face and root on OD of bend.
(3) Interpolated from 1000°F, 8 and 10 hour aging data in task 3.
(4) 1000°F for 8 hours.
(5) Specimen Configuration: Figure A1

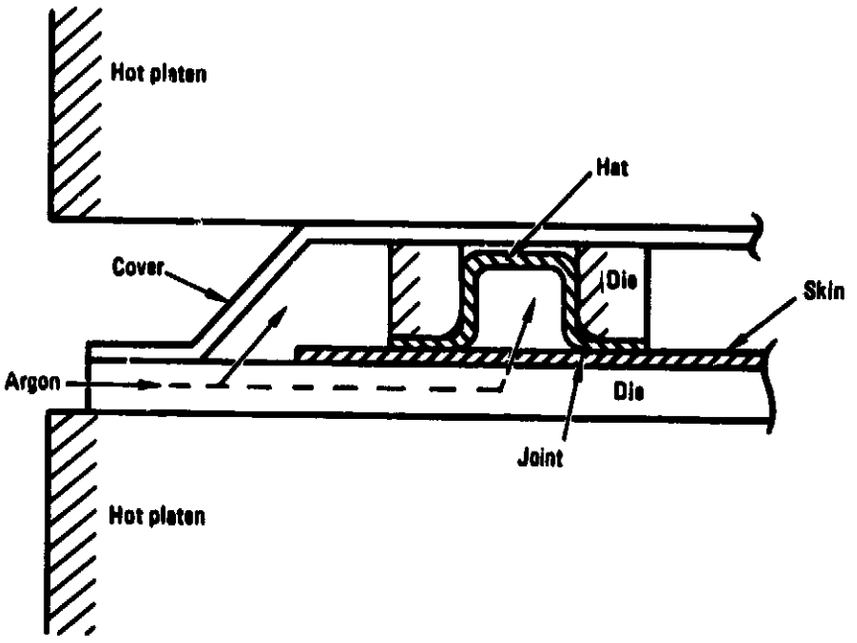

Figure 51. - Isothermal brazing concept.

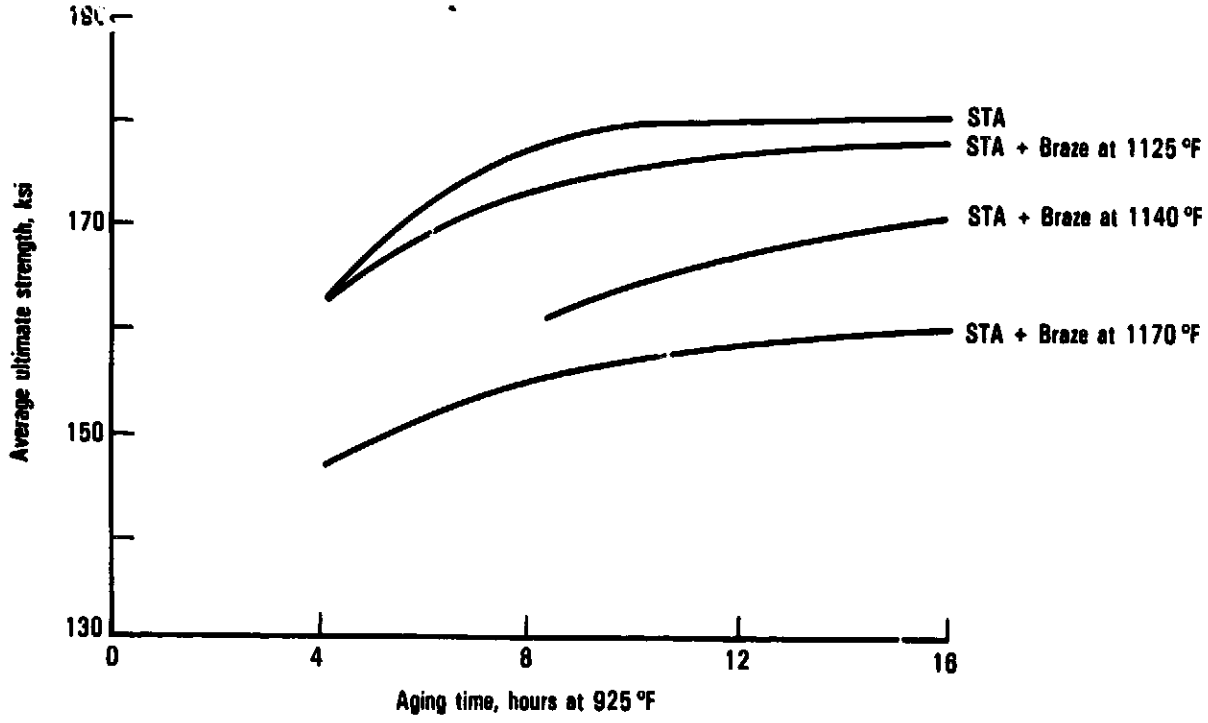

Figure 52. - Effect of braze cycle on tensile strength of Ti-15-3 sheet.

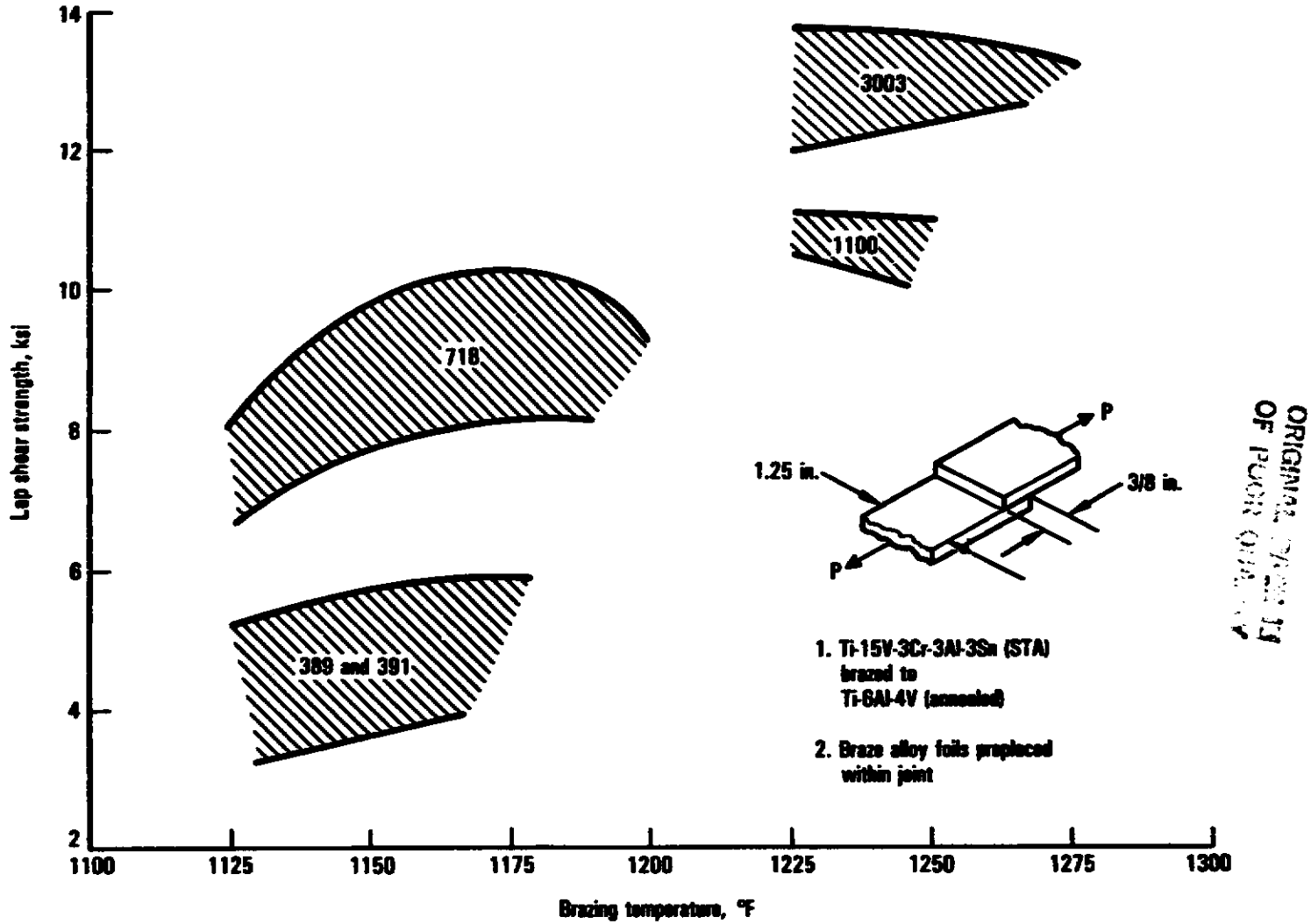

Figure 53. - Room temperature brazed joint shear strength of some candidate aluminum brazing alloys.

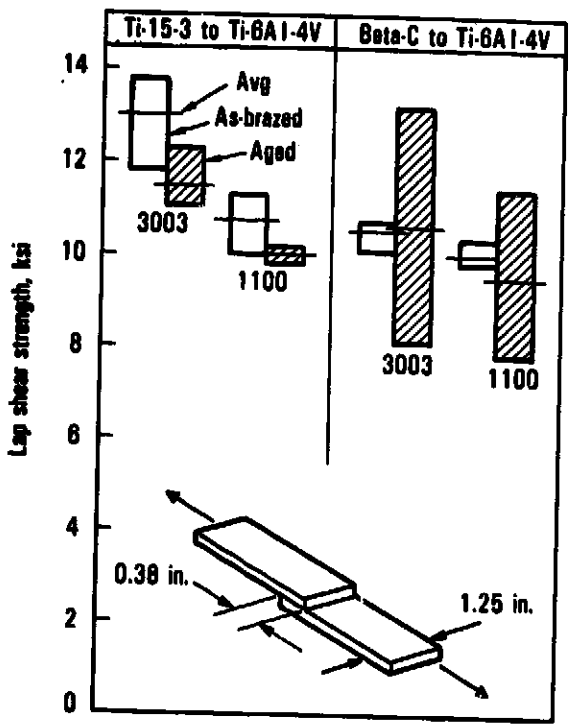

Figure 54. - Room temperature shear strength of brazed titanium joints.

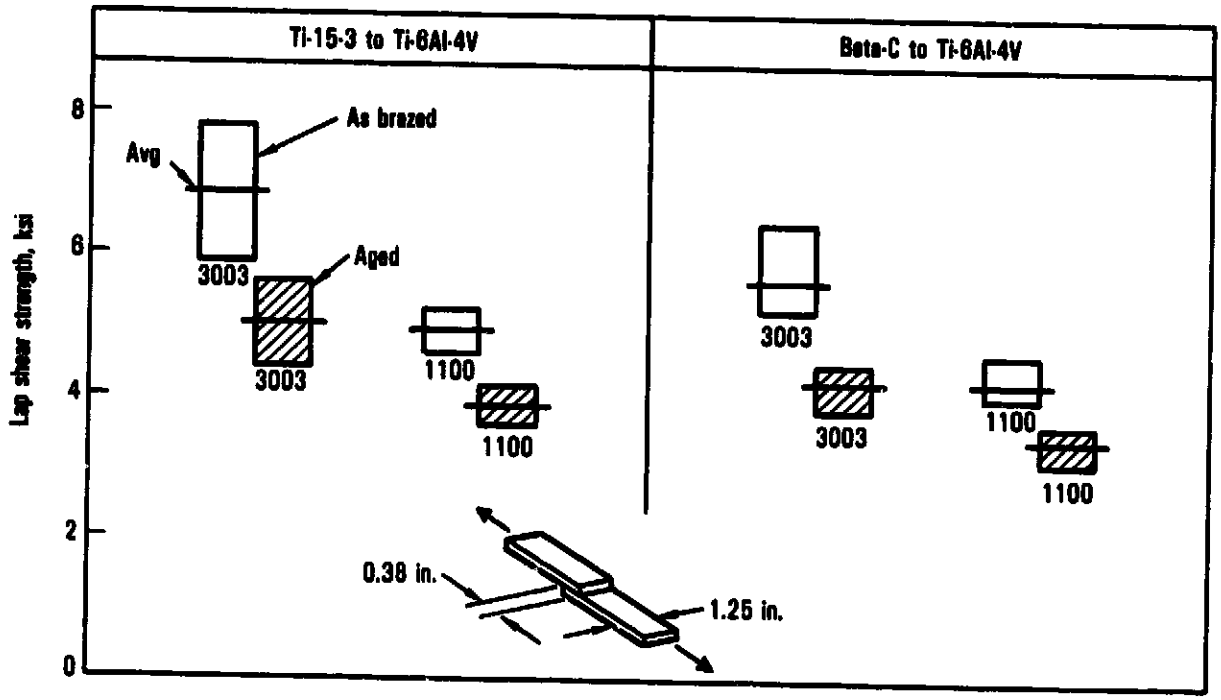

Figure 55. - 600°F shear strength of brazed titanium joints.

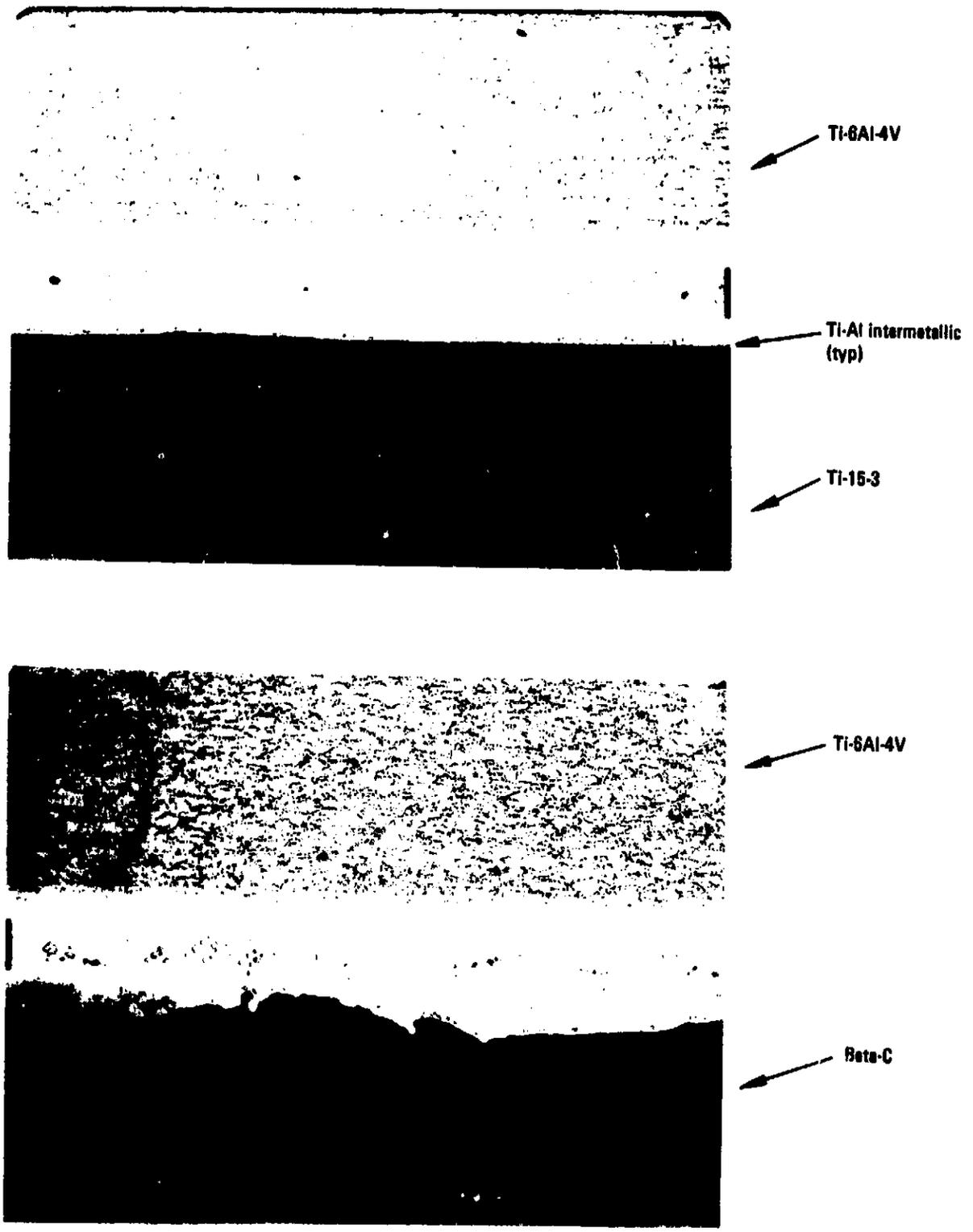

Figure 56. - Sections thru 3003Al isothermal brazed joints. (Top) Ti-15-3/Ti-6Al-4V, aged 940°F-12h; (bottom) Beta-C/Ti-6Al-4V, aged 1000°F-8h. Mag. 250X.

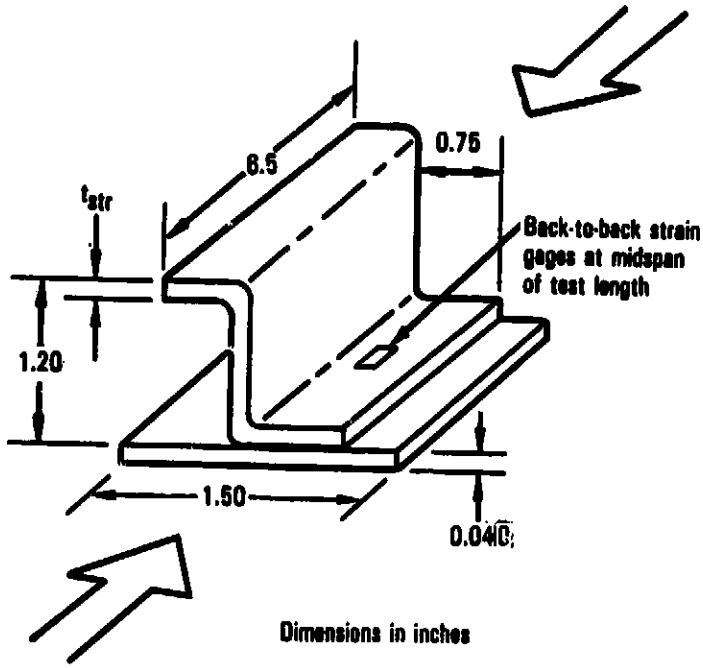

Ti-15-3 stringers (specimens 2 and 4): t_{str} = 0.063

Beta-C stringers (specimens A and B): t_{str} = 0.069

Figure 57. - Specimen geometry for short column crippling tests of zee-stiffened elements.

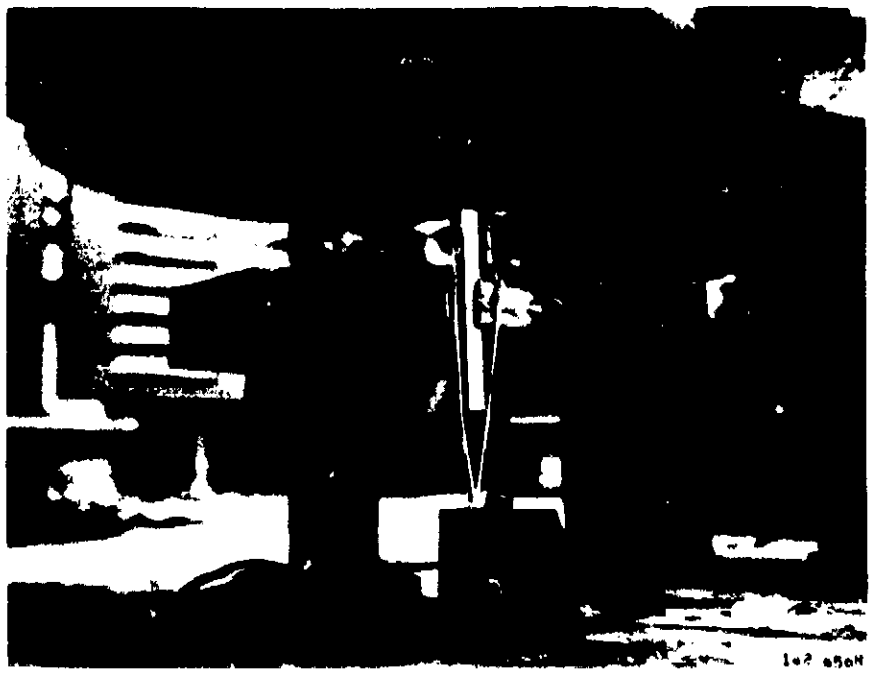

Figure 58. - Typical test installation - short column crippling tests of zee-stiffened elements.

Figure 59. - Ti-15-3 zee-stiffened elements after crippling test.

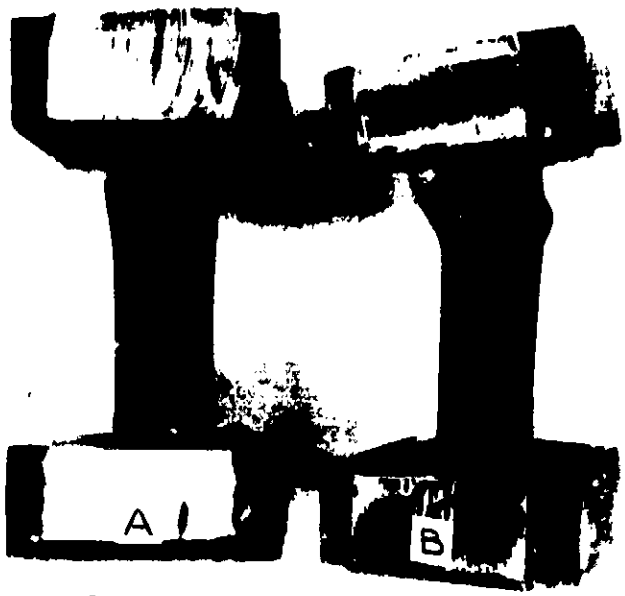

Figure 60. - Beta-C zee-stiffened elements after crippling test.

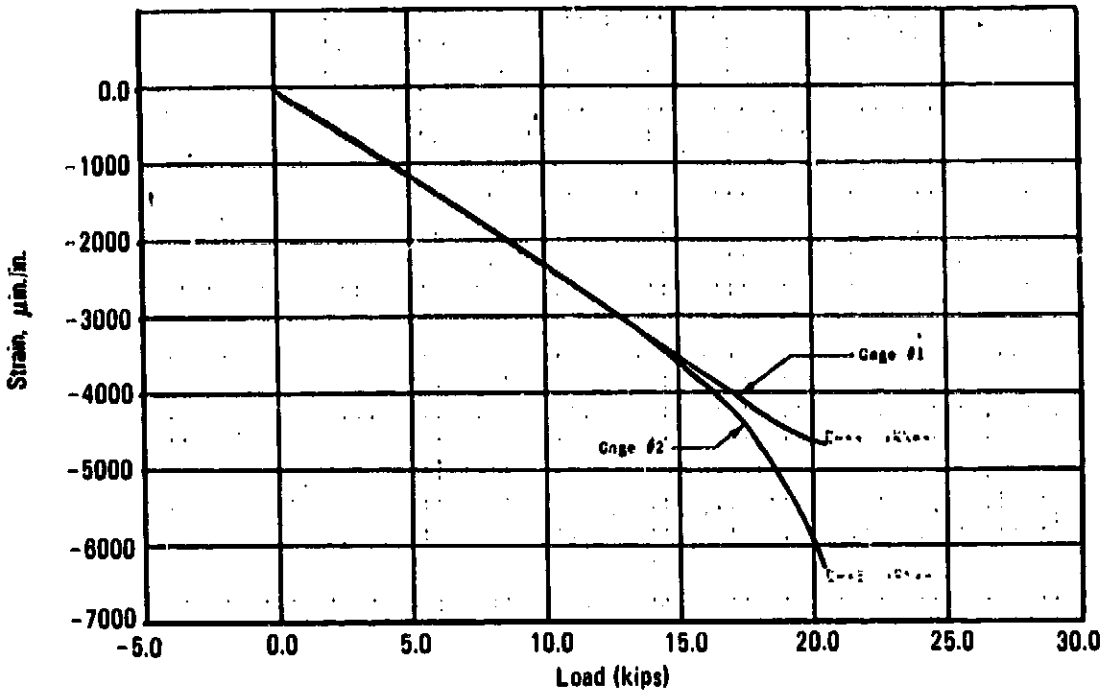

(a) Specimen B, strain vs load

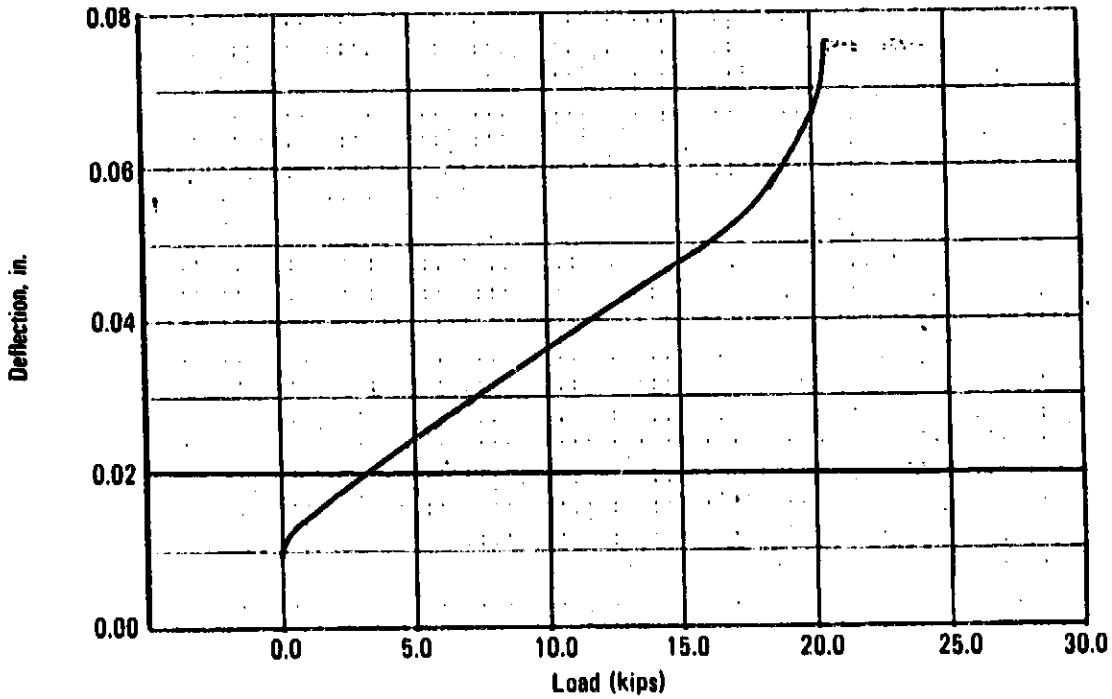

(b) Specimen B, deflection vs load

Figure 61. - Examples of load/strain and load/deflection curves - short column crippling test of Beta-C zee-stiffened element - specimen B.

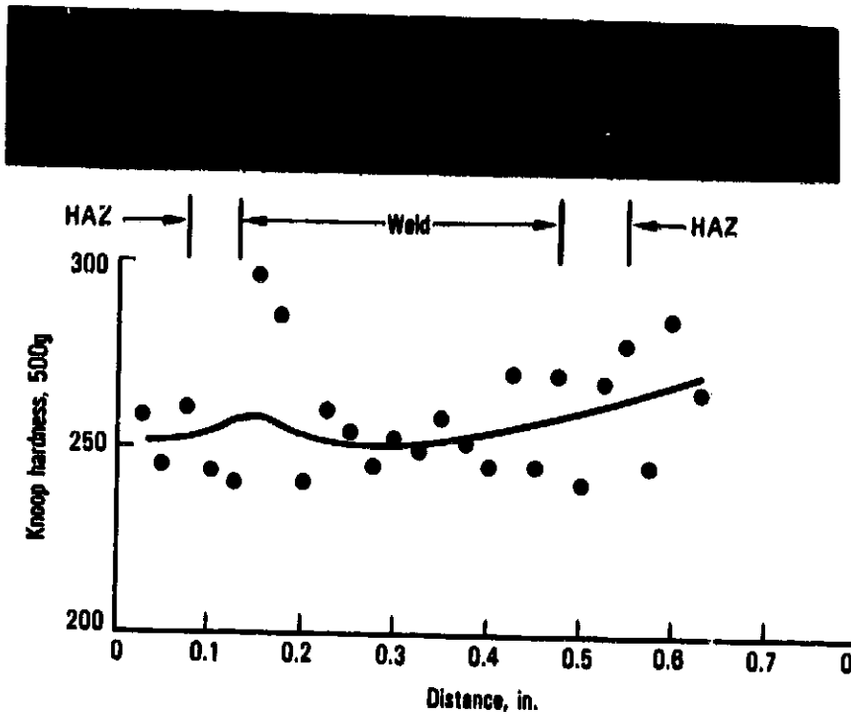

(a) Condition: ST + Weld

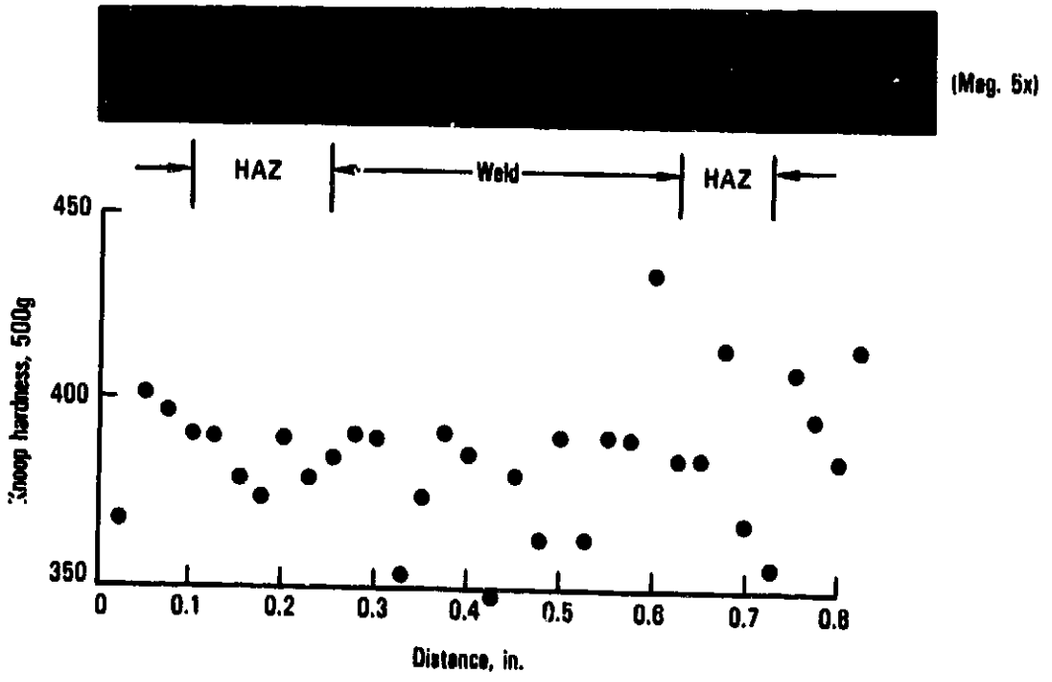

(b) Condition: ST + Weld + Age (925^{0}F/12h)

Figure 62. - Hardness traverse of TIG butt welds in 0.080 in. Ti-15-3 sheet.

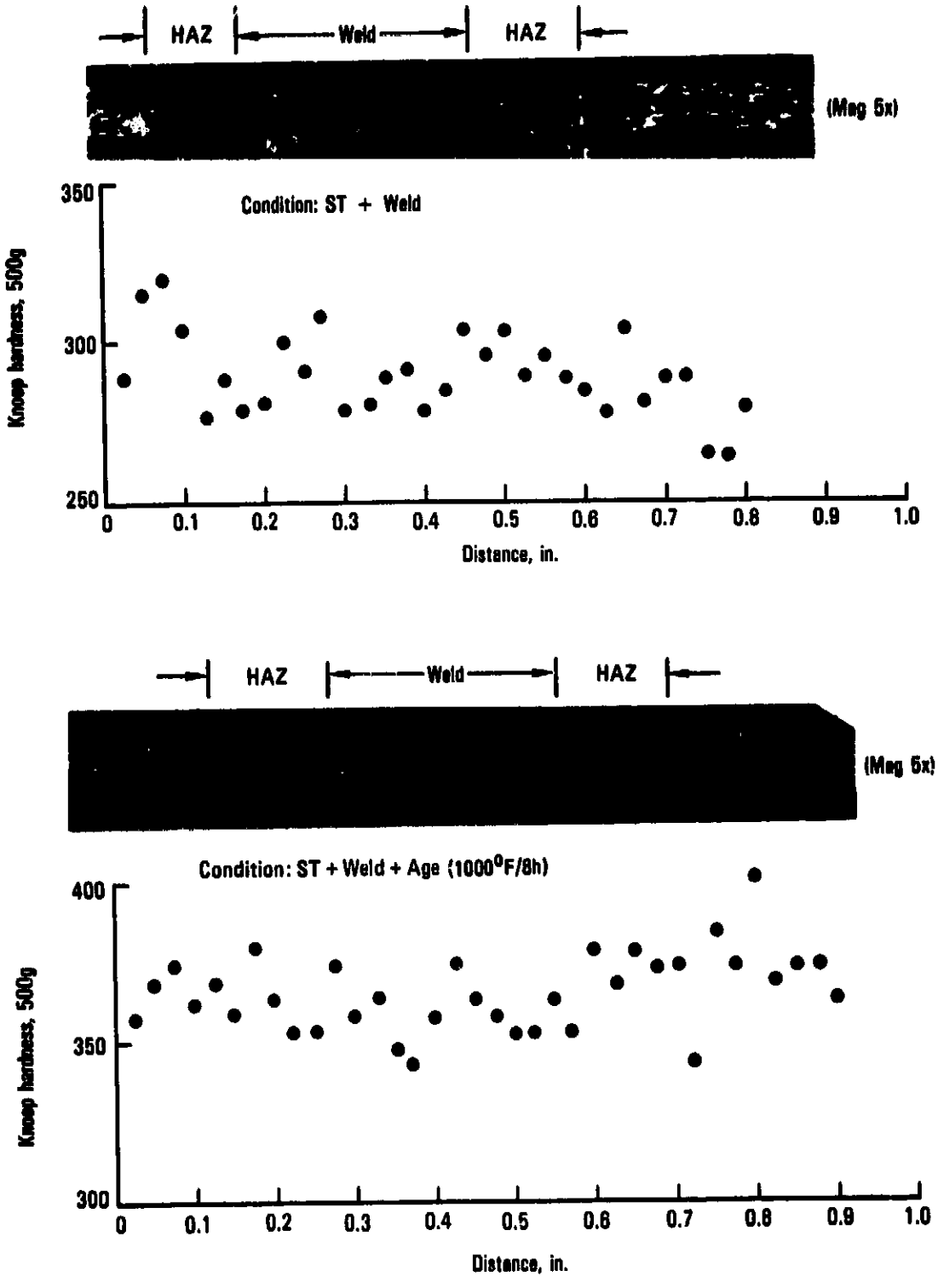

Figure 63. - Hardness traverse of TIG butt welds in 0.065 in. Beta-C sheet.

TASK 6 - PANEL SPECIMEN FABRICATION

Design and Fabrication

Lockheed's analytical studies for NASA in the design of supersonic cruise vehicles have involved all aspects of airframe design for vehicles with cruise speeds ranging from Mach 2.0 to Mach 2.7. In one of these studies, under contract to NASA LaRC (ref. 27), a comprehensive analytical study was performed to assess the various structural/material approaches for design of primary wing and fuselage structure of a Mach 2.7 arrow-wing supersonic cruise aircraft. Various wing structural arrangements were investigated. Among these, a spanwise stiffened wing structural arrangement was evaluated for various wing surface panel concepts including the zee-stiffened, integral zee-stiffened, hat-stiffened, and blade-stiffened concepts. The least weight concept (most structurally efficient) for this arrangement was the hat-stiffened.

A weight penalty was associated with an all beta titanium design due to the large amount of wing surface area that is lightly loaded. Hence, the lower modulus/density ratio of the candidate beta alloy (Beta-C at that time) presented heavier designs than those of the corresponding Ti-6Al-4V (annealed) designs. However, in highly loaded regions, such as the wing box near the root chord, the Beta-C designs showed promise of weight savings because the stress levels are sufficiently high to take advantage of higher inelastic strength capability of the beta alloy. Also, considerable cost savings are available using a beta alloy due to its cold forming capability when compared with the hot forming requirements of Ti-6Al-4V. Therefore, a hybrid design using a Ti-6-4 surface skin and beta alloy stringers joined by isothermal brazing appears to present an efficient structural arrangement.

To demonstrate the compressive buckling capability of the isothermal brazed hat-stiffened panel design, a series of six short-column compression tests was conducted. The cross-sectional geometry of the test panels approaches optimum proportions: the stresses for local and general instability failure modes are approximately equivalent. Each of the panels had three beta titanium stringers which were brake formed to the hat configuration, then isothermal brazed to an annealed Ti-6-4 skin using 3003 aluminum brazing alloy. Four of the panels had Ti-15-3 stringers and two had Beta-C stringers. After brazing, the Ti-15-3 panels were aged in a vacuum at 940°F for 12 hours and the Beta-C panels were aged at 1000°F for 8 hours. Nominal panel dimensions and a completed panel are shown in figure 64.

Testing

Four panels with Ti-15-3 stiffeners were tested, two at room temperature and two at 600°F. One Beta-C stiffened panel was tested at room temperature and the other at 600°F. Test length of the panels was 13 inches after potting and machining the ends. The panel edges were supported during test by slotted tubes, as shown in figure 65, to prevent premature buckling. Ten strain gages were installed on each of the room temperature panels, as also indicated in figure 65. A clamshell radiant heating arrangement was used for the elevated temperature tests with thermocouples attached to the panels to monitor temperature. Test temperature was held within ±25°F. An LVDT-type deflection transducer measured machine head travel continuously during testing. The panels were tested in a 400-kip universal static test machine. Typical test installations for the room temperature and elevated temperature tests are shown in figure 66.

The initial buckling mode for these panels was that of the Ti-6-4 skin. The initial buckling stress was predicted using the method described on pages 368-371 of reference 28, and assuming simply supported boundary conditions. Both the skin widths under the stringers and between stringers were analyzed, and the predicted location of initial buckling for all six panels was between the stringers.

Panel failure was by crippling of the cross section. The crippling stress was predicted as in task 5. A conservative estimate (ref. 28, pages 371-376) of the effective width of the between-stringer skin sections was used to account for buckled skin, and inelasticity was taken into account where applicable. The crippling analysis indicated that the Ti-6-4 skin stresses at failure were in the inelastic region for all six panels, but the only stringer stresses in the inelastic region were those of the Ti-15-3 elevated temperature panels.

The material properties used for Ti-6-4 were taken from reference 13, and measurements made in task 4 provided the stress-strain curves used for the beta alloy stringers. The predicted initial buckling and crippling failure stresses and the corresponding test results are summarized in table 40. A discussion follows:

- Of the four panels with Ti-15-3 stringers, panel 6-9, tested at room temperature, failed within one percent of the predicted value and panel 6-8, tested at 600°F, failed within 8 percent of the prediction. Panels 6-10 and 6-11 had considerably larger differences between predicted and test failure loads, 18 and 17 percent, respectively; the suspected reason for the low test failure loads for these two panels is a variation in aging response of the Ti-15-3 stringers because stringers for panels 6-8 and 6-9 were from one sheet and those for 6-10 and 6-11 from another sheet. Photographs of the failed panels are presented in figure 67. A typical load/strain curve is shown in figure 68.

- The initial compression buckling stress of the Ti-15-3 panels as indicated by the divergence in the strain gage recordings, fell within 20 percent of the calculated buckling strength of the widest element on the Ti-6Al-4V skin segment, the skin between the stringers. In three of the four cases the prediction was conservative.

- The room-temperature Beta-C stiffened panel No. 6-5 failed within 2 percent of the predicted value, with an initial buckling load about 15 percent higher than predicted. Beta-C panel 6-1, tested at 600°F, failed 22 percent below the predicted load, and was at a load about 25 percent lower than the predicted value when its skin began to buckle. Photographs of the panels after testing are shown in figure 69.

- In all six tests the brazed joints remained intact until after panel failure. Disbonding after failure was generally minimal and confined to the immediate vicinity of the crippled flanges.

TABLE 40. - ANALYSIS AND TEST RESULTS OF SHORT COLUMN CRIPPLING TESTS OF HAT-STIFFENED PANELS

Specimen ID	Stringer/Skin	Test Temp	Initial Buckling* (ksi)		Failure (ksi)		Comments
			Prediction	Test	Prediction	Test	
6-5	Beta-C/Ti-6-4	Room	65.0	75	116.0	118.1	Failure occurred 4 inches from top of panel Stringers fractured at several locations along failure line 3 to 4 inch disbond after failure
6-1	Beta-C/Ti-6-4	600°F	60.1	45	92.2	75.8	Crippling failure occurred at midspan Slight disbond noted after failure
6-9	Ti-15-3/Ti-6-4	Room	62.9	76	120.7	121.3	Crippling failure occurred 9 inches from top of panel Slight disbond noted after failure
6-11	Ti-15-3/Ti-6-4	Room	80.7	66	121.7	104.4	Crippling failure occurred in lower 1/4 length Buckle not straight across panel Stringers cracked on bends at failure location 3 to 4 inch disbond noted after failure
6-8	Ti-15-3/Ti-6-4	600°F	52.0	62	91.9	84.8	Crippling failure occurred 4 inches from top of panel Slight disbond noted after failure
6-10	Ti-15-3/Ti-6-4	600°F	63.8	70	92.4	78.4	Crippling failure occurred 4 inches from top of panel Slight disbond noted after failure

* Initial buckling was determined from strain gage recordings for room temperature tests and by visual observation for elevated temperature tests. In all cases, initial buckling occurred on the skin between the stringers.

Note: All stresses are averaged.

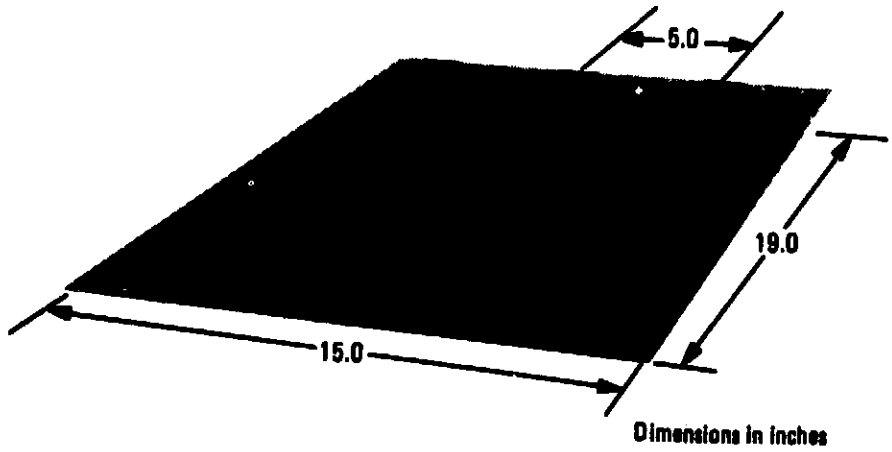

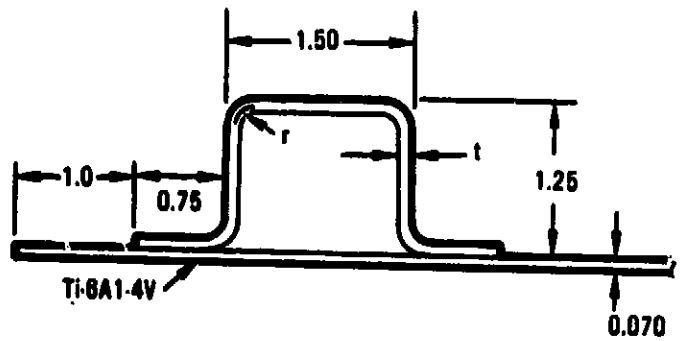

Beta-C stiffener: t = 0.065, r = 0.282
Ti-15-3 stiffener: t = 0.080, r = 0.227

Figure 64. - Specimen geometry for short column crippling tests of titanium hat-stiffened panels.

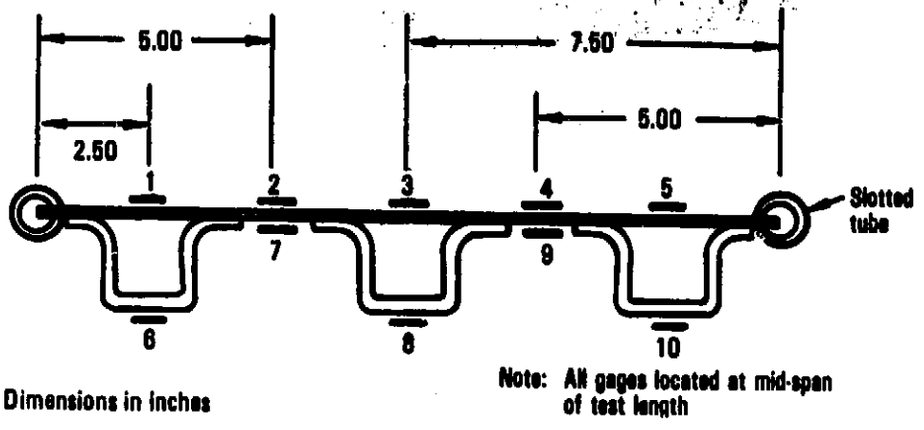

Figure 65. - Strain gage locations on room temperature panels - short column crippling tests of hat-stiffened panels.

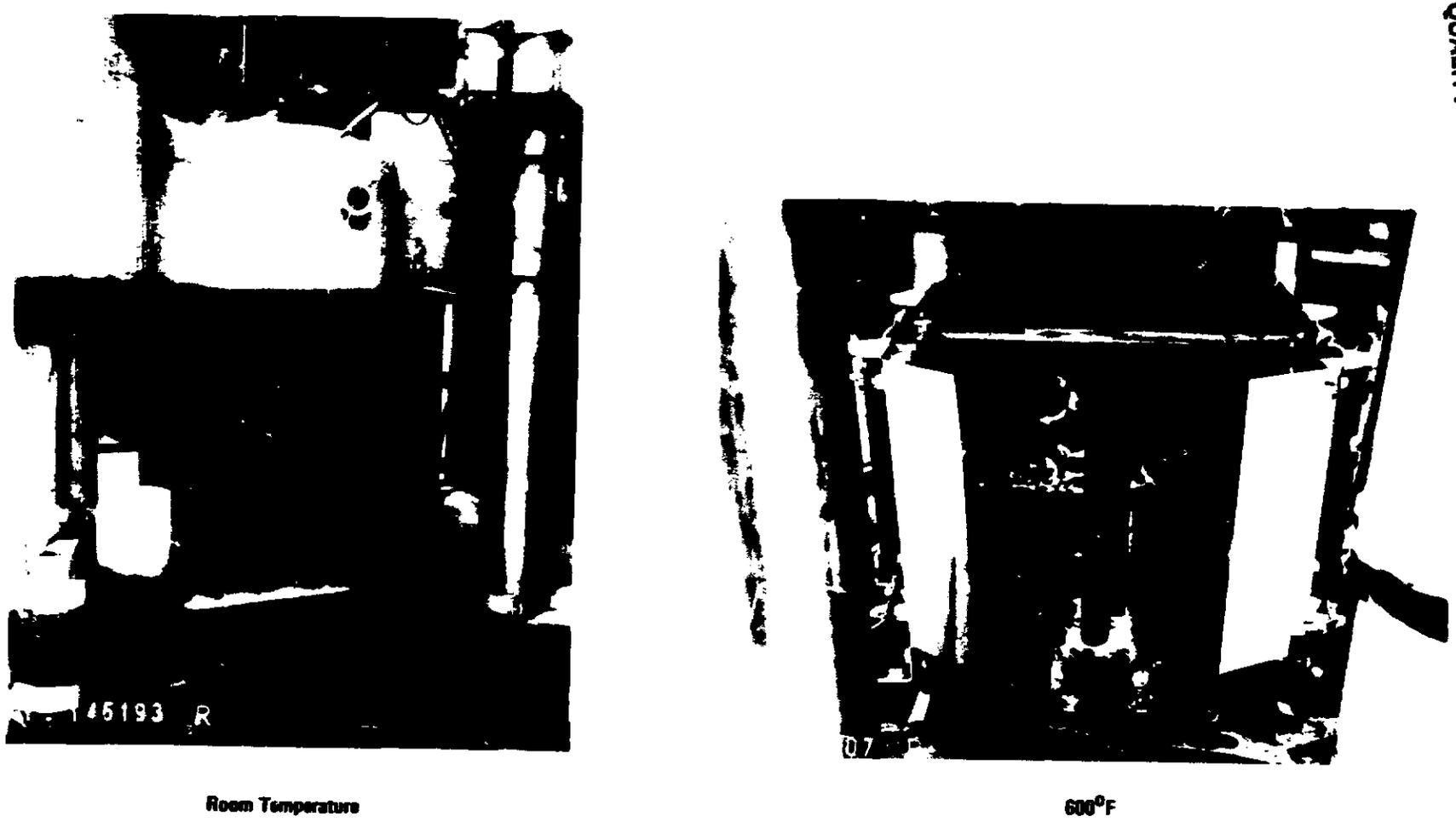

Room Temperature

600°F

Figure 66. - Typical test installations for short column crippling tests of hat stiffened panels.

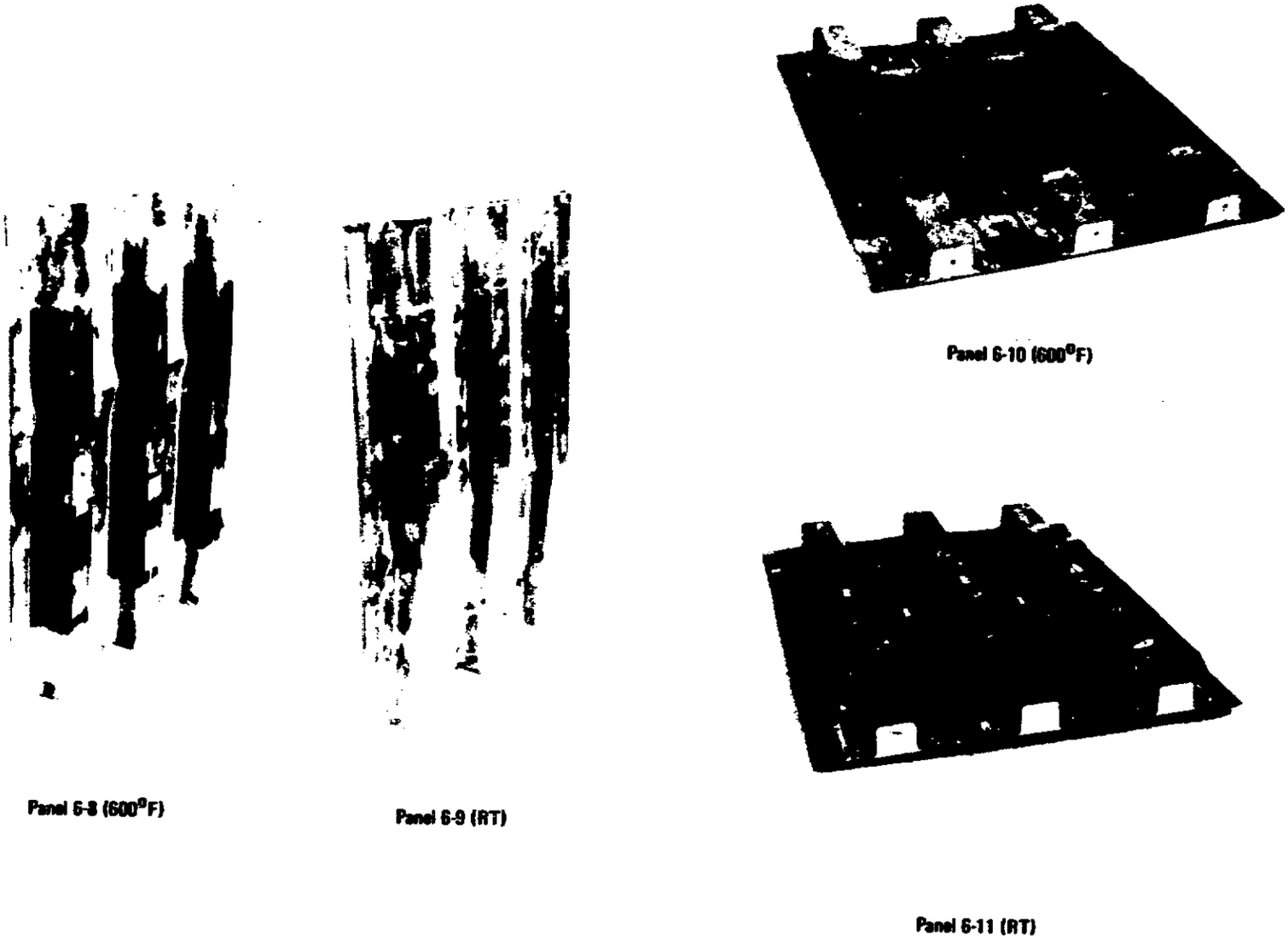

Figure 67. - Failed panels with Ti-15-3 stringers - short column crippling tests of hat-stiffened panels.

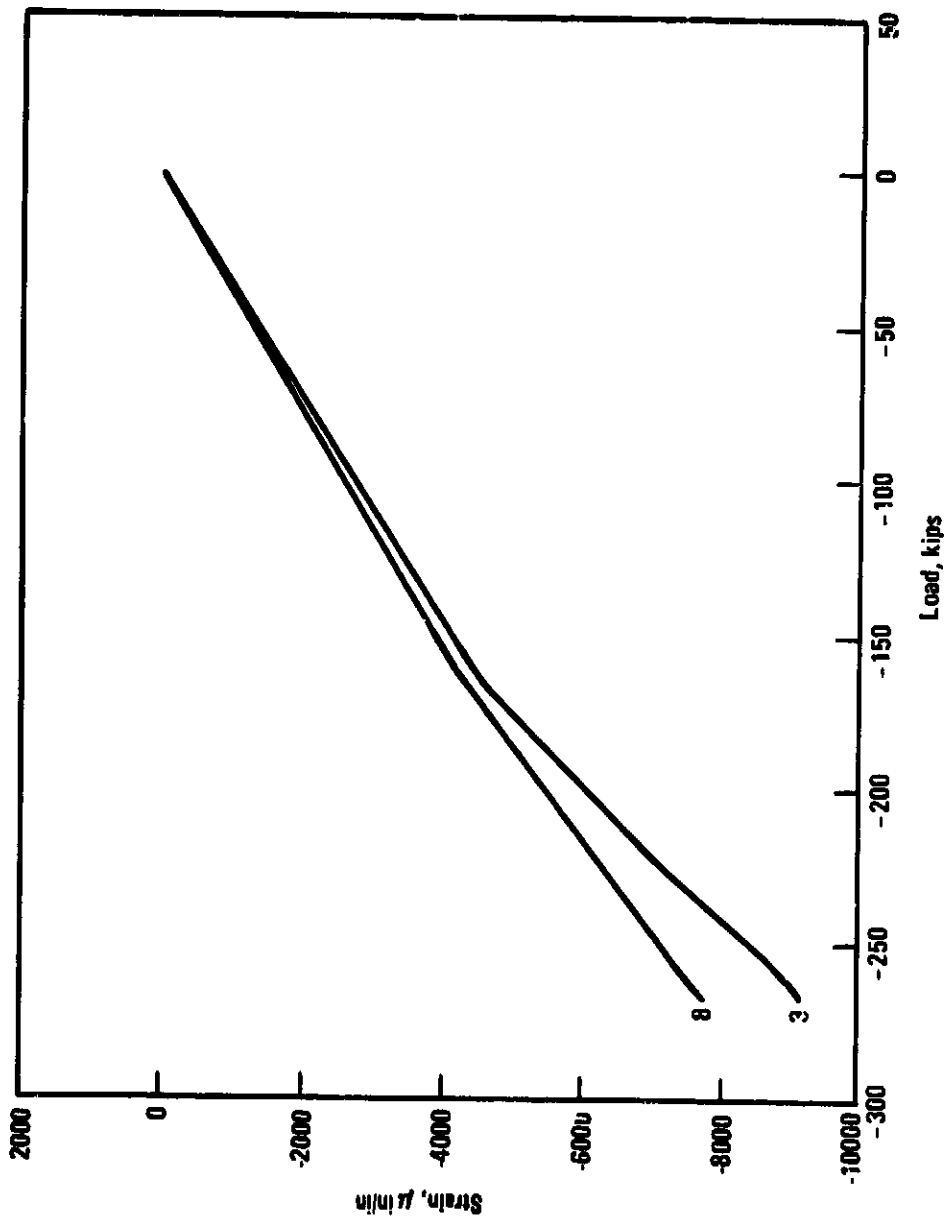

Figure 68. - Panel 6-9, strain vs load (gages 3 and 8) - short column crippling tests of hat-stiffened panels

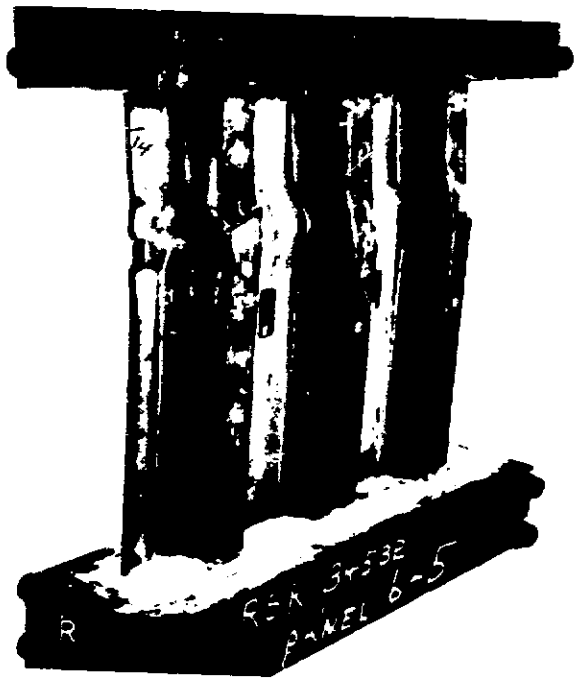

Panel 6-5 (RT)

Panel 6-1 (600°F)

Figure 69. - Failed panels with Beta-C stringers - short column crippling tests of hat-stiffened panels.

TASK 7 - WING PANEL FABRICATION

Four relatively large hat-stiffened panels were fabricated using Ti-15-3 cold-formed stringers isothermal brazed to a Ti-6-4 skin. Three of the panels, simulating wing upper surface panels of an SCV, were tested to provide insight into the long-column compression and damage tolerance characteristics of panels fabricated using beta titanium alloys. The fourth panel was a demonstration component delivered to the NASA-Langley Research Center.

Design and Fabrication

The panel design represents an SCV wing upper surface panel between two ribs. The panels were 20 inches wide by 48 inches long, containing four brake-formed Ti-15-3 stringers isothermal brazed to a Ti-6-4 skin using 3003 aluminum brazing alloy. Cross-sectional proportions and pitch were the same as those of the crippling panels in task 6. After brazing, the panels were aged in a vacuum at 940°F for 12 hours with no restraint fixturing. Flatness was checked before and after aging by means of deviation from a straight edge. The panels stayed essentially flat (within 0.030 inch), demonstrating that brazing in the fixture appears to effectively size and stress relieve. A completed panel is shown in figure 70.

Static Compression Tests

One panel was tested at room temperature and one at 600°F. Test length of the panels was 40 inches after potting and machining the ends. For full fixity, the effective panel length or distance between points of contraflexure approximates an SCV rib spacing of 20 inches with the ribs providing simple support to the skin.

Strain gages were installed and the edges were supported by slotted tubes as depicted in figures 71 and 72. An LVDT-type deflection transducer was used to measure machine head travel and clamshell radiant heating was used for the 600°F panel. Test temperature was held within ±25°F. Figures 73 and 74 show the installations of the test panels in the 400-kip Universal static test machine. Load rate was 1200 pounds per second for the RT test and 1000 pounds per second for the 600°F test.

Skin buckling, cross-section crippling, and Euler column buckling were analyzed prior to testing. The crippling stress was calculated only to confirm that crippling would not be the principal failure mode. A summary of the correlation between the analysis and test results is presented in table 41.

Panel failure was in the long-column mode. The analysis based on full end fixity indicated that for the room temperature panel, both the skin stress and the stringer stress were in the elastic region of the stress/strain curve at failure. For the panel tested at 600°F, only the stringer stress was in the elastic region. A typical load/strain curve is shown in figure 75.

Both the room and elevated temperature test results correlate closely with calculated values using Euler's long column theory with an end fixity of 3.0. For this fixity, the distance between points of contraflexure corresponds to a simply supported column with a length of 23 inches. In both cases, the deformed shape of the panel at maximum load was characteristic of a classic column failure. The maximum variation between the calculated values and the test results was less than 4 percent. No local buckling was evident, and no cracks, braze separation or other damage was found in post-test visual, X-ray, and ultrasonic inspections.

Fatigue/Crack Growth Tests

Fatigue/crack growth tests of a representative hat-stiffened wing upper surface panel for an SCV were conducted to investigate the durability aspects of the isothermal brazing process. The panel was subjected to an initial 20,000 flight lifetime variable amplitude flight-by-flight fatigue spectrum. Then a flaw was introduced in the panel, and a second lifetime of fatigue loadings was applied. Finally, the panel was statically tested to failure in compression to determine its residual strength. All testing was performed at room temperature.

The fatigue loading spectrum was based on Spectrum C, which was developed in the mid-1960's by the Lockheed-California Company. Spectrum C represents service loadings on a lower surface panel in the wing root region of a supersonic transport aircraft, and is comprised primarily of tensile loadings. Since this study is based on the requirements for an upper surface panel in the wing root region, Spectrum C required some alterations to create a series of compression-dominated loadings appropriate for this application.

In Spectrum C, the lower surface mean stress was 25 ksi and the mean load ratio for the climb segment was 1.0. The mean load ratios for the cruise and descent segments of each flight were derived from this ratio by adding (or subtracting) factors representing the fuel decrement and the thermal stress increment applicable to that flight segment. For the upper surface spectrum used in this test, the same mean stress, mean load ratio, fuel and thermal stress factors were used, with their signs reversed when appropriate. The

resulting spectrum is predominately composed of compression-compression loadings reflecting the upper surface mean and variable loads associated with the climb, cruise, and descent segments of a flight. Tension-tension fatigue loadings are included in the loading spectrum to represent the loads applied to the wing upper surface panel during the landing and taxi segments of a flight. The reference stress used for Spectrum C, in combination with the minimum stress ratio in the loadings for the upper surface, was compared with the calculated crippling stress to prevent premature failure of the panel during fatigue loading. The spectrum applied to the panel is presented in table 42. Figure 76 diagrams a unit flight profile. Table 42 lists the variable loadings applied at the indicated intervals during the 20,000 flight lifetime.

A preflaw was introduced into the Ti-6-4 skin between the two center Ti-15-3 stiffeners after the first lifetime of spectrum fatigue testing. Crack growth analyses were conducted to estimate the initial preflaw size that would grow to the edge of the hat stiffener within the second lifetime (20,000 flights). The analyses were conducted using the methods described in reference 29 and the effectiveness of the flanges of the hat stiffeners in slowing the crack growth rate as the crack approached the stiffeners was considered. The value of $R_c = -0.36$ used in the analysis was derived from constant amplitude fatigue crack growth data at R=-1.0 and at R=0.1 using an analytical relationship between the R value for a constant amplitude loading and the associated crack growth. These data indicated that compression loadings associated with R values less than -0.36 have the same effect on crack growth as a loading cycle of $R_c = -0.36$ with the same maximum tension stress.

The ends of the panel were enclosed in a fixture designed to distribute the loads evenly throughout the panel cross-section. The fixture, illustrated in figure 77, consisted of maple wood fillers between and under the stringers, aluminum doublers in a cascading arrangement on each side of the panel, with steel plates and gussets outside of the doublers. The fixturing was bolted and adhesive bonded to the panel, leaving an unreinforced panel length of 20 inches. The edges of the panel were supported by slotted tubes and the ends of the panel/fixture were machined flat, square, and parallel. Flexures were installed at the ends of the unreinforced portion of the panel to prevent lateral deflection of the panel during fatigue loading. The flexures were not used during the residual compression test.

Sixteen strain gages were installed on the panel as shown in figure 78. Load/strain and load/deflection data were recorded periodically during the fatigue portion of the test and continuously during the residual compression test. In the 220-kip MTS fatigue test machine, the deflections were measured by a position feedback transducer on the loading jack of the test machine. For the static residual strength test, an LVDT-type deflection transducer was used. Photographs of the panel installed in the 220-kip MTS fatigue test machine and in the 400-kip Universal static test machine are presented in figure 79.

After installation of the panel in the test machine, preliminary load/strain surveys were performed and the fatigue loadings were applied to the test panel. Data were recorded periodically to ensure that the test machine was achieving the required stress levels. Typical loadings recorded during flight number 1000 are shown in figure 80. Explicitly, the cycles of loadings within any given flight is found by summing the columns ("Unit flight" through "20000 flights") which are exactly divisible into the number of this given flight. Thus for flight number 1000, the complete listing of loadings applied would include the summation of loadings for columns "Unit flight", "100 flts," "500 flts", and "1000 flts" in table 42.

At slightly less than 10,000 flights, a disbond between the panel skin and one of the wood fillers was noted. Each subsequent load/strain survey during the two lifetimes of fatigue testing showed distinct, though relatively small, increases in the stringer strains for a given compression load, probably indicating a slight redistribution of the load over the panel cross-section because of the disbonding in the text fixture. No other problems were encountered throughout the remainder of the testing.

X-ray inspection at the end of the first lifetime (20,000 flights) showed no evidence of cracks or growth of existing voids in the braze as a result of testing. A 0.98-inch cut was made in the skin between the two middle stringers (figure 78) and a constant amplitude loading cycle, S_{max}=15,000 psi and R=0.1, was applied until the cut propagated to a length of 1.196 inches. Then a second lifetime of fatigue loadings was applied, and the crack growth was measured periodically, as plotted in Figure 81.

At the end of the second lifetime, the crack length was 2.537 inches, extending slightly into the brazed region of the skin at the two adjacent stringer flanges. As can be seen in figure 82, the crack grew much slower than predicted. Tension-tension constant amplitude loading with S_{max} = 15,000 psi and R=0.1 was applied to further extend the crack before the residual compression test. After approximately 46,000 cycles of this loading, the crack had grown through the flanges of both of the adjacent hat stiffeners and was beginning to grow up the side of one stiffener, as shown in figure 83. At this point, the fatigue loading was stopped. In situ X-ray inspection showed no evidence of testing-related flaws other than the induced crack.

The panel was removed from the 220-kip MTS fatigue test machine and installed in the 400-kip Universal static test machine. A final load/strain-load/deflection survey was taken before the residual compression test was initiated. Strain gage readings during testing indicated initial skin buckling at 190,000 pounds which was 13 percent below the predicted value. The panel failed in crippling at a load of 341,000 pounds; there was no lateral deflection indicative of long-column failure. The brazed joints remained intact until panel failure, but disbonded over the entire unsupported panel length of 20 inches at failure. A representative load/strain curve is presented in figure 84 and a photograph of the failed panel is shown in figure 85. The panel's residual compressive strength was above 95 percent of the calculated strength for an undamaged panel.

Weight Study

A theoretical weight comparison was made between a conventional, hot-formed and riveted all Ti-6-4 hat-stiffened panel and an isothermal brazed panel with cold-formed Ti-15-3 hat stiffeners and Ti-6-4 skin. The Ti-15-3 brazed panel was chosen as the baseline and crippling was considered to be the critical failure mode. The room temperature crippling load of the brazed panel (361,400 pounds) was used as the design load for the riveted panel. Two approaches were investigated in designing an all Ti-6-4 riveted panel based on the large (20-by 48-inch) wing panel geometry. In one case, the stringer thickness was held constant at 0.080 inch and the skin thickness was increased until the design load was reached. In the second, both skin and stringer thicknesses were increased. In each case, 3/16 inch diameter rivets were used to attach the stiffeners to the skin and sufficient width was added to the flanges of the stiffeners to ensure proper fastener edge distance. Table 43 summarizes the results of this study. Both design approaches showed that the brazed panel with Ti-15-3 stiffeners was about 16 percent lighter than the conventional titanium panel.

Cost Study

A preliminary cost analysis was made to compare the cold-formed/isothermal brazed beta titanium fabrication method for a 20-inch by 48-inch hat stiffened wing panel with state-of-the-art hot-formed/riveted assembly of a comparable Ti-6-4 structure. Panel geometry was kept as nearly constant as practical. The riveted panels required slightly wider flanges to maintain proper edge distance. The analysis included factors of raw materials, processing, tooling, equipment, and associated recurring and nonrecurring costs. Where applicable, labor hours were taken from the Lockheed-California Company "Engineering Cost Handbook" and planning/operation sheets.

Table 44 gives projected unit costs for quantities of 50, 100, and 200. Compared with the conventional Ti-6-4 panel, the cold-formed/isothermal brazed structure composed of Ti-15-3 stringers and a Ti-6-4 skin shows projected savings of at least 25 percent.

TABLE 41. - ANALYSIS AND TEST RESULTS OF LONG-COLUMN COMPRESSION TESTS OF REPRESENTATIVE TITANIUM WING PANELS

Panel ID	Stringer/Skin	Test Temp	Long Column Buckling Stress		Comments
			Calculated* (ksi)	Test (ksi)	
7-2	Ti-15-3/Ti-6-4	Room	66.0	64.8	Failure in potting material after attaining maximum load No braze separation
7-1	Ti-15-3/Ti-6-4	600°F	60.3	58.2	Strain gage #3 recorded no data during test No braze separation

*Based on end fixity of 3.0

Note: All stresses are averaged

TABLE 42. - FATIGUE LOADING SPECTRUM FOR PANEL 7-3

Flight Segment	f_{mean} / $f_{1g_{Ref}}$ *	f_{very} / $f_{1g_{Ref}}$ *	Unit Flight	Growth Cycles Added Every:						Cycles Per 20000 Flights		Cyclic Rate (Hz)
				100 flts	500 flts	1000 flts	5000 flts	10000 flts	20000 flts	Per Load Level	Cumulative	
Taxi	0.24	0.51	1							20000	25015	3
		0.61		22	1	1				4460	5015	3
		0.71		2	2					480	555	2
		0.81			1	1	1	1		66	75	2
		0.91					2			8	9	2
		1.01							1	1	1	1
Climb	-1.00	0.15	7							140000	199117	10
		0.25	2							40000	59117	6
		0.35		62						12400	19117	4
		0.45		22						4400	6717	3
		0.55		7						1400	2317	3
		0.65			13					520	917	2
		0.75			6					240	397	2
		0.85			2					80	157	2
		0.95			1					40	77	2
		1.05				1				20	37	1
		1.15					2			8	17	1
		1.25					1			4	9	1
		1.35						1		2	5	1
		1.45							2	2	3	1
		1.55							1	1	1	1
Cruise	-0.25	0.15	3	30						76000	87239	10
		0.25		48						9800	11239	6
		0.35		7						1400	1639	4
		0.45		1						200	239	3
		0.55				1	3			32	39	3
		0.65					1	1		6	7	2
		0.75							1	1	1	2
Descent	-1.00	0.15	7	75						155000	187412	10
		0.25	1	30						26000	32412	6
		0.35		25						5000	6412	4
		0.45		5	2					1080	1412	3
		0.55		1	1					240	332	3
		0.65				3	1			64	92	2
		0.75				1				20	28	2
		0.85						3		6	8	2
		0.95							2	2	2	2

*$f_{1g_{Ref}}$ = 26 ksi

TABLE 43. - WEIGHT COMPARISON - REPRESENTATIVE WING PANEL

Panel description	• 4 Hats, 5 in. pitch • Length = 48 in. • Width = 20 in.	Weight	
		LB	Δ%
Cold-formed, isothermal brazed Beta Ti stringers	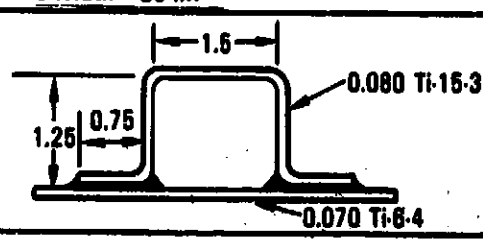	24.35	Baseline
Hot-formed, riveted all Ti-6-4 panel	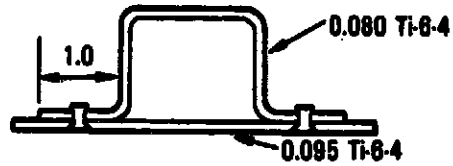	29.05	+18.2
	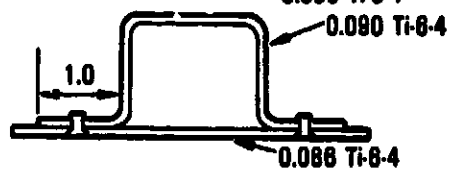	29.19	+18.6

TABLE 44. TITANIUM WING PANEL COST SUMMARY

Material Stringer/Skin	Ti-6-4/Ti-6-4			Ti-15-3/Ti-6-4		
Fabrication Method	Hot Form, Rivet			Cold Form, Isothermal Braze		
Quantity	50	100	200	50	100	200
Recurring Costs ($)	2307	2116	1945	1405	1347	1295
Nonrecurring Costs, Amortized ($)	323	161	81	569	284	142
Total Unit Cost ($)	2630	2277	2026	1974	1631	1437
Net Program Savings (%)	Baseline →			25%	28%	29%
Implementation Cost ($)	16140 →			28449 →		
Panel size: 20 x 48 inches with 4 stringers						

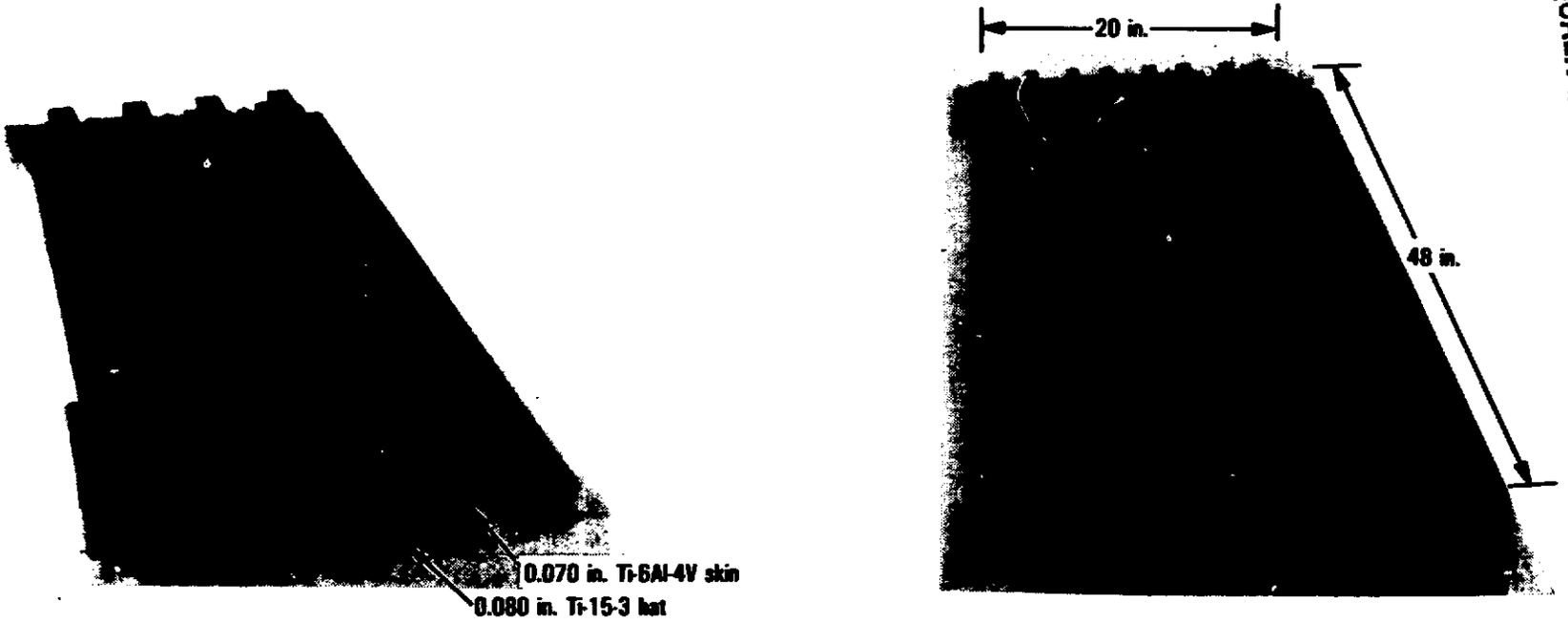

(Cross-section dimensions same as figure 64)

Panel No. 7-1	600 °F	static compression test
Panel No. 7-2	RT	static compression test
Panel No. 7-3	RT	spectrum fatigue → crack growth → residual strength
Panel No. 7-4	Deliver to NASA Langley	

Figure 70. - Cold-formed, isothermal brazed representative titanium wing panels - task 7.

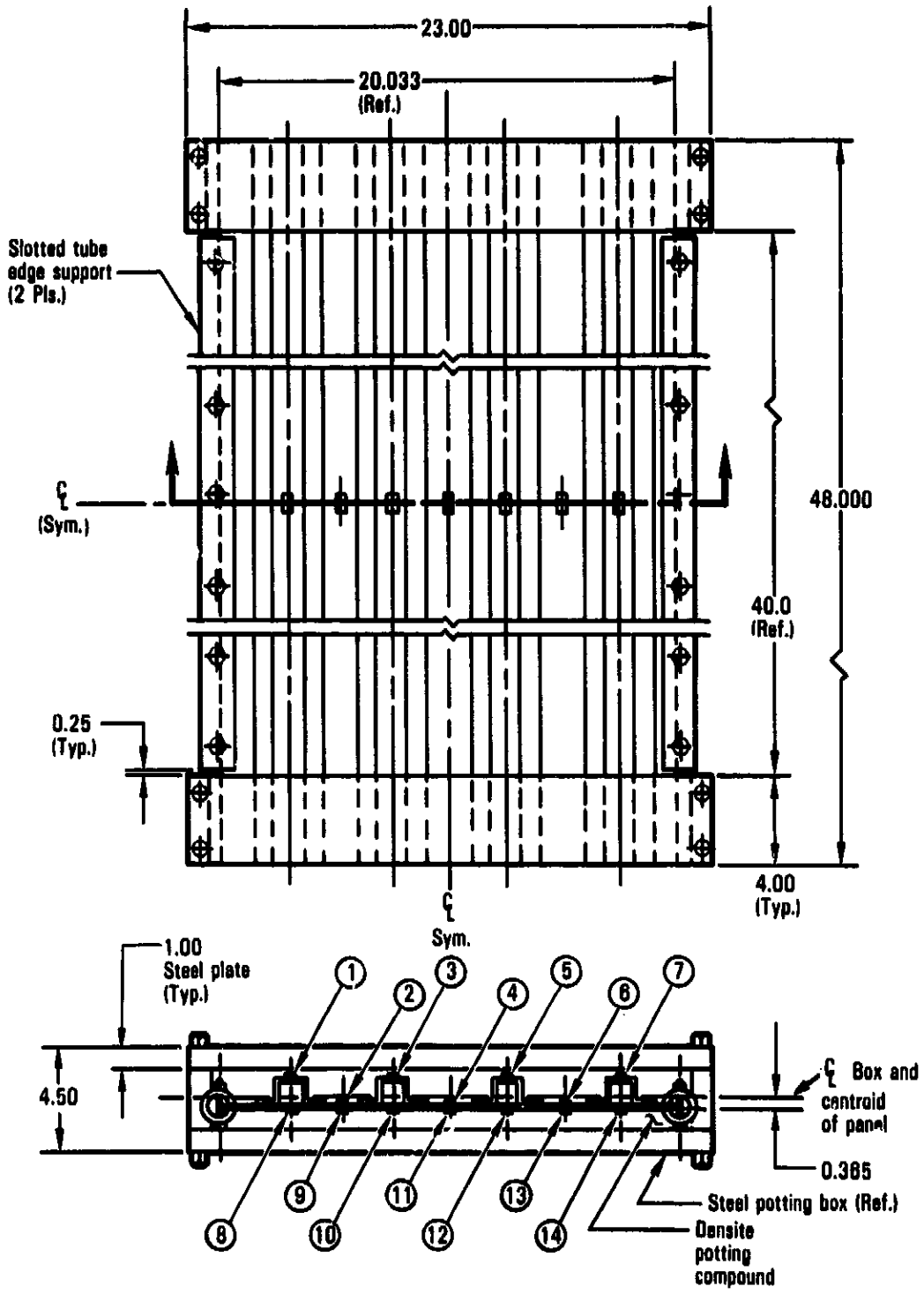

Figure 71. - Strain gage locations, edge clamp details, potting box installation, Panel 7-2. Room temperature long column compression test of representative wing panel.

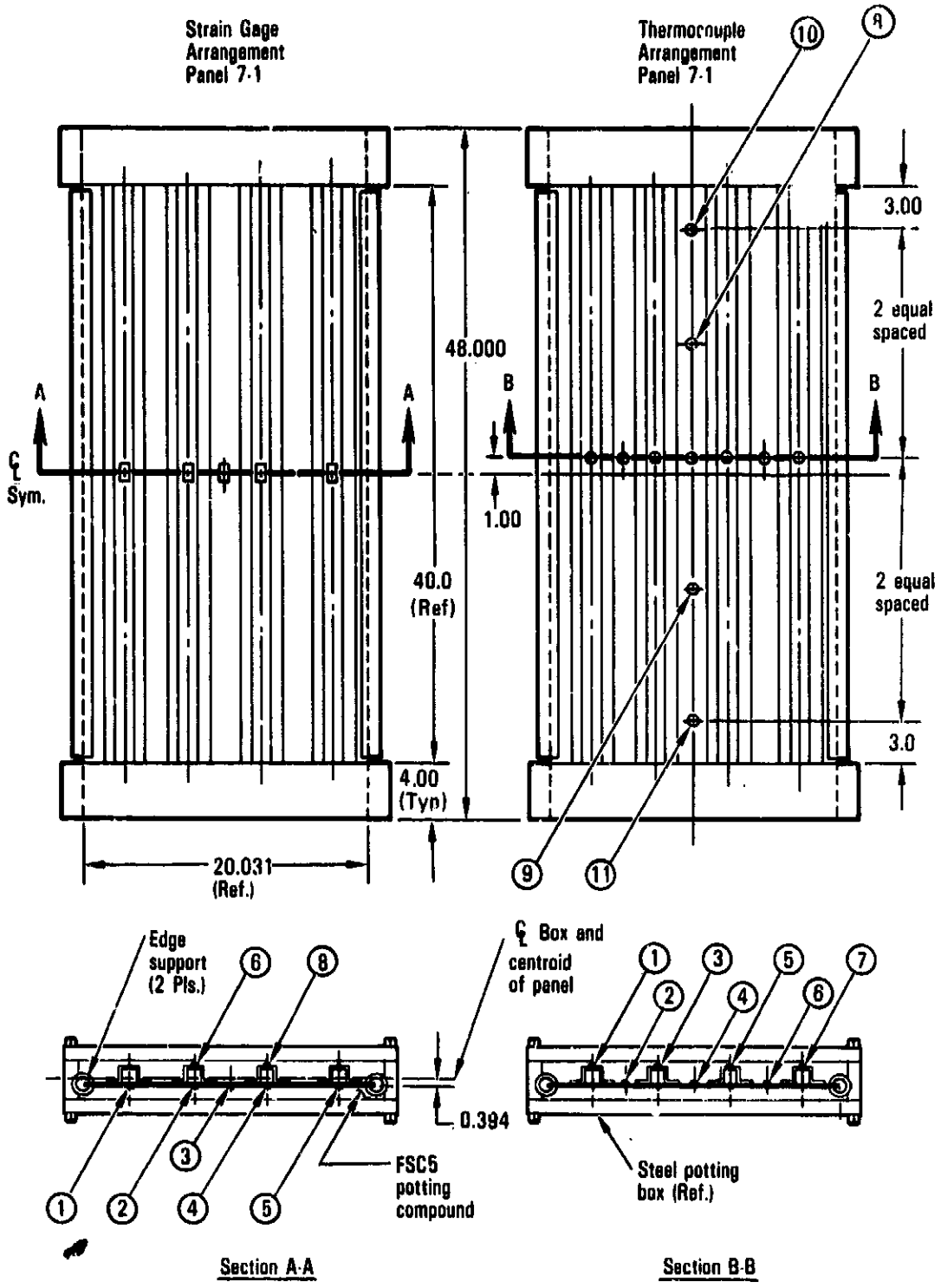

Figure 72. - Strain gage and thermocouple arrangements, panel 7-1. Elevated temperature long column compression test of representative wing panel.

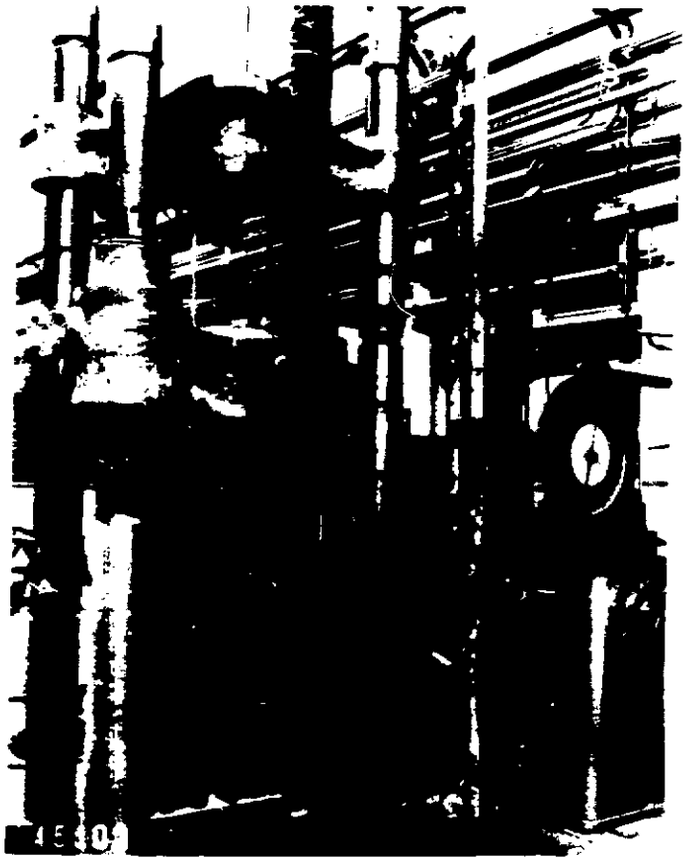

Figure 73. - Installation of panel no. 7-2 in the 400-kip Universal static test machine for room temperature long column compression test of representative wing panel. (LVDT deflection transducer is at the top of the fixed head).

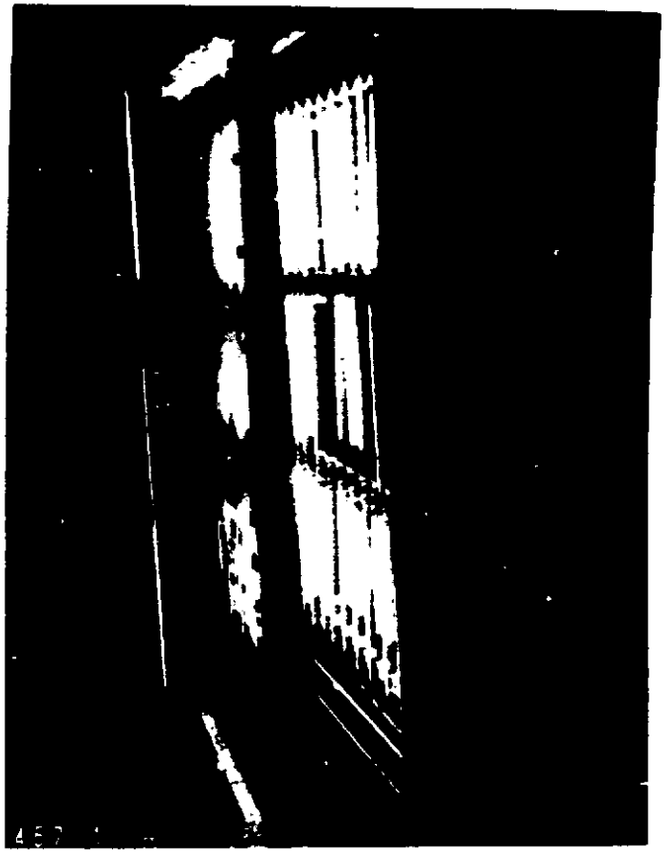

Figure 74. - View of panel no. 7-1 during elevated temperature long column compression test. (Inside of one of the heaters is visible).

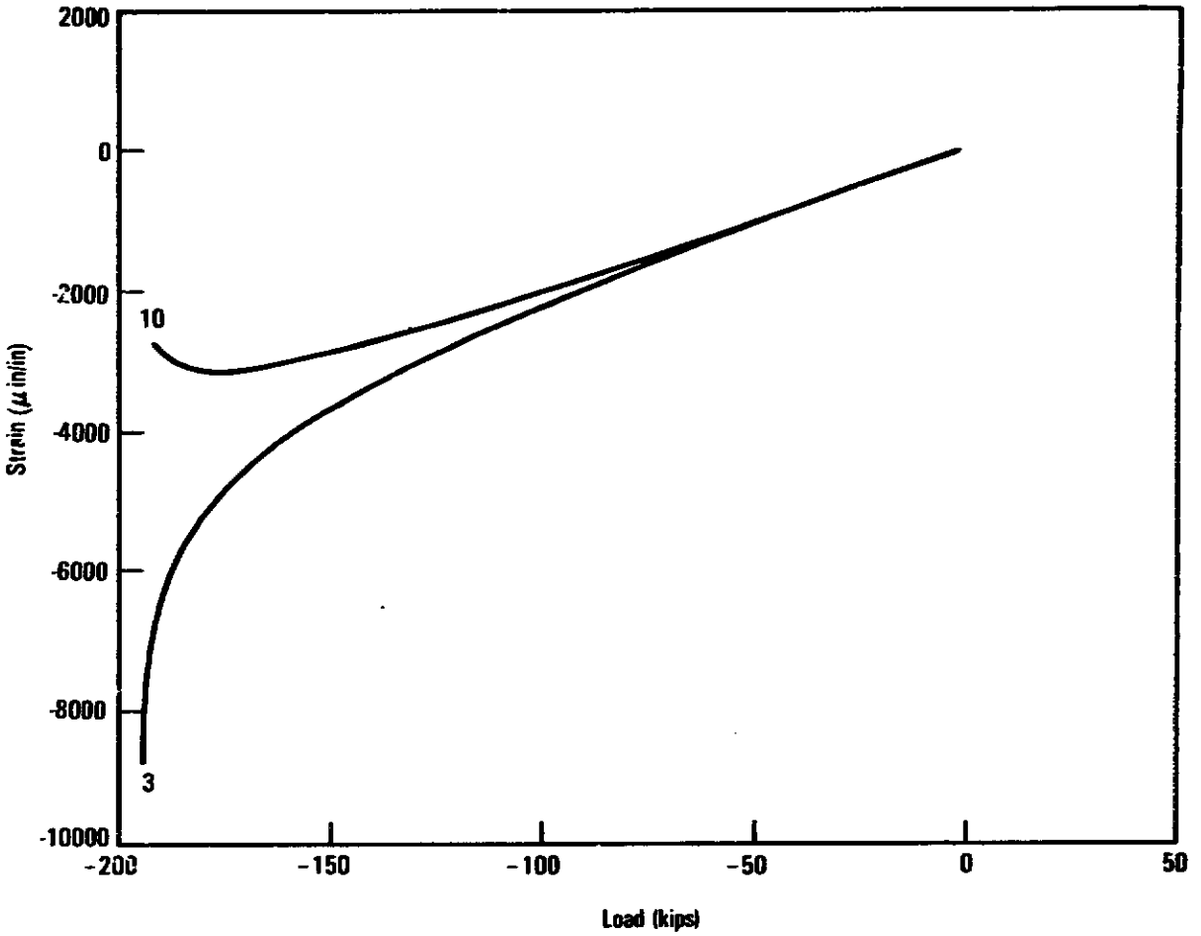

Figure 75. - Panel 7-2, load/strain curves (gages 3 and 10), long column compression tests of representative wing panels.

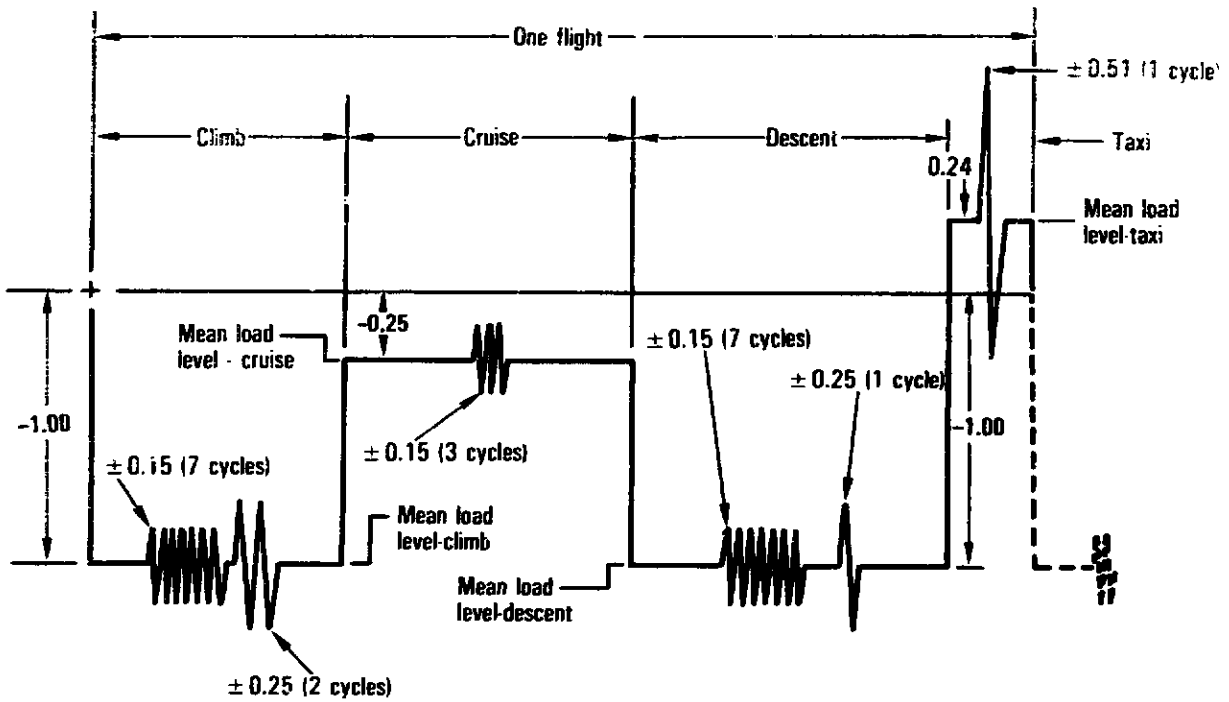

Note: Ordinate indicates ratio of stress to $f_{1g_{Ref}}$

where $f_{1g_{Ref}}$ = 25000 psi

Growth in magnitudes of cycle loads with time is given in Table 42.

Figure 76. - Unit flight loading sequence and magnitudes for beta titanium alloys study, upper surface panel.

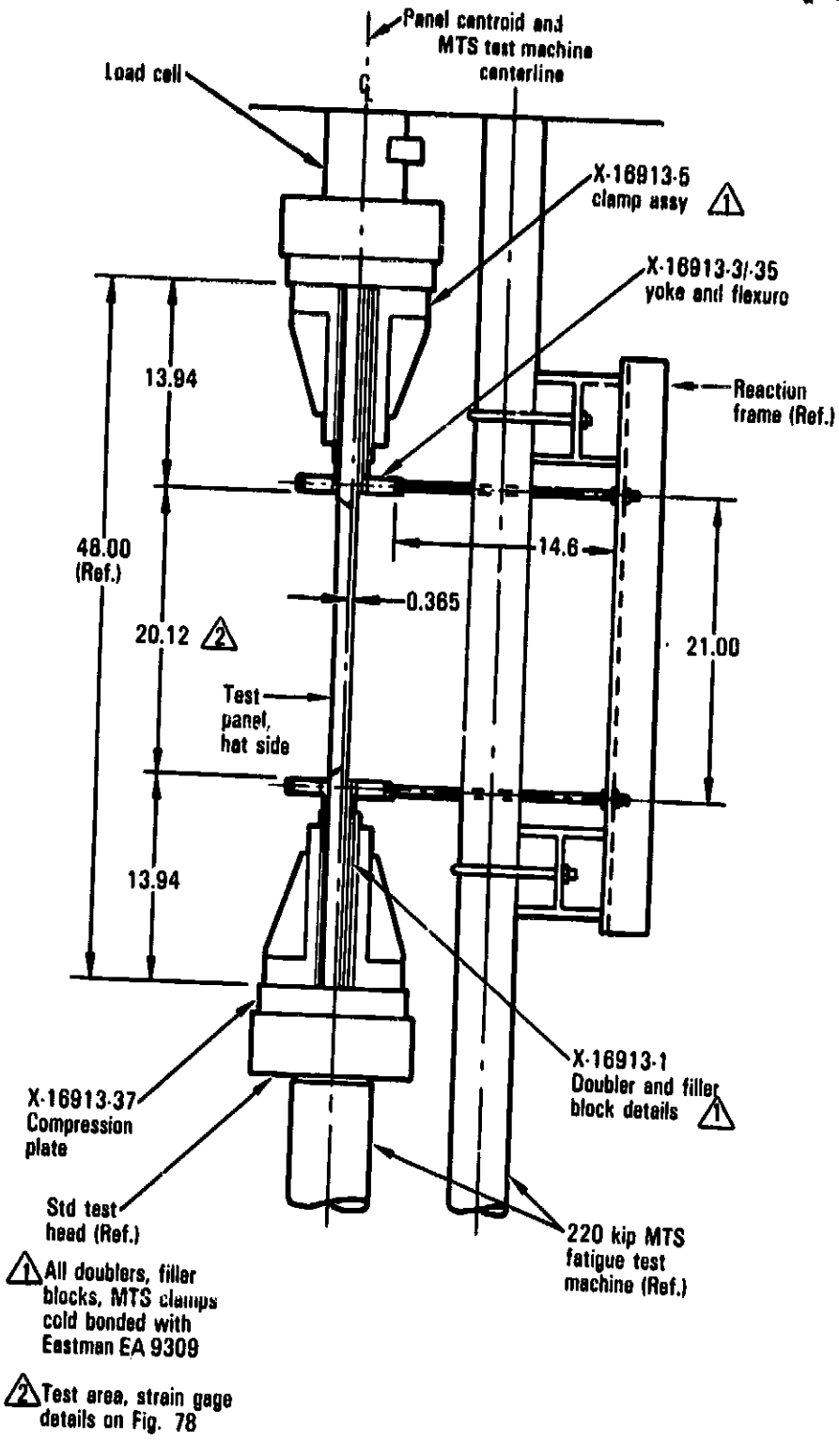

Figure 77. - Fatigue test setup, panel 7-3.

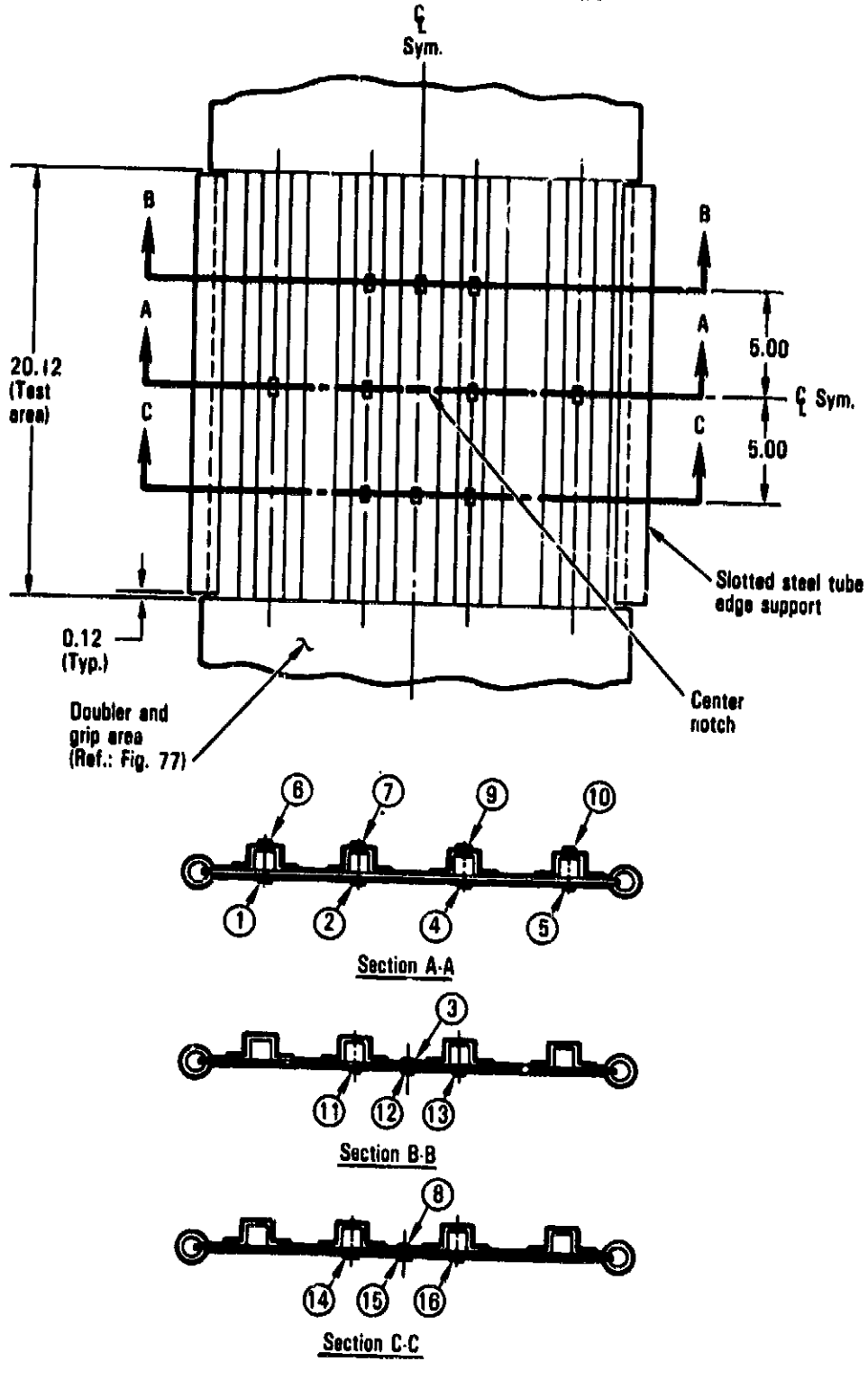

Figure 78. - Strain gage locations - fatigue/crack growth panel 7-3.

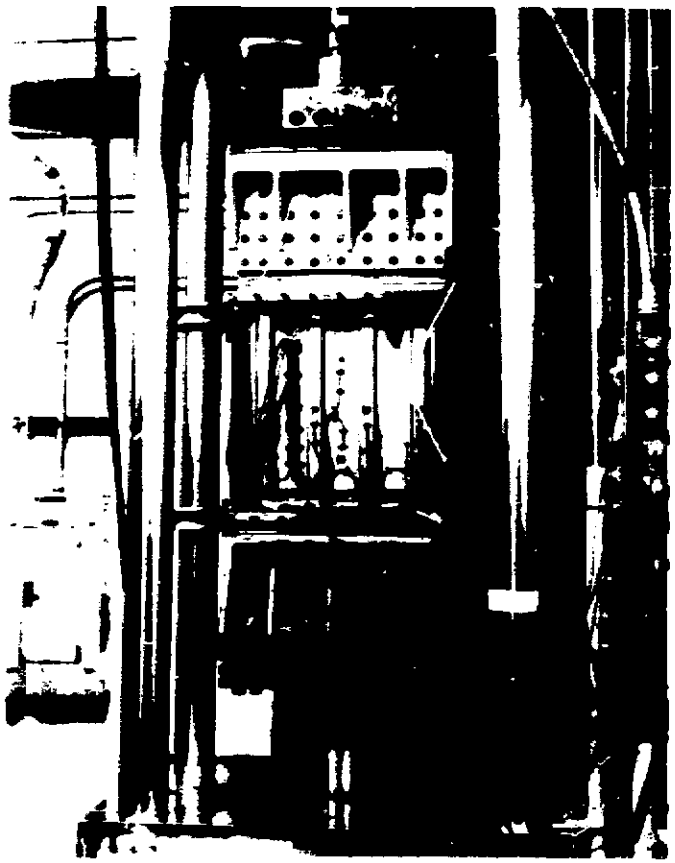

Fatigue/Crack Growth Test. Installation
in 220-kip MTS Fatigue Test Machine

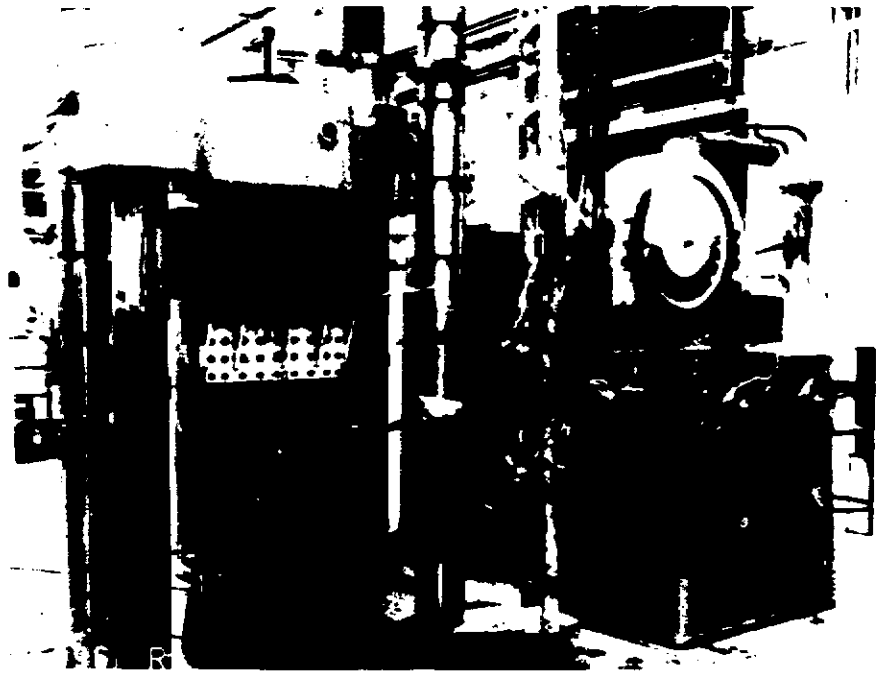

Residual Compression Strength Test. Installation
in 400-kip Universal Static Test Machine

Figure 79. - Fatigue and static compression test installations of panel no. 7-3.

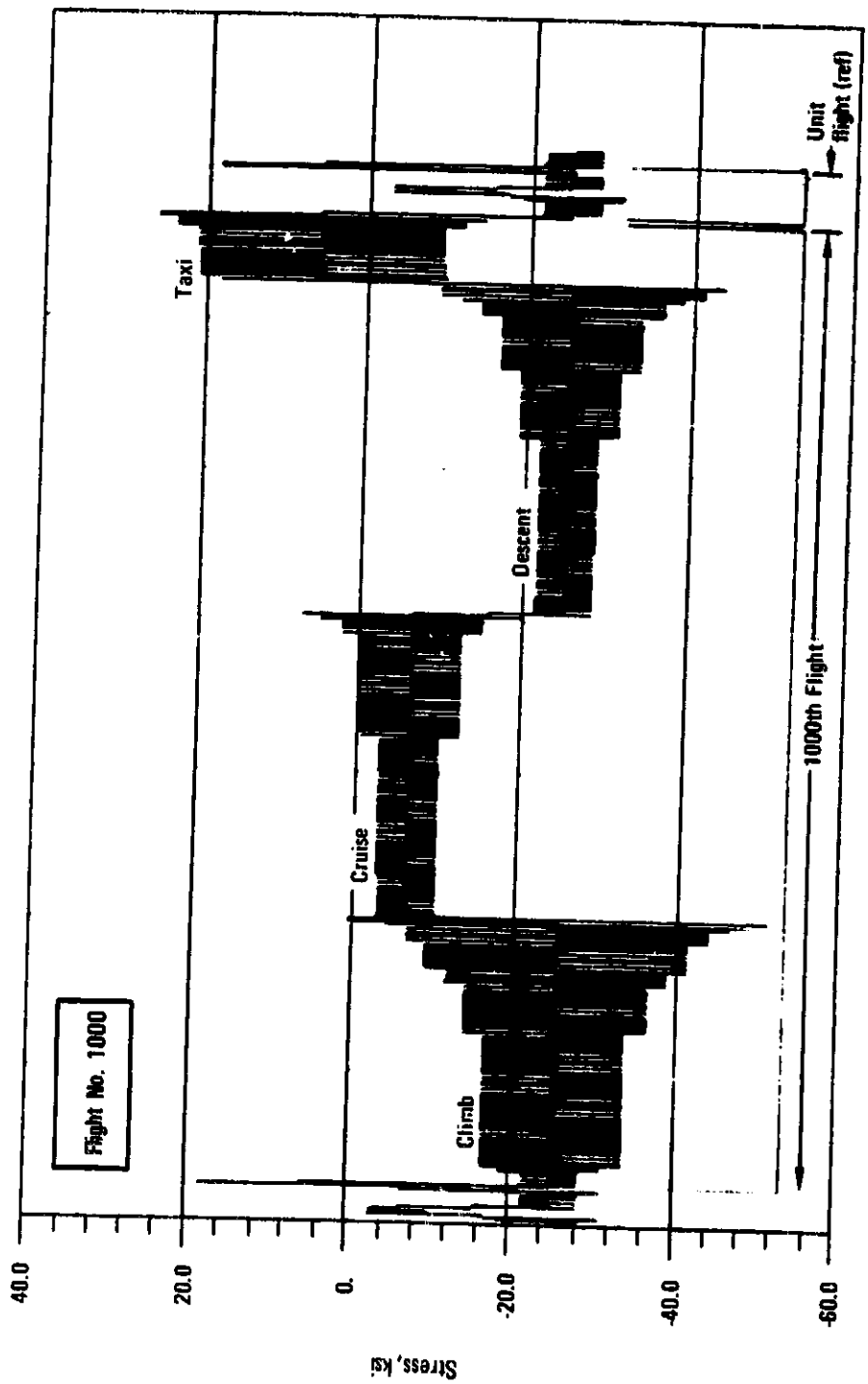

Figure 80. - Computer loading scan during flight 1000 - fatigue/crack growth test of representative wing panel 7-3.

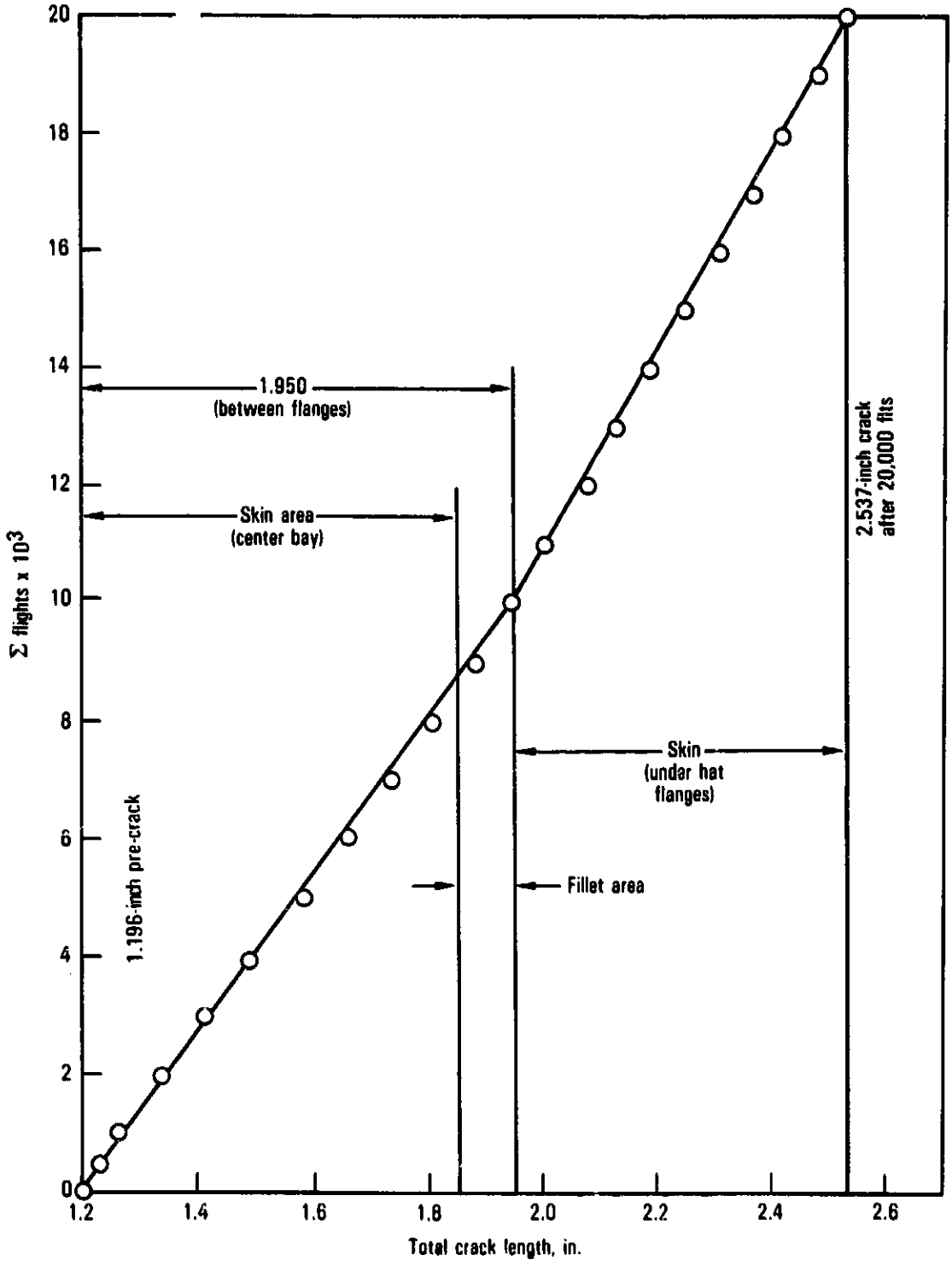

Figure 81. - Crack growth in Ti-6Al-4V skin during second application of 20,000 - flight spectrum, panel 7-3.

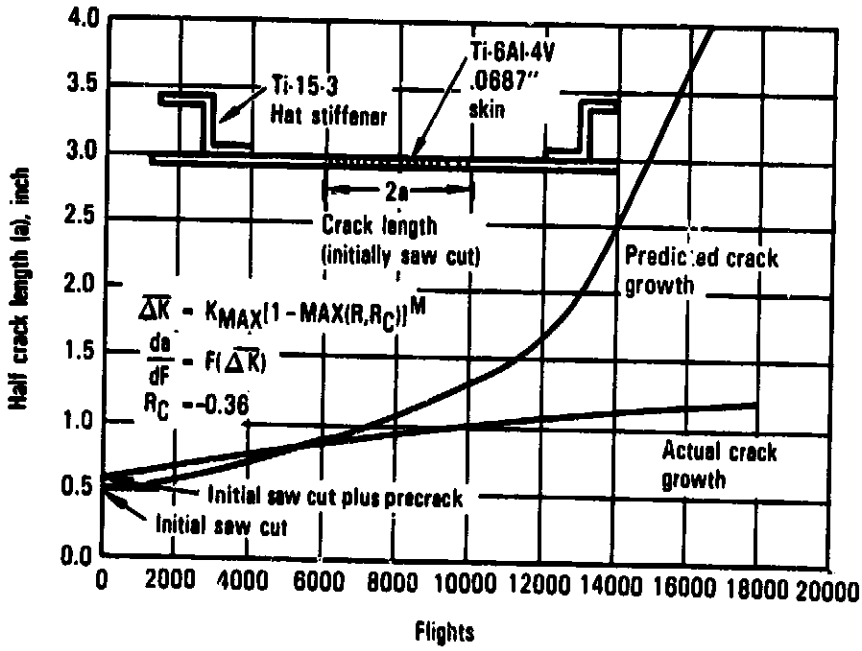

Figure 82. - Predicted and actual crack growth history - fatigue/crack growth test of representative wing panel 7-3.

Figure 83. - Two views of panel 7-3 crack geometry immediately prior to residual strength compression test. (Top) hat side, (bottom) skin side.

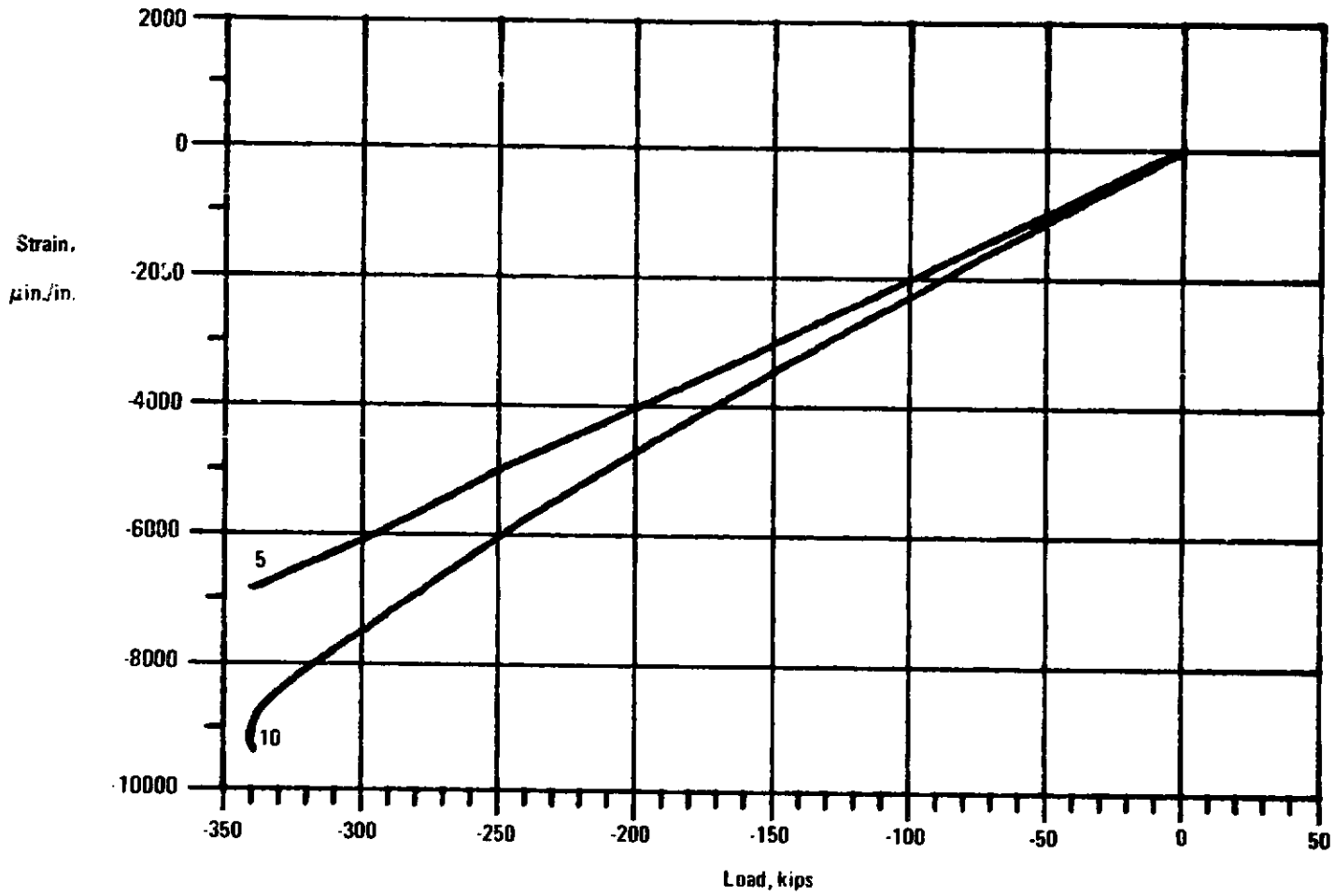

Figure 84. - Panel 7-3, strain vs load (gages 5 and 10), residual compression strength test following fatigue/crack growth test of representative wing panel.

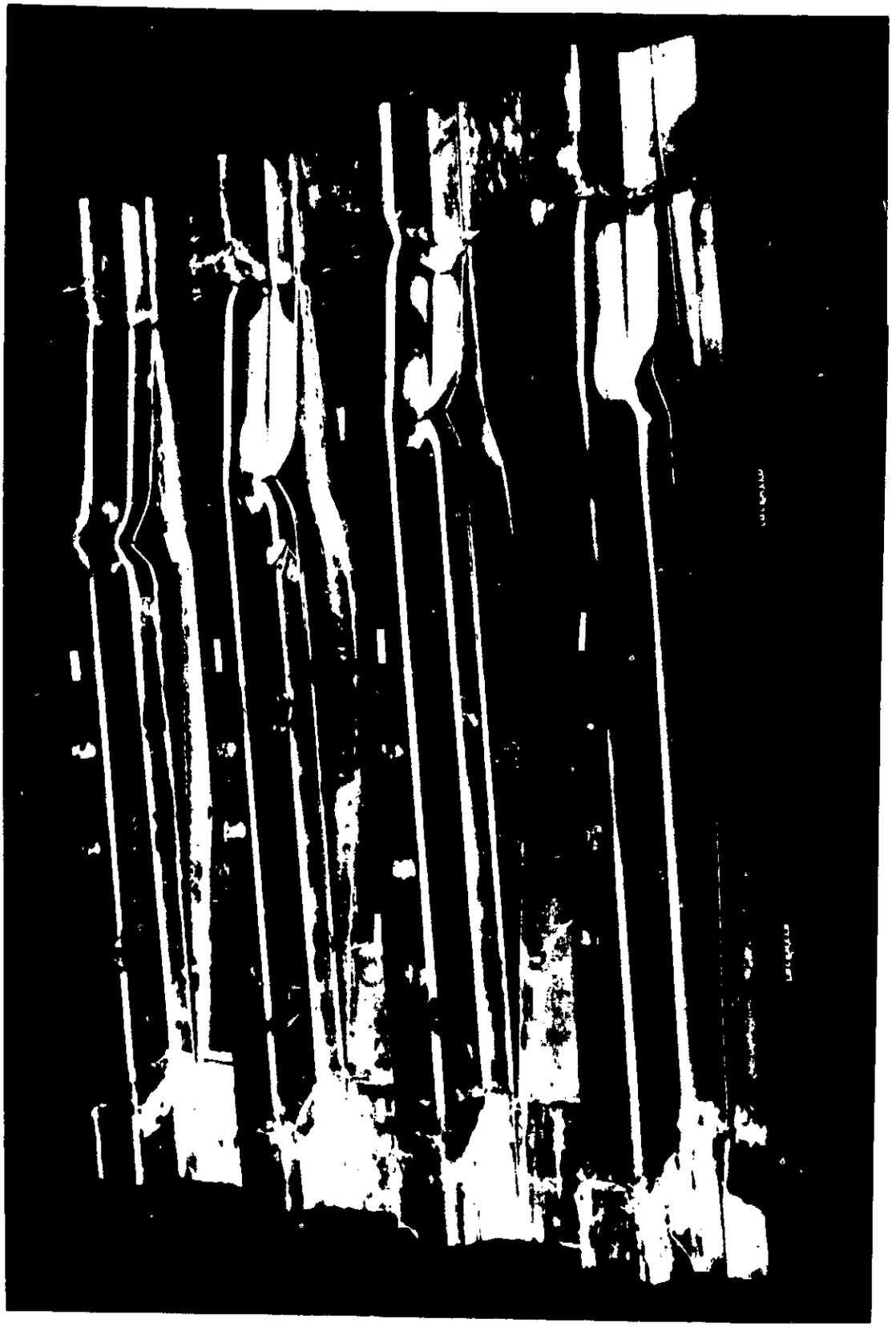

Figure 85. - View of panel 7-3 following residual compression test failure. (End fixtures and strain gage leads removed).

TASK 8 - METAL MATRIX COMPOSITE (MMC) SELECTIVE REINFORCEMENT CONCEPTS

This task investigated the feasibility of using metal matrix composite to selectively reinforce beta titanium structural components on an SCV. It involved the design, analysis, fabrication and testing of coupons and short elements of selected structural concepts, and assessing the data for scaling up the concepts to selectively reinforce full-size wing panels.

Design and Analysis

The Ti-15-3 zee-stiffened skin/stringer configuration of task 5 was chosen for assessing the metal matrix composite selective reinforcement concepts. The task 5 crippling test results thus provided baseline data for the unreinforced skin/stringer configuration. From a producibility and structural stability standpoint, the unsupported (upper) flange of the zee stiffener was the selected reinforcement location. Initially three candidate design concepts as depicted in Figure 86 were reviewed to select two concepts for evaluation having the most promising combinations of fiber/matrix system and compatible joining process.

Two fiber/matrix systems used for preliminary sizing of the reinforcement were state-of-the-art products of AVCO Specialty Materials Division: 1) SCS-6/Ti-6-4 consisting of 35 volume percent silicon carbide (SiC) continous filaments consolidated in a matrix of Ti-6Al-4V foil by diffusion bonding, and 2) SCS-2/6061 containing 45 volume percent SiC in a 6061 aluminum matrix. The analysis indicated an optimum reinforcement thickness of 6-plies for either MMC system, with a reinforcement width of 0.5 inch. The outer skin of matrix alloy was then increased to facilitate subsequent joining to the beta titanium structure.

The three candidate design concepts (figure 86) were analyzed to assess the effect of the MMC material and joining method on their load-carrying capability and weight. The crippling stress of the cross-section was determined, then the optimum column length (simultaneous column and cripping failure) and associated weight were calculated for each concept. This theoretical weight comparison is summarized in table 45. Concept 1 (SiC/Ti-6-4, isothermal braze) was used as the baseline. Concept 2 (SiC/Ti-6-4, spotweld) requires a MMC 2-plies thicker than Concept 1 to carry equal crippling load, but their relative weights remain essentially equal. Concept 3 (SiC/6061, LID diffusion bond) was 6-percent lighter than the other two concepts. Concept 3, however, was eliminated because it was felt that the 6061 aluminum would lose its shear transfer capability at the 600°F service temperature.

Fabrication

SiC/Ti-6-4 composite. - The MMC laminates received from AVCO were 6-plies of 35v/o SiC/Ti-6-4 with a nominal 8 mil skin of Ti-6-4 on each side, resulting in a total thickness of 0.064 inch, a. . 30v/o SiC. The material was ordered in machined specimen widths of 0.250 and 0.500 inch for compression and component tests, and in a sheared specimen width of 1. in. for the lap shear tests. The reported tensile strengths of the MMC varied considerably from panel to panel. Thus, for the purpose of correlating the test data, the first number of a test specimen ID identifies the parent MMC panel number. (Example: specimen 8-1 is from panel no. 8.)

Brazing development. - Concept 1 (figure 86) required establishing the brazeability of Ti-15-3 to the SiC/Ti-6-4 composite using the isothermal brazing process and 3003 aluminum brazing alloy.

Nitric-HF acid cleaning of the MMC resulted in a scattered, dark surface smut. EDAX of the smut revealed nitrogen enrichment which is thought to be a residual from the consolidation stage (possibly boron nitride stopoff). This smut condition was mechanically removed by vapor honing prior to brazing.

The braze shear strengths shown below for SiC/Ti-6-4 to Ti-15-3 lap joints were below the 11.0 to 13.7 ksi range obtained in task 5 for Ti-6-4 to Ti-15-3. Contamination due to surface smutting could be a factor.

Joint Combination (Braze alloy 3003 Al)	Shear Strength (psi)	
	As-Brazed	Aged 940°F-12h
0.063 in. SiC/Ti-6-4	7,850	9,650
to	8,180	10,500
0.063 in. Ti-15-3	8,740	10,700
	10,200	
	10,300	

Microstructure of the SiC/Ti-6-4 isothermal brazed to Ti-15-3, and then aged at 940°F for 12 hours, is shown in figure 87. Good wetting was achieved, and no detrimental fiber/matrix interactions were readily observed.

NOTE: Brazing a single flat strip of Ti-15-3 to the SiC/Ti-6-4 composite causes significant lengthwise bow, apparently a result of differential thermal expansion and contraction rates of the materials. This is evidence that more symmetric MMC placement is preferred.

Spotwelding Development. - The two spotweld joint combinations required for design concept 2 (figure 86) were 0.063 in. Ti-15-3 (aged) to 0.040 in. Ti-6-4 (annealed), and 0.063 in. Ti-15-3 (aged) to 0.063 in. SiC/Ti-6-4 composite. The Ti-15-3 was aged 940°F-12 hours before spotwelding, and the joints were evaluated in the as-welded state. A summary of the spotweld procedure development evaluation is given in table 46.

Spotwelds between Ti-15-3 and Ti-6-4 displayed satisfactory shear strengths, regular nugget shape and size, and no evidence of internal defects. Photomicrographs of a transverse center section of a representative spotweld are shown in figure 88. Longitudinal sections exhibited identical micrographic features. The symmetrical columnar growth within the weld nugget suggested thorough mixing of the two alloys and symmetric solidification. This was further verified through SEM study and EDAX. A vanadium X-ray map of the fusion zone exhibited uniform distribution of vanadium over the entire region. Quantitative EDAX analysis of the weld nugget showed almost identical compositions on both sides of the interface with about 12 percent vanadium in both locations. Thus, thorough mixing of the Ti-6Al-4V and Ti-15V-3Cr-Sn-3Al alloys is indicated.

Spotwelds between the Ti-15-3 and SiC/Ti-6-4 composite were unsatisfactory. The presence of SiC filaments completely changed the weld nugget structure.

A transverse section of the SiC/Ti-6-4 away from the spotweld location is illustrated in figure 89. Though gaps from the consolidation stage were observed between the filaments, their distribution was fairly regular.

Transverse and longitudinal sections through the center of the spotwelds are shown in figures 90 and 91 at several magnifications. The size of the fuzed zone has decreased. X-ray mapping indicated that the nugget was poor in vanadium, which substantiates that melting was mostly confined within the SiC/Ti-6-4 composite material and little mixing has occurred with the Ti-15-3.

Spotwelding caused bending of the filaments and some cracks were observed in the filaments. Figure 90 also illustrates the formation of shrinkage cracks around the filaments. Most of these cracks were located near the center of the nugget which is the area that solidifed last. The columnar grain growth of the Ti-15-3/Ti-6-4 weld (figure 88) was absent in the Ti-15-3/MMC weld nugget. Instead, a fine dendritic structure was observed within this area which suggests a rapid solidification process, and an annular ring of a fine cellular structure was observed around the SiC filaments (figures 90 and 91). Figure 92 is an SEM photograph of a filament and its adjacent matrix area containing some shrinkage cracks. Quantitative EDAX performed at locations A, B, C, and D (figure 92) revealed that the white cellular growth at location A was rich in silicon (14 percent). The silicon content decreased sharply as the distance from the filament increased. Around

2 wt. percent silicon was measured at locations B and C on either side of the crack, and the silicon content was reduced to 0.82 wt. percent at D. The 2 wt. percent silicon in titanium can increase the temperature difference between solidus and liquidus over 300°F, which encourages dendritic growth, and in turn makes the alloy more prone to shrinkage cavity formation. The dendritic solidification pattern is evident at the shrinkage cracks in figure 92 (right-hand bottom side of the filament). Apparently, the filaments being of lower thermal conductivity dissipate less heat; consequently, molten material around the filaments freezes last and shrinkage cracks develop.

An attempt was made to limit weld nugget penetration to the outermost 8 mil Ti-6-4 skin of the SiC/Ti-6-4 composite by adjustment of the spotwelding parameters and heat balance. Transverse and longitudinal sections through the center of the bond made between Ti-15-3 and the SiC/Ti-6-4 are shown in figure 93. Microscopic examination indicates that the interface has the nature of a solid state diffusion bond, although some melting has taken place within the composite (where resistivity might be highest) as evidenced by presence of the fine solidification structure. Fiber distortion was minimal and no shrinkage cracks were seen. As shown in table 46, the shear strength of the resistance bond was comparable to the strength of the spotwelds which had a high degree of penetration. The reliability and repeatability of this type of bond is yet undetermined, and work on the resistance spotweld approach for joining SiC/Ti-6-4 to beta titanium was discontinued.

Testing

Coupon and short element compression tests of the selective reinforcement design concepts were performed.

Coupon tests. - The effects of the joining processes and heat treatment on the compressive properties of the SiC/Ti-6-4 MMC were evaluated. Tests included the baseline MMC, MMC with simulated brazing cycle, MMC joined to Ti-15-3 by isothermal brazing or spotwelding, and spotwelds between Ti-6-4 and Ti-15-3. Ti-6-4/Ti-15-3 brazed joints were covered in task 4.

The basic test coupon configuration is shown in figure A8 of the appendix. The 0.90 in. gage length was selected based upon spanning at least two spotwelds for the maximum spotweld pitch tested (5/8 inch). Two strain gages were attached back-to-back in the test section. Using hydraulic grips, loading was primarily in shear through bonded grip tabs. End loading was also available in the grips. The loading rate was 0.010 inch per minute.

Results of the coupon compression tests are presented in table 47. All coupons failed by buckling (or bending) in the test section. These limited tests show that the brazing and/or aging thermal cycles had negligible effect on the compression strength or modulus of the SiC/Ti-6-4 composite. Test results of the spotweld and brazed joint specimens are generally inconclusive, although the brazed joint strengths were higher.

Short element tests. - Two crippling tests were conducted for design concept 1 of figure 86. The specimen configuration is identical to the Ti-15-3 zee-stiffened elements in task 5 (see figure 57), with the addition of the SiC/Ti-6-4 composite unidirectional reinforcement on the unsupported flange of the stringer.

Ti-15-3 stringers were made from 0.063 in. sheet brake formed to the zee shape. The MMC, stringer, and Ti-6-4 skin segment were isothermal brazed using 3003Al brazing alloy, then the specimens were aged in a vacuum furnace at 940°F for 12 hours. The test length of the specimens was 4 inches after potting and machining the ends. Testing details were essentially the same as described in the task 5 crippling test section. The analysis and test results are summarized in table 48, and the failed specimens are displayed in figure 94.

As the loading on specimen 0-27 approached its maximum value, the specimen twisted slightly. This twist became more pronounced as the loading gradually dropped off. The MMC reinforcement did not crack but folded over on itself, delaminating at the fold and separating from the stringer flange over a 1.5 inch length. The skin and stringer crippled slightly at failure but did not crack. The brazed skin/stringer joint separated slightly over a length of less than 1/4 inch.

The MMC reinforcement on specimen 0-28 buckled and delaminated slightly, but only cracked part of the way through its thickness. The brazed joint between the reinforcement and the stringer remained intact until the load had reached its maximum value and was in the process of being relieved. The stringer and skin exhibited a crippling-type failure, but did not crack or disbond.

Less than a 2 percent variation was recorded between the predicted failure stresses and the test results of the two brazed specimens. Indications of initial skin buckling were within 12 percent of the prediction. Properties for the MMC reinforcement used in the analysis were derived from test data obtained on other Lockheed programs. The modulus values shown in table 47 of this report agree closely with the derived data, but the buckling failure mode precluded obtaining compressive yield strength properties. The average failure stress of the reinforced configuration (126.5 ksi) is about 11 percent higher than that for unreinforced specimens in task 5.

Weight/Cost Study

Weight comparison. - A theoretical weight comparison was made between a baseline unreinforced panel and the MMC reinforced panel concepts. The basic task 7 configuration for a SCV wing upper surface hat-stiffened skin panel 20 in. wide and 48 in. long was maintained; reinforcement location was on the crown of the hats (figure 95).

Table 49, which includes results of the earlier task 7 weight study, shows that all three designs incorporating Ti-15-3 stiffeners provide a considerable theoretical weight savings over the conventional Ti-6-4 riveted panel. The reinforced spotwelded panel is about 9 percent lighter than the conventional panel and the unreinforced brazed panel (task 7 configuration) is 16 percent lighter. The reinforced brazed panel shows the greatest theoretical weight savings, 22 percent, over the conventional titanium panel. Viewing the unreinforced brazed configuration as the baseline, only the reinforced brazed panel is lighter.

Cost comparison. - A preliminary cost assessment was made for scaling up the MMC selective reinforcement of beta titanium structure to fabricate a full size wing panel for a SCV. The basic hat-stiffened wing panel configuration of task 7 was used, with the reinforcement located on the crown of the hats as depicted in figure 95. Projected costs for the selectively reinforced concepts are viewed as rough order of magnitude (ROM) estimates because of the lack of familiarity with MMC fabrication limitations. Table 50 compares projected costs, based on a quantity of 100, for the MMC-reinforced concepts and baseline unreinforced panels. The costs of the spotwelded and brazed reinforced panel concepts are, respectively, about 40 percent and 60 percent higher than the conventional Ti-6-4 panel.

TABLE 45. - WEIGHT COMPARISON OF A Ti-15-3 ZEE-STIFFENED ELEMENT REINFORCED WITH MMC

Concept	Joining Method	Heat Treat*	MMC Reinforcement			Optimized Panel Length in.	Relative Weight
			Description	Width in.	Thickness in.		
1	Isothermal Braze (Baseline)	After Brazing	SCS-6/Ti-6-4 (35v/o SiC)	0.50	0.063	20.56	1.000
2	Spotweld**	Before Welding	SCS-6/Ti-6-4 (35v/o SiC)	0.50	0.079	20.62	1.003
3	Liquid Interface Diffusion Bond	After Bonding	SCS-2/6061 Al (45v/o SiC)	0.50	0.059	20.53	0.940

*Aged at 940°F for 12 hours.

**Maximum spotweld spacing to prevent inter-weld buckling = 1-3/16 in.

TABLE 46. - SUMMARY OF SHEAR STRENGTH AND METALLURGICAL FEATURES OF SPOTWELDS

Two Sheet Combinations	Avg. Shear* (lbs)	Avg. Nugget Dia. (in.)		Max. Penetration (%)		Internal Quality
		L	T	L	T	
0.040 in. Ti-6-4 (Ann.) to 0.063 in. Ti-15-3 (Aged)	2890	0.199	0.208	72 87	70 84	Clear (Ref. figure 88)
0.063 in. SiC/Ti-6-4 to 0.063 in. Ti-15-3 (Aged) (High Nugget Penetration)	1820	0.210 0.179	0.229 0.153	88 57	84 44	SiC fibers displaced with some fracturing Shrinkage cracks around fibers near middle of weld nugget. (Ref. figures 90, 91, 92)
0.063 in. SiC/Ti-6-4 to 0.063 in. Ti-15-3 (Aged) (Minimum Nugget Development)	1580	N/A	N/A	N/A	N/A	Solid state bond at interface, slight melting within composite Minimal SiC fiber distortion No shrinkage cavities evident (Ref. figure 93)

*Single spot specimens 1 in. wide with 1 in. overlap.

TABLE 47. - ROOM TEMPERATURE COMPRESSION TEST RESULTS OF METAL MATRIX COMPOSITE TEST COUPONS AFTER VARIOUS PROCESSING CYCLES

Coupon ID(1)	Material(2)	Condition(3)	Buckling Stress (ksi)	Initial Tangent Modulus (Msi)	Remarks
8-1	MMC	As-fabricated	268.7	29.0	
8-2	MMC	As-fabricated	277.2	29.4	
Avg.			272.9	29.2	
8-3	MMC	Age	268.6	28.6	
8-4	MMC	Age	280.4	29.5	
Avg.			274.5	29.0	
8-5	MMC	Braze Cycle	277.5	29.7	
8-6	MMC	Braze Cycle	286.2	29.1	
Avg.			281.8	29.4	
8-7	MMC	Braze Cycle + Age	283.5	29.7	
8-8	MMC	Braze Cycle + Age	272.8	30.2	
Avg.			278.2	29.9	
8-9	MMC/Ti-15-3	Braze + Age	236.1	–	Lengthwise bow 0.085 in.
8-11	MMC/Ti-15-3	Braze + Age	211.5	–	Lengthwise bow 0.081 in.
Avg.			223.8		
0-16	MMC	As-fabricated	Failed in set-up		
0-17	MMC	As-fabricated	225.7	29.1	
0-18	MMC	Age	213.4	29.4	
0-19	MMC	Age	221.7	28.9	
Avg.			217.6	29.2	
0-22	MMC/Ti-15-3	Braze + Age	218.8	–	Lengthwise bow 0.040 in.
0-23	MMC/Ti-15-3	Braze + Age	227.2	–	Lengthwise bow 0.040 in.
Avg.			223.0		
0-20	MMC/Ti-15-3	Spotweld (5/8 in. pitch)	182.6	22.4	
0-26	MMC/Ti-15-3	Spotweld (5/8 in. pitch)	173.2	22.4	
Avg.			177.9	22.4	
C-1	Ti-6-4/Ti-15-3	Spotweld (5/8 in. pitch)	104.4	–	
C-X	Ti-6-4/Ti-15-3	Spotweld (5/8 in. pitch)	105.0	–	
Avg.			104.7		
9-8	MMC/Ti-15-3	*Res. Bond (3/8 in. pitch)	185.4	23.6	
9-11	MMC/Ti-15-3	*Res. Bond (3/8 in. pitch)	215.2	23.9	
Avg.			200.3	23.7	
9-12	MMC/Ti-15-3	*Res. Bond (5/8 in. pitch)	184.1	23.3	
9-13	MMC/Ti-15-3	*Res. Bond (5/8 in. pitch)	165.4	22.2	
9-14	MMC/Ti-15-3	*Res. Bond (5/8 in. pitch)	157.4	22.7	
Avg.			169.0	22.7	

(1)First number in ID identifies original MMC panel number. Specimen Configurations: Figure A8.

(2)MMC = 0.063 in. SiC/Ti-6-4 (6-ply, 30v/o); Ti-15-3 = 0.063 in.; Ti-6-4 = 0.040 in.

(3)Age = 940°F - 12h in vacuum. (Note: Ti-15-3 portion of all spotweld coupons is aged prior to spotwelding).

*Refers to resistance spotbond of table 46 with zero nugget penetration.

TABLE 48. - ANALYSIS AND TEST RESULTS OF ROOM TEMPERATURE SHORT COLUMN CRIPPLING TESTS OF SELECTIVELY REINFORCED SKIN/STRINGER ELEMENTS

Description	Spec. ID	Initial Buckling Stress (psi)		Failure Stress (psi)		Comments
		Calculated	Test	Calculated	Test	
Ti-15-3 stringer Ti-6-4 skin SiC/Ti-6-4 reinforcement Brazed with 3003A1	0-27	116,000	120,000	128,700	125,800	Specimen twisted slightly just before it reached maximum load. Showed some evidence of separation at both braze interfaces.
	0-28	114,000	100,000*	128,600	127,300	Showed no visible evidence of separation at either braze interface before failure.

*Based on visual observation, not on strain gage data.

Note: All stresses are averaged.

TABLE 49. - THEORETICAL WEIGHT COMPARISON OF MMC-REINFORCED AND BASELINE WING PANEL CONCEPTS

Panel Description (20 by 48 in. with 4 stringers)	Theoretical Weight		
	Lb	Percent Change	
		Riveted Baseline	Brazed Baseline
BRAZED PANEL Ti-15-3 Stringers, t = 0.080 in. Ti-6-4 Skin, t = 0.070 in.	24.4	-16%	-
RIVETED PANEL Ti-6-4 Stringers, t = 0.080 in. Ti-6-4 Skin, t = 0.095 in.	29.0	--	+19%
SPOTWELDED REINFORCED PANEL Ti-15-3 Stringers, t = 0.080 in. Ti-6-4 Skin, t = 0.076 in. SCS-6/Ti-6-4 Reinforcement, t = 0.063 in.	26.3	-9%	+8%
BRAZED REINFORCED PANEL Ti-15-3 Stringers, t = 0.080 in. Ti-6-4 Skin, t = 0.048 in. SCS-6/Ti-6-4 Reinforcement, t = 0.063 in.	22.6	-22%	-7%

TABLE 50. - ROM COST COMPARISON OF MMC-REINFORCED AND BASELINE WING PANEL CONCEPTS

Material Stringer/Skin	Ti-6-4/Ti-6-4	Ti-15-3/Ti-6-4	Ti-15-3/Ti-6-4 (SiC/Ti-6-4 Reinforced)	Ti-15-3/Ti-6-4 (SiC/Ti-6-4 Reinforced)
Fabrication Method	*Hot Form, Rivet	*Cold Form, Isothermal Braze	Cold Form, Isothermal Braze	Cold Form, Spotweld
Recurring Costs ($)	2116	1347	3340	3106
Nonrecurring Costs, Amortized ($)	161	284	276	46
Total Unit Cost ($)	2277	1631	3616	3152
Δ Cost vs. Baseline (%)	Baseline	−28%	+58%	+38%
Implementation Cost ($)	16140	28449	27613	4626

Panel Size: 20 by 48 inches with 4 stringers.

Quantity: 100

*Data from task 7, table 44.

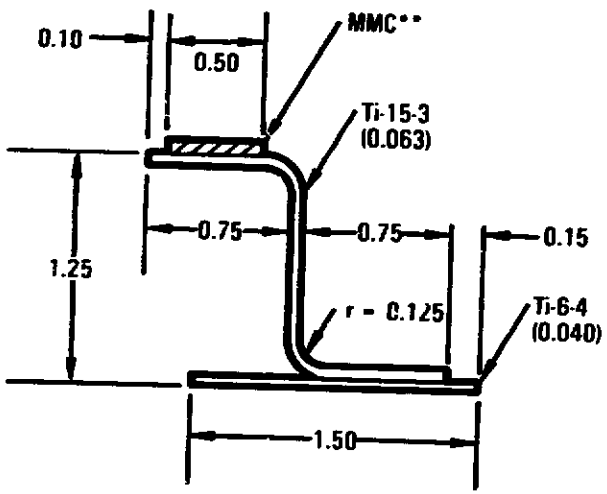

Dim. in inches

Concept	MMC	Joining Method
1	35v/o SiC/Ti-6-4	Isothermal Braze
2	35v/o SiC/Ti-6-4	Spotweld
3	45v/o SiC/6061A ℓ	Diffusion Bond (LID)*

*Rohr Industries proprietary liquid interface diffusion (LID) bonding process
**SiC fiber orientation (0°) into page

Figure 86. - Candidate metal matrix composite selective reinforcement concepts.

Longitudinal section 8.5X

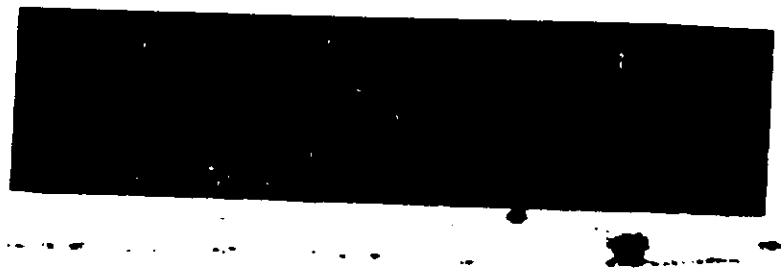

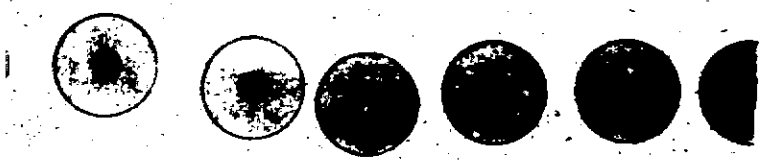

Transverse section 100X

Transverse section 500X

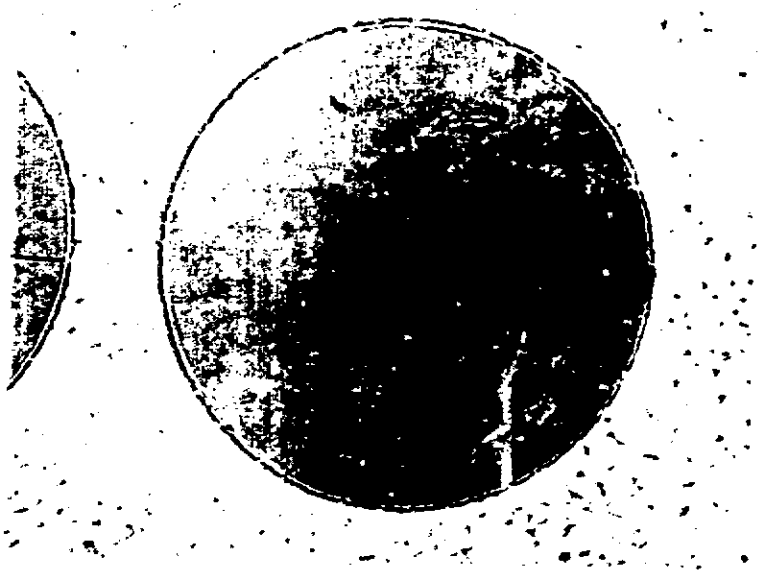

Transverse section 500X

Figure 87. - Microstructure of Ti-15-3 and SiC/Ti-6-4 brazed with 3003 Al and aged 940°F for 12 hours.

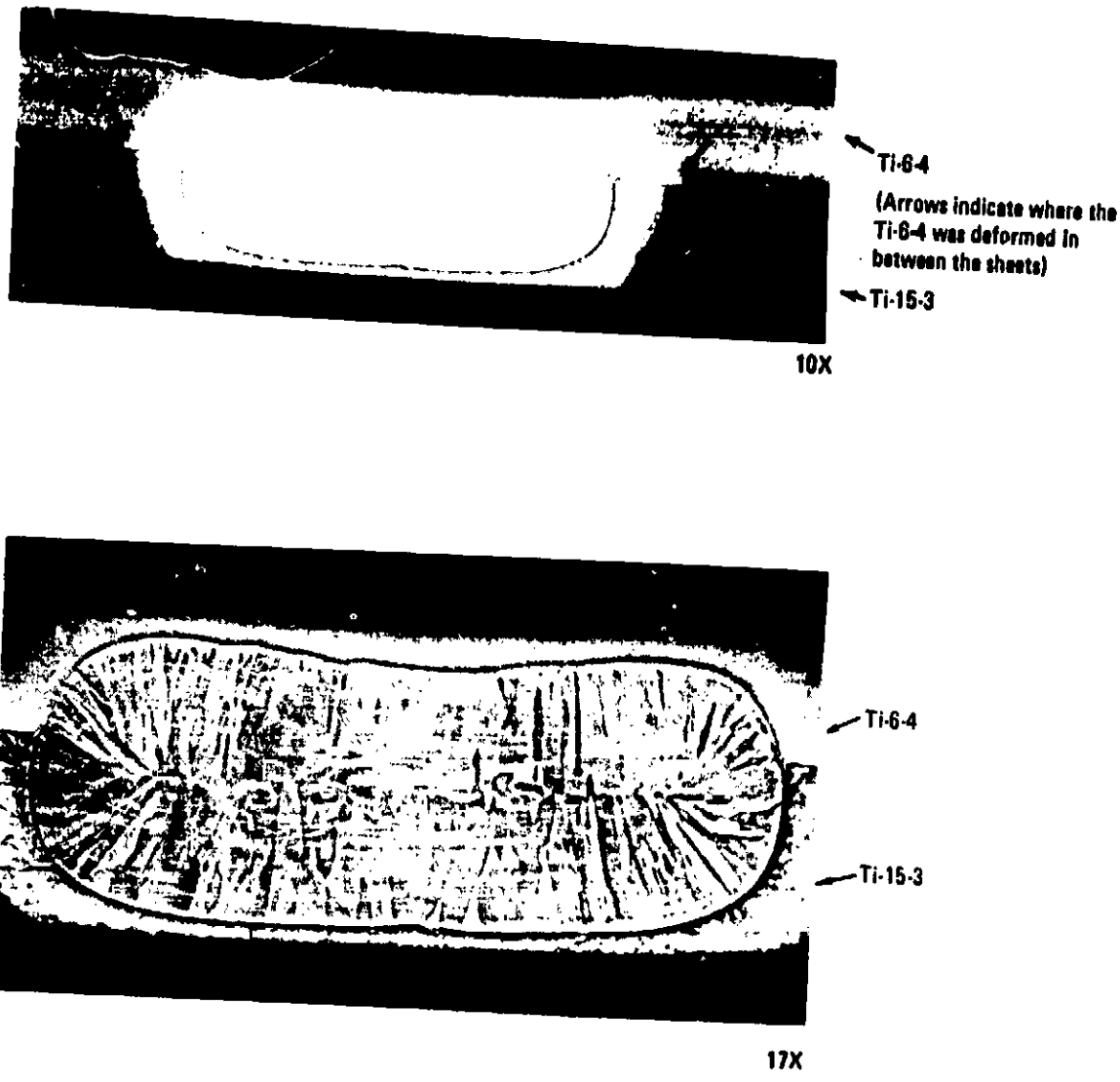

Figure 88. - Photomicrographs of the transverse section through the center of a spotweld between 0.040 in. Ti-6-4 (Ann.) and 0.063 in. Ti-15-3 (Aged).

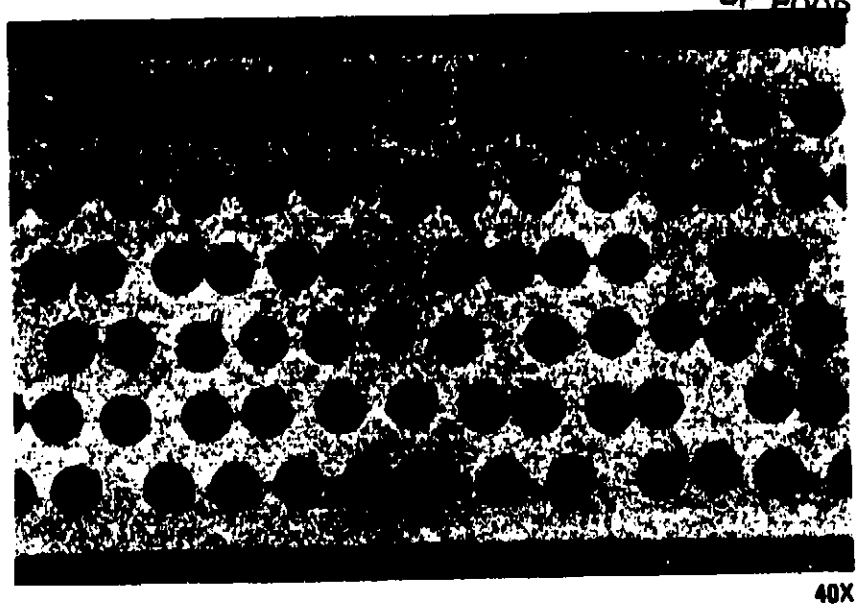

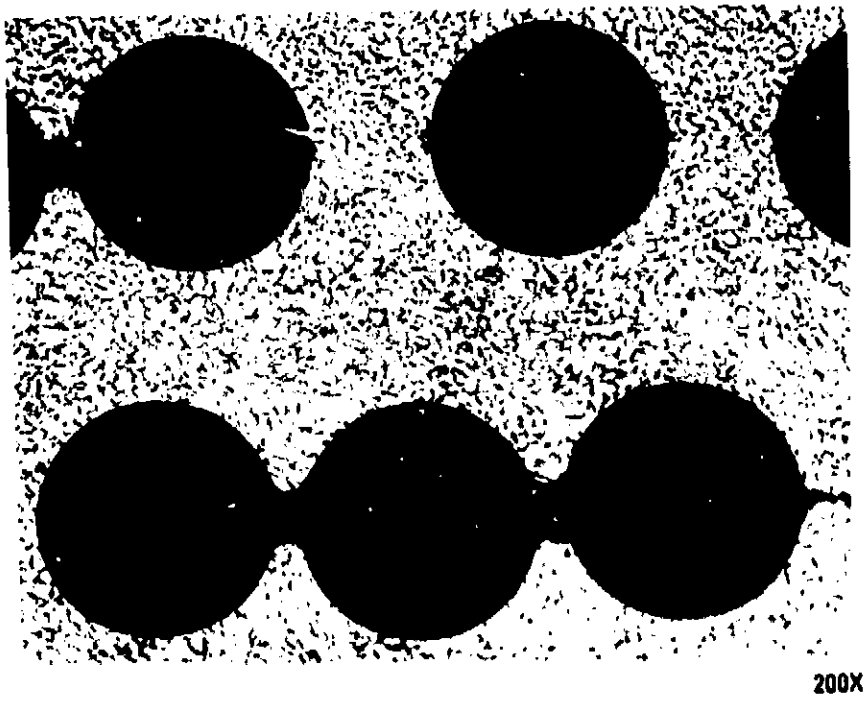

Figure 89. - Photomicrographs of the transverse section of the SiC/Ti-6-4 composite away from the spotweld area showing the distribution of SiC filaments. Note evidence of unfilled gaps between the filaments (arrows in upper photo).

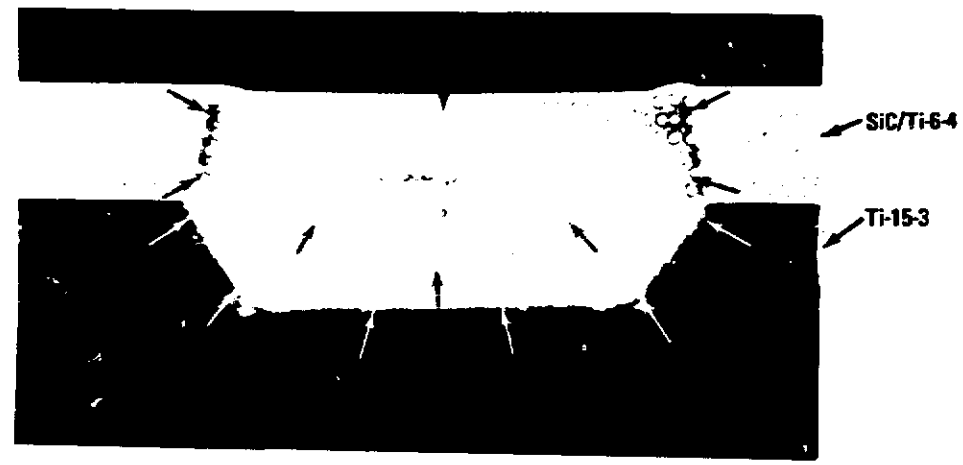

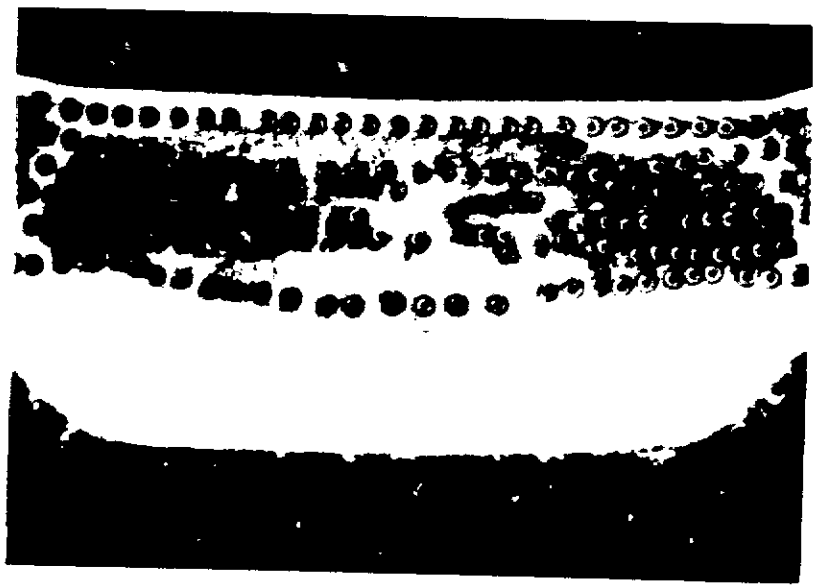

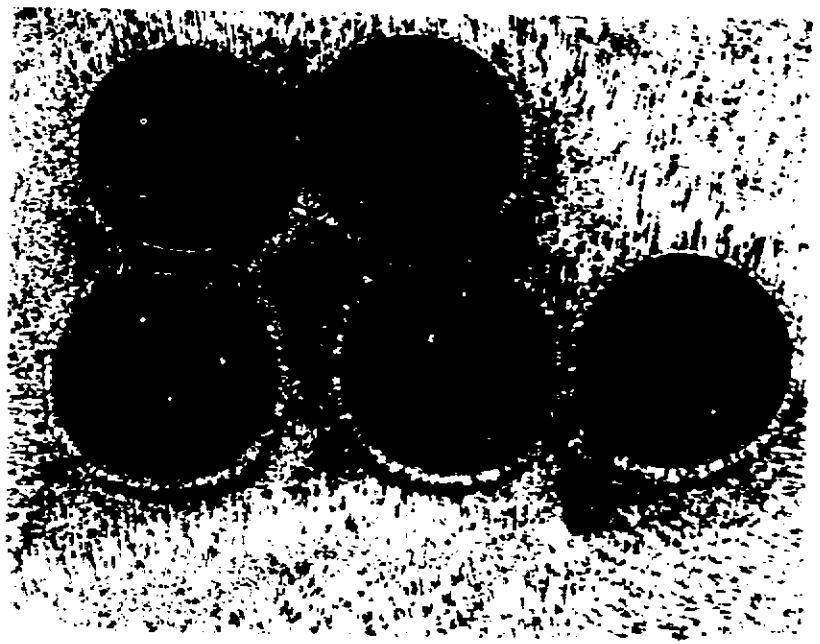

Figure 90 - Photomicrographs of the transverse section through the center of the spotweld between Ti-15-3 and SiC/Ti-6-4. Note the fine solidification structure and the shrinkage cracks around the SiC filaments. Black arrows delineate the molten region of the weld nugget. White arrows outline the heat-affected region in the beta titanium alloy.

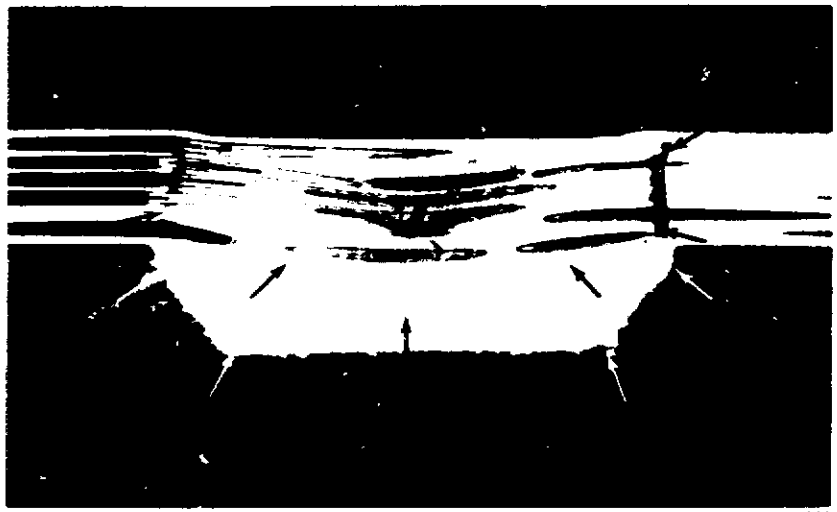

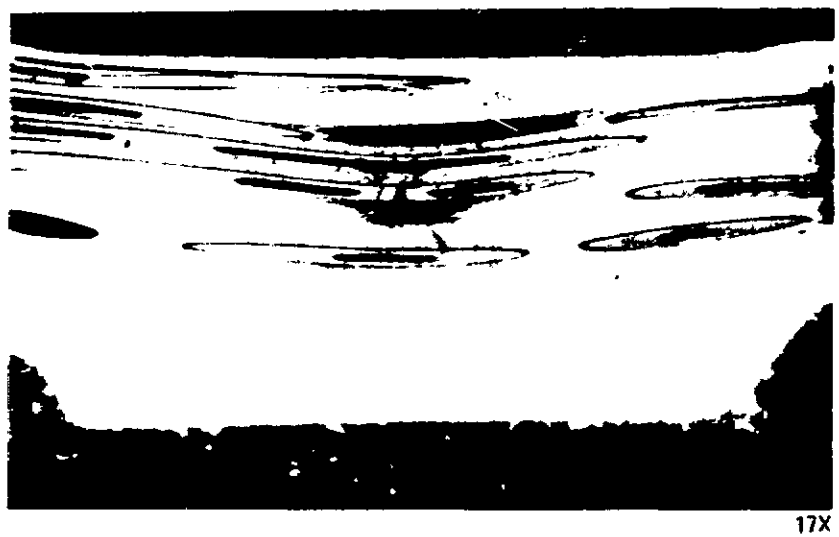

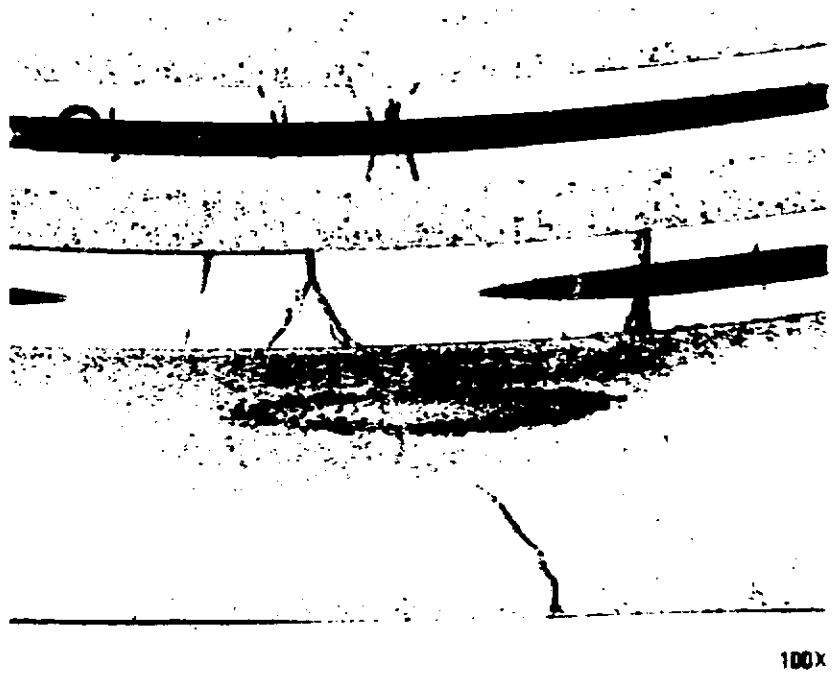

Figure 91. - Photomicrographs of the lc gitudinal section through the center of the spotweld between Ti-15-3 and SiC/Ti-6-4. Note bending of the SiC filaments.

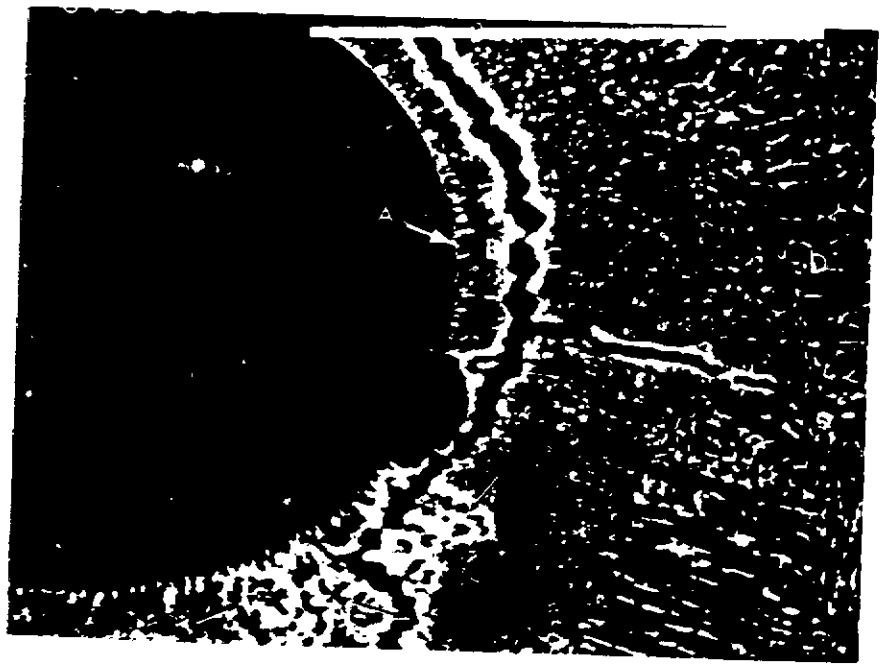

Elements	Composition in wt. % (EDAX)			
	Location A	Location B	Location C	Location D
Al	3.06	5.30	5.40	6.03
Si	14.12	2.07	2.40	0.82
V	2.53	6.80	5.97	4.44
Ti	80.29	85.83	86.23	88.72

Figure 92. - A SEM photograph of a silicon carbide filament and its adjacent area taken from the molten region of weld nugget showing shrinkage cracks and dendritic solidification pattern (arrows) within these cracks. Letters A, B, C and D denote the locations quantitative EDX analyses were made. 680X

Longitudinal 10X

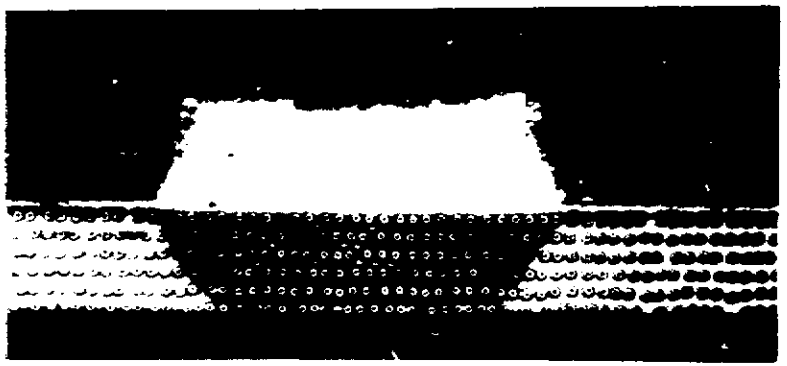

Transverse 10X

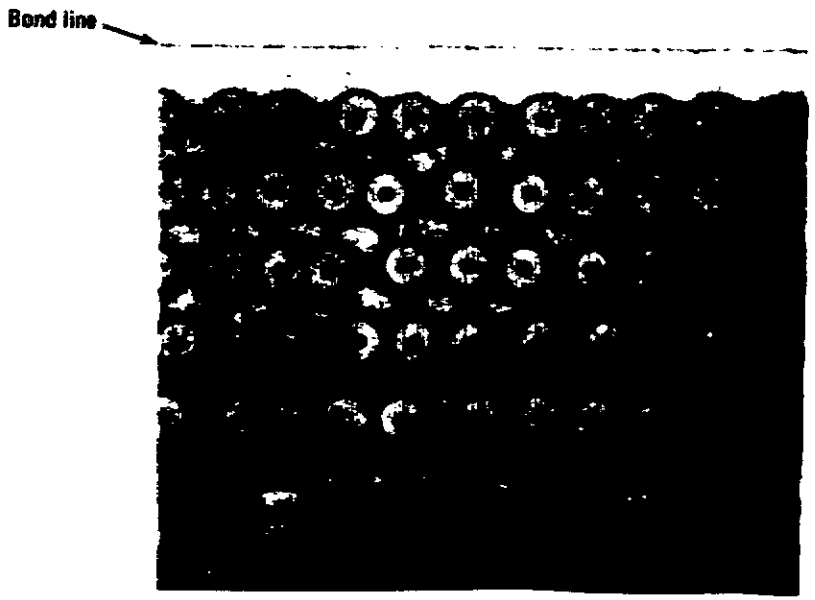

Transverse 40X

Figure 93. - Sections through the center of resistance bonds between Ti-15-3 and SiC/Ti-6-4 with no melting at the interface. Outline of HAZ is visible.

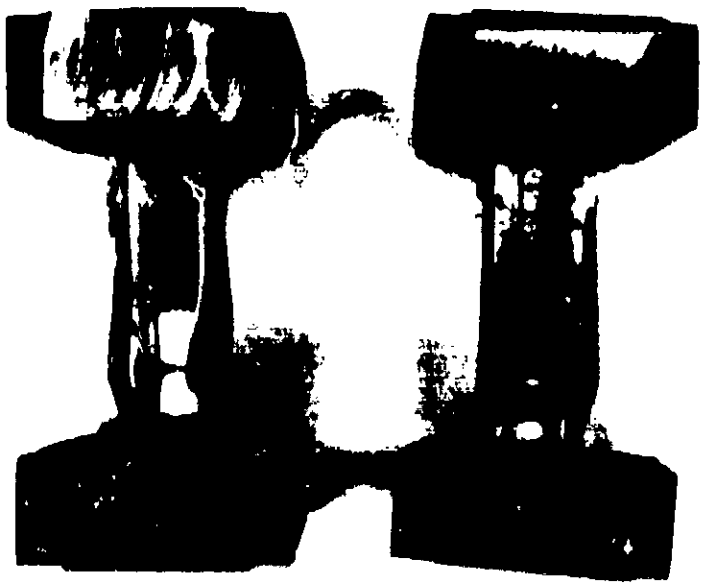

Figure 94. - Brazed zee-stiffened elements reinforced with SiC/Ti-6-4 MMC, after crippling test.

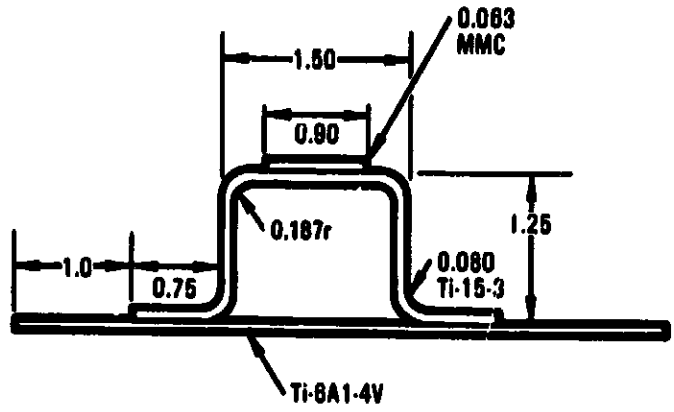

Note: Skin thickness varies
Dimensions in inches

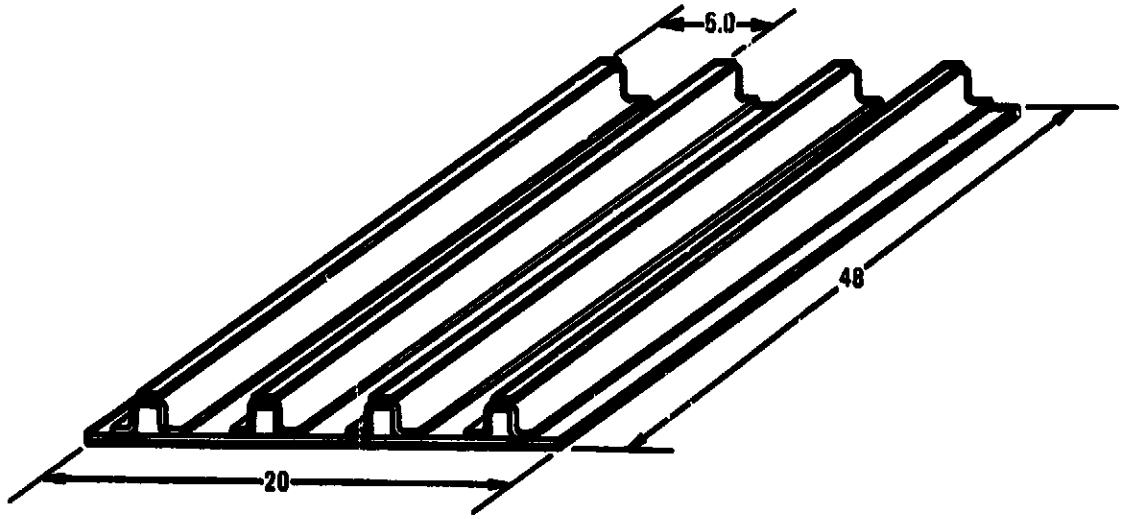

Figure 95. - Representative wing panel configuration with MMC reinforcement for task 8 weight/cost study.

C-3

CONCLUDING REMARKS

Low-cost methods for titanium structural fabrication using advanced cold-formable beta alloys have been studied for use in a Mach 2.7 supersonic cruise environment. The principal alloy investigated was Ti-15V-3Cr-3Al-3Sn (Ti-15-3), and a more limited evaluation of the Ti-3Al-8V-6Cr-4Mo-4Zr (Beta-C) alloy was made. Major findings of this investigation were as follows:

- Solution treated Ti-15-3 has good formability in terms of both mechanical properties and actual forming behavior. Cold formability of Ti-15-3 appears comparable with low-strength grades of commercially pure Ti and much better than Ti-6-4; e.g., their average minimum bend radius is 2.4t (Ti-15-3), 3.0t (C.P.-A40), 5.0t (Ti-6-4).

- Aged Ti-15-3 displays high mechanical properties over the postulated SCV temperature range of -65°F to 600°F. Beta-C in limited tests showed similar characteristics.

- Ti-15-3 showed exceptionally good high-cycle notched fatigue strength. Brazing or cold-working before aging adversely affected notched fatigue strength.

- Fatigue crack growth rates of Ti-15-3 were found to be insensitive to prestrain or a salt water environment, while the fracture resistance was reduced considerably as a result of prestrain.

- For fracture toughness considerations, mill annealed Ti-6-4 is superior to Ti-15-3 STA sheet at relatively high yield strength levels such as above 160 ksi. It is recommended that fracture toughness and notch sensitivity versus strength level of Ti-15-3 be further defined.

- Ti-15-3 and Beta-C were readily TIG-weldable in the annealed condition. As-welded and welded plus aged butt joints achieved full joint efficiency with good ductility.

- A unique low-cost isothermal brazing process has been developed which achieves rapid out-of-furnace brazing in an argon atmosphere. Ti-15-3 and Beta-C were readily brazed in the annealed condition to Ti-6-4 using aluminum brazing alloys, and they responded well to post-braze aging.

- Structural efficiency of small skin/stringer panels composed of cold-formed beta alloy stringers and Ti-6-4 skin joined by isothermal brazing was indicated in short column crippling tests at room temperature and 600°F.

- Further structural verification of cold-formed, isothermal brazed beta titanium structure was obtained in long-column compression at room temperature and 600°F, spectrum fatigue, and damage tolerance testing of large-scale representative wing upper surface panels of an SCV.

- Cold-formed and isothermal brazed beta titanium fabrication methods can save at least 25 percent cost and 16 percent weight over a conventional hot-formed and riveted Ti-6-4 assembly.

- Feasibility of using continuous filament SiC/Ti-6-4 metal matrix composite to selectively reinforce a beta titanium skin/stringer component has been shown. The reinforced isothermal brazed configuration has increased structural capability and weight savings potential. Spotweldability was poor and needs further development to eliminate local composite degradation. Present costs of the MMC selective reinforcement concepts studied would be prohibitive for many applications.

APPENDIX A
TEST COUPON CONFIGURATIONS

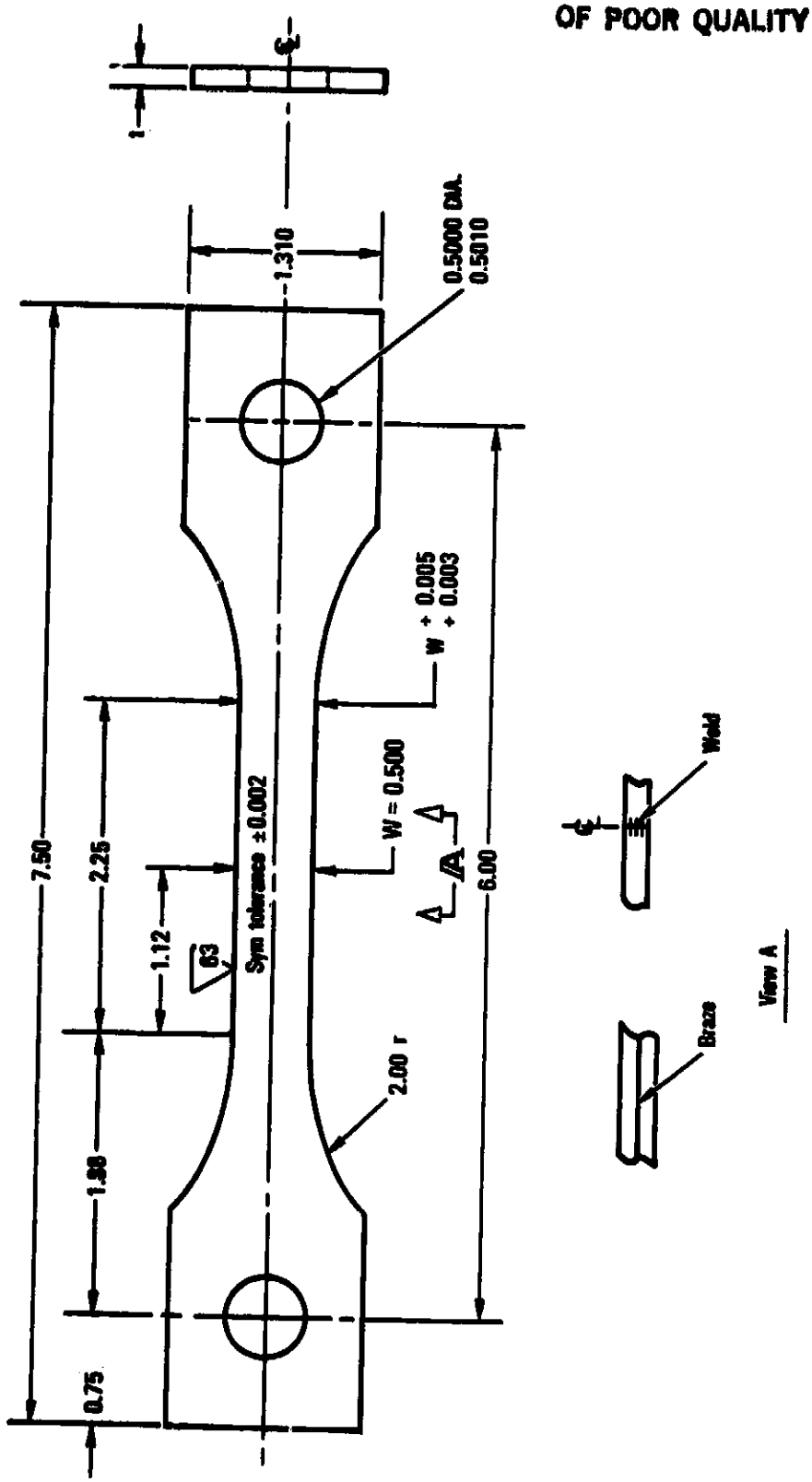

Figure A1. - Tensile and creep coupons.

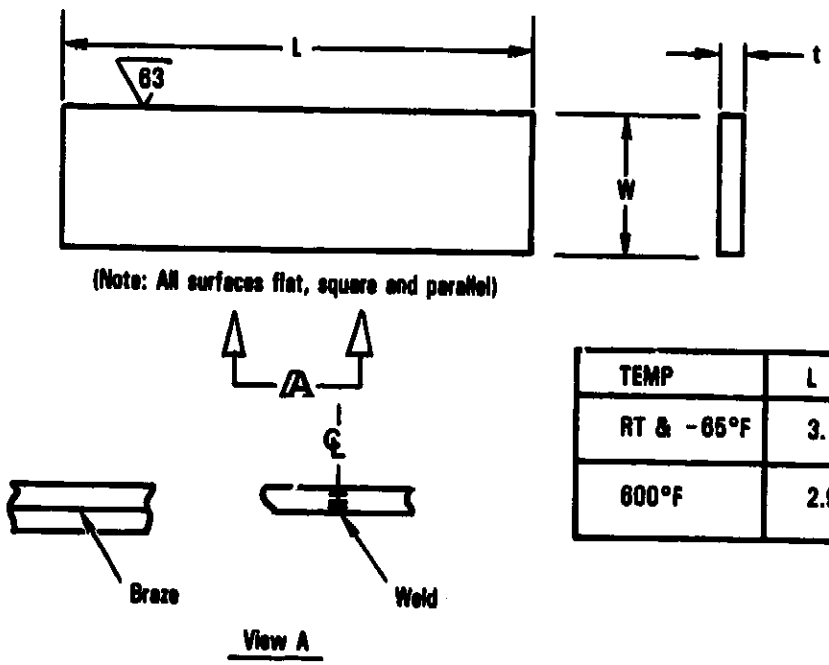

TEMP	L	W
RT & -65°F	3.100	0.625
600°F	2.900	1.000

Figure A2. - Compression coupons.

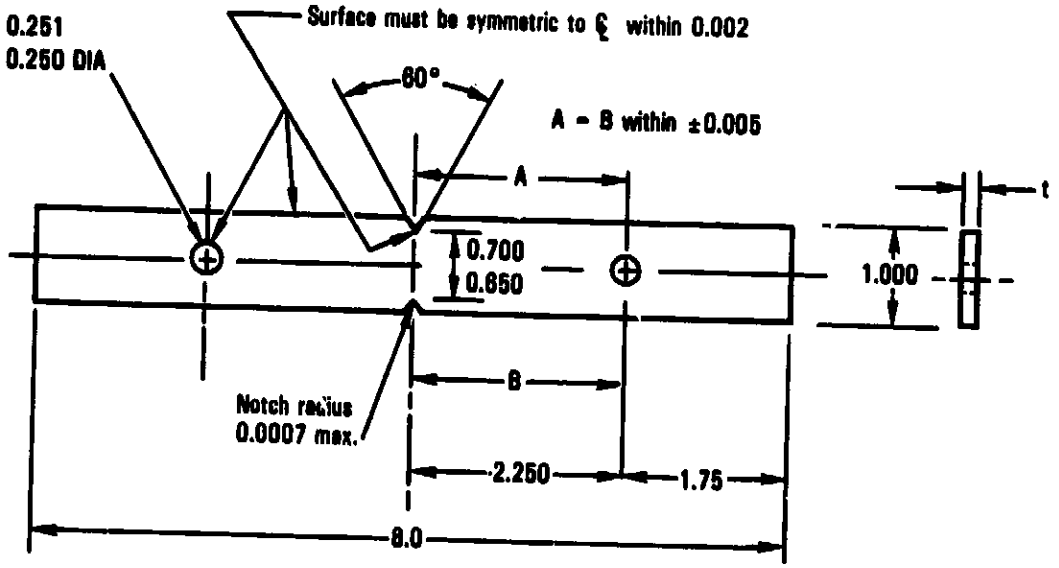

Figure A3. - Sharp edge-notch coupon (ASTM E338).

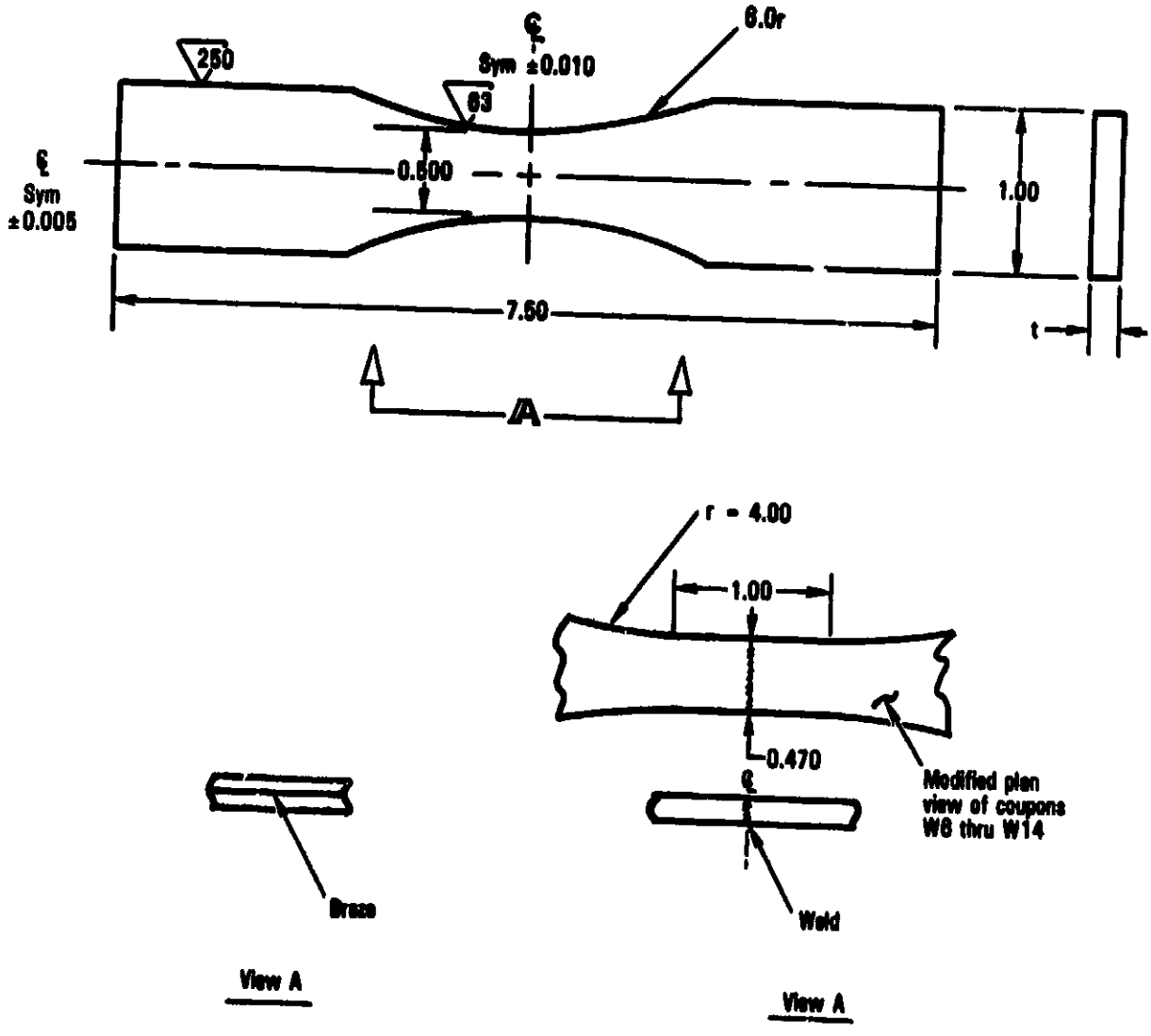

Figure A4. - Smooth fatigue coupons (K_t=1.0).

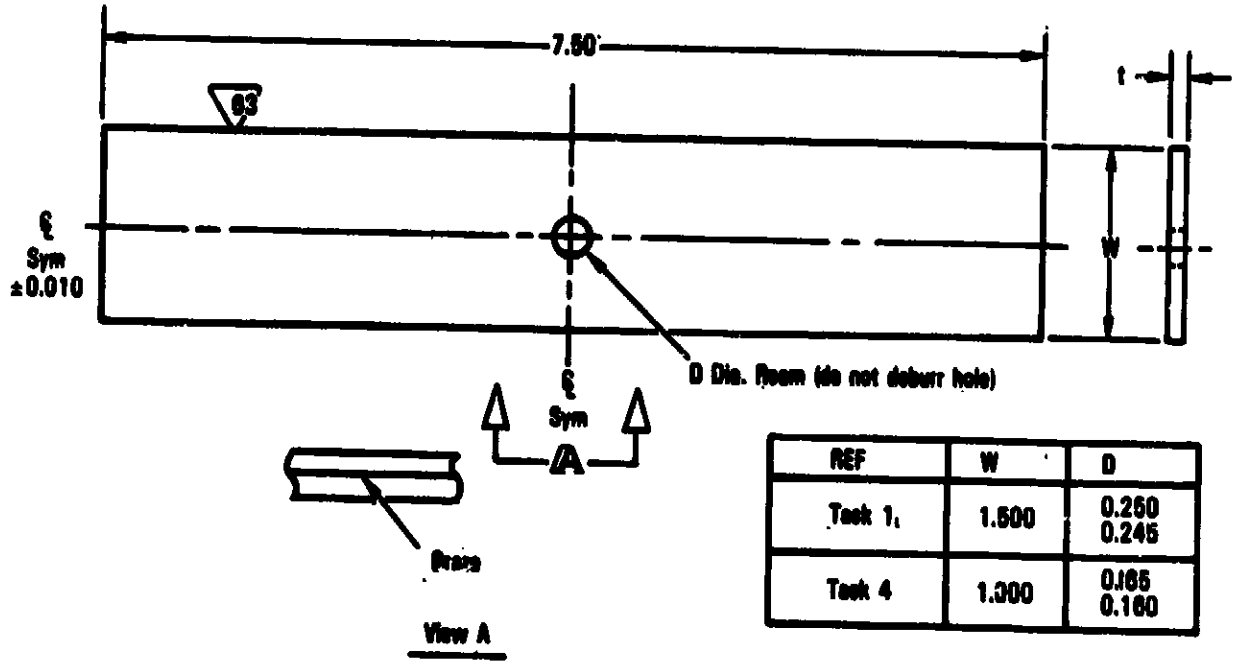

REF	W	D
Task 1,	1.500	0.250 0.245
Task 4	1.000	0.165 0.160

Figure A5. - Notched fatigue coupons (K_t=2.6).

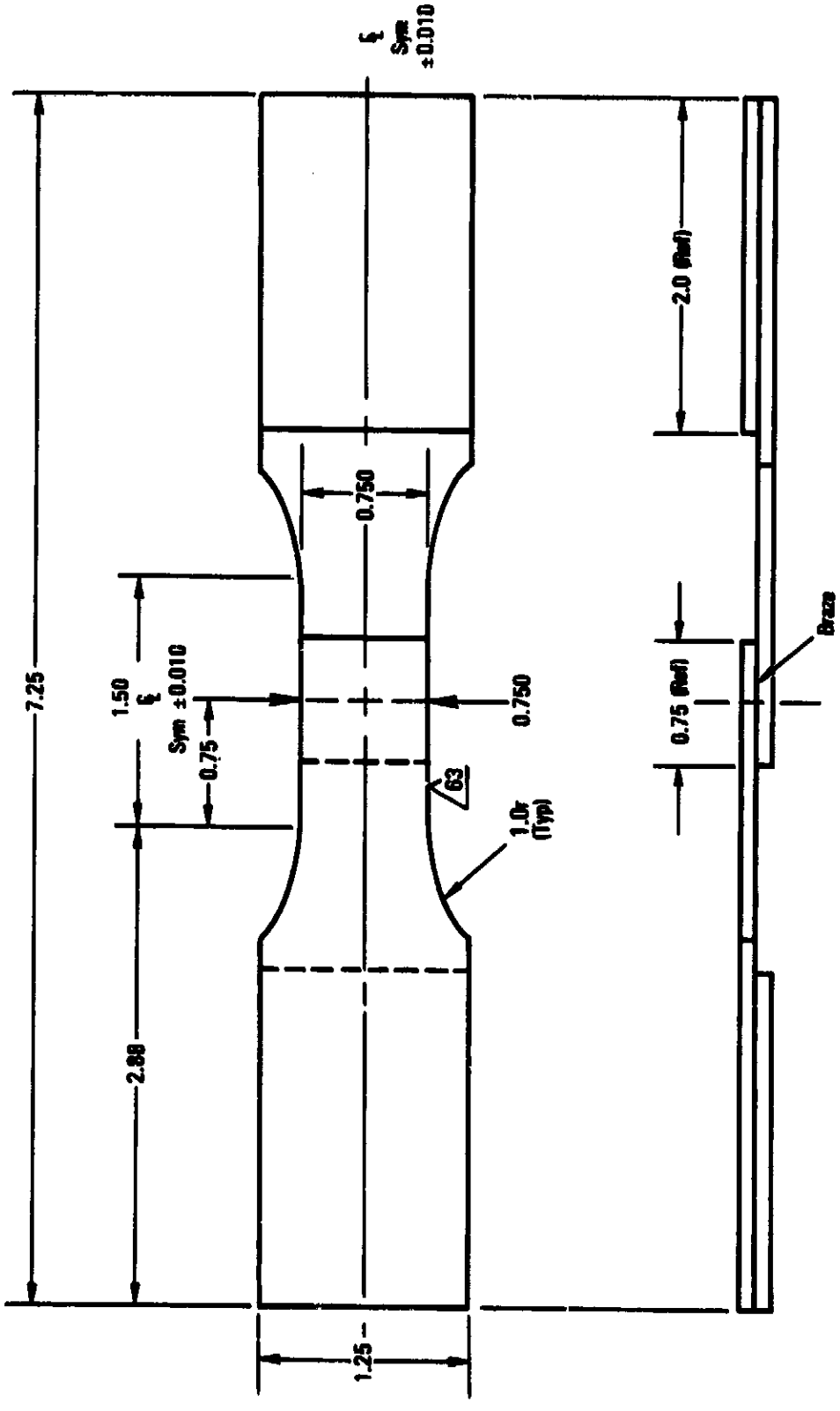

Figure A6. - Braze lap shear fatigue coupon.

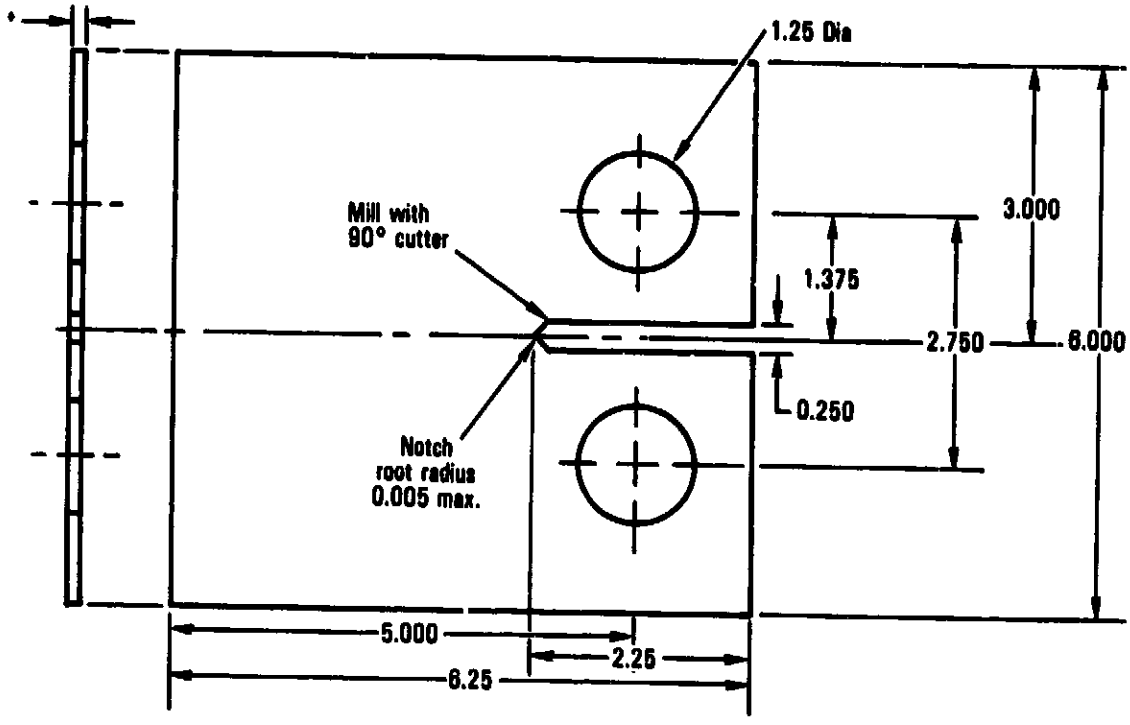

Figure A7. - Compact tension coupon (ASTM E561).

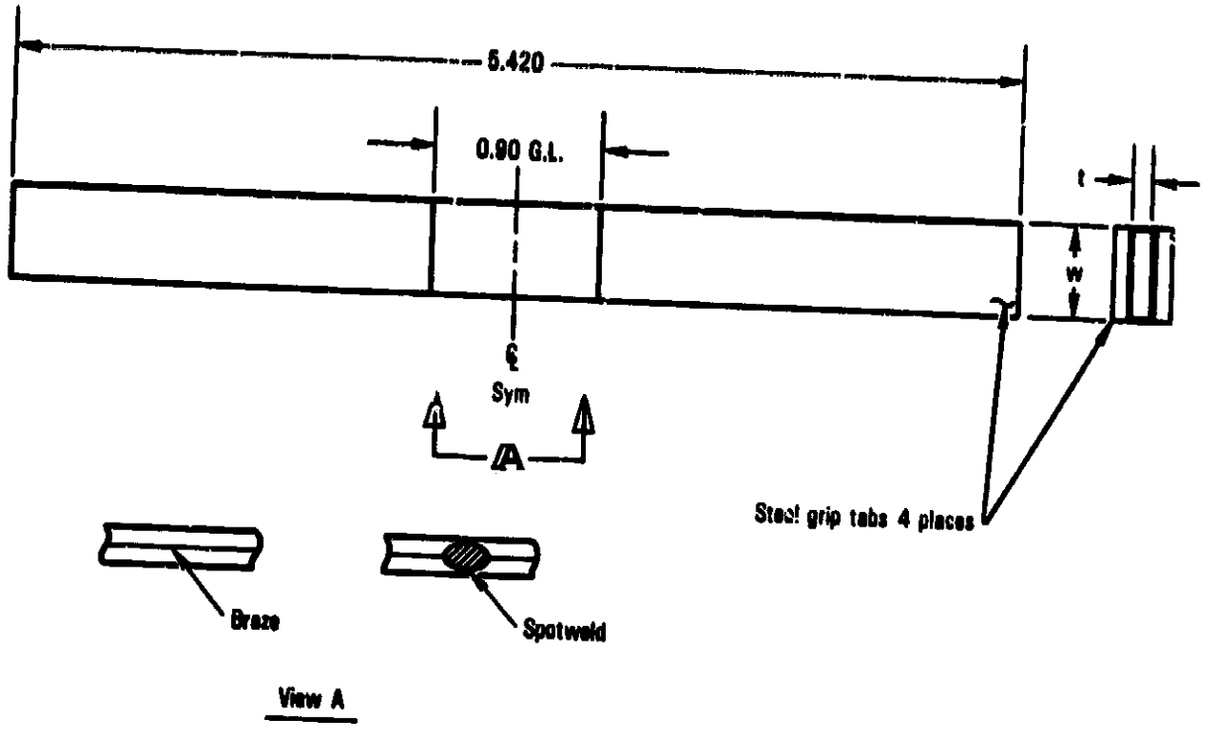

NOTE: 1. W = 0.250 to 0.500
2. 0.90 gage length was selected to span at least two spotwelds of 5/8 inch max pitch
3. Sides and ends machined square and parallel where required by diamond wheel grinding

Figure A8. Metal matrix composite compression coupons.

REFERENCES

1. R.S. Kaneko, G.W. Davis, C.A. Woods, and D.M. Royster, "Low Cost Fabrication of Sheet Structure Using a New Beta Titanium Alloy," Vol. 27, 27th National SAMPE Proceedings, 1982.

2. R.A. Wood, D.N. Williams, J.D. Boyd, R.L. Rothman, and E.S. Bartlett, "Strain Transformable Beta Titanium Base Alloys," AFML-TR-70-257, Battelle Memorial Institute, Dec. 1970. (Available from DTIC as AD 877 899.)

3. H.W. Stemme, "Development of a Formable Sheet of Titanium Alloy," AFML-TR-73-49, Lockheed-Georgia Company, April 1973. (Available from DTIC as AD 761 515.)

4. T.L. Wardlaw, H.W. Rosenberg, W.M. Parris, "Development of Economical Sheet Titanium Alloy," AFML-TR-73-296, Titanium Metals Corp., Dec. 1973. (Available from DTIC as AD 775 358.)

5. G. Lenning, "Formable Sheet Titanium Alloys," AFML-TR-76-45, Titanium Metals Corp., TIMET Div., August 1976. (Available from DTIC as AD A033 187.)

6. F.A. Crossley and J.M. Van Orden, "A New Titanium Alloy for Forms and Weldments," Metals Engineering Quarterly, Vol. 13, May 1973.

7. R.A. Wood, "Beta Titanium Alloys," MCIC-72-11, Battelle Columbus Laboratories, Ohio, September 1972. (Available from DTIC as AD 753 439.)

8. RMI Company, Technical Bulletin, "Properties of Ti-3Al-8V-6Cr-4Mo-4Zr," June 1978.

9. R.A. Wood and k.J. Favor, "Titanium Alloys Handbook," MCIC-HB-02 (Contracts F33615-72-C-1227 and DSA 900-73-C-0922), Battelle Columbus Lab., Dec. 1972. (Available from DTIC as AD 758 335.)

10. J.W. Hegemeyer and D.E. Gordon, "Properties of Two Beta Titanium Alloys after Aging at Several Different Temperatures," Titanium Science and Technology: Proceedings of the Second International Conference, Vol. 3, 1973, pp. 1957-1968.

11. Mechanical Properties Data Center, Battelle Columbus Lab.: Aerospace Structural Metals Handbook - 1980 Publication. (Formerly AFML-TR-68-115.)

12. V.C. Peterson, J.B. Guernsey, and R.C. Buehl, "Manufacturing Procedures for a New High-Strength Beta Titanium Alloy Having Superior Formability," AFML-TR-69-171, Part III, Crucible Steel Company of America, June, 1969.

13. "Metallic Materials and Elements for Aerospace Vehicle Structures," MIL-HDBK-5C, 15 September 1976.

14. "Titanium and Titanium Alloy Sheet, Strip and Plate," MIL-T-9046H, 14 March 1974.

15. B.R. Wright, et al., "Supersonic Cruise Vehicle Technology Assessment Study of an Over/Under Engine Concept," NASA CR-159003, 1978.

16. R.A. Wood and H.R. Ogden, "The All-Beta Titanium Alloy (Ti-13V-11Cr-3Al)" DMIC Rept. 110 (DTIC AD 214002), Battelle Mem. Inst., April 17, 1959.

17. E.H. Rennhack and D.D. Crooks, "Elevated Temperature Plastic Anisotropy of Ti-6Al-4V Plate," Metallurgical Transactions, 1979, Vol. 10A, p. 457.

18. E.H. Rennhack, "How Normal Anisotropy Influences Formability of Aluminum Alloys," Metals Engineering Quarterly, 1976, Vol. 16, p. 58.

19. W.T. Lankford, S.C. Snyder and J.A. Bauscher, "New Criteria for Predicting the Stress Performance of Deep Drawing Sheets," Transactions ASM, 1950, Vol. 42, p. 1197.

20. R.L. Whiteley, "The Importance of Directionality in Drawing Quality Sheet Steel," Transactions ASM, 1960, Vol. 52, p. 154.

21. S.S. Hecker, "Formability of Aluminum Alloy Sheets," Transactions of the ASME (Journal of Engineering Materials and Technology), January 1975.

22. S.S. Hecker, "Simple Technique for Determining Forming Limit Curves," Sheet Metal Industries, November 1975.

23. A.K. Gosh, "The Effect of Lateral-Drawing-In on Stretch Formability," Materials Engineering Quarterly, August 1975.

24. V. Nagpal and T. Altan, "Mathematical Modeling of Sheet Metal Formability Indices and Sheet Metal Forming Processes," AFML-TR-78-140, Battelle Columbus Lab., October 1978. (Available from DTIC as AD B036 118L.)

25. R.G. Hocker, "Weldbraze Airframe Components," AFML-TR-77-171, Northrop Corporation, Hawthorne, Calif., Nov. 1977. (Available from DTIC as AD A054 042.)

26. T.T. Bales, D.M. Royster, W.E. Arnold, Jr., "Development of the Weld-Braze Joining Process," NASA TN D-7281, 1973.

27. I.F. Sakata and G.W. Davis, "Evaluation of Structural Design Concepts for an Arrow-Wing Supersonic Cruise Aircraft," NASA CR-2667, 1977.

28. D.J. Peery, "Aircraft Structures," McGraw Hill Book Company, 1950.

29. T.R. Brussat, "Rapid Calculation of Fatigue Crack Growth by Integration," presented at the 7th Symposium on Fracture Mechanics, College Park, MD., August 27-29, 1973.

★U.S. GOVERNMENT PRINTING OFFICE:1983-639-008/ 30